



Terms and Conditions of Use of Digitised Theses from Trinity College Library Dublin

Copyright statement

All material supplied by Trinity College Library is protected by copyright (under the Copyright and Related Rights Act, 2000 as amended) and other relevant Intellectual Property Rights. By accessing and using a Digitised Thesis from Trinity College Library you acknowledge that all Intellectual Property Rights in any Works supplied are the sole and exclusive property of the copyright and/or other IPR holder. Specific copyright holders may not be explicitly identified. Use of materials from other sources within a thesis should not be construed as a claim over them.

A non-exclusive, non-transferable licence is hereby granted to those using or reproducing, in whole or in part, the material for valid purposes, providing the copyright owners are acknowledged using the normal conventions. Where specific permission to use material is required, this is identified and such permission must be sought from the copyright holder or agency cited.

Liability statement

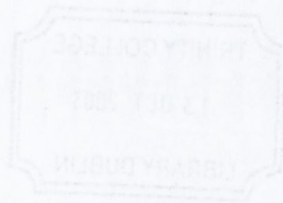
By using a Digitised Thesis, I accept that Trinity College Dublin bears no legal responsibility for the accuracy, legality or comprehensiveness of materials contained within the thesis, and that Trinity College Dublin accepts no liability for indirect, consequential, or incidental, damages or losses arising from use of the thesis for whatever reason. Information located in a thesis may be subject to specific use constraints, details of which may not be explicitly described. It is the responsibility of potential and actual users to be aware of such constraints and to abide by them. By making use of material from a digitised thesis, you accept these copyright and disclaimer provisions. Where it is brought to the attention of Trinity College Library that there may be a breach of copyright or other restraint, it is the policy to withdraw or take down access to a thesis while the issue is being resolved.

Access Agreement

By using a Digitised Thesis from Trinity College Library you are bound by the following Terms & Conditions. Please read them carefully.

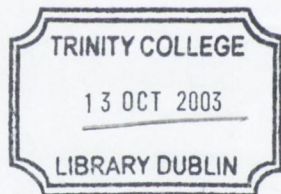
I have read and I understand the following statement: All material supplied via a Digitised Thesis from Trinity College Library is protected by copyright and other intellectual property rights, and duplication or sale of all or part of any of a thesis is not permitted, except that material may be duplicated by you for your research use or for educational purposes in electronic or print form providing the copyright owners are acknowledged using the normal conventions. You must obtain permission for any other use. Electronic or print copies may not be offered, whether for sale or otherwise to anyone. This copy has been supplied on the understanding that it is copyright material and that no quotation from the thesis may be published without proper acknowledgement.

METAL SPINNING,
AN
INCREMENTAL FORMING PROCESS



Eamonn Quigley

Submitted in fulfillment of the requirements for the award of the degree of
Doctor of Philosophy to the University of Dublin, Trinity College, 2003.



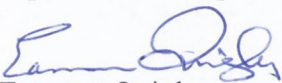
TH681S
~~9475~~
7359

Handwritten text in black ink, consisting of three lines: 'TH681S', a crossed-out '9475', and '7359'.

Declaration

I declare that the present work has not been submitted as an exercise for a degree at any other university. This thesis consists entirely of my own work except where references indicate otherwise.

I agree that the library of the University of Dublin, Trinity College, Dublin may lend or copy this thesis upon request.



Eamonn Quigley

Acknowledgements

The author wishes to express his sincere gratitude and appreciation to the following people:

to my wife Eimear thank you for your patience and encouragement with my studies over many years.

to my supervisor Professor John Monaghan.

to my engineering colleagues at the Institute of Technology, Tallaght and at Trinity College who encouraged and supported me in this work.

to my colleagues in the Languages Dept at IT Tallaght who helped me with German and Japanese texts.

to my children who have seen me disappear into my 'lighthouse' very many times in the course of this project.

Summary

Recent changes in product development processes have increased the demand for sheet metal parts manufactured in low volumes with the minimum investment in tooling. Spinning and a related process called 'incremental stretch forming' have shown potential for meeting this demand. Metal spinning is a long established process with low tooling costs that can be used to form a flat sheet metal blank into a hollow rotationally symmetric part. For the purposes of this project spinning was taken as a representative incremental forming process, i.e. a process where the deformation is achieved incrementally.

Spinning to this day is a process that is reliant on the skill and intuition of those involved. The deformation processes involved in both spinning and incremental stretch forming are complex three dimensional processes that cannot be readily analysed by conventional closed form analytical techniques. Consequently, a major objective of this project was to apply finite element analysis to spinning in order to develop an understanding of the nature of the tool contact involved and to characterise the process in terms of the forces required, the tool contact area and the thickness change in the workpiece.

As contact is a central issue to this analysis, classical or Hertzian static contact analysis was used as a starting point to provide a reference for comparison with the results of physical experiments and the results of finite element simulations. The predictions of classical contact mechanics supported the results of finite element analysis of static contact. With this validation the finite element analysis of static contact was extended to study compression of a workpiece between elastic tools and other loading scenarios. These static analyses highlight the advantages of using low elastic modulus tools or a combination of steel and low elastic modulus tooling. These static analyses provide insight into what tool rigidity is demanded by an incremental forming process and so can inform tool and machine design as well as forming strategy or tool path design.

Because the static contact simulations were run using two dimensional finite element analysis they were particularly cost effective in terms of solution times (computation cost). This was particularly evident because of the relatively high computation cost of running a full process simulation of a spinning operation. Nonetheless full process simulations were achieved and these provide significant insight into the deformation involved in a spinning process. These full process simulations were coupled with local mesh refinement to develop a new description of the deformation mechanisms involved. Thus this work contributes to an understanding of the key parameters of spinning, as an incremental forming process, and to providing a foundation for designing new strategies for incremental forming and for designing of incremental forming processes and equipment.

CHAPTER 1. INTRODUCTION.....	1
1.1. BACKGROUND TO INVESTIGATION	1
1.2. CURRENT RESEARCH ON INCREMENTAL STRETCH FORMING	1
1.1.1. Spinning.....	2
1.1.2. Spinning as an Archetypal Incremental Forming Process.....	3
1.1.3. Analysis of Contact Loads and Stresses.....	3
1.1.4. Shear forming	4
1.1.5. Main Project Objectives	5
CHAPTER 2. A REVIEW OF SPINNING & RELATED PROCESSES	6
2.1. TECHNOLOGY.....	6
2.1.1. The historical development of spinning	6
2.1.2. Spinning Technology -terminology.....	10
2.1.3. Examples of spinning operations.....	11
2.1.4. Spinning Process Limitations	12
2.1.5. Advantages of spinning.....	13
2.1.6. Disadvantages and Limitations of Spinning Process and Process Understanding.....	13
2.1.7. Spinning; the practical requirements.....	14
2.1.8. Spinning - Conventional Spinning	15
2.1.9. Strain predictions for Conventional Spinning.....	19
1.1.10. Shear forming	21
1.1.11. Shear Forming; a Comparison of Thickness Strains and Principal Strains	24
1.1.12. Metal Spinning Compared with Machining on a Lathe	28
1.1.13. Programming the roller path.....	28
1.1.14. Surfaces of revolution with minimum tooling	30
1.2. SPINNING DEFORMATION MECHANISMS.....	32
1.2.1. Analyses of Shear forming	32
1.3. CLASSICAL ANALYSIS OF CONTACT MECHANICS.....	36
1.3.1. Contact Mechanics an Analytical approach.....	36
1.3.2. Uniform pressure and other contact pressure distributions	37
1.4. ELASTOPLASTIC FEA	41
1.4.1. Introduction and Summary	41
1.4.2. The selection of the MARC finite element code	43
1.4.3. Simulation of contact using MARC.....	44
1.4.4. Element Selection and Mesh Definition.....	44
1.4.5. Material Model	45
1.4.6. Validation of Finite Element Model.....	46
CHAPTER 3. EXPERIMENTS PHYSICAL & FE MODELS	49
3.1. INTRODUCTION.....	49
3.2. DIRECT STATIC CONTACT: PHYSICAL EXPERIMENTS;.....	52

3.2.1. <i>The Purpose of Analysing Direct Contact</i>	52
3.2.2. <i>The Direct Static Contact Physical Experiments: Materials Used</i>	52
3.2.3. <i>Experimental investigation of the contact area</i>	53
3.3. DIRECT STATIC CONTACT: FE SIMULATIONS.....	56
3.3.1. <i>Simulating the Workpiece Loading as Uniform Pressure</i>	60
3.3.2. <i>Simulating the Workpiece Loading as Opposing Pressures</i>	63
3.3.3. <i>Simulating Workpiece Contact Load with Rigid Tool Surfaces</i>	66
3.3.4. <i>Simulating Workpiece Contact Load as Direct Compression by Elastic Tools</i>	71
3.4. THE EXPERIMENTAL SPINNING PROCESS.....	73
3.4.1. <i>Overview of Spinning Experiments</i>	73
3.4.2. <i>Measurement of Part Shape</i>	75
3.4.3. <i>Measurement of Strains</i>	76
3.4.4. <i>Measurement of Work-hardening</i>	77
1.1.5. <i>Measurement of Forces</i>	78
1.1.6. <i>The Spinning Equipment</i>	80
1.1.7. <i>The tool path including NC code</i>	83
1.5. THE SPINNING PROCESS: FE SIMULATIONS.....	86
1.5.1. <i>An Approach to Simulation of Spinning using 2D-Axisymmetric FEA</i>	86
1.5.2. <i>Simulating the Spinning Process with 3D FEA</i>	89
1.6. SUMMARY OF EXPERIMENTAL WORK	99
CHAPTER 4. RESULTS AND ANALYSIS.....	100
4.1. INTRODUCTION TO RESULTS AND ANALYSIS.....	100
4.2. RESULTS OF STATIC CONTACT ANALYSIS	101
4.2.1. <i>Hertzian Analysis Applied to the Roller and Former in Static Contact</i>	101
1.1.2. <i>Finite Element Predictions of Static Contact</i>	108
1.1.3. <i>FE predictions of Static Contact with the Workpiece in place:-</i>	110
1.1.4. <i>The Results of Static Contact Physical Experiments</i>	120
1.1.5. <i>Linking the study of contact areas involved in direct contact to spinning</i>	121
1.1.6. <i>The Results from Uniform Pressure FE Model</i>	122
1.3. SPINNING PROCESS EXPERIMENTS.....	130
1.3.1. <i>Experimental shape: spun part geometry as measured by CMM</i>	130
1.3.2. <i>Comparison of Experimental Forces with Published Results</i>	131
1.3.3. <i>Thickness strain measurements</i>	132
1.3.4. <i>Tool Force Line Stiffness in Spinning</i>	134
1.3.5. <i>Comparison of Experimental Strains with Strains for Landmark Processes</i>	136
1.4. FINITE ELEMENT SIMULATION OF THE SPINNING PROCESS.....	138
1.4.1. <i>Comparison of experimental strains with FE predictions</i>	138
1.4.2. <i>FE predictions of spinning forces using full 3D process simulation</i>	139
1.4.3. <i>Presentation /Analysis of force in surface normal coordinate system</i>	140
1.4.4. <i>Tool Force Line Stiffness in Spinning from FEA</i>	143
1.4.5. <i>Comparison of experimental strains with FE predictions</i>	145

1.1.6. Contour plots of Strains from FE models	146
1.1.7. Strain variation through thickness from FE analysis.....	148
1.1.8. Strain hardening results.....	156
1.5. USING MESH REFINEMENT TO STUDY CONTACT	158
1.5.1. Results showing size of contact area.....	158
1.5.2. Offset Contact Forces and Areas (insight Deformation Mechanics in spinning)	161
CHAPTER 5. CONCLUSIONS	165
5.1. CONCLUSIONS	165
5.2. RECOMMENDATIONS FOR FUTURE WORK.....	168
REFERENCES	169
APPENDIX 1 FLOW CURVES FROM PLANE STRAIN COMPRESSION.....	172
APPENDIX 2 NC CODE	177
APPENDIX 3 FORTRAN 6.6 CODE FOR AXISYMMETRIC SPINNING PROCESS SIMULATION	178
APPENDIX 4 FORTRAN 6.6 CODE FOR ROTATING FULL THREE DIMENSIONAL SIMULATION.....	199

LIST OF FIGURES AND TABLES

Figure 1.1 Simple setups for a spinning operation	2
Figure 2.1 Example of Metal spinning from first century AD [10]	6
Figure 2.2 Wood cut of manually powered spinning operation [12]	7
Figure 2.3 Hand Spinning, Lange 1990 [18]	8
Figure 2.4 Typical path used in manual spinning comprising seven tool passes [17]	9
Figure 2.5 Manually generated tool path (a) recorded by a playback NC lathe (b) [20]	9
Figure 2.6 Spinning:-central area shear formed, outer area conventional spinning [20]	11
Figure 2.7 Selection of spun parts [26]	12
Figure 2.8 The basic requirements for a spinning operation	14
Figure 2.9 Successive Spinning Passes –Idealised constant thickness spinning	15
Figure 2.10 Successive spinning passes [18]	16
Figure 2.11 Conventional spinning of a large workpiece [20]	16
Figure 2.12 Initial elastic deformation	17
Figure 2.13 Deformation in spinning after [17]	18
Figure 2.14 Conventional spinning (constant thickness forming)	20
Figure 2.15 Conventional spinning compared to shear forming	21
Figure 2.16 Thickness reduction in shear forming	22
Figure 2.17 Comparison of Principal Strain with Thickness Strain in Shearforming	24
Figure 2.18 Directions of Principal Strains and Thickness Strain in Shearforming	25
Figure 2.19 Comparison of Strains in shear forming and conventional spinning	26
Figure 2.20 Thickness reduction in shear forming [33]	26
Figure 2.21 Wall thickness variation in shear forming [34]	27
Figure 2.22 Roller Passes based on Evolute Curves [36]	29
Figure 2.23 Spinning:- contact with former only occurs near the tool	30
Figure 2.24 Spinning without a mandrel [7]	30
Figure 2.25 Spinning without mandrel support or internal supporting roller [38]	32
Figure 2.26 Hardness distribution in shear formed copper cone [39]	33
Figure 2.27 Deformation of Shear forming Wada [40]	34
Figure 2.28 Compatibility with flange (impossible flange shape).	35
Figure 2.29 Contact pressure distribution –Johnson [41] (a) Contours of principal stresses (b) Trajectories of principal stress directions (c) Stress distribution due to uniform and Hertz pressure distribution.	38
Figure 2.30 Contact pressure distribution [43]	39
Figure 2.31 Contact pressure distribution (dimensionless contact stress) [44]	40
Figure 2.32 Cantilever Test Apparatus	46
Figure 2.33 Solid element aspect ratios	47
Figure 2.34 Typical Finite Element Model	47
Figure 3.1 Different Static Contact Load Arrangements	50
Figure 3.2 Instron 8516 with Roller and Flat for Indentation Experiment	53
Figure 3.3 Close-up view of Typical Indentation Experiment	54
Figure 3.4 Fuji Prescale film principle of operation	54
Figure 3.5 Contact Area Detected by Fuji Prescale film	55

Figure 3.6 Contact Pressure Applied to One Side of Thin Workpiece	57
Figure 3.7 Contact Pressure Applied to One Side of Thick Workpiece	57
Figure 3.8 Simulating Loading as Opposing Uniform Pressures on Workpiece	58
Figure 3.9 Load Applied by Rigid Tools	58
Figure 3.10 Finite element models with different test piece thickness	60
Figure 3.11 Axisymmetric FE Model, mesh and boundary conditions	62
Figure 3.12 Axisymmetric FE Model uniform pressure load, typical stress contours	62
Figure 3.13 Axi-symmetric finite element model with pressures applied	64
Figure 3.14 Axisymmetric FE Model Opposing Pressures, a typical result	65
Figure 3.15 An Example of One Quarter Segment of Contacting Solids	67
Figure 3.16 Configurations of Roller and Former	68
Figure 3.17 Axisymmetric FE model, mesh between rigid body tools	70
Figure 3.18 Axi-symmetric finite element model –contact bodies	71
Figure 3.19 Axisymmetric FE model –Elastic Tools Typical Stress Result	72
Figure 3.20 An example of a spun part (with steel rule).	74
Figure 3.21 Measurement of Parts on TESA CMM	75
Figure 3.22 The Etching Process	76
Figure 3.23 Etched Circle Grid (a) on part, (b) detail, (c) on flat workpiece.	77
Figure 3.24 Beuhler Microhardness Tester (a), Part mounted for test (b) and (c).	78
Figure 3.25 Roller Tool Mounted in the Kistler 9121 Dynamometer	79
Figure 3.26 Basic dimensions of former	80
Figure 3.27 Roller	80
Figure 3.28 Roller holder	81
Figure 3.29 Tailstock	82
Figure 3.30 Experimental spinning process	82
Figure 3.31 Basic Tool Motion Equidistant from the Surface of Former	83
Figure 3.32 First roller pass showing the position of the roller edge radius	84
Figure 3.33 Second and Third Roller Pass	85
Figure 3.34 2D-Axisymmetric Model of Spinning	86
Figure 3.35 2D-Axisymmetric Model of Spinning Typical Deformed Shape	86
Figure 3.36 Roller Path in Axisymmetric Simulation of Spinning Process	87
Figure 3.37 Detail of Roller Path in Axisymmetric Simulation	87
Figure 3.38 Optimum mesh definition	90
Figure 3.39 Three Dimensional Mesh	91
Figure 3.40 A Section of Mesh Generated by Rotation	91
Figure 3.41 Mesh Based on Curvature of Formed Part	93
Figure 3.42 Mesh Based on Uniform Element Area	94
Figure 3.43 A Practical Compromise in Mesh Definition	94
Figure 3.44 Spinning model with rigid roller and rigid former	96
Figure 3.45 Roller model-rigid surface with attached mesh	97
Figure 3.46 Spinning model with deformable elements on roller and rigid former	98
Figure 4.1 Configurations of Roller and Former	103

Figure 4.2 Force variation with Prescribed Displacement (Hertz theory)	107
Figure 4.3 Contact area against Force from Hertz Theory	107
Figure 4.4 Comparison of Hertz and FE Predictions of Contact Force (No Workpiece)	109
Figure 4.5 Comparison of FE predictions of force for positions 1 and 2 (no workpiece)	110
Figure 4.6 FE Predictions of contact force for position 1 (workpiece and no workpiece compared).	111
Figure 4.7 Stiffness predictions from finite element models (with workpiece).	112
Figure 4.8 Axisymmetric Model –different sizes of contact areas (red on detail))	113
Figure 4.9 Contact Area Relationship with Force: Finite Element Prediction Vs Hertz.	114
Figure 4.10 Contact Area Relationship with Force: Finite Element Prediction.	115
Figure 4.11 Workpiece contact area Vs Prescribed displacement from FE (roller position1).	116
Figure 4.12 Thickness reduction variation with prescribed displacement.	117
Figure 4.13 Thickness reduction variation with applied force.	118
Figure 4.14 Axisymmetric Finite Element Model Constant pressure typical results	122
Figure 4.15 Stress contours for a pressure load (a) analytical [41] Vs (b) FE solution	123
Figure 4.16 Analytical and FE prediction of Stress Vs dimensionless distance below the surface generated by a uniform pressure.	124
Figure 4.17 Equivalent Stress variation with distance below the surface in Different Thickness plates (uniform pressure load, “no support”).	125
Figure 4.18 Stress Variation with distance below the surface in 1mm thick plate	126
Figure 4.19 Stress variation with supported area	127
Figure 4.20 Plastic strain occurring under uniform pressure	128
Figure 4.21 Plastic Strain Results Axi-symmetric finite element model	129
Figure 4.22 A typical profile of a spun part as measured on the CMM (in mm)	130
Figure 4.23 Typical forces in a spinning operation.	131
Figure 4.24 Force Measurement Coordinate System	132
Figure 4.25 Experimental Thickness Variation	133
Figure 4.26 Experimental Force History Curves for different Prescribed Displacements	134
Figure 4.27 Force Variation with Prescribed displacement of Roller	135
Figure 4.28 Theoretical strains for shear forming a spherical part of radius 95mm	136
Figure 4.29 Ideal constant thickness and shear forming strains for the experimental shape.	137
Figure 4.30 Experimental thickness strain compared with theoretical process strains	138
Figure 4.31 Predicted forces from FEA compared with experimental forces.	139
Figure 4.32 Force Components in Surface Normal Coordinate System	141
Figure 4.33 Prediction of deformed shape during first pass (t=1.0s)	141
Figure 4.34 Prediction of deformed shape during second pass (t=3.1s)	142
Figure 4.35 Force Vs Prescribed displacement (experimental and FE full process)	143
Figure 4.36 Predicted top surface strains from FEA compared with experimental grid circle strains.	145
Figure 4.37 Equivalent strains from finite element model.	146
Figure 4.38 Principal plastic strain tensors	147
Figure 4.39 A section of the finite element model during spinning	149
Figure 4.40 Strain Variation through Sheet Thickness at ‘(a)’ near tailstock	149
Figure 4.41 Strain Variation through Sheet Thickness at ‘(b)’(of Figure 4.39)	150

Figure 4.42 Strain Variation through Sheet Thickness at '(c)'	151
Figure 4.43 A section of the finite element model - spinning completed	152
Figure 4.44 Strain Variation through Sheet Thickness at '(d)'	152
Figure 4.45 Strain Variation through Sheet Thickness at '(e)'	153
Figure 4.46 Strain Variation through Sheet Thickness at '(f)'	153
Figure 4.47 Strain Variation through Sheet Thickness at '(g)'	154
Figure 4.48 Strain Variation through Sheet Thickness at '(h)'	154
Figure 4.49 Strains from FE simulation compared to theoretical	155
Figure 4.50 Typical hardness profile	156
Figure 4.51 Strength from hardness measurements and FE predicted	156
Figure 4.52 Mesh divided into four domains (spin020128)	158
Figure 4.53 Contact area between roller and workpiece	159
Figure 4.54 Contact area between roller and workpiece using adaptive meshing (spin 020128-4ad)	160
Figure 4.55 Offset of contact areas on roller and former	161
Figure 4.56 Workpiece contact stress contours	162
Figure 4.57 Workpiece contact stress contours	162
Figure 4.58 Contour plots of Equivalent Plastic Strain Rate	163
Figure 4.59 Plots of Equivalent Plastic Strain Rate with stress contours superimposed.	163

LIST OF TABLES

Table 2.1 Applications of static contact theory to spinning.	37
Table 2.2 Various FE Options in the Simulation of Spinning.	42
Table 3.1 Roller, Workpiece and Support Surfaces Investigated	52
Table 3.2 Area-pressure calculations	65
Table 3.3 Table Principal Radii (-all dimension in mm.)	69
Table 3.4 Variations in materials used	72
Table 4.1 Hertzian elastic contact predictions (roller touching former with no workpiece)	105
Table 4.2 Experimental Measurements of contact area	120

Glossary

Contact stiffness

This may be thought of as similar to a spring stiffness it is the force generated by a given prescribed displacement divided by the prescribed displacement. It has dimension of force divided by length.

Prescribed displacement

When two elastic solids are brought into contact with a given force the displacement, that occurs after initial point contact as the force is applied, can be measured as the reduction in distance between points in each solid that are remote from the area of contact. This change in position of the tools is termed a 'prescribed displacement'. It has dimension of length.

Shear forming

A process where compression is the primary cause of plastic deformation and which may be termed flow forming

Spinning, also termed conventional spinning

A process where the workpiece is deformed plastically through a combination of compression and tension and where change in wall thickness is not essential.

Nomenclature

<i>Symbol</i>	<i>Unit</i>	<i>Description</i>
$e_x e_y e_z$		engineering strain components
e_h		hoop strain
e_t		thickness strain
e_r		radial strain
F_z	N	axial force component
F_r	N	radial force component
F_t	N	tangential force component
R_{eq}	mm	equivalent radius in two dimensions of a doubly curved three dimensional surface
R_n	mm	normal distance from the axis of spinning
t	mm	thickness of the blank
α		angle between surface normal and spinning axis
γ		defining angle of shear deformation
$\varepsilon_x \varepsilon_y \varepsilon_z$		natural strain components
θ		half cone angle
σ_z	N/mm^2	stress in the z direction (direction of the applied pressure)
σ_r	N/mm^2	stress in the r direction (perpendicular to applied pressure)
τ	N/mm^2	shear stress

CHAPTER 1. INTRODUCTION

1.1. Background to Investigation

Currently there are few processes available for the low volume manufacture of complex three dimensional sheet metal products. There is increasing market demand for low volume manufacture of such sheet metal parts involving fast turnaround for product development purposes and for the manufacture of low volume niche goods. This market is currently served by techniques such as selective laser sintering and fused deposition for non sheet metal parts. These rapid prototyping techniques are layer-based additive processes and are not suited to the production of thin walled metal parts such as those made by deep drawing or stamping. Spinning has some capability to meet the demand for low volume manufacture but is restricted to rotationally symmetric parts. Spinning does, however, have the advantage that tool costs are relatively low.

An ideal process for the production of complex three dimensional sheet metal parts would accept a digital description of the required part geometry and without further intervention produce the required shape using flat sheet as the input material. Any such process might operate on the basis of incrementally forming the sheet to the required shape. Existing processes are effectively process chains that produce soft tools for deep drawing or pressing the required parts. These soft tools are produced using a variety of process chains usually involving casting directly or indirectly from a rapid prototype master. A prototyping process that avoids the cost of soft tools entirely would offer major economic advantages given that typical tool costs for a modest pressed part say 300 by 500mm could easily exceed €100,000.

1.2. Current Research on Incremental Stretch Forming

Matsubara[1], Jeswiet[2], Bramley[3] and Strano[4] have all demonstrated real processes which can all be termed incremental stretch forming and which go part of the way towards this ideal process. Variations within these demonstrated processes range from the use of a fixed edge clamp, through the use of a floating edge clamp with a central support, to the use of a rapid prototype model as an internal former with a floating edge clamp. It is clear from this variety of processes that the role of the internal support is not universally agreed.

Metal spinning is a long established process and is generally carried out using a former to provide internal support, and the workpiece is usually clamped centrally on the former while the periphery of the workpiece is unsupported. Therefore, the development of an understanding of the former – workpiece – roller interaction in spinning will, in the context of incremental stretch forming, enable the development of more useful processes. If the mechanisms of deformation involved in metal spinning are better understood then they can be more easily applied to complex 3D free form parts. It is in this context that the work in this research project was undertaken.

1.2.1. Spinning

Spinning is an incremental sheet forming process, which has a large variety of industrial applications. Sheet forming using metal spinning competes with deep drawing in the manufacture of rotationally symmetric parts, also spinning allows the manufacture of shapes that cannot easily be deep drawn. Conventional spinning is a rotational forming process that does not set out to change the wall thickness i.e. both the blank and the finished product have roughly the same thickness. Among the advantages that spinning has over deep drawing is the fact that the investment in tooling is minimised. Figure 1.1(a) shows a simple setup for hand spinning. The cost of a mandrel is small compared to that of a stamping tool typically consisting of a punch, blankholder and die. In situations of low production volumes this advantage is compelling. Spinning can also be used as a process to manufacture the prototypes of parts that will eventually be deep drawn or stamped.

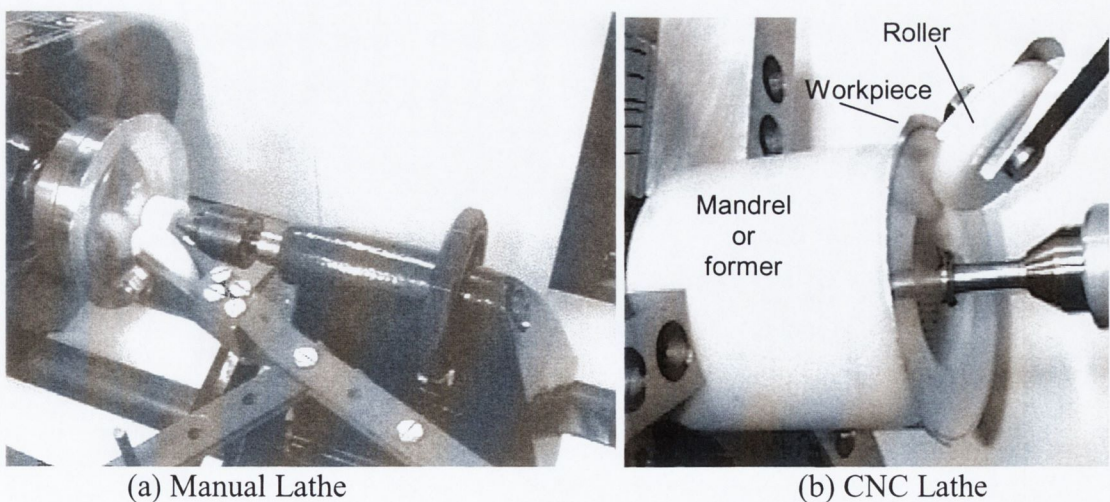


Figure 1.1 Simple setups for a spinning operation

1.2.2. Spinning as an Archetypal Incremental Forming Process

In this project, spinning is explored as an archetypal process for a variety of incremental forming processes. Spinning is very similar in nature to other incremental forming processes for sheet metal. The processes described by Matsubara [1, 5], Iseki[6] belong to the same family of sheet metal forming processes. It is shown that stretching and bending are part of the spinning process. Spinning is an ideal point to start exploring the wide range of incremental forming processes as categorised for rotational processes by von Finckenstein [7] or by Jeswiet [8] in the wider context of non-rotational incremental sheet forming processes. Spinning is assessed in terms of how close it is to a homogenous deformation process. Idealised deformation sets a minimum deformation required by part geometry and this is compared with the strains imposed by metal spinning. Applying finite element analysis to assess the amount of redundant work imposed on the material enables the planning of spinning operations to produce parts with known material properties and to optimise the material condition in critical part regions. In this way it should be possible to avoid premature failure such as might occur when a formed part is left with excessive residual stresses.

1.2.3. Analysis of Contact Loads and Stresses.

During spinning (or any incremental sheet forming process) the most active deformation occurs at or close to the contact zone between workpiece and tool. This contact imposes locally high stresses and accomplishes the required deformation. The stresses arising from contact are explored for the situation where the workpiece is unsupported in the contact region and also where it is supported by a mandrel or former. Various models of the contact between the roller and the workpiece and the mandrel are presented in chapter 3. These show the limitations of the simulation of the overall process and give a detailed insight that would be difficult to incorporate in the overall process model. Another advantage of these models is that they allow investigation of the contact with the roller, which is difficult to approach experimentally.

1.2.4. Shear forming

In this project the results in earlier literature relating to shear forming are explored with the benefit of computer simulation tools. In the literature relating to shear forming the influence of many parameters: material, blank thickness, roller nose radius, cone angle, roller feed, mandrel speed etc. are evaluated. While the effects of changing these parameters has been previously established empirically, this project sets out to analyse the spinning process in detail and thereby to establish how some of these parameters influence the outcome of a spinning process. In this project the mechanics of the spinning process were investigated by experimental testing and by the use of elasto-plastic finite element analysis (FEA). The ideal processes of constant thickness spinning and shear forming and their associated theoretical strain distributions are presented. These strain distributions form a reference for the results of both finite element simulations and practical spinning.

In this project the shape selected for analysis was dish shaped with a spherical central region and a fillet of smaller radius around the periphery of the part rather than the more typical cone shape. This choice was made in order to explore a variety of forming conditions.

1.2.5. Main Project Objectives

This investigation of spinning leads to definition of key parameters that can be extended to three-dimensional free-form sheet manufacturing processes. Finite element analysis has been used to predict the spinning process. The prediction of the forces in a spinning process was taken as a clear objective in order to develop a more efficient process in terms of tool forces and tool life. The finite element simulation was applied to predict material condition in the workpiece.

In outline the objectives were;

- (1) to use 3D finite element analysis to quantify the size of contact areas and contact stresses between workpiece and tools (roller and former) in a spinning operation
- (2) to compare roller contact in a stationary and in-process situation,
- (3) to characterise the contact zone and the force displacement characteristics of a spinning process,
- (4) to investigate the use of a roller and / or former made of low elastic modulus materials through finite element analysis and experiment.
- (5) to use experimental force measurements to validate those predicted by the finite element simulations.
- (6) to validate the 3D finite element simulation using an actual spinning process implemented on a CNC lathe,
- (7) to analyse the stresses that occur in the contact zone considering both static contact and in-process stresses.
- (8) to determine the nature of material deformation in conventional metal spinning, characterising deformation as shearing stretching compression etc. as appropriate.
- (9) to investigate the role of stresses or constraints applied by the surrounding material on the deformation zone

The predictions of plastic strains from the finite element simulations can then be compared with measured strains with some confidence leading to a new analysis of the plastic strains involved in metal spinning. This analysis will support the characterisation, and understanding of the force displacement behaviour, of a spinning process.

CHAPTER 2. A REVIEW OF SPINNING & RELATED PROCESSES

2.1. Technology

2.1.1. The historical development of spinning

Hand spinning is a process that dates back into the ancient world [9]. This source identifies bronze cladding for a chariot wheel dating from over two thousand years ago as showing definite evidence of spinning. An early example of metal spinning in Ireland dates from the first century AD [10]. Figure 2.1 shows an example of a bronze bowl dating from the first century AD. This is catalogued as the Keshcarrigan bowl after the place in Co. Leitrim, Ireland where it was found. It bears chuck marks on its base where it was held by a lathe [11]. Obviously the handle was attached after the bowl itself was formed.



Figure 2.1 Example of Metal spinning from first century AD [10]

Spinning certainly has been an established manufacturing technique for many hundreds of years. More recent history can be traced to resurgence of spinning in England in the 14th century. A spinning operation from the middle ages with a completely manually powered lathe operated by two workers is shown in Figure 2.2 [12].



Figure 2.2 Wood cut of manually powered spinning operation [12]

Spinning as an ancient technique found favour with metal workers because of the relatively low power and particularly low forces involved while offering the possibility of a surface finish that would be otherwise difficult to achieve. Hand spinning where the tool is pushed directly against the workpiece by hand or manipulated with some lever to provide mechanical advantage is long established. Traditional hand spinning relies heavily on the skill and intuition of the operator, it is a process that requires an intuitive sense of material behaviour and how best to take advantage of their properties. This is achieved by interacting with the structural transformations that are occurring as the sheet or disk blank is formed around the mandrel. Fletter [13] emphasises that ‘developing a feel for the material with all of one’s senses allows one to push the material and the spinning process to yield a perfect part effortlessly’. While this statement is perhaps a little optimistic it does point to how a direct awareness of the force required will help the process. In hand spinning the operator feels the force directly because the force is applied to the workpiece by hand either directly or with a system of levers. The sound of the process will alert one to impending wrinkling or to the part being seated on the mandrel and the smell of burning lubricant will be noticeable if the workpiece is heating excessively. In fact recent work [14] has been undertaken to study acoustic emissions during spinning operations.

Within the last century spinning has found an extremely wide range of applications. Some texts [15] from the 1960's describe metal spinning as being in the realm of the hobbyist however the German language publication on spinning with steel sheet [16] shows clearly that spinning is a process with many industrial applications. Manufacturing and metal forming textbooks, for example [17 Lange1985], describe the different types of spinning operations and their applications.

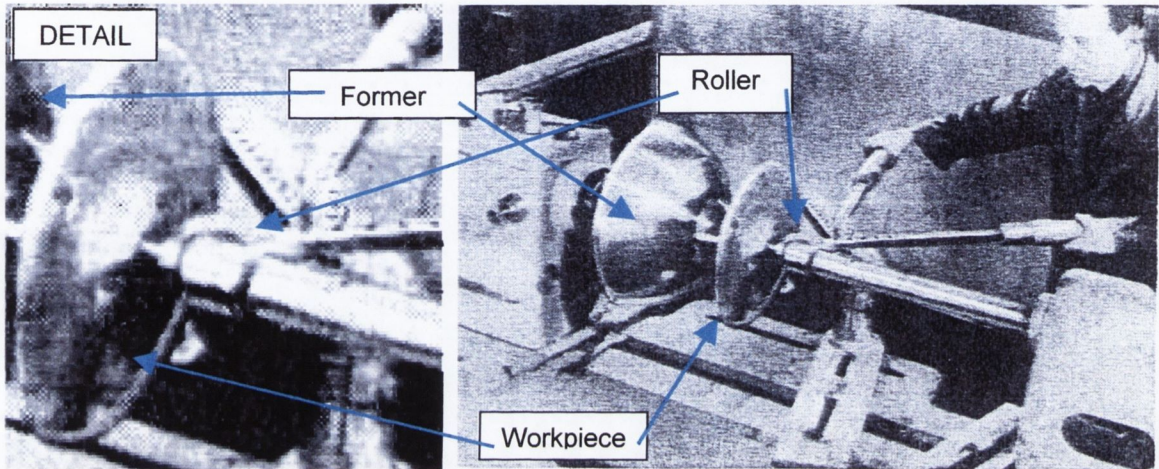


Figure 2.3 Hand Spinning, Lange 1990 [18]

In the 1950's power spinning machines came into widespread use. Prior to this hand spinning or manual spinning was the rule, where all of the force applied to the workpiece was the result of the physical effort of the operator or spinner. Figure 2.3 shows a typical hand spinning operation [18]. At this stage the distinction between spinning and shear forming had not been made. Shear forming became possible with the introduction of higher powered and automatic machines. Modern machines are usually dedicated to one or the other process. Early metal spinners would apply a series of hand tool movements based on their knowledge and experience of the behaviour of the metal. The major process limitation was muscle power. Skill in manipulating the metal by a series of tool movements was the domain of the craft of spinning. A typical tool path for a hand spinning operation is shown in Figure 2.4 [19]. It can be seen in this diagram that seven tool passes were used to form the blank to the required cylindrical shape.

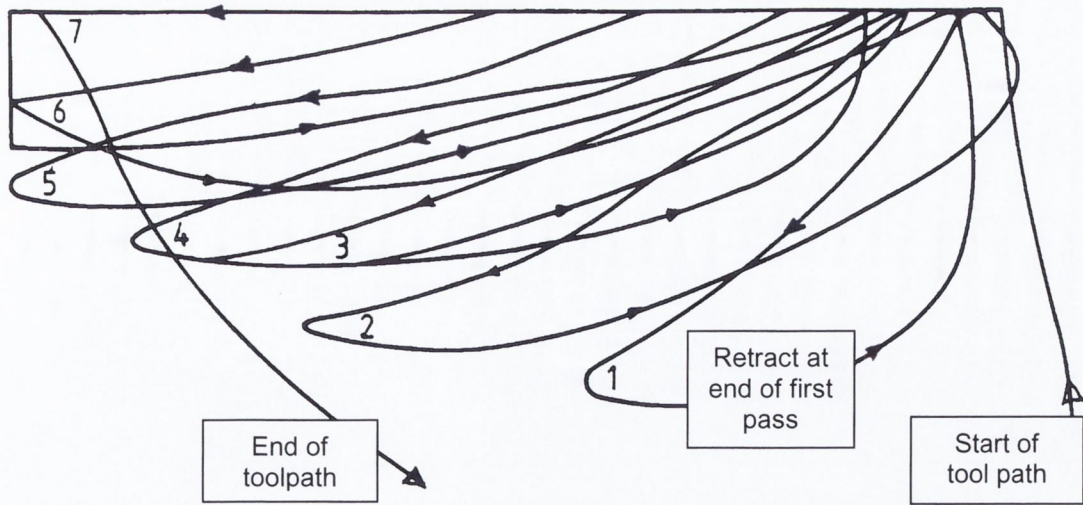


Figure 2.4 Typical path used in manual spinning comprising seven tool passes [17]

Power spinning first took the physical effort out of the process by providing joystick control of the tool movement. The first high performance machines for the mass production of spun parts worked with copying controls. These were directly dependent on a copying template and the range of movements was restricted. Due to the complexity of the spinning operation, the development of control systems in recent years has once again allowed craft skills to be applied to the process. This has resulted in the playback control system which has become industry standard in conjunction with CNC. A roller tool path generated on a playback NC machine is shown in Figure 2.5 [20] and a modern playback NC spinning lathe is also shown. Roller holders are used with integral sensors to balance out the fluctuations inherent in the process. Spinning machines can now run fully automatically with automatic part feeders.

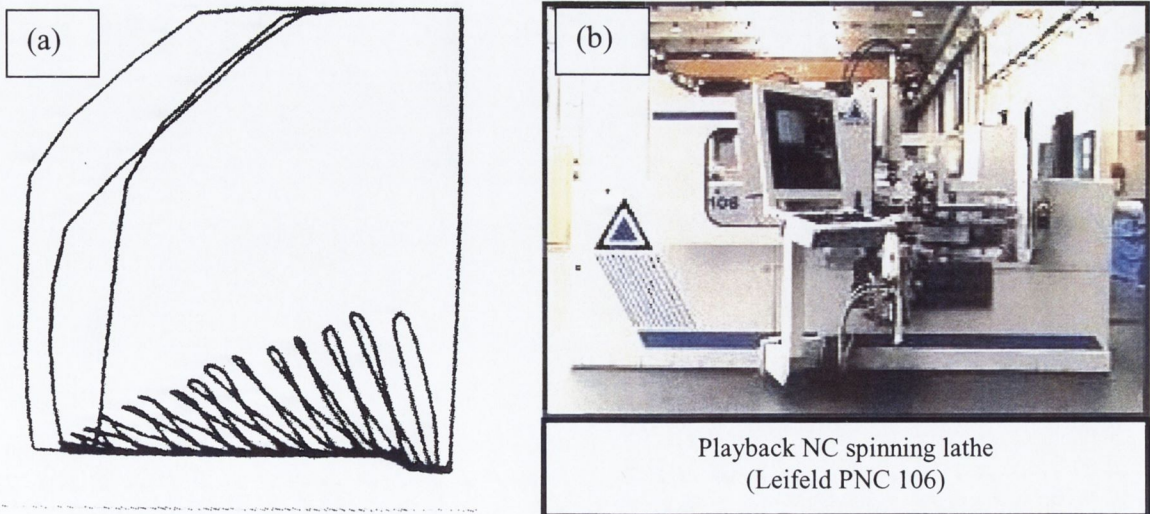


Figure 2.5 Manually generated tool path (a) recorded by a playback NC lathe (b) [20]

2.1.2. Spinning Technology -terminology

The traditional term 'spinning' encompasses, as a general concept, a group of forming processes for the production of rotationally symmetric hollow shapes. Common to all is the rotation of the workpiece, and tools (usually rollers) which are moved in carefully designed paths against the workpiece to produce a variety of shapes [20]. In **spinning**, also termed **conventional spinning**, the workpiece is deformed plastically through a combination of compression and tension. This can be distinguished from other spinning type processes where compression is the primary cause of plastic deformation and which may be termed **flow forming**. Within flow forming a further distinction can be drawn between **shear forming**, also termed spin forging or flow turning, and **cylindrical flow forming**, also termed tube spinning. Shear forming is dealt with in greater detail in section 2.1.10, page 21. Tube spinning may be characterised as either backward or forward tube spinning. Both of these processes can be used to accomplish a reduction in wall thickness or diameter much as in a conventional tube drawing process. Tube spinning has been found to be particularly suited to producing long thin walled tubes of small diameter from certain materials. [21]. In this report the term 'spinning' will be used to denote conventional spinning.

The reality is that there is a continuum of spinning type processes including certain well defined landmark processes such as constant thickness spinning and shear forming. Terms such as under-spinning, shear spinning and over-spinning have been applied and these distinctions will become apparent as the various spinning operations are described.

Since the 1960s, sheet spinning has been explored by many researchers using a variety of analytical and experimental approaches. These have largely focused on the analysis of shear forming. Shear forming is described [22] as a more desirable process because there is no difficulty due to instability in the flange of the workpiece. In the shear forming of a cone shaped product the outside diameter of the blank is exactly the diameter of the finished part. Shear forming is characteristically a single roller pass operation with a constant gap between roller and mandrel and so more readily lends itself to analysis. Shear forming can also be represented as an idealised process in which the hoop strain in the workpiece is zero.

A second idealised spinning process is referred to as constant thickness spinning. In this process the thickness of the product is the same as that of the blank and therefore the thickness strain is zero. Close approximations to both processes can be found in practice. A third idealised process in which there is no radial strain can also be considered. This requires the thickness to increase so that the hoop dimension can be reduced to form the

blank around the mandrel. This is not easily accomplished because of the tendency for buckling during the forming process, however some increase in sheet thickness can be observed at the edge of the workpiece particularly in conventional spinning operations. It can be seen that there are several different processes that fall under the title of sheet metal spinning and in fact a wide range of deformation patterns can be found within conventional spinning.

2.1.3. Examples of spinning operations

Metal spinning can take many different forms. Tube spinning can be used to manufacture precision thin walled tubes, or to achieve a closure of high-pressure gas bottles. Sheet metal spinning operations similarly vary. In one case multi-pass spinning operations may be carried out with the deliberate intention of avoiding any change in thickness. At the other extreme a part could be designed requiring a change in wall thickness, so with single pass spinning operations the blank used may well have a far larger thickness than is desired in the finished part. Such a process is termed shear forming.

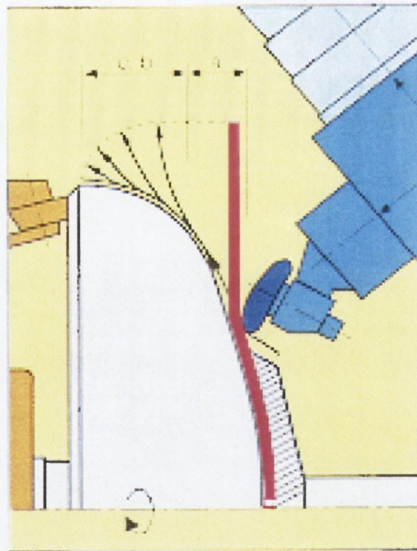


Figure 2.6 Spinning:-central area shear formed, outer area conventional spinning [20]

Conventional spinning and shear forming can be combined for some workpieces. In Figure 2.6 Runge [20] describes the forming of an elliptical tank-end that is first shear formed in the centre by a single roller pass and then spun conventionally at the outside. The central area marked 'a' in the diagram is shear formed while the outer area indicated by 'c,b' is conventionally spun by several passes of the roller.

2.1.4. Spinning Process Limitations

A metal part that is deep drawn is limited by the ductility of the material. A part that is spun is subject to far greater compressive stresses and therefore the limit of forming may in fact be due to buckling rather than tensile failure. Recent work by El Shiekh [23] investigated factors influencing the maximum achievable drawing or spinning ratio, i.e. the limiting ratio of blank diameter to cup diameter. This work suggests that a spinning ratio of 3 is achievable which contrasts with a theoretical [24] limiting deep drawing ratio of 2.7 which allows drawing ratios of slightly more than 2 to be achievable in production operations. Achievable drawing ratios can be influenced by the quality of the sheet material. A sheet metal that has appropriate anisotropy is better able to resist thinning. While many texts admit that there are no laws defined which place the process variables in a clearly defined mathematical relationship, work by Dierig [25] has resulted in the development of a thorough practical guide to spinning and the various process parameters involved.

There are other generally reported process limitations, such as the fact that it is difficult to form a cone with a cone angle of less than 15 degrees in a single pass. Similarly a very flat cone, with a cone angle of say 170 degrees, can be difficult to form [20]. Nonetheless a large variety of shapes and sizes of products can be manufactured by spinning. Figure 2.7 illustrates some examples of spun parts [26].



Figure 2.7 Selection of spun parts [26]

2.1.5. Advantages of spinning

Spinning and flow forming represent exceptions to the usual rule that a high level of investment in tooling and equipment is required for the cold working of metal parts. Compared to chip forming processes associated with machining the economy of material utilisation is very attractive. Spinning and flow forming can be applied to a great variety of hollow parts of widely differing shape and variable wall thickness. Changes in shape can be produced in any part of the component. Thus spinning is an economical process suitable not only for medium and large scale production but also for small batches and even for prototypes. Any metal that can be cold worked can be spun. Hot working is applied only in exceptional cases. As a cold working process spinning can produce the desired work hardening, and generally optimal properties can be generated by this cold working.

Spinning is frequently used for the manufacture of rotationally symmetric shapes where press tooling might not be justified or practical on the grounds of component size or production volumes. Spinning also provides the possibility of producing parts that cannot be formed by deep drawing. In this report, spinning is taken as a rotational forming process that does not set out to change the wall thickness. Both the blank and the finished product have roughly the same thickness. The term **constant thickness spinning** may be applied to such a process. The objective of changing the shape of the blank to a new desired product shape without a significant change in wall thickness is common to both spinning and deep drawing.

2.1.6. Disadvantages and Limitations of Spinning Process and Process Understanding

The above description of spinning processes very much emphasises the compressive nature of shear forming but others report that shear forming can be achieved without the use of a mandrel and as such would appear to be a stretch forming process. This anomaly will be explored in the course of this investigation. It may be then possible to address the generally reported process limitations such as those associated with very flat and very deep cones.

Spinning process is limited to rotationally symmetric products. Through a better understanding of the spinning process it is hoped to enhance its use to a greater variety of product forms.

2.1.7. Spinning; the practical requirements.

The following is a list of the most basic requirements for a spinning process and Figure 2.8 illustrates the concepts. The spinning lathe is normally equipped with:-

- 1 A former, spindle or shaped tool that will help determine the shape of the finished workpiece, shown cutaway in Figure 2.8.
- 2 A tool, usually a roller, which is in most cases a toroidal shape but may have a different leading and trailing radii
- 3 The workpiece, a blank or preform that is to be worked, shown cutaway in figure 2.8.
- 4 A tailstock, used to clamp the workpiece against the former (if the workpiece has a central hole it can be attached directly to the former without the use of a tailstock).
- 5 The process requires some means of centering the workpiece as it is being clamped
- 6 A tool path comprising a number of roller passes along the workpiece which gradually bring it to the required shape
- 7 A trimming operation is often carried out with a cutting tool to eliminate any eccentricity of the workpiece which may have arisen from poor centering or uneven metal flow during spinning due to anisotropy of the raw material.
- 8 Depending on the nature of the spinning operation a backing disk or roller is sometimes used to steady the un-worked area of the disk blank. This helps to avoid buckling of the flange.

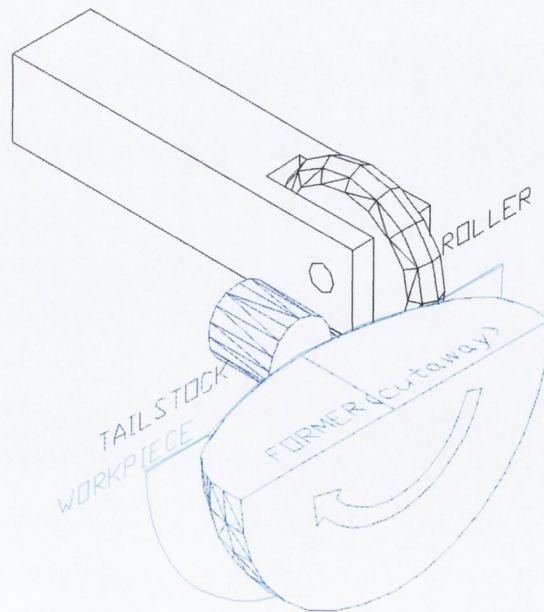


Figure 2.8 The basic requirements for a spinning operation

2.1.8. Spinning - Conventional Spinning

Spinning (conventional spinning) is a process in which the objective is to maintain an unchanged wall thickness from blank to finished work piece. The radial position of each element changes significantly while the wall thickness remains largely unaltered.

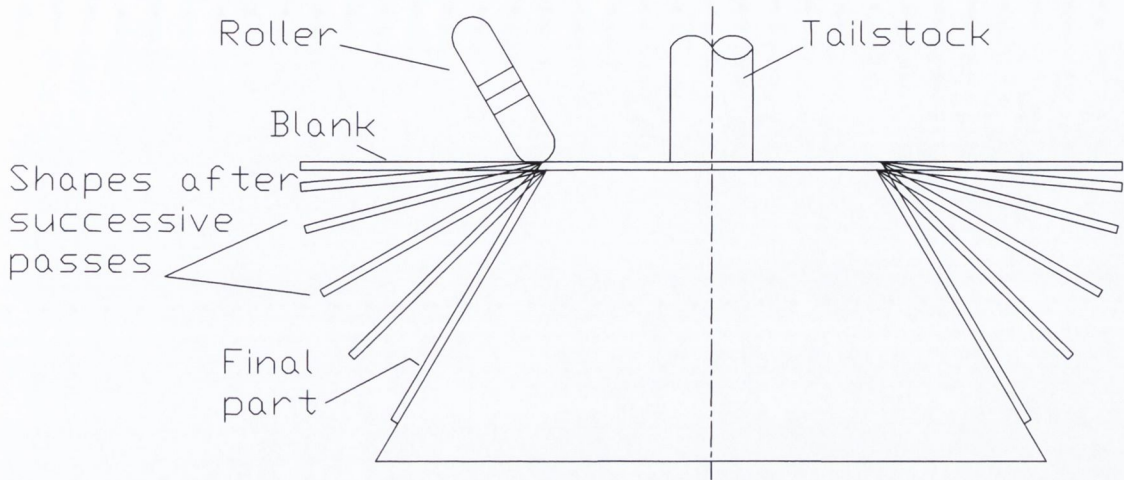


Figure 2.9 Successive Spinning Passes –Idealised constant thickness spinning

Conventional spinning is by its very nature a multi-pass operation. The strains required are larger than what can be compatibly achieved in a single pass. The desired deformation or strains on the inner part near the tailstock would produce buckling in the outer part (flange) before the pass was finished if they were attempted in a single pass. Correspondingly the process could simultaneously fail by the roller producing an undesired thickness reduction or necking in the sheet. It would then no longer approach a constant thickness process.

The nature of multi-pass spinning is evident from the diagram given in Figure 2.9. Consider the flange after each pass, there is a reduction in the outside diameter implying circumferential or hoop compressive strains and simultaneously there is an increase in the radial distance measured along the part from the edge to the un-deformed central area consequently there are tensile strains in this direction. It is assumed that the sheet thickness remains constant.

While this is an idealised version of conventional spinning other authors have presented diagrams of the intermediate stages where the intermediate form of the flange is not simply conical but is concave and so being doubly curved is more resistant to buckling during spinning. This is shown in Figure 2.10 from Lange 1990 [18]

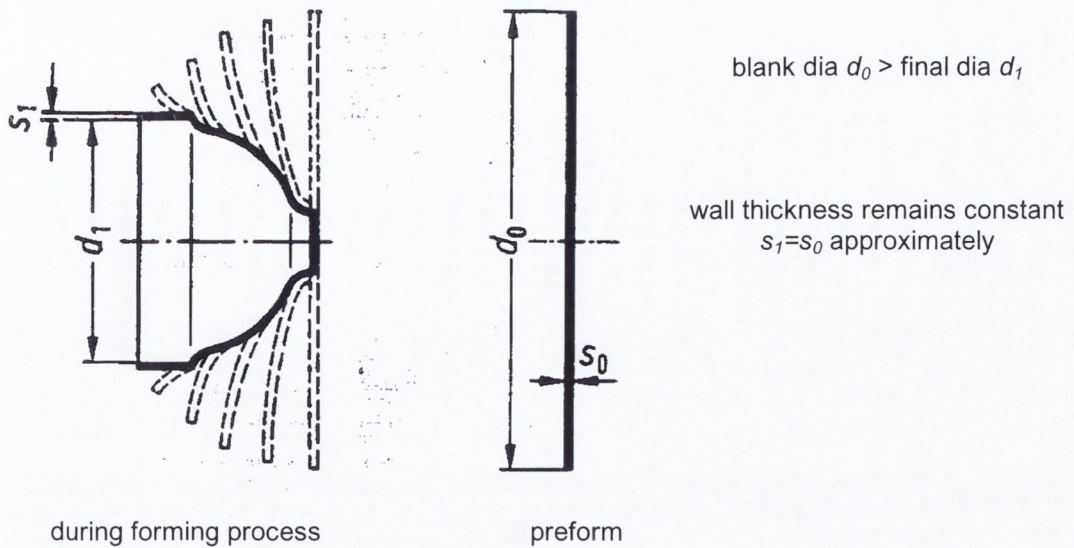


Figure 2.10 Successive spinning passes [18]

The fact that the form of the intermediate shape is not simply conical means that the strains imposed on the workpiece include some additional bending and radial strains, which contribute to achieving the final compressive hoop strains required to give the part its form.

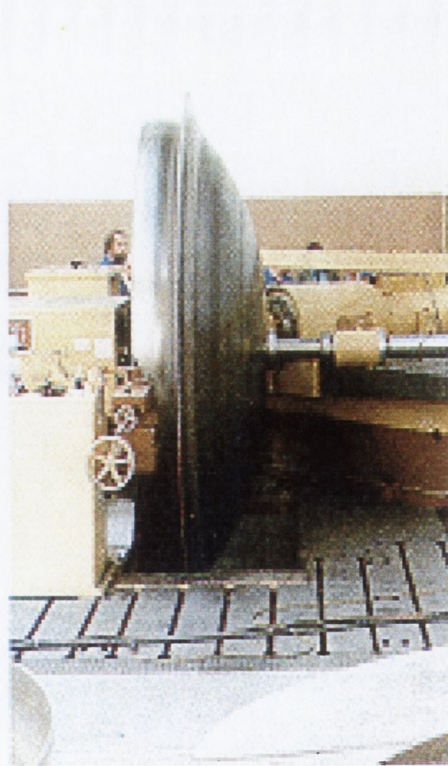


Figure 2.11 Conventional spinning of a large workpiece [20]

This process can be applied to large and small workpieces. Figure 2.9 may well be a typical shape for a small saucepan, but Figure 2.11 shows a part being worked that is over 3 meters in diameter. This large workpiece is being formed around a mandrel of the desired shape. (The face of a man can just be seen to the left of the former).

Rationale for Multi-pass spinning; it can be observed that there are a number of distinct stages in the production of a part using multi pass spinning.

At first when the roller comes into contact with the spinning disc or blank the disc is bent elastically as a cantilever. This is the approach stage of the first pass and is illustrated in Figure 2.12. (The roller was brought into contact with a non-rotating blank for the purposes of this figure and the roller can be seen contacting the blank at the lower left hand corner of the picture).



Figure 2.12 Initial elastic deformation

The next stage creates the initial doming of the blank. It can be considered that the bending, as in Figure 2.12, has reached the plastic limit and so a permanent deflection of the blank from its original flat state is achieved as it is rotated under the action of the roller. On the area of the blank between the roller and the tailstock the deformation mechanism is by bending, as shown in Figure 2.12, leading to plastic deformations. An analysis of this deformation was proposed by Qiang [27] in order to provide a theoretical basis for the forces involved in spinning.

At the region close to the roller, plastic deformation occurs in a localised area. Figure 2.13 shows this mechanism, it involves stretching near the 'point' of contact and bending also as the workpiece conforms locally to the curvature of the roller, at least in the contact zone. Although this cross section shows the roller deflecting the workpiece into contact with the former, a deformation of this nature may take place during several roller passes before the workpiece contacts the former.

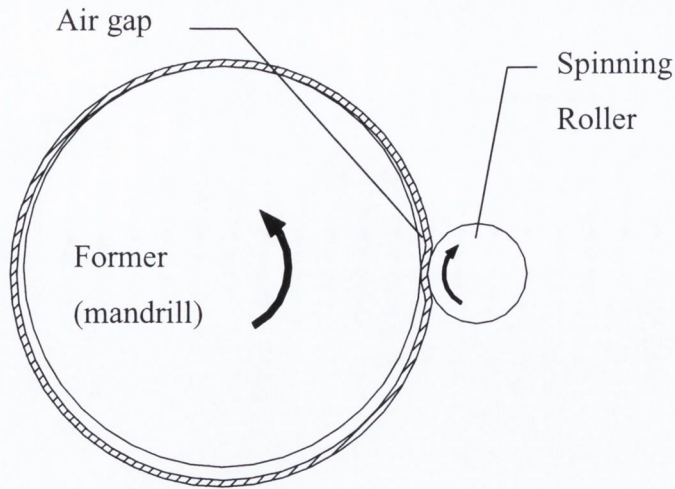


Figure 2.13 Deformation in spinning after [17]

After the workpiece has achieved some depth, it becomes much stiffer due to geometry changes and strain hardening and can react much larger roller forces, even while it is not yet in contact with the mandrel or former during most of the roller pass. Once it is no longer flat it has far greater stiffness to resist the deflection mode illustrated in Figure 2.12. Controlled deforming of the dome can now take place by a series of successive roller passes.

While this gives some insight into what happens during the spinning process it is still very much a three dimensional problem. The work piece is being held by the tailstock and ultimately working forces have to be carried through this clamped area until the situation of Figure 2.13 arises when the workpiece is touching the former and transmitting roller forces more directly to the former. Once this situation occurs, the force on the roller, and therefore on the workpiece, is very sensitive to roller position. If the roller is moved to try to create an interference with the workpiece the force will increase rapidly. In the case of a manual spinning process the operator is intuitively conscious of this. In the case of spinning with automated equipment the position of the roller must be carefully controlled. If the automated equipment is hydraulically actuated there is some possibility of limiting the force by limiting the hydraulic pressure.

2.1.9. Strain predictions for Conventional Spinning

A knowledge of the strains involved in the manufacture of any particular part is useful in predicting how much work hardening is caused and therefore the strength of the material in the finished piece. Identifying the regions of high strain can also help to identify difficult to form regions for any particular part. A knowledge of the strains allows the possibility of calculating the total energy input required to form the workpiece and consequently the forces required. This section presents an analysis by the author of the deformation required for conventional spinning based on volume constancy and part shape.

If the conventional spinning process is taken as a constant thickness process i.e. with no change in thickness from the blank to the final part, then by calculating the volume of the part the size of the required blank can be calculated. This volume constancy can reasonably be applied to all plastic deformation processes [24]. It follows that the blank's outer diameter D_{blank} is given by

$$D_{blank} = \sqrt{\frac{Vol_{part}}{(\frac{\pi}{4})t}} \quad \text{equation 2.1}$$

The change in outer diameter from blank to part is then known and the hoop strain can be calculated as

$$\epsilon_{hoop} = \ln\left(\frac{D_{part}}{D_{blank}}\right) \quad \text{equation 2.2}$$

and because thickness is constant there must be a reciprocal radial dimensional change or strain in a direction perpendicular to hoop and thickness directions. This direction lies in the sheet parallel to its surface, or more correctly perpendicular to its local surface normal and perpendicular to the hoop or circumference direction. This approach can be applied to any part or any portion of a part and so strains can be calculated for any given position, for any given part geometry.

If the conventional spinning process is assumed to be a true constant thickness process it is possible to calculate the strains that are imposed during the forming of any particular shaped part. This has been done by this author for the experimental part used [28] and is now outlined briefly. The part was formed on a mandrel with outer diameter 100mm and with central section consisting of a spherical surface of radius 95mm and a blend radius between the cylindrical and the spherical areas of 17mm. It is a similar shape to that used

in an investigation of working forces in conventional spinning by Qiang [27]. In order to calculate the strains for constant thickness spinning it is necessary to consider the volume of the blank and that portion of the part that it forms.

Thus to evaluate the strains involved consider any arbitrary portion of the blank of radius r then V_b the volume of this portion of the blank is given by

$$V_b = \pi r^2 t \quad \text{equation 2.3}$$

where t is the thickness of the blank.

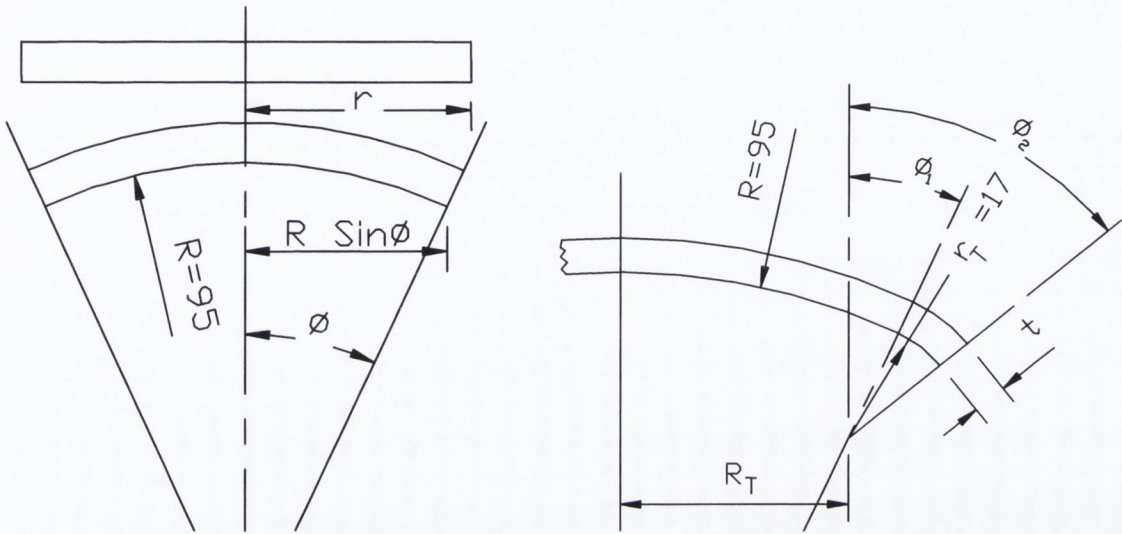


Figure 2.14 Conventional spinning (constant thickness forming)

Next consider the portion of the final shape that is formed by this volume of metal. Its volume V_f is given by

$$V_f = (2/3)\pi [(R+t)^3 - R^3] \cdot (1 - \cos\phi) \quad \text{equation 2.4}$$

where ϕ is the cone angle and R is the radius of the spherical part of the required shape i.e. 95mm. Since the volume of this arbitrary part is known from equation 2.4 above by equating these volumes V_b and V_f an equation can be solved for ϕ . The radius at the perimeter of this portion of the worked piece can be calculated as $R \sin\phi$

The circumferential or hoop strain can now be considered. The original circumference is $2\pi r$, the new circumference is $2\pi R \sin\phi$ so the hoop strain is

$$e_h = (2\pi R \sin\phi - 2\pi r) / 2\pi r$$

$$e_h = (R \sin\phi - r) / r \quad \text{equation 2.5}$$

This is valid only for the spherical part of the worked shape, however the strain for the part of the worked shape with radius 17mm between the spherical and cylindrical sections can be evaluated in a similar way by considering the geometry involved. This part is toroidal in shape where R_T and r_T are the determining radii. For the chosen part these have values

of $(95-17)\text{Sin}\Phi_1$ and 17 respectively, where Φ_1 is the limiting angle for the spherical portion of the part. The volume of the section of the torus between Φ_1 and Φ_2 as shown in Figure 2.14 is

$$V_{\text{torus}(\Phi_2 - \Phi_1)} = \pi R_T (r_T)^2 \cdot (\Phi_2 - \Phi_1) + [2\pi (r_T)^3 / 3] (\text{Cos } \Phi_1 - \text{Cos } \Phi_2) \quad \text{equation 2.6}$$

the radial distance from the spinning axis is now $R_s \text{Sin}\Phi_1 + r_T \text{Sin}\Phi_2$ and again the radial strain can be calculated.

Figure 2.15 illustrates the contrast between conventional spinning and shear forming which is described in 2.1.10

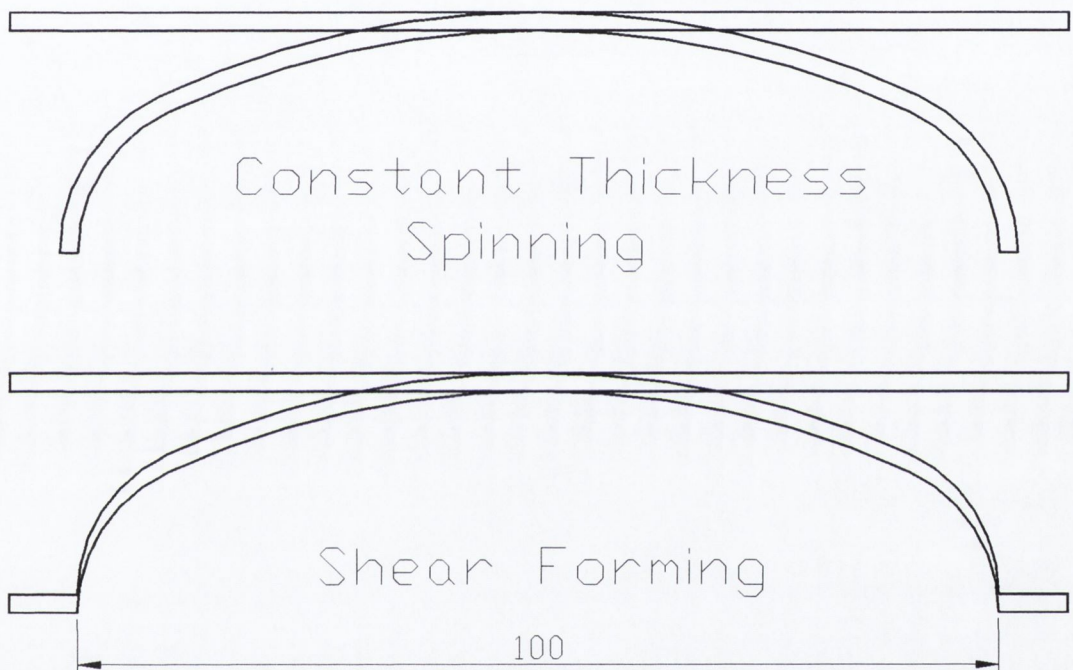


Figure 2.15 Conventional spinning compared to shear forming

2.1.10. Shear forming

Shear forming is a process similar to conventional spinning but with certain distinguishing characteristics. Unlike a conventional spinning process it involves a substantial change in sheet thickness. In shear forming the radial position of an element does not change, i.e. the normal distance from the axis of spinning is constant. In spite of this strain in a radial direction lying in the tangent plane can be large. It can be considered as the reciprocal of the thickness reduction. The thickness reduction is evident in Figure 2.14. In practice the

sharp corner shown in this figure does not occur because of the radius of the roller. With shear forming it is impossible to produce a cylindrical part from a flat blank as this would imply that the wall thickness was reduced to zero.

Shear forming (spin forging) is a process where the hoop strain is zero. With shear forming, as it is termed by Packham [29], or spin forging, as it is termed by Kobayashi [30] and Nagarajan [31], the radial position (distance from the axis of rotation) of any element is unaltered.

The following analysis of strains involved in shear forming is again taken from an analysis by this author [28] which compares the strains in pure shear forming with those involved in conventional spinning. It is based on a particular simple workpiece shape. The shape in question provides a variety of forming conditions. As already described the shape consisted of final diameter 100mm with central section consisting of a spherical surface of radius 95mm with a blend radius between the cylindrical and the spherical sections of 17mm. The part shape shown in Figure 2.15 reflects these dimensions.

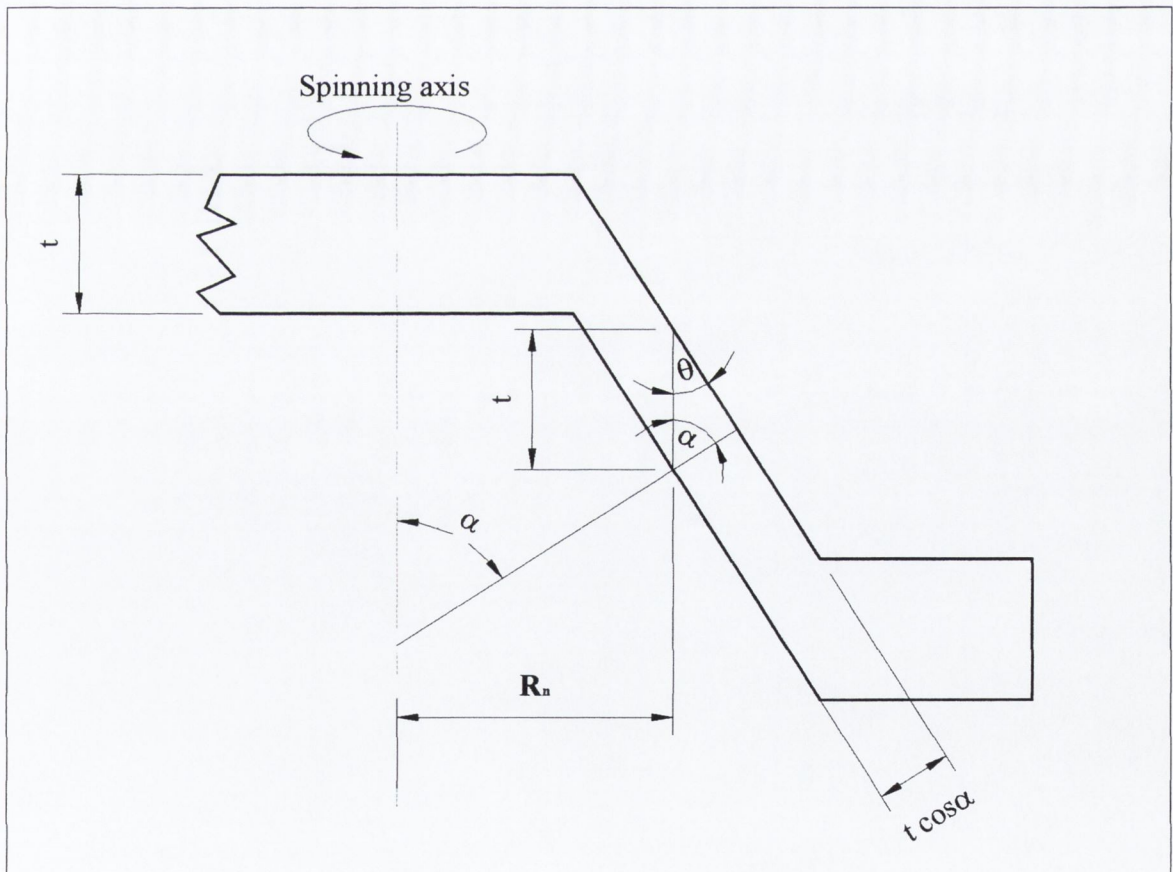


Figure 2.16 Thickness reduction in shear forming

Thickness reduction in shear forming of a cone shaped part is illustrated in Figure 2.16. The thickness reduction is commonly given as $t\sin(\theta)$ where θ is the half cone angle of the part being manufactured. Thus if the cone angle is small the part thickness is small compared to the blank. If α is the angle that the surface normal of this element makes with the spinning axis and t is the thickness of the blank then the thickness of the part after shear forming is $t\cos(\alpha)$. This is a more useful way of considering thickness reduction for a part that is not a straight cone. It is an identical statement as $(\theta + \alpha = \pi/2)$. In the case of a cone shaped part the angle is fixed, however for a spherical or other shaped part the angle varies with the position on the workpiece. When shear forming the radial position of an element remains unchanged, i.e. the normal distance R_n from the axis of spinning is unchanged.

It follows that the circumference of any circular element $2\pi R_n$ is also unchanged. If the circumference of any element is unchanged then the hoop strain e_h is zero. If volume constancy is now considered it is apparent that there must be a strain in a direction perpendicular to the thickness strain. As e_h is zero this strain must be in a radial direction so let e_r denote this strain.

The change in thickness is $t\cos\alpha - t$ which gives a negative quantity implying a thickness reduction and so the thickness strain e_t is given by

$$e_t = \frac{(t\cos\alpha - t)}{t} \\ = \cos\alpha - 1$$

when simplified.

Volume constancy tells us that

$$(1 + e_r) \cdot (1 + e_t) \cdot (1 + e_h) = 1$$

for engineering strains [Johnson and Mellor, 1973]

but since $e_h = 0$ we can write that

$$(1 + e_r) \cdot (1 + e_t) = 1$$

and substituting for e_t that

$$(1 + e_r) \cdot (1 + (\cos\alpha - 1)) = 1$$

and so this can be solved for e_r

and it is found that the corresponding perpendicular strain from volume constancy is

$$e_r = \frac{1}{\cos\alpha} - 1$$

2.1.11. Shear Forming; a Comparison of Thickness Strains and Principal Strains

Of course the question must be raised as to whether these are the principal strains, and the reality is that they are not. However for small values of the cone angle theta (very deep cones) or large values of alpha these strains are quite close to the principal strains but as the cone angle changes this is not the case. The shear angle can be used to calculate the principal strains. Spencer [32] provides a clear analysis of a simple shear deformation defined by the angle gamma that is not dependent on the shear angle being small as is typically assumed in texts dealing with elastic strains.

If gamma, γ or identically alpha, α as in Figure 2.16 is the defining angle of the shear deformation then the principal strains are given by

$$e_1, e_2 = ((1/\cos \beta) \pm \tan \beta) \quad \text{equation 2.7}$$

$$\text{where} \quad \beta = \tan^{-1} ((1/2)\tan \gamma)$$

The simple consequence of this is that the thickness strain, which is rather easier to calculate, is not a principal strain and is considerably less in magnitude than the principal strain for small shear angles. A finite element analysis using very simple single element 2D model can confirm this. For a shear angle of 60 degrees, where it gives 88% of the principal strain, and for larger shear angles it is a reasonable estimate of the principal strain. This point is illustrated in Figure 2.17 and Figure 2.18.

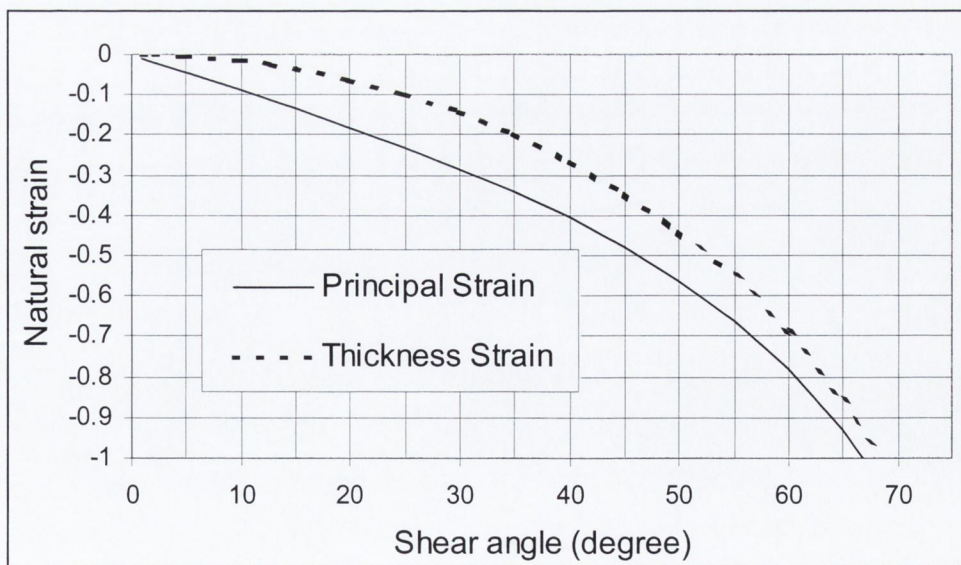


Figure 2.17 Comparison of Principal Strain with Thickness Strain in Shearforming

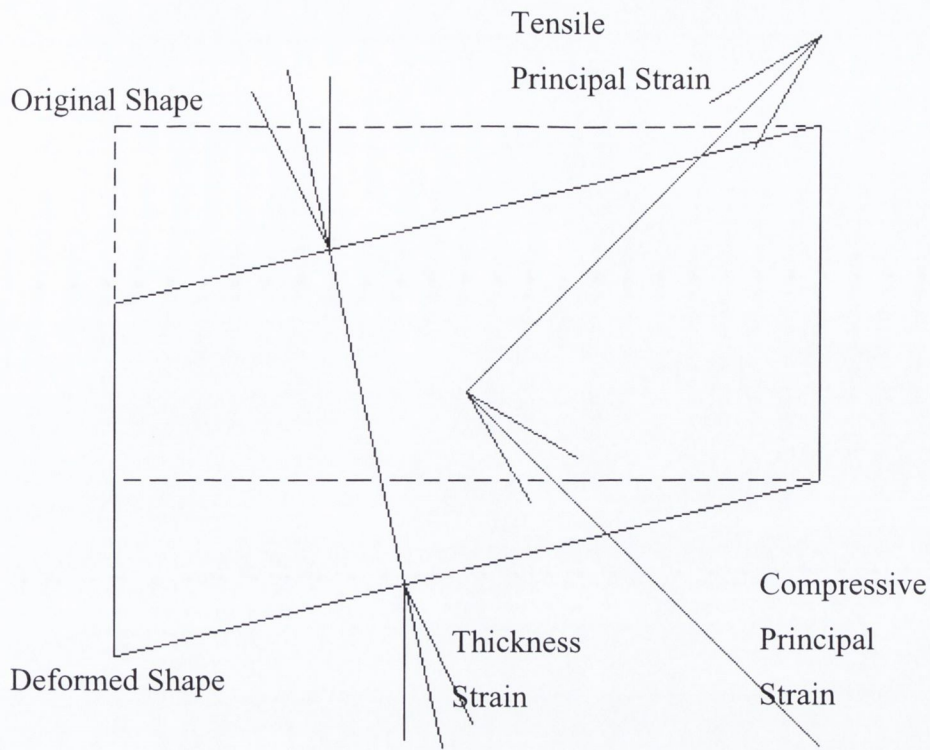


Figure 2.18 Directions of Principal Strains and Thickness Strain in Shearforming

The fact that thickness strain is not a principal strain does not invalidate the calculations of thickness strain used to determine the deformed geometry assuming volume constancy, but does indicate that it would be inappropriate to calculate equivalent plastic strain on the assumption that thickness strain and radial strain were principal strains if shear forming is assumed to be the nature of the deformation. Figure 2.19 compares the theoretical hoop, radial, and thickness strain for the part shape illustrated in Figure 2.15. Shear forming causes thickness strain and radial strain while hoop strain is zero. Constant thickness forming generates a hoop and radial strain and as the name implies the thickness strain is zero.

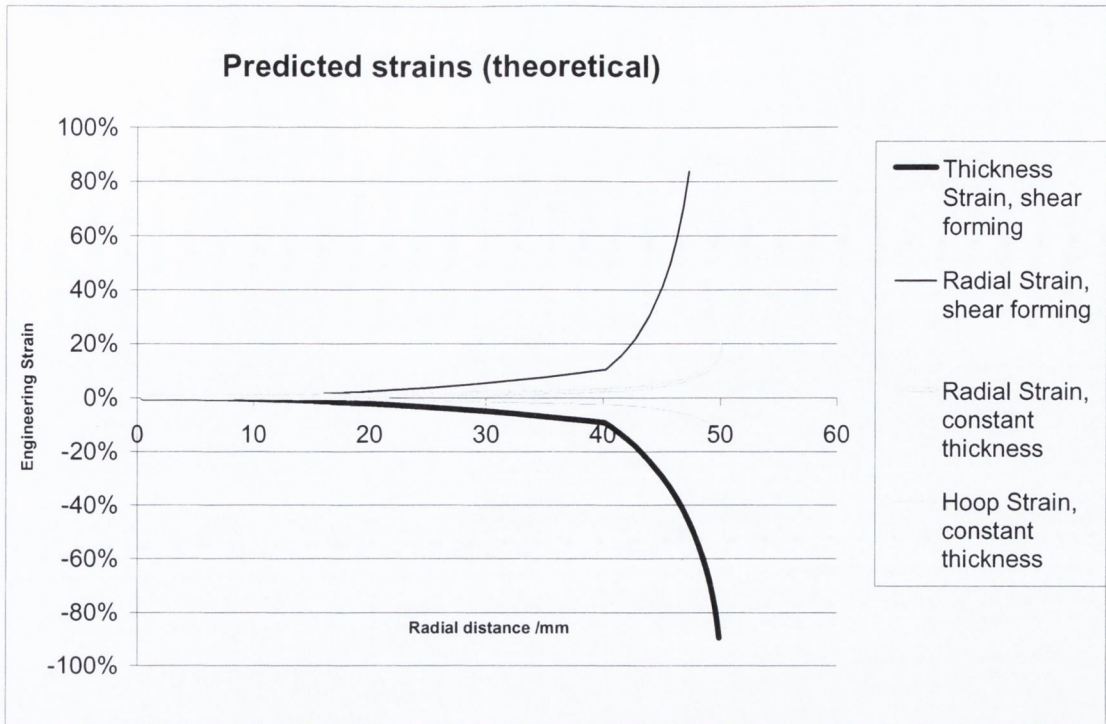


Figure 2.19 Comparison of Strains in shear forming and conventional spinning

While the calculation of shear forming strains based on Figure 2.16 was relatively straightforward and could be obtained directly from the geometrical position of the element, however Figure 2.15 and Figure 2.16 represent an idealised version of shear forming. In fact the roller has a real radius and there is no sharp corner between the formed part and the flange. Figure 2.20 from Wada and Nanba [33], shows a more realistic representation of shear forming in progress particularly of the deformation zone.

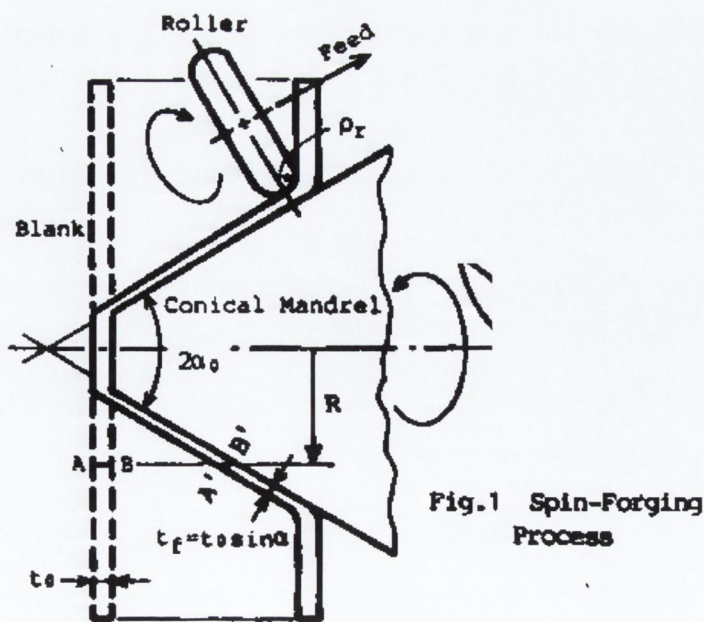


Figure 2.20 Thickness reduction in shear forming [33]

The shear forming process has been a subject of analysis by a number of authors using various methods, including upper bound and deformation energy methods. The practical interest of these analyses lay in calculating the tangential force component. Because once this force component is known it is relatively simple to calculate the power requirement for the particular spinning operation.

The results of the analyses by a number of authors found that the wall thickness was not uniform but reduced more at the beginning of the process and as some compressive stresses build up in the flange the thickness approaches that of a pure shear forming process. The results reported by Sortais [34] are typical of these and are presented in Figure 2.21.

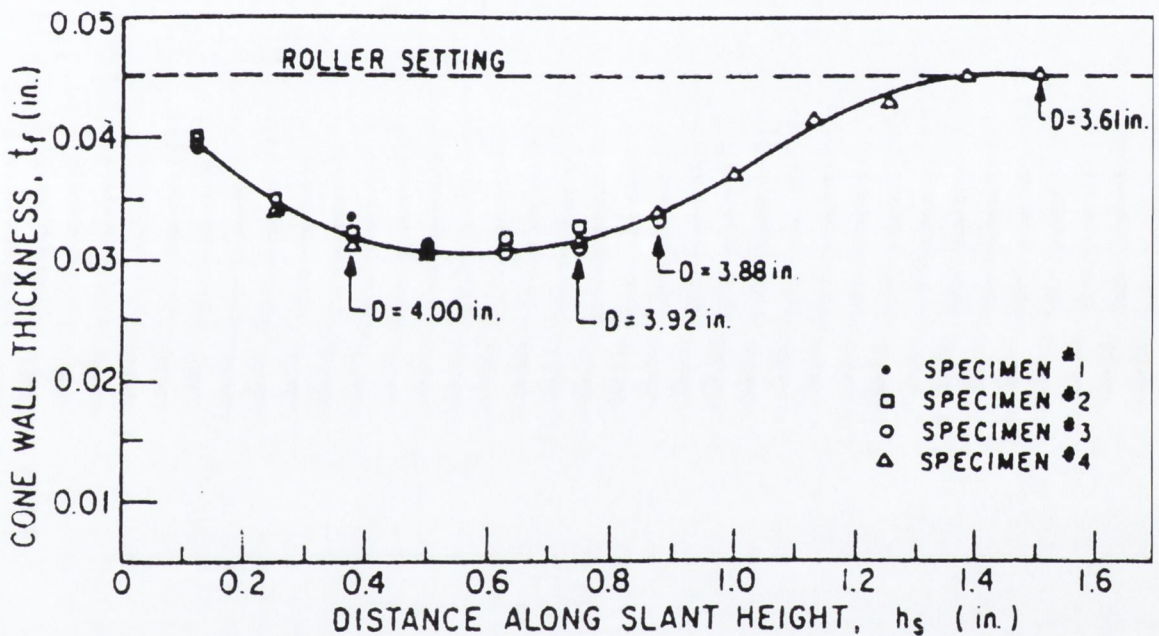


Figure 2.21 Wall thickness variation in shear forming [34]

In Figure 2.21 the 'roller setting' is the distance from the roller to the former and it is maintained constant for this operation and so 'should' allow the production of a uniform wall thickness. It quickly becomes apparent that even shear forming is not easily analysed although it involves only a single roller pass. The idealised geometry used as the basis for calculation of strains are just that, an idealised or theoretical version of a more complex reality, but nonetheless shear forming and constant thickness forming provide interesting landmarks in a wide spectrum of spinning operations.

2.1.12. Metal Spinning Compared with Machining on a Lathe.

Spinning may appear similar to conventional turning but several striking differences are apparent.

1. Spinning offers better efficiency in terms of the use of material as spinning involves no chip formation.
2. Spinning can be accomplished using multiple rollers offset around the workpiece. For example the use of three rollers offset at 120° to each other is quite typical. This has the advantage of balancing the forces on the former and thus reducing the load on the spindle bearings in the headstock of the machine.
3. Roller movement is sometimes controlled by hydraulic power rather than by the DC motors common on a conventional lathe.
4. The force system is quite different in spinning as the tangential force component is much smaller than that encountered in metal cutting. When it is considered that it is a roller that is in contact with the workpiece this is not surprising.
5. There is of course one major difference and that is the tool path, as illustrated in Figure 2.4 and Figure 2.5. Toolpaths in machining are relatively easily determined. Once a cutter has been chosen to suit a particular material then recommended feed, speed and depth of cut are usually well documented and quickly guide the definition of the toolpath. This is not the case for a metal spinning process. Each tool pass must give the workpiece a compatible intermediate shape without buckling. A curved intermediate shape offers greater resistance to buckling than a straight cone hence a curved tool path is frequently used.

2.1.13. Programming the roller path

The toolpath is critical in a conventional spinning operations because it must move the roller to deform the workpiece into a sequence of compatible shapes that incrementally allow the required product to be formed. Each intermediate shape between the initial blank and the final product must be formed without buckling or tearing the material, thus these intermediate shapes dictated by the toolpath must be compatible.

As spinning developed with the automation of machine tools of the period some investigations were done into how tool paths could be programmed. Tool path programming in multipass spinning is described by Kohne [35] and can be seen as very different from the tool path during metal cutting. In metal cutting the raw material diameter must be compared with the required finished size and the material to be removed can be divided into a number of roughing and finishing cuts. By contrast in metal spinning

each pass brings the work piece to a new partly formed shape. The strains imposed by this working must be sufficiently low so that the workpiece does not tear, buckle or crack. Each of these failure modes are discussed by Lange [17]. Material will fail in tension (tear) if the roller radius is too small or the roller force too great. Buckling will occur if too much change is attempted in one pass and cracking will occur on the flange if wrinkles are bent and unbent repeatedly during the spinning operation.

Each tool pass must impose additional deformation that cumulates to produce the final part shape required. The strains applied by any one roller pass must be compatible in all regions of the work piece. The total amount of work hardening that imposed on the metal must be considered. At any stage it may be desirable to include an annealing operation before proceeding with the next step of working of the metal. The manually generated spinning toolpaths such as those shown in Figure 2.4 and Figure 2.5 are difficult to produce as an analytical curve using an NC controller that will provide the same or similar metal working as a manual operation. One proposal uses a series of evolute curves as a roller tool path. Kawai [36]. Figure 2.22 illustrates this approach, note how different this is from the manually generated paths presented in Figure 2.4 and Figure 2.5.

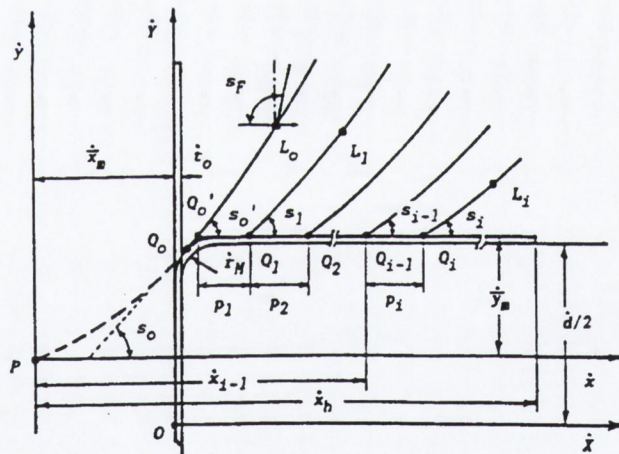


Figure 2.22 Roller Passes based on Evolute Curves [36]

In fact these tool paths are effectively segments of circular arcs with a slightly higher curvature nearer to the mandrel i.e. there is a slightly larger radius of curvature at the edge of the flange. The important feature of these paths is that they are not straight lines and so leave the intermediate shapes as doubly curved shapes as illustrated earlier in Figure 2.10 for a different part.

2.1.14. Surfaces of revolution with minimum tooling

If it is desired to produce a rotationally symmetric part with the least possible investment in tooling, spinning or flow forming must be considered. Generally spinning is done against a form tool but the work piece is only in contact with a very small part of the form tool at any one time. Figure 2.23 illustrates this point.

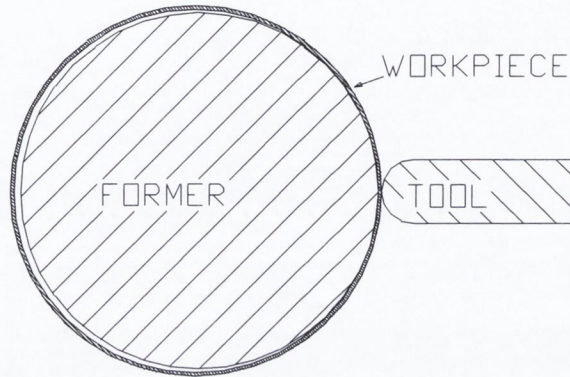


Figure 2.23 Spinning:- contact with former only occurs near the tool

The internal radius of the work piece will always be slightly larger than the radius of the former. So that pressure from the tool (roller) will bring only a certain portion of the workpiece into contact with the former. The former does not have to be made of a high strength material.

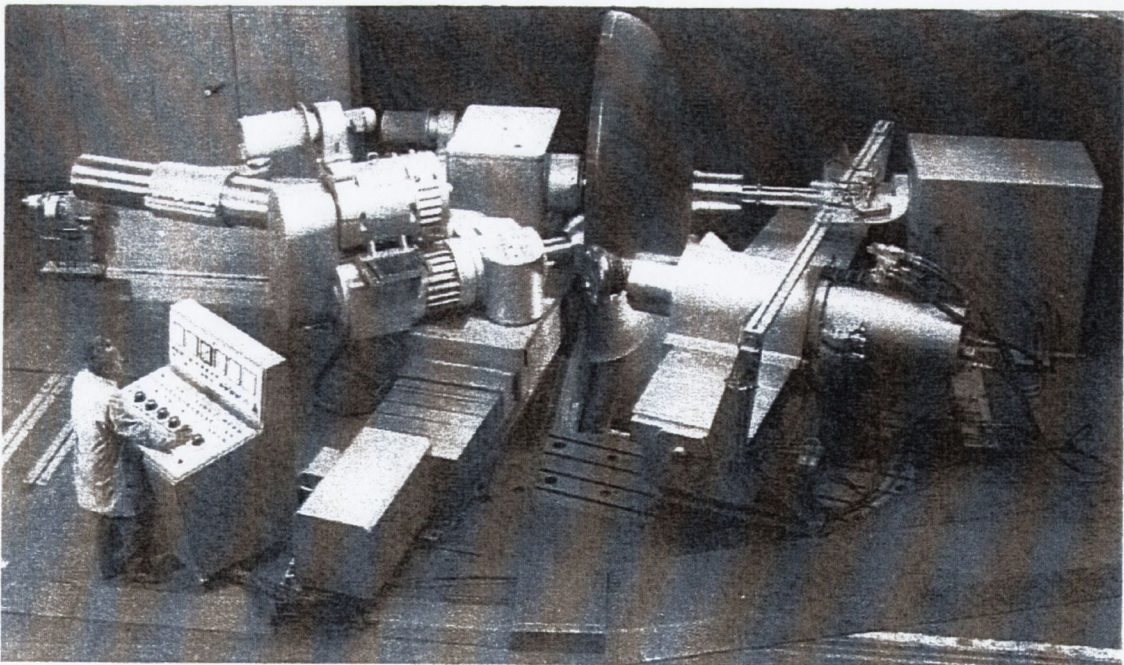


Figure 2.24 Spinning without a mandrel [7]

Lange [18] describes how spinning can be performed with a moving roller replacing the form tool. Figure 2.24] shows this implemented for a large part where obviously there

would be large cost savings in dispensing with a mandrel. This could be implemented for free form 3 dimensional sheet metal parts if the contact areas of the roller and former are well understood. Some insight into this problem is presented by the author in later chapters.

Winkelmann et al [37] describe the manufacture of flanged wheel type parts from a flat disk of sheet metal using a splitting roller and two backing rollers. In this case the deformation of the workpiece when using controlled rollers is more typical of bulk metal forming processes than sheet forming processes. So for a rotationally symmetric part spinning can offer the possibility of virtually tool-less manufacture.

In fact recent work by Kawai et al. [38] has investigated cone spinning without a mandrel. Satisfactory cone spinning has been carried out using only a straight spindle to hold the work piece. This process requires that some of the flange remains un-deformed and so the flange is itself providing the constraint. So in Figure 2.25 [38] the minimum size of flange is illustrated.

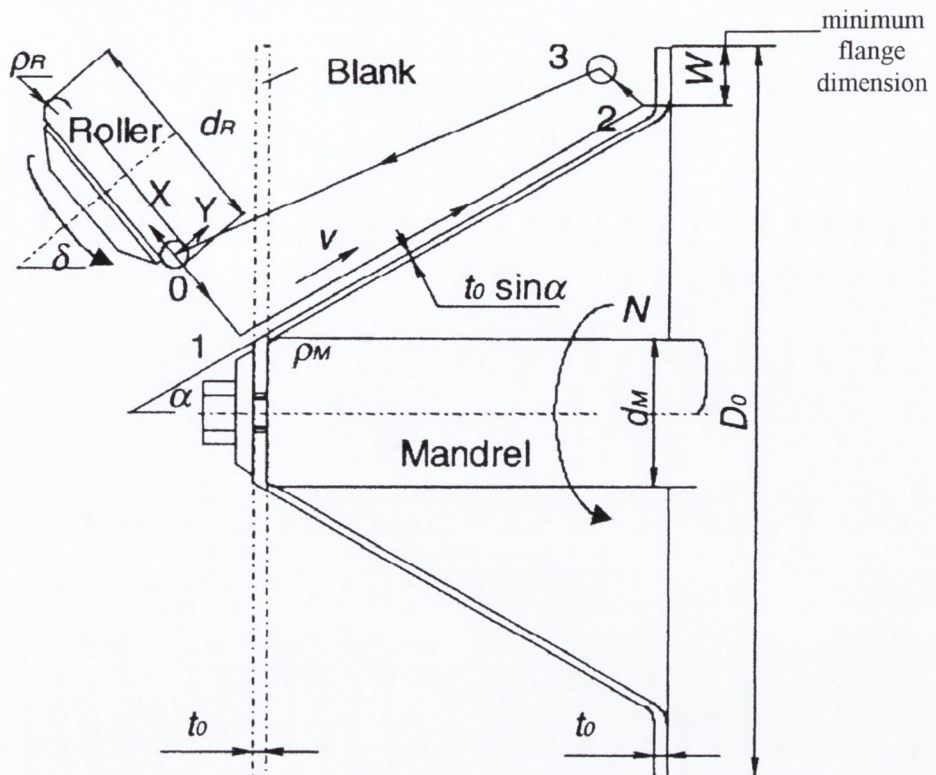


Figure 2.25 Spinning without mandrel support or internal supporting roller [38]

2.2. Spinning Deformation Mechanisms

2.2.1. Analyses of Shear forming

The contact of the roller is described for shear forming by Slater [39]. He reports that the greater mechanical working of the part does actually happen on the surface in contact with the roller. Mechanical working of the metal changes hardness from 54 on the Rockwell Hardness F scale in the unworked region to 88 on the roller contact surface and 85 on the former/mandrel side. So although there is a difference it is relatively small. Figure 2.26 shows the constant hardness contours in a section through a copper cone. It is apparent from this diagram that plastic deformation happens in material that is not directly in contact with the roller. Hardening has taken place in the material that has not directly made contact with the roller. Provided the feed per revolution is small it is evident that all the workpiece will make contact with the roller i.e. will touch the roller during the spinning process.

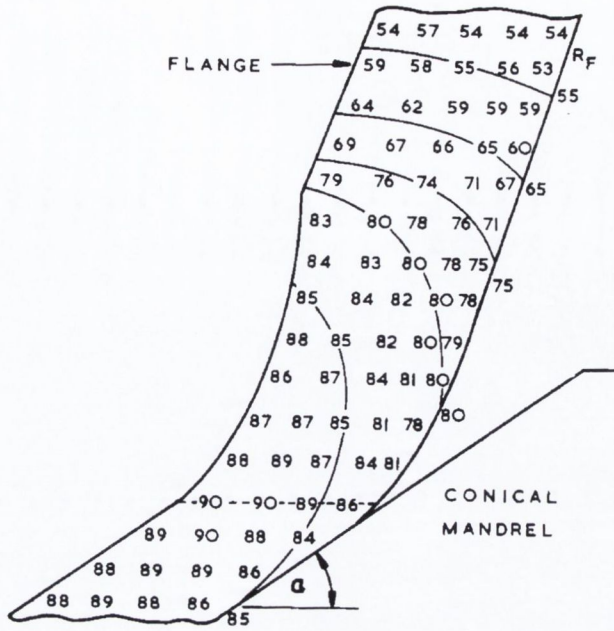


Figure 2.26 Hardness distribution in shear formed copper cone [39]

Wada [40] investigated the nature of the deformation process in shear forming and highlights the fact that it is not a simple shear deformation process that the name might imply. Rather this process is a combination of bending, stretching and pure shearing. The following figure taken from this paper shows how the material flow is studied on two perpendicular planes passing through the centre of contact. Wada's analysis relies on the feed revolution being 'very low'. By studying Figure 2.27 the problem of imposing a large feed per revolution is evident – the flange which is essentially a flat plate is required to elastically accommodate the step change in position in the deformation zone.

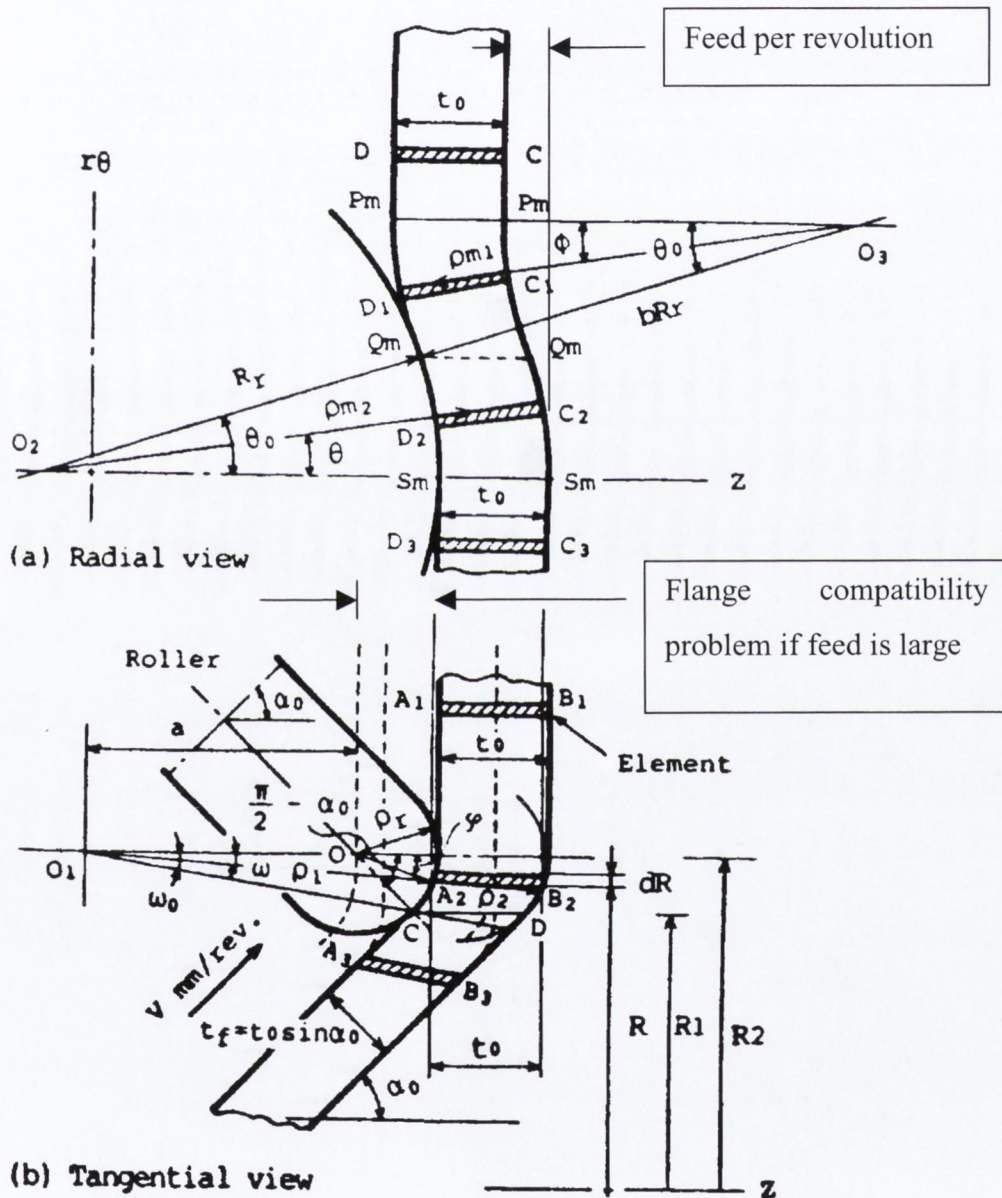


Figure 2.27 Deformation of Shear forming Wada [40]

It is worth noting that the analysis given by Wada [40] assumes that plane sections remain plane. However in the previous Figure 2.26 it can be seen that there is some difference in

deformation between the two surfaces of the workpiece and in particular the surface not in contact with the roller undergoes a different strain process, as can be seen from the variation in hardness values reported. At a simple level it would be surprising if there was simple shear strain happening at a workpiece surface where there was no tool contact and so there could be no shear stress.

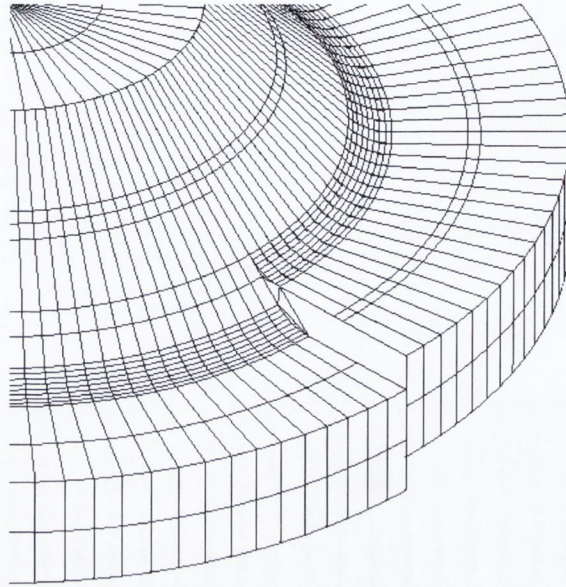


Figure 2.28 Compatibility with flange (impossible flange shape).

Even if plane sections remained plane there still is a problem of compatibility between a flat flange that is essentially undeformed and a cone that is being formed by the roller where a newly formed region has a width equal to the feed per revolution of the roller. The flange must elastically accommodate the plastic deformation imposed by the roller, as it cannot simply take up the shape illustrated in Figure 2.28.

These limitations relating to the assumption that plane sections remain plane do not invalidate the evaluation of plastic work done to provide the finished cone, and its application to the calculation of working force required to complete the shear forming process. Referring again to Figure 2.26 it can be seen that the plastic deformation zone extends into the flange and beyond the region that is directly in contact with the roller.

2.3. Classical Analysis of Contact Mechanics

Roller, Former and Workpiece Contact: Analysis of Contact Loads and Stresses.

The entire process of spinning is centered on the deformation that occurs in a relatively small area of the workpiece i.e. within and around the region of the workpiece that is in contact with the roller. Understanding what goes on in this region is key to understanding the process. This contact imposes locally high stresses and accomplishes the desired deformation.

Various finite element models that offer differing degrees of detail of the contact zone are presented later in Chapter 3. While these computer simulations enable more complex contact problems to be studied, nonetheless considerable useful understanding of the contact problem can be gained by applying classical contact analysis to the tool contact problem. The contact stresses in an actual spinning process will of course differ from those of a stationary situation that can be analysed using classical contact mechanics applied to the rolling contact of an actual spinning process. However this theory can be used to estimate the tool force line stiffness and the contact area that arises with stationary contact. These predictions can be compared to the results of spinning process finite element simulations and physical experiments. Both *stiffness* and *contact area* are important in order to develop an understanding of deformation occurring in the contact zone.

The stiffness of the contact will influence the dimensional variations that can be tolerated in the roller and former profile, as well as having implications for the rigidity of both the roller holder and the lathe or machine tool. The stiffer the contact the greater accuracy that is required of the former and roller shape.

There are two basic and distinct contact situations one where the workpiece is unsupported in the contact region and the other where support is provided by a mandrel or former.

The applicability of elastic contact theory to questions about spinning is summarized in table 2.1 and the following sections outline some of this theory.

2.3.1. Contact Mechanics an Analytical approach

While it is of interest to develop an analysis of what shape or deformation mode the flange of the workpiece may adopt in the vicinity of the roller, it is perhaps useful to look at how the workpiece and tools (roller and former) might make contact under static conditions. Admittedly the analytical solutions are for static contact and not for dynamic contact with a plastically deforming workpiece, nonetheless the analytical solution will yield some information on stresses in the roller and former and on the deflection of the former and roller surfaces.

Table 2.1 Applications of static contact theory to spinning.

	Classical Hertz Theory	Shell/plate theory (K.L. Johnson etc)	Assumed constant pressure
Contact Between ----	Elastic solid	Elastic shell or plate	Tool (roller or former)
	Elastic solid	Elastic shell/plate or rigid body	Workpiece
and -----			
Application in Spinning	Study of pressure distribution and calculation of contact area if tools are moved together without workpiece allows calculation of tool force line stiffness and stress in tools	Study of pressure distribution and calculation of contact area and elastic stress and strain if workpiece elastically conforms to the tool shape. Predictions of stiffness will be low as it does not deal with entire tool force line	Stress in workpiece can be predicted requires contact area to be known either measured or estimated from elastic theory

A simplified approach to modelling this region is to consider the force applied to the workpiece as a uniform pressure acting on a small area of a flat sheet i.e. the workpiece at the start of the process. Even with the contact stress represented as a uniform pressure some interesting characteristics can be demonstrated that can be applied to spinning.

2.3.2. Uniform pressure and other contact pressure distributions

Admittedly the choice of a uniform pressure will ultimately have limitations but the resulting stress distributions are similar for constant pressure and Hertz pressure distribution. Johnson [41] compares the effects of a Hertz contact pressure distribution of contacting bodies with that arising from a uniform distribution Figure 2.29. The Hertz contact model (developed in 1882) is useful for validating finite element models, and also

it gives some initial understanding of how the contact pressure is reacted by a solid, however it only represents an analytical solution applicable to contact between two solids. It is obvious that models of plates or shells in contact with a solid are more appropriate because the workpiece thickness is small compared to the size of the roller and former. The use of a uniform pressure model is certainly useful for a preliminary investigation of the spinning process. However significant differences are to be expected between the first contact of the roller with the flat disk and the contact of the roller with a doubly curved surface. In the case of initial contact the model by Essenburg [42] for axisymmetric contact of a paraboloid with a thin plate may be of use. In the latter case the model by Updike and Kalins [43] for the compression of a spherical shell by a rigid flat surface may also be useful. Figure 2.30 is taken this paper and illustrates the distribution of pressure for contact between a flat plate and a spherical shell. This type of pressure distribution is equally expected with a thin flat plate and a curved rigid body. Johnson [41] describes the anticipated pressure distribution stating that for thin plates in contact with a cylindrical body the pressure is a minimum in the center, rising to a maximum at the edges of the contact area.

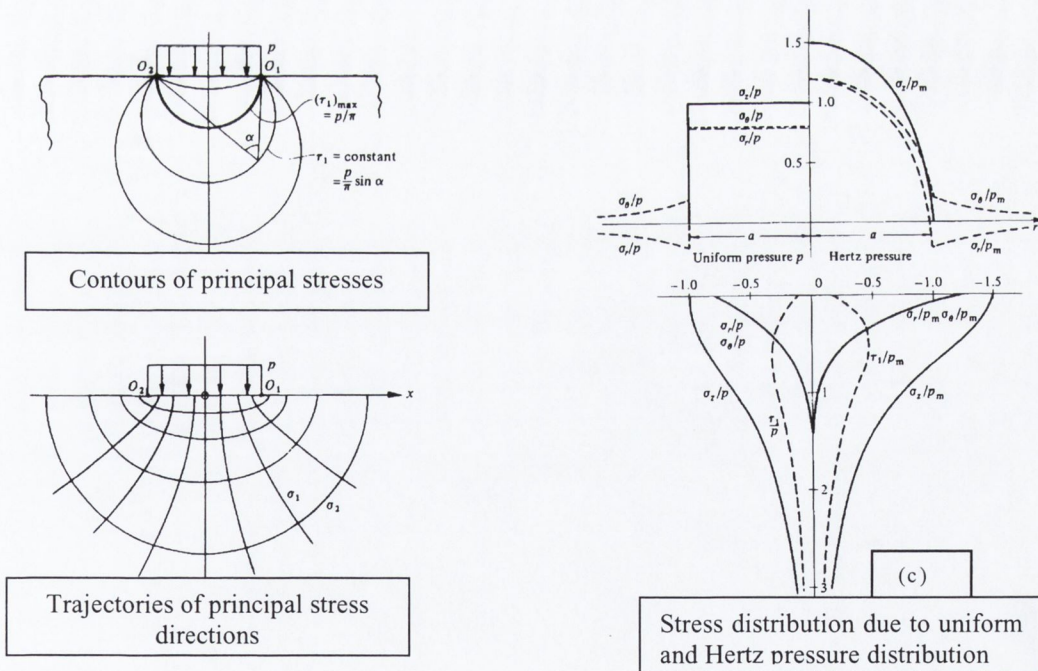


Figure 2.29 Contact pressure distribution –Johnson [41]
 (a) Contours of principal stresses (b) Trajectories of principal stress directions
 (c) Stress distribution due to uniform and Hertz pressure distribution.

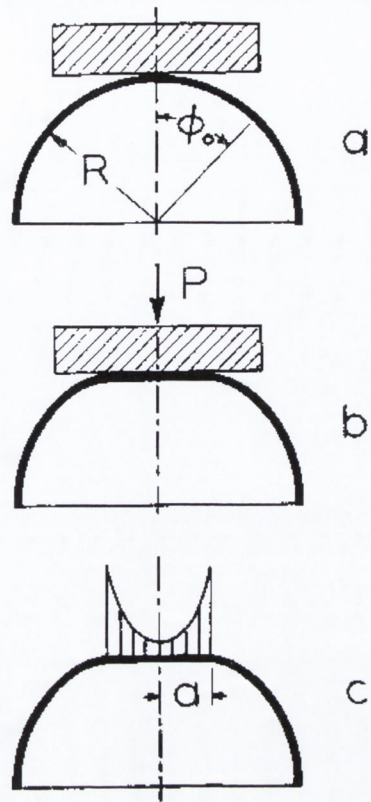


Figure 2.30 Contact pressure distribution [43]

As the thickness of the plate or spherical shell is increased the results change from that of Figure 2.30 through the range of distributions illustrated in Figure 2.31

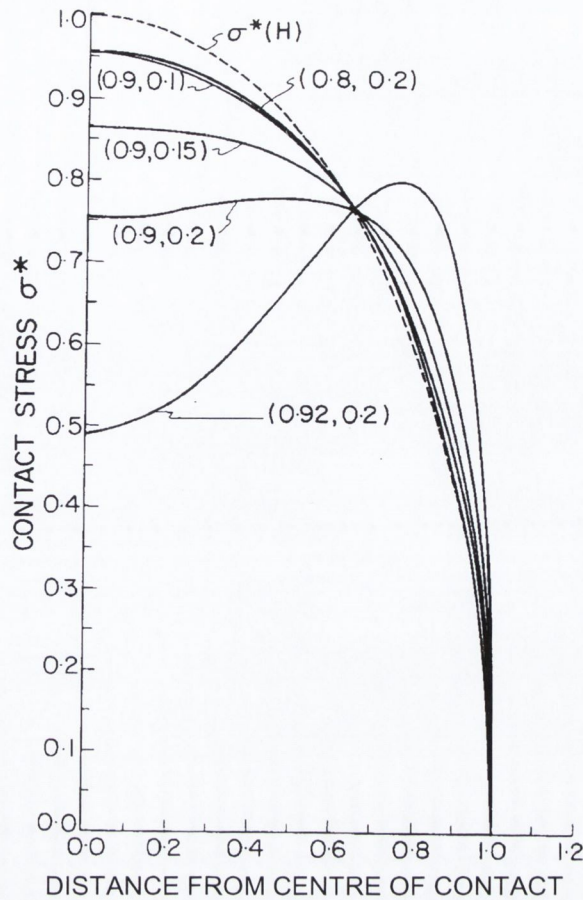


Figure 2.31 Contact pressure distribution (dimensionless contact stress) [44]

The plausibility of a spiked pressure distribution is a little questionable particularly when the workpiece is more than a simple thin shell. So a useful analysis is given by Gladwell [44] for contact between a rigid flat surface and a hollow sphere. Figure 2.31 presents the variation of normalised contact stress i.e. contact stress divided by the maximum contact stress that would occur with a pure Hertzian contact stress distribution for the same load. The horizontal axis represents the distance from the center of the contact area divided by the radius of the contact area. The two ratios that determine the nature of these curves are given in parenthesis in Figure 2.31 for each curve; these are the ratio of internal to external radius and the angle subtended by the contact area. The graphs of normalised contact stress presented Figure 2.31 can be seen to vary from a Hertzian type of pressure distribution with a central maximum, to a distribution with a maximum near the edge of the contact region which is becoming similar to that shown previously in Figure 2.30.

2.4. Elastoplastic FEA

Finite element analysis can be used to study the deformation of a workpiece and how the forces involved in spinning are producing this deformation.

2.4.1. Introduction and Summary

The finite element method is essentially a numerical method for providing an approximate solution to practical engineering problems. There are several commercial codes that can be used to simulate metal forming problems. The work undertaken for this thesis sets out to develop new insights into spinning with the aid of elasto-plastic finite element simulations. As part of this project the reliability of these simulations is validated experimentally by examination of part shape and by determining the tool forces. These simulations allow investigation of aspects of metal spinning that would otherwise be extremely difficult to undertake experimentally.

A variety of FE models have been developed in this project to investigate various aspects of metal spinning. While the ultimate objective is to produce a full 3D simulation of the entire spinning process there are several useful aspects of spinning that can be investigated using 2D analysis.

Simple changes such as changing the material of the roller or former to use a more or less compliant material can also be investigated without physically building a new set of tools for each variation or experiment. A 2D analysis of such changes is useful and effective in terms of solution times.

It will be demonstrated that changing the roller's elastic modulus can have significant benefits for the spinning process.

Bending and stretching are clearly demonstrated in the full 3D simulation. In fact it is shown that the intrinsic bending nature of the process arises because of an offset between the contact region on the roller and the contact region on the former on opposite sides of the workpiece.

Table 2.2 Various FE Options in the Simulation of Spinning.

Model	Element type	Mesh type	Forces Applied	Boundary conditions
2D	4 node full integration plane strain		uniform pressure	fixed edge and constrained onto axis of symmetry
			uniform pressures	edge nodes constrained constrained onto axis of symmetry
	4 node full integration axi-symmetric		elastic indenters (roller and former)	constrained onto axis of symmetry
			rigid former +elastic roller	fixed at centre
3D	8 node full integration	non adaptive	rigid former +elastic roller	'glued' to tailstock
		adaptive	rigid former +elastic roller	'glued' to tailstock

It is only the rapid growth in the availability of increasingly powerful low cost computers that an analysis based on an elasto-plastic finite element simulation of the spinning process can be undertaken. This is particularly true for a spinning because of the incremental nature of the process. Consequently the number of computational cycles is much greater than for other processes such as deep drawing. (The tool has to travel much further along the surface of the workpiece than with say deep drawing or stamping).

There are intrinsic difficulties associated with the simulation of spinning using finite element analysis. In order to understand the particular difficulties that metal spinning presents for finite element analysis the nature of metal spinning itself must be considered. As was mentioned above spinning is an incremental forming process in which deformation is achieved with relatively small forces. Although any model must consider the equilibrium of the entire workpiece in spinning there is only a small portion of the workpiece in contact with the roller or forming tool at any given time. Consequently the

FE mesh must be fine enough to allow some continuity of contact as the nodal forces transfer from one element to the next as the elements pass under the roller. If the mesh is too fine the solution times required become impossible, while if it is too coarse there is little hope of getting meaningful answers from the analysis.

It is particularly worthwhile to look at the contact stresses. These are central to gaining an understanding of how the forming load is applied to the workpiece and how tools of low elastic modulus materials, and even tools of low strength materials, can create the necessary stresses in the workpiece without the tools being permanently deformed.

As well as the mesh definition the division of the process into an appropriate number of time steps or increments must be considered. If the increments are set too large the model will not solve because there are too many nodes making contact with, and separating from, the roller at any given instant. In order that the analysis will provide accurate results the length of the time increment must be considered in terms of the speed of rotation of the workpiece. The time increment can be made so small that each node spends several increments approaching the roller but the cost of this will be very long solution times. These, and a variety of other issues, are key decisions that need to be addressed when building a working finite element model of the spinning process.

2.4.2. The selection of the MARC finite element code

The Marc finite element code was chosen because although it is a general purpose multi-physics code it has reasonable capabilities to simulate elasto-plastic material behaviour. It also has a direct constraint contact algorithm that is very useful in simulating the movement of the roller in contact with the workpiece. Marc has been used by other researchers in the field of incremental metal forming, such as Powell [45].

Type of Elements available in MARC: For all the models produced in this project isoparametric elements were used (4 node in 2D and 8 node in 3D). Multi-noded elements with midside nodes were avoided because of their inability to detect contact on the midside nodes even though it may be possible to better simulate bending with such higher order elements. Other options include the use of reduced integration elements for those elements located away from the area of interest. However for spinning each area of the workpiece becomes the area of interest as it passes under the roller.

2.4.3. Simulation of contact using MARC

The definition of contact is clearly critical for the effective modelling of an incremental forming process. One of the key reasons for the selecting MARC is its capability to handle contact without the need to define the specific nodes of one body that are going to touch particular elements of another body. The Marc software uses a direct constraint contact algorithm. In this procedure the motion of the bodies is tracked and when contact occurs direct constraints (both kinematic and nodal force) are applied to the motion as boundary conditions [46] A contact tolerance is used to define a zone on either side of the contact surface. This tolerance volume is checked for nodes that have entered. When nodes are detected within the contact volume they are constrained onto the contact surface and the equilibrium of the mesh is solved again. The validity of the contact forces arising from the contact constraint is then checked. If the contact force on the node is negative (there is a negative contact pressure) the node is released and the equilibrium of the mesh is solved again. This procedure may need to be repeated several times in order to give a valid solution. It follows that there is substantial computational work required to model contact. The Marc software enables this zone can be biased so that it is unevenly distributed on either side of the contact surface. This is useful in that the contact zone does not have to be very thin to avoid dragging non-contacting elements onto the surface. It enables a reasonable tolerance to be used, and avoids nodes passing through the surface. Determination of the optimum contact parameters to be used in any contact model is by no means straightforward. There is no obvious ideal value for contact tolerance contact bias, release force etc..

2.4.4. Element Selection and Mesh Definition.

Shell elements are widely used for the simulation of sheet forming processes. The area of the sheet is divided into rectangular and or triangular elements. While the shell elements in MARC have the capability of making contact on both sides of a surface or workpiece, there are certain limitations because of the fact that a single element is required to model the sheet material passing between two tool surfaces. In this case the node can only be constrained to be in contact with one of the tool surfaces and perhaps the effect of the second tool surface could be simulated as a pressure acting on the mesh. The ability of the element to model bending is also central to a successful modelling of a spinning or incremental forming process as a significant amount of bending and unbending occurs as the metal is formed by contact with the tool. Thus setting a different number of integration layers for a shell element directly affects the accuracy of the model.

Solid elements are widely used in the simulation of bulk metal forming operations, as well as for structural analysis of arbitrary shaped components. The volume of the component is divided into bricks, wedges or tetrahedrons to define the mesh. Modelling of sheet metal forming processes with solid elements facilitates the simulation of the sheet passing between two tool surfaces. However a greater number of solid elements may be required to model a given area of sheet material than when shell elements are used. A single solid element through the thickness would be expected to offer poor simulation of a pure bending load and so a minimum of two or three elements would be expected to give a more reasonable simulation. However the MARC finite element code offers an option called 'assumed strain' [46] which can be used with an eight node brick element. Normally an eight node brick does not capture the linear variation in shear strain which is present in bending when a single element is used in the bending direction. With the assumed strain option the interpolation functions are modified so that the shear strain variation can be better represented resulting in enhanced simulation of bending loads.

With the choice of either a shell or a solid element it is essential that the element has the ability to function effectively both with large strain plastic deformations and large displacements. There will be areas of the workpiece that as well as undergoing plastic strain are also displaced from their original position in the blank.

The mesh design is fundamentally constrained by the number of elements that can be used while allowing a reasonable solution time to be achieved. This is particularly true with spinning because of the incremental nature of the process. As each element passes through the contact zone the equilibrium of the entire mesh must be solved. Meshes used with the various models are described in section 3.3 for the static contact models and in section 3.5 for the spinning process models.

Adaptive meshing

Adaptive mesh refinement has been applied to a number of simulations in the course of this project but is not very effective for total process simulation because ultimately every element will require remeshing when it comes into contact with the roller. However it can be applied in order to study the process in detail at particular stages as will be demonstrated in section 4.5 page 158.

2.4.5. Material Model

The nature of incremental forming processes, such as spinning and dieless incremental stretch or bulge forming, is that a deflection rather than a load is imposed on the workpiece as CNC machine tools are position controlled. In order for the finite element simulation to

accurately predict the part shape it is essential that elastic recovery after deformation must be handled effectively. It follows that in defining the stress strain behaviour of the material it is of great importance that the slope of the elastic recovery is accurate. A rigid plastic formulation would be undesirable. Over-stiff models will under predict elastic recovery and vice versa models that under estimate elastic stiffness will over predict the elastic recovery.

Large stress strain behaviour for the workpiece material was determined by plane strain compression testing. The experimental investigation of the flow curve for the material used in the workpiece is described in Appendix 1 Flow Curves from Plane Strain Compression. More information about property determination and the specific flow curve used in the simulations is presented in the chapter 3.

Because of the repeated loading and reversal of loads and following the recommendations of the Marc user documentation [47] the kinematic hardening option was used. This is preferable to isotropic hardening in the case where plastic strain occurs in situations of load reversals. In simple terms the yield surface shifts rather than increases the diameter of the von Mises yield surface. Anisotropic material behaviour was not considered.

2.4.6. Validation of Finite Element Model

An investigation [48] was carried out by this author of the effects of mesh design on the accuracy of the predictions of the force displacement characteristics for a simple experiment. This experiment involved a simple cantilever test that produced plastic bending. The experiment chosen for this purpose is illustrated in Figure 2.32.

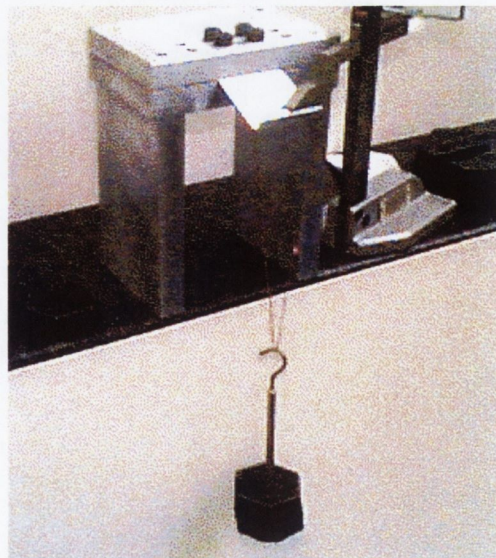


Figure 2.32 Cantilever Test Apparatus

This experiment was then modelled using a variety of different mesh options and the accuracy of the finite element models evaluated. The shape of the elements used was varied from the ideal to the marginal as illustrated in Figure 2.33.

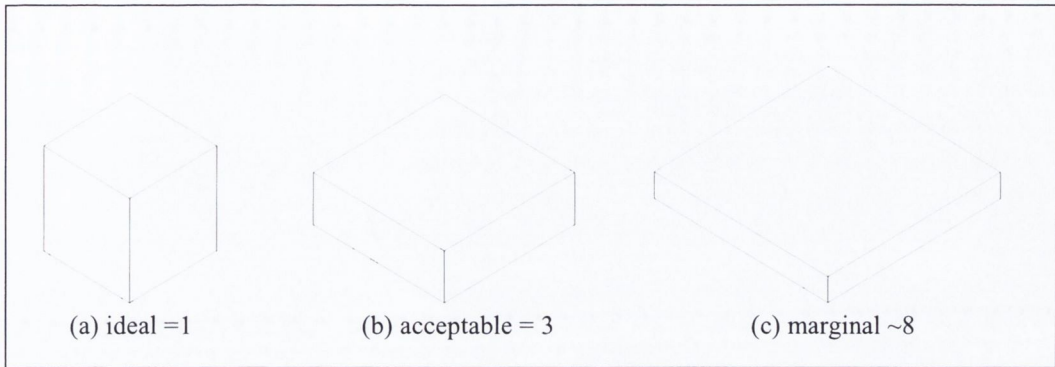


Figure 2.33 Solid element aspect ratios

The first approach to improving the accuracy of the finite element simulation might be to use elements of compromised aspect ratio in order to increase the accuracy of the prediction of stress variations through the thickness of the testpiece. This approach is illustrated in Figure 2.34

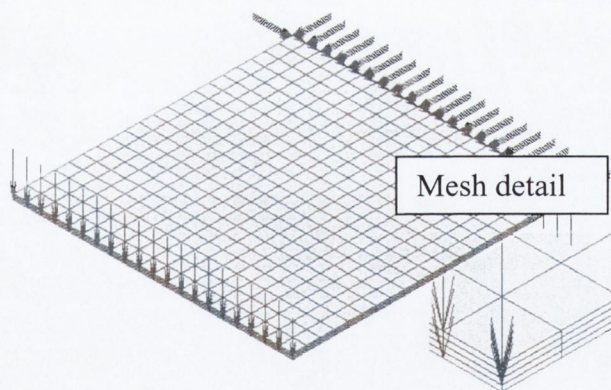


Figure 2.34 Typical Finite Element Model

However it was found by this author [48] that the accuracy of the simulation was better served by increasing the number of elements along the beam rather than by using several rather flat elements through the thickness. In fact it is reported that the error due to parasitic shear [49] with solid elements increases with the square of the aspect ratio. For example the model in Figure 2.34 has 1600 elements (20 elements long x 20 elements wide x 4 elements thick) and has the same accuracy as a model with 200 elements (20 elements

long x 20elements wide x 1 elements thick). So a better solution (more accurate for the same number of elements) was obtained by using a single element through the workpiece thickness. The use of shell elements was also explored and found to be effective provided that the mesh did not have to simulate contact on both sides of the surface. The design of the mesh for the spinning process simulations is described in chapter 3, section 3.5

CHAPTER 3. EXPERIMENTS PHYSICAL & FE MODELS

3.1. Introduction

This chapter outlines both the physical and simulation experiments carried out by the author in the course of this work. The results of these various experiments and simulations are presented and analysed in the Chapter 4. Recalling that the major objective of this project is to better understand the deformation process in spinning and the nature of the roller workpiece and workpiece former interactions, the structure of this chapter is as follows;

- 3.2 Direct Static Contact: Physical Experiments;
- 3.3 Direct Static Contact: FE Simulations
- 3.4 The Experimental Spinning Process
- 3.5 The Spinning Process: FE Simulations

To explain this approach; two distinct situations were investigated, firstly the static or direct contact of the tool with the workpiece, and secondly the condition of rolling or moving contact during the spinning process. The first experiments set some expectations for the results of the second and have some counterparts in classical closed form analytical theory. It may be expected that the stiffness of the tool force line obtained from the static experiments will also be found in the moving experiments.

It is reasonable to assume that the area of contact with the roller for static load conditions would be expected to reflect the area determined in the moving experiments. The results of the static experiments and the predictions of the static simulations can thus be validated to a greater or lesser extent by classical theory and so provide some insight and confidence in the results of the rolling / spinning experiments and the subsequent simulations.

Another attraction of the static simulation experiments is that their cost is much less than that of computer-based spinning process simulations because the solution times are very much shorter than for an actual spinning process simulation.

The static simulation experiments show the limitations associated with the simulation of the overall process. In particular the static finite element simulations provide a detailed insight that would be difficult to incorporate in the overall or spinning process simulation. The overall process models allow investigation of the contact or interaction between the workpiece, former and roller. The computer-based simulations allow a level of analysis which is impossible to achieve by physical experiment.

The shape of the contact area will be quite different with moving contact compared with stationary conditions, and does not need to be centered on the common surface normal of the roller and former as it is with stationary contact.

The static contact investigations cover two scenarios; one where there is no direct support behind the workpiece when the roller makes contact and the other where the workpiece is supported, such as by the former during an actual spinning operation. These two conditions would be expected to demonstrate a wide variation in contact stiffness. The two conditions are illustrated in figure 3.1.

Where there are two solids touching a **prescribed displacement** can be imposed to study contact stress etc. When two elastic solids are brought into contact with a given force the displacement that occurs after initial point contact as the force is applied can be measured as the reduction in distance between points in each solid that are remote from the area of contact. This change in position of the tools is termed a 'prescribed displacement'. It has dimension of length. If the applied force is divided by the prescribed displacement it gives a measure of force over distance which can be termed **contact stiffness**. This may be thought of as similar to a spring stiffness it is the force generated by a given prescribed displacement divided by the prescribed displacement. It has dimension of force divided by length.

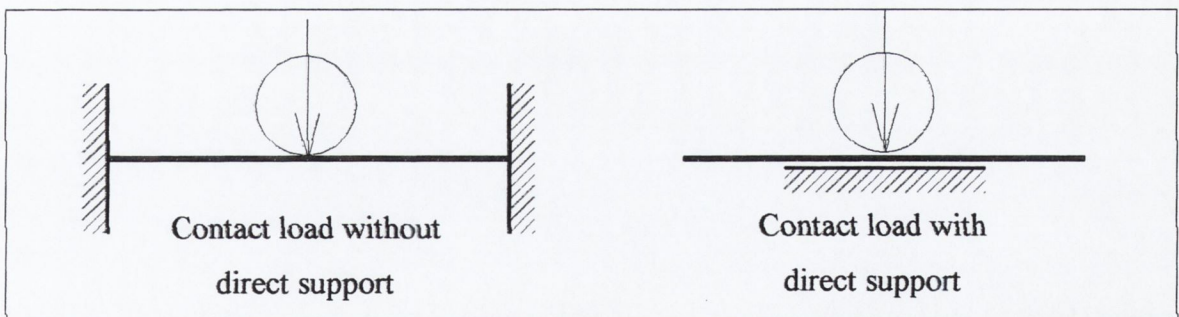


Figure 3.1 Different Static Contact Load Arrangements

These provide useful comparisons with the physical spinning process, which in part may be characterised as unsupported contact and elsewhere as directly supported contact. They also provide insight into the nature of the spinning process by providing an indication of the size of the contact area and the scale of the plastic strains that can be induced by a given contact force.

Typically the reality of the spinning process is that where the roller makes contact with the workpiece some of the workpiece is unsupported and some of the workpiece is directly supported. The material on the flange side of the contact zone is without direct support and the material on the formed side of the contact zone has support from the former or mandrel. It is known from standard stress analysis [50] that the distance to the clamped edges will influence the result of the experiment. In the finite element simulation of the unsupported direct contact the clamped edge is 9mm from the centre of the applied load. This is entirely arbitrary but gives a point where comparisons can be made as workpiece thickness is changed relative to the fixed area to which pressure is applied.

While roller contact with the workpiece is rarely either completely unsupported or simply directly supported in metal spinning, it is useful to look at the effects of both support arrangements because they represent both ends of a wide range of possible load situations.

3.2. Direct Static Contact: Physical Experiments;

3.2.1. The Purpose of Analysing Direct Contact

Simple static contact (non-spinning) experiments were conducted to obtain some indication of the size of the contact area. Experiments involved (1) two solids with no workpiece i.e. Hertzian contact, (2) two rigid solids ‘forging’ a deformable workpiece. Various representative shapes of solids and thickness of workpiece were used. The results of these investigations of the contact area were used to validate the finite element models of direct contact. It was anticipated that these experiments would also help to answer the question of whether conventional spinning is an incremental forging process or an incremental stretch forming process.

For example, if the working forces in spinning are much less than those required to produce the same thickness reduction by forging then stretch forming rather than forging must be considered to better characterise the spinning process. This may even be shown to be true for so called shear forming.

3.2.2. The Direct Static Contact Physical Experiments: Materials Used

The material used for these experiments was 0.5 and 1.0mm thick commercially pure Aluminium in the half hard condition. It was purchased as Al 99.0-Werkstoff 30205, Material condition HH, 0.2% yield 110 MPa and is an equivalent to Al 1100 H12. Large strain stress behaviour for the test material was determined by plane strain compression testing. This is described in Appendix 1.

Table 3.1 Roller, Workpiece and Support Surfaces Investigated

	Material	Young's modulus	Geometry /Size
Roller (Indenter)	Nylon OR Steel	2.8GPa 208GPa	Wheel (100Diameter 8mm Edge Radius)
Test Piece	Aluminium	69GPa	1.0mm OR 0.5mm thick
Support Surface	Nylon OR Steel	2.8GPa 208GPa	Spherical Surface 95mm Radius

3.2.3. Experimental investigation of the contact area

The contact areas were investigated experimentally using Fuji Prescale Film [51]. Using an Instron 8516 servo-hydraulic universal test machine with a 10kN load cell a 300N test load was applied. A roller (a spinning tool) was used with Aluminium sheet samples of 0.5 and 1.0mm thickness. The support surfaces used included flat and curved surfaces. The curved supporting surface used was a convex spherical surface, which was in fact the radius 95 spherical area of a spinning former. Table 3.1 outlines the various combinations that were tested. A typical experimental setup is shown in Figure 3.2 where the roller is held in the upper hydraulic jaws and a flat surface in the lower jaws.

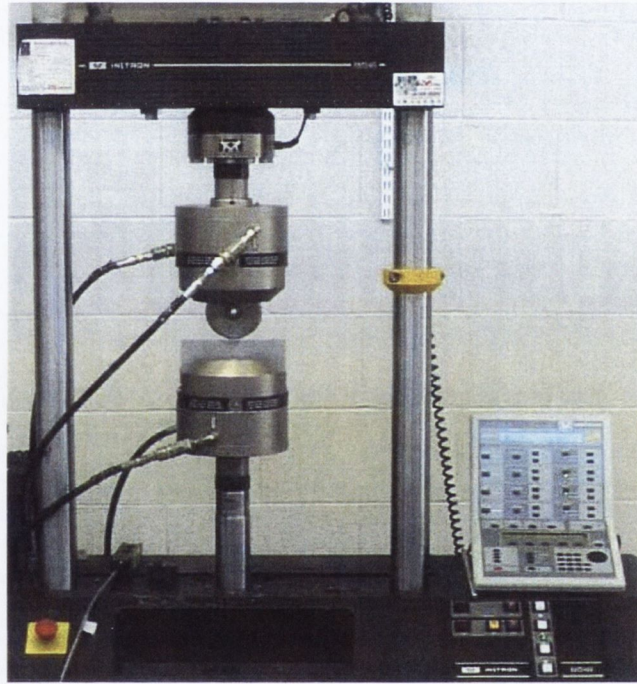


Figure 3.2 Instron 8516 with Roller and Flat for Indentation Experiment

The detail view given in Figure 3.3 shows the workpiece or test specimen placed on top of the flat surface with a small area of Fuji Prescale Film between it and the roller. Fuji film was placed on both sides of the test specimen.

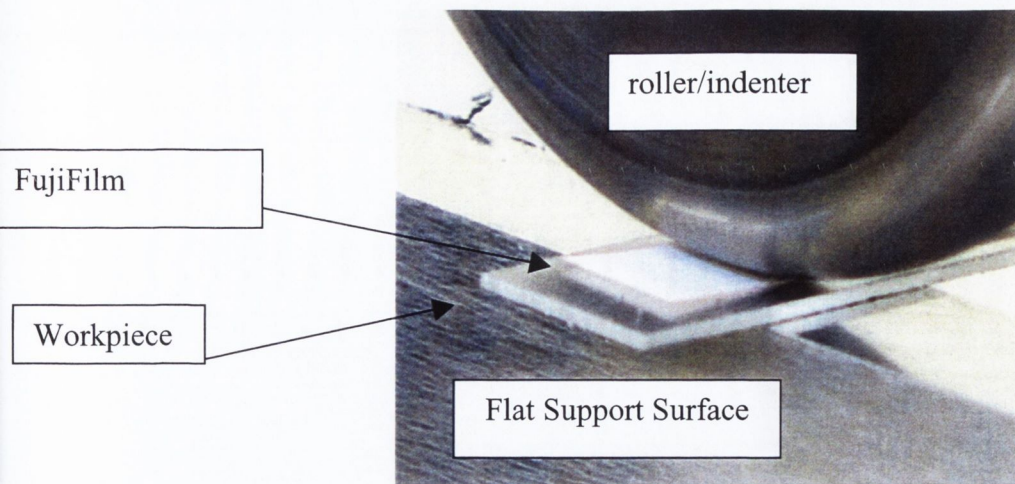


Figure 3.3 Close-up view of Typical Indentation Experiment

The Fuji Prescale film used is composed of an A-film, comprising of a PET base and a layer of microcapsulated color-forming material and a C-film, featuring a layer of colour developing material on a PET base (Fuji Color Film Technologies). Although this film can be used to measure pressure directly from the density of the colour pattern produced, in this case it was simply used to study the area of contact. The two layers of film have a combined thickness of 0.2mm. This might be felt to be a potential source of error in the experiment but in fact the film suffers no visible permanent deformation after use, so it was assumed that it maintains a reasonably uniform thickness during the test and so does not interfere with the results. In fact the material has a modulus of elasticity similar to that of Nylon and would therefore be less likely to interfere with the cases where Nylon is the material of either the roller or the support surface. The principle of operation of this film is explained by the schematic in Figure 3.4

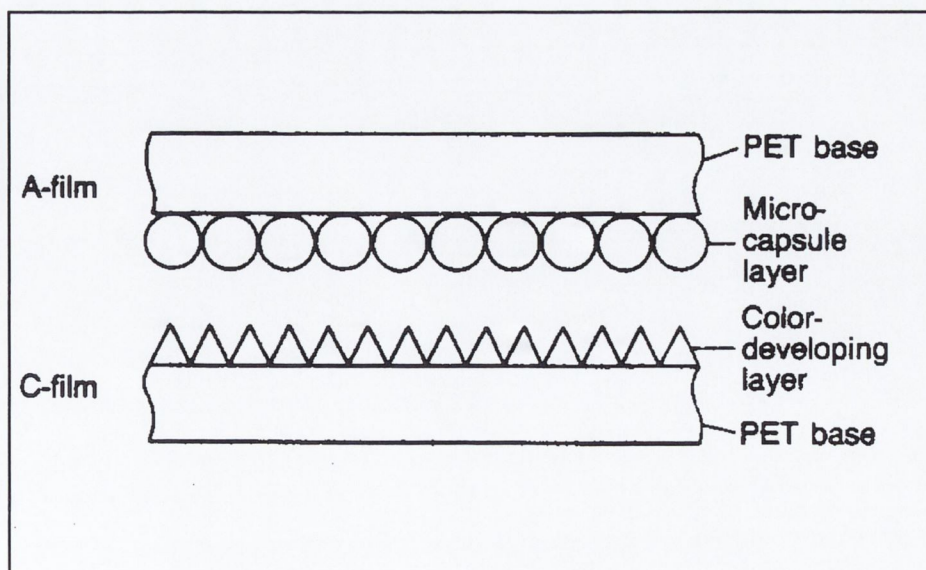


Figure 3.4 Fuji Prescale film principle of operation

This special purpose film is available in a variety of sensitivities. A medium sensitivity film was used and this is rated to detect contact pressures in the region of 100 to 500 kgf/cm² or approximately 10 to 50 MPa. It will be seen that some of the contact pressures calculated are less than 10MPa so the accuracy of these results is not as good as those for the higher pressures. This fact was evident from the colour patterns obtained. The contact area was clearly defined for the smaller contact areas with a well-developed colour area on the film i.e. the higher contact pressures obtained with the stiffer materials gave sharper results. The lower contact pressures yielded a less well-defined area. A typical well-defined contact pattern is shown in Figure 3.5.

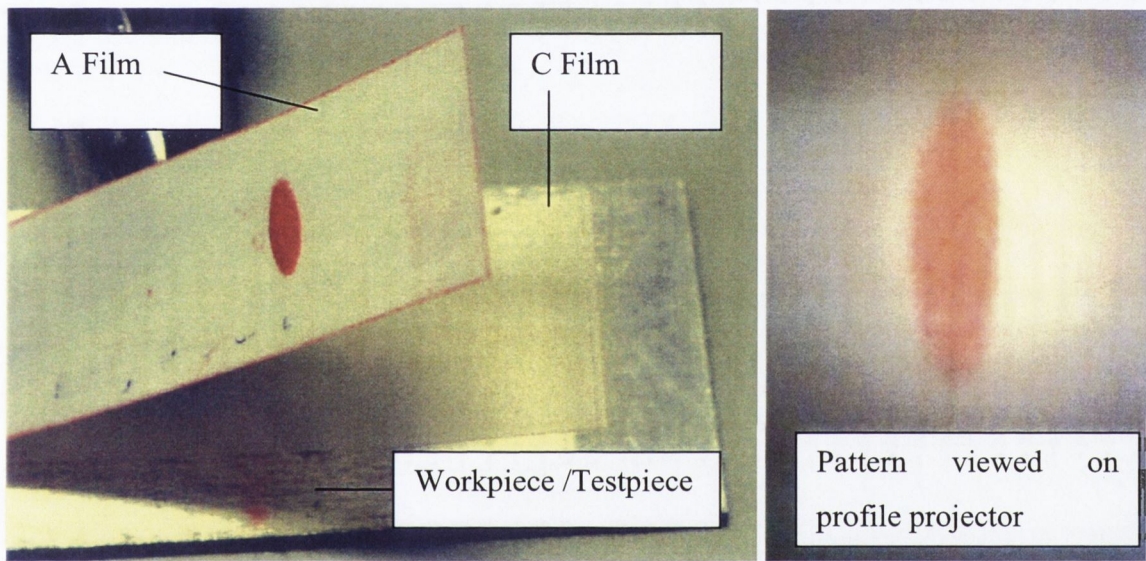


Figure 3.5 Contact Area Detected by Fuji Prescale film

3.3. Direct Static Contact: FE Simulations

This Section 3.3 describes axisymmetric finite element models that are used to study the stress in the workpiece under local loading and also to study the contact of the workpiece with the roller and former. These models do not simulate the loading conditions in a full spinning process but allow the investigation of the stresses created by a given force. These models enable static contact to be characterised in terms of compression of the workpiece and deflection of the tools by a given force. In these finite element models the areas of contact with the tools are directly aligned on opposite sides of the workpiece and the load is applied at the center of the test piece. As stated previously the typical reality of the spinning process is that where the roller makes contact with the workpiece some of the workpiece is unsupported and some of the workpiece is directly supported. The material on the flange side of the contact zone is without direct support and the material on the formed side of the contact zone has support from the former or mandrel. Because the roller contact with the workpiece is rarely either completely unsupported or simply directly supported in metal spinning, it is useful to look at the effects of both support arrangements because they represent two extremes of a wide range of possible load situations. Simulation of the spinning process will allow investigation of the offset of the contact areas on either side of the workpiece, these models are described later in section 3.5.

This section 3.3 dealing with the direct static contact simulations is divided into four sub sections as follows:-

Firstly the finite element simulation of the workpiece being loaded from one side is described in section 3.3.1. The concept of the unsupported workpiece is illustrated in Figure 3.6 and Figure 3.7 and this finite element simulation investigates how the equivalent stress varies through the thickness of the workpiece for this load arrangement and how this variation changes for workpieces of different thickness.

The loaded area has a radius of 1mm, the support that prevents rigid body motion is provided at a radius of 9mm i.e. at the edge of the mesh. In these models the effect of stress caused by a central load will be dependent on the distance to the support and whether it is simply supported or fixed (clamped).

It is known from standard analysis [50] of stress on a circular area at the center of a round plate that the distance to the clamped edges will influence the result of the experiment. In the finite element simulation of direct contact, the unsupported sheet is clamped 9mm from the center of the applied load. This is entirely arbitrary but this value is chosen so that

comparisons can be made as workpiece thickness is changed relative to the fixed area, of radius 1mm, carrying the load.

This stress variation through workpiece thickness was simulated for a number of workpieces of different thickness, Figure 3.7 illustrates the situation with a thicker workpiece. The area of interest in these models is the area subjected to the pressure loading. These models have boundary conditions applied at the edge of the mesh to prevent rigid body motion. These boundary conditions are a reasonable distance from the area of interest and so should not cause any local anomalies.

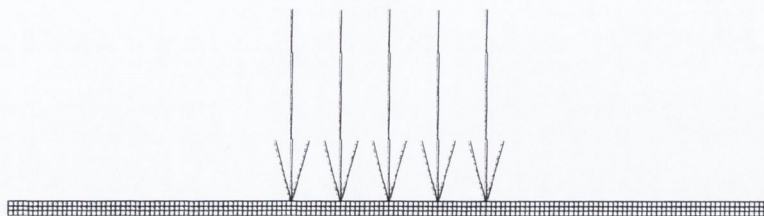


Figure 3.6 Contact Pressure Applied to One Side of Thin Workpiece

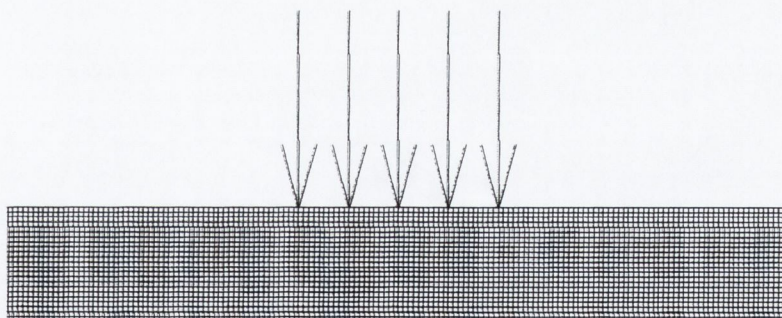


Figure 3.7 Contact Pressure Applied to One Side of Thick Workpiece

Secondly the finite element simulation of the workpiece being loaded from both sides is described in section 3.3.2. The loading of the workpiece by equal loads generated by different uniform pressures acting on different areas is illustrated schematically in Figure 3.8. Pressures as such do not directly force any shape change as a tool surface would, but these models do show the effect of such loads in generating significant strains in the workpiece. Opposing loads applied to different areas will occur in the physical world as

long as the radius of curvature of the loading surfaces is different on either side of the workpiece, as is usually the case in spinning i.e. roller and former do not usually have the same radius of curvature.

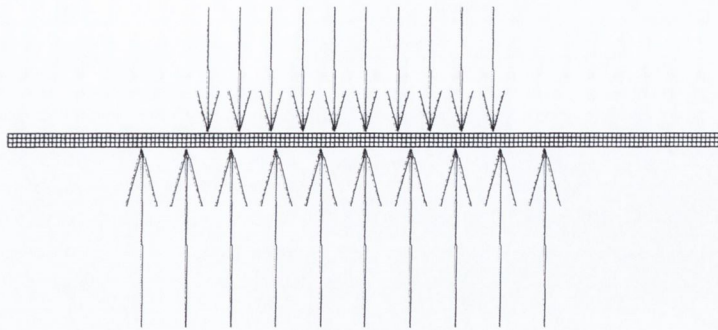


Figure 3.8 Simulating Loading as Opposing Uniform Pressures on Workpiece

Thirdly in section 3.3.3 the finite element model used to simulate the workpiece being indented by rigid tools is described. This is effectively a local forging operation on the centre of a large sheet. Figure 3.9 presents a diagram of the situation being simulated but of course using an axisymmetric model only half of the model is actually defined and solved. The stiffness (force displacement characteristic) of this contact is useful for comparison with the stiffness of the elastic contact of tools having differing material properties (stiffness) that might be used in an actual spinning process. This simulation will also show the development of plastic strain with prescribed displacement. The thickness reduction produced by this indentation can be compared with that achieved in a physical spinning process that uses a similar tool arrangement and forces.

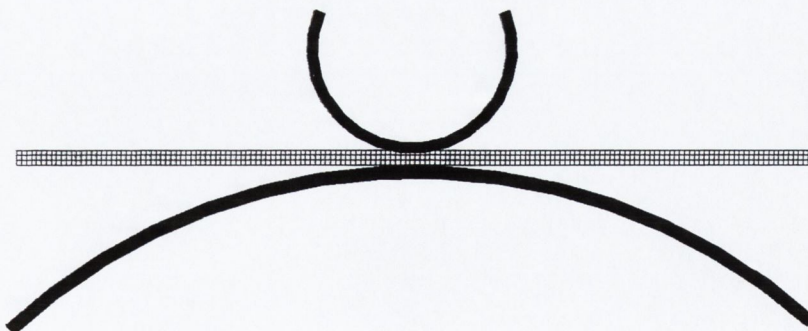


Figure 3.9 Load Applied by Rigid Tools

Finally section 3.3.4 is a development of the previous section with the rigid tools replaced by elastic tools. Each tool is represented by a deformable mesh to enable the simulation of elastic contact behaviour. These models are used to investigate whether a steel roller can

be regarded as a rigid tool when working commercially pure aluminium, or if in fact the elastic deformation of the contact surface, that is clearly demonstrated with soft (nylon) tools, is also significant with stiffer materials such as steel. Thus the contact stiffness (i.e. the force generated by a given prescribed displacement divided by the prescribed displacement) predicted by any one model can be compared to the results of the physical spinning experiments. These are the finite element models that most closely replicate the contact that occurs in spinning without actually introducing the issue of moving contact. The development of plastic strain, and the predicted contact area are very relevant to the definition of a full spinning process simulation.

Finite element modelling of material behaviour:

Details of the material flow properties are given in Appendix 1 (Al 99.0-Werkstoff 30205, Material condition HH, 0.2% yield 110 MPa). The material model used a value of 69000N/mm^2 for Young's Modulus and a value of 0.35 for Poisson's ratio, i.e. these are typical values for the properties of aluminium. The initial yield strength was entered as 96 MPa and the tangent modulus (slope of flow curve) was 25 MPa [ref c199, c253]

3.3.1. Simulating the Workpiece Loading as Uniform Pressure

The following section gives a more detailed description of the models used, in terms of the loads applied, the boundary conditions and other parameters.

This is the first of the stationary contact simulations and it involves applying the load as a uniformly distributed pressure on a relatively small 'contact' area. In this case using the finite element model it is possible to investigate how the stress pattern changes as the thickness of the workpiece varies from a semi-infinite solid to a thin sheet. Figure 3.10 shows two examples of the models being described. Both models have the same boundary conditions and differ only in the thickness of the test piece being simulated. The centre of the test piece is at the right hand edge of the mesh because using an axisymmetric model only half of the model is actually defined and solved.

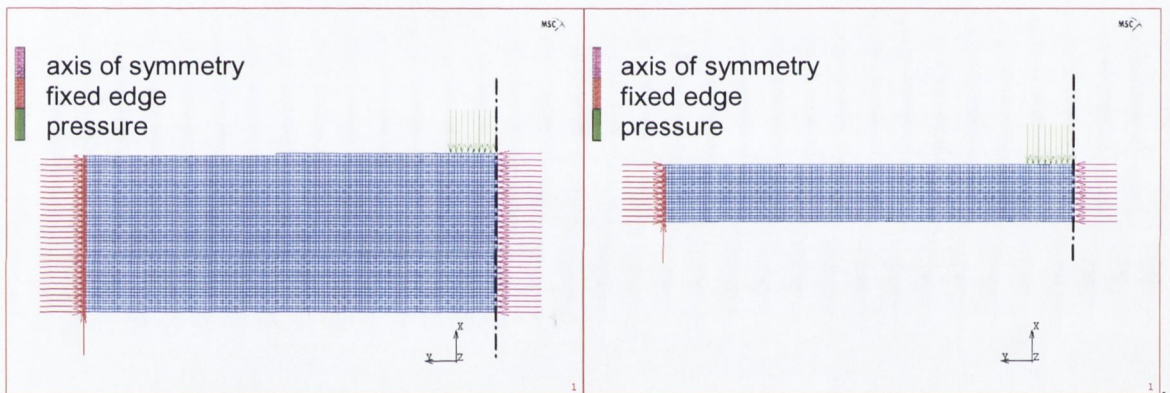


Figure 3.10 Finite element models with different test piece thickness

These models investigate how the application of a relatively low contact stress (well below the elastic limit of the material) to a thin workpiece can produce much higher stress in the workpiece. This higher stress may even be close to the yield stress. These models also investigate how with increasing contact stress much of the thickness of the sheet is loaded above its elastic limit.

The justification for modelling the contact problem using a uniform pressure to simulate the contact load is as follows.

It has been seen that the stresses arising in elastic solids due to a uniform pressure are similar to those due to a contact load. The variation in stress directly beneath the applied pressure (along the center-line or surface normal at the center of contact) was shown by Johnson [41] to be similar for constant pressure and for Hertzian contact this similarity was

presented in Figure 2.29. Making use of this similarity the contact stress was modelled as a uniformly distributed pressure.

The variation in stress along a line (the surface normal) through the workpiece thickness at the centre of the load was plotted. Then the thickness of the elastic solid was changed in a number of models from large solid to thin plate and the results are presented later in Chapter 4 as a family of stress curves.

This can be expected to show increasing stress as the thickness of the supporting plate (elastic solid) is reduced but also will demonstrate how the ratio of pressure to equivalent stress changes demonstrating how a tool applying a given contact stress can produce much larger equivalent stress in the plate.

Description of Finite Element Model with Workpiece Loaded by Uniform Pressure

A number of different finite element models involving workpiece thicknesses from 16mm to 1mm were created using the axisymmetric element type number 10 in the MARC finite element code. The number of elements varied from 36 864 for the 16mm thick plate, to 2 304 for the 1mm thick sheet. Solution times were all less than ten minutes. The MARC type 10 element is a full integration, four-node, axisymmetric element. The element edge length was 0.0625mm. Material thickness was set as 16mm initially to model a semi-infinite solid and this was reduced to 1.0mm over a number of models. This thickness dimension is marked t in Figure 3.11. The particular model shown in this figure has a thickness of 2.5mm. The mesh was defined to represent an 18mm diameter testpiece. The boundary conditions were (1) the constraining of the central nodes onto the axis of symmetry, (2) secondly the zero displacement constraint on the perimeter of the material 9.0mm away from the center of the pressure load and finally (3) the pressure load itself. The displacement constraint at the edge of the mesh is effectively a perfectly rigid support. Although the effect of this support would change if the diameter of the testpiece were changed because the diameter is fixed these models are used to study stress variation with changing testpiece thickness. Also because the load is applied to an area of radius 1mm at the center of the testpiece and this is the area of interest, any stress concentrations that occur at the edges are not the subject of this investigation.

The load due to the applied pressure was calculated as an edge load. The radius of the contact area was chosen to be 1.0mm i.e. a contact area of 3.14mm^2 . In order to apply a load of 250N, a load per unit area or pressure of $79.6\text{N}/\text{mm}^2$ must be applied to the edge of

the mesh i.e. a pressure boundary condition in the finite element model. These parameters were chosen as being representative of typical contact areas and working forces for the spinning process being studied. The 1mm radius of the loaded area is small compared to the largest sheet thickness of 16mm, therefore justifying this model as being a reasonable representation of a semi-infinite solid. The material constants used in the model are those of the material used in the physical experiments i.e. values to represent typical properties for aluminium.

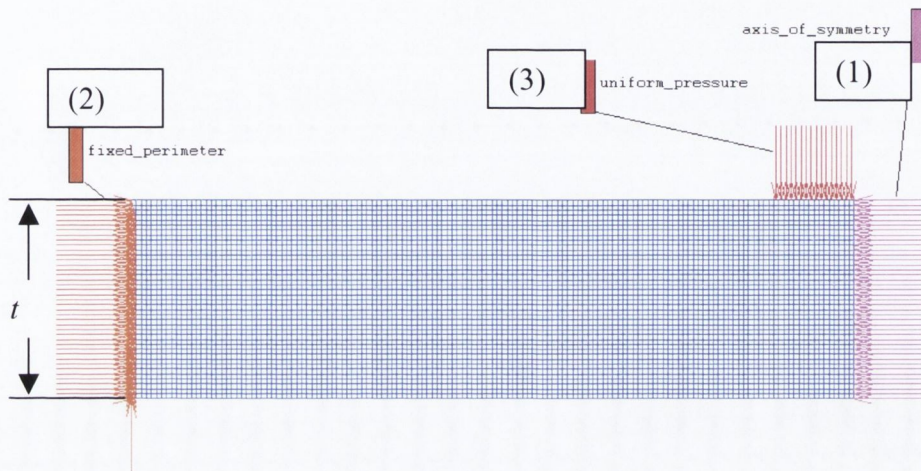


Figure 3.11 Axisymmetric FE Model, mesh and boundary conditions

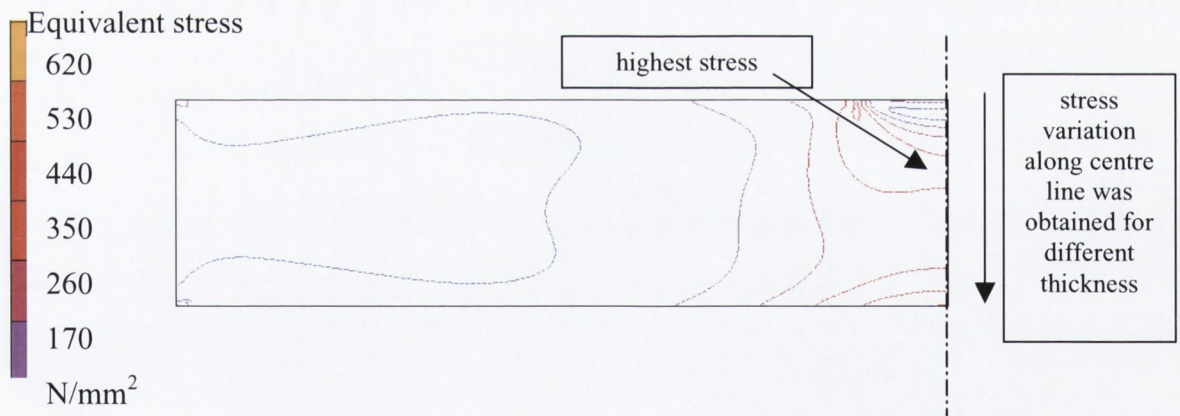


Figure 3.12 Axisymmetric FE Model uniform pressure load, typical stress contours

Figure 3.12 shows typical stress contours obtained from this finite element model. The stress contours clearly show that the region of highest stress occurs beneath the center of contact within the thickness of the material. These results are presented and discussed in Chapter 4 and comparisons are made between different sets of stress contours obtained with different sheet thickness.

3.3.2. Simulating the Workpiece Loading as Opposing Pressures

These simulations explore how a tool applying a certain contact stress can produce a much larger equivalent stress in the workpiece i.e. the loading of the workpiece by equal loads generated by different uniform pressures applied to different areas on opposite sides of the workpiece. These loads could be applied by tools made of a low stiffness material such as nylon. Applied pressures as such do not force any shape change but these models investigate the effect of such pressures in generating significant stresses and strains within the workpiece. Balancing forces applied to different areas will occur in the physical world as long as the radius of curvature is different on the loading tools (the roller and the former).

The purpose of modelling the contact problem using opposing uniform pressures to simulate the contact load was as follows. Although the actual contact areas may seem to be flattened elastically as the roller and the former touch the workpiece, as long as they have different surface curvatures the contact areas will differ on either side of the workpiece. The plastic strain caused by such loading will be compared to the level of strain required to deform the workpiece to the final product shape. The results of this model will also be used for comparison with the results for contact simulation using elastic tools, which is described in section 3.3.3.

This present model can be expected to show increasing stress as the difference in area increases. In spite of the fact that the forces are equal. It is of interest is to see how a combination of pressures (contact stresses) can create equivalent stress in the workpiece of greater intensity than the pressure applied to the outside of the workpiece. As the area of the supporting pressure is increased (and intensity reduces) the stress amplification will approach that of a uniform pressure applied to only one side of the workpiece and will give a result similar to the results of the simulation described in the previous section 3.3.1.

Description of Finite Element Model with Workpiece loaded by Opposing Pressures

The following finite element model applies the calculated opposing pressures to a sheet modelled as a two dimensional problem with an axis of symmetry.

Similar to the models described in section 3.3.1 the problem was treated as axisymmetric and a mesh was defined using the MARC finite element code. The element type used was a full integration, four node, axisymmetric element (MARC type 10). The element edge length was 0.0625mm. Material thickness was set as 1mm. The mesh consisting of 2304

elements was defined to represent an 18mm diameter workpiece and is illustrated in Figure 3.13. The boundary conditions were as follows; (1) the central nodes were constrained of onto the axis of symmetry, (2) the uniform pressure was applied on the 1mm radius area, (3) the uniform pressure supporting the workpiece was applied and finally (4) the perimeter of the workpiece 9.0mm away from the centre of the applied pressure was constrained to have zero displacement which in fact applied little to no force to the mesh but ensured stability i.e. prevents any rigid body motion.

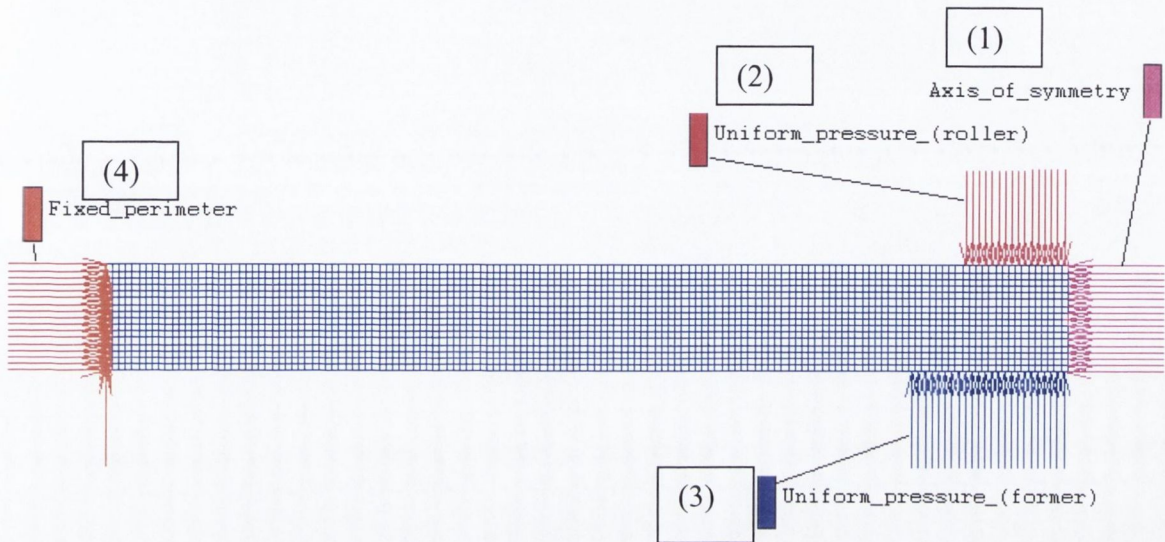


Figure 3.13 Axi-symmetric finite element model with pressures applied

The range of simulations covered

For these simulations workpiece thickness was maintained at 1mm and the contact area i.e. the area subjected to uniform pressure, extended 1mm from the centre-line on the upper surface. This corresponds to a contact area of 3.14mm^2 . On the other side, the lower surface, the contact area was varied. Initially the area of this supporting pressure was set equal to that on the upper surface i.e. 1mm from centre. This was changed in a series of models out to 6mm from the centre as detailed in Table 3.2.

Table 3.2 Area-pressure calculations

Finite Element Model Number	radius of supporting area	area	supporting pressure (load =250N/area)
Ndnt011229j	1	3.1416	79.5775
Ndnt011229k	1.0625	3.5466	70.4908
Ndnt011229l	1.125	3.9761	62.8760
Ndnt011229m	1.1875	4.4301	56.4317
Ndnt011229n	1.25	4.9087	50.9296
Ndnt011229o	1.5	7.0686	35.3678
Ndnt011229p	2	12.5664	19.8944
Ndnt011229q	4	50.2655	4.9736
Ndnt011229r	5	78.5398	3.1831
Ndnt011229s	6	113.0973	2.2105

This pressure on the top surface was applied as an edge load. The area where this load is applied has a radius of 1.0mm. To apply a load of 250N the load per unit area can be calculated as 79.6N/mm^2 and so this is the value given to the edge or pressure boundary condition in the finite element model. A similar calculation for the edge load on the lower surface produced the values in table 3.2.

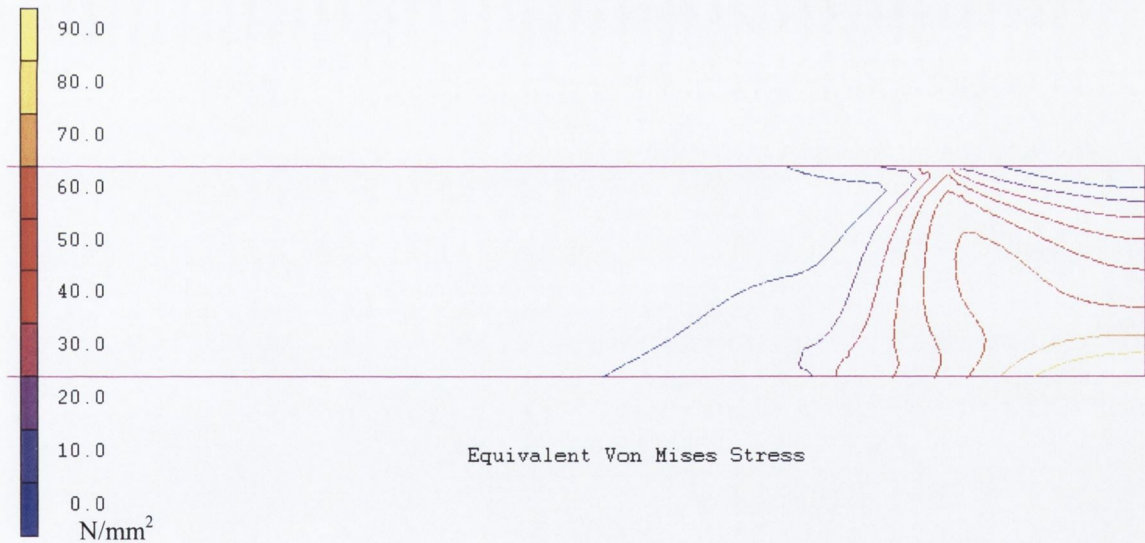


Figure 3.14 Axisymmetric FE Model Opposing Pressures, a typical result

This Figure 3.14 shows typical stress contours for equivalent stress obtained from the model. This result shows that with a very soft or spreadout support force a very significant equivalent stress can be generated by a contact pressure. Equivalent stresses can be larger than the contact pressure. The results from this model, which are presented in section 4.2.6, quantify this effect. This effect is very relevant to a spinning process because of the offset in contact areas that occurs in the spinning process and will be discussed in section 4.5.2.

3.3.3. Simulating Workpiece Contact Load with Rigid Tool Surfaces

These simulations are designed to predict stiffness of the contact and to allow resulting strains to be plotted against increasing loads. These models predict the load required to achieve a given (or prescribed) displacement, and also the resulting area of contact and the contact pressure. It will be shown later that a more accurate prediction of stiffness can be achieved with the model described in the following section 3.3.4. Nonetheless it is of interest see what prediction of stiffness occurs because of the use of rigid bodies rather than deformable bodies to represent the roller and former. In the three-dimensional models of spinning, which are described in section 3.5, it is not practical to model both the roller and former as deformable bodies hence an understanding of the possible effects of this limitation is necessary.

The load is applied using a rigid indenter with an appropriate radius. In the case where the tools have spherical surfaces it is straightforward to use the radius of the sphere as the radius of the rigid body in a 2D axisymmetric analysis. However in the case where the surface is say, ellipsoidal or toroidal, the contacting surface has to be represented by a single radius to enable the use of axisymmetric FEA. The local principal radii of the surfaces must be calculated and then combined to get a single or equivalent radius, R_{eq} that can be used in the finite element model.

The approach of calculating an equivalent radius is adopted in developing Hertz contact theory i.e. classical closed form solutions to contact of elastic bodies [c76 K.L. Johnson]. In Hertz contact theory an equivalent radius R_{eq} for a sphere touching a flat surface is calculated as

$$R_{eq} = \frac{1}{\left\{ \frac{1}{R_1} + \frac{1}{R_2} + \frac{1}{R_3} + \frac{1}{R_4} \right\}} \quad \text{equation 3.1}$$

Where R_1 , R_2 , R_3 and R_4 are the local principal relative radii of any two contacting solids. An example of the four radii involved is shown in Figure 3.15.

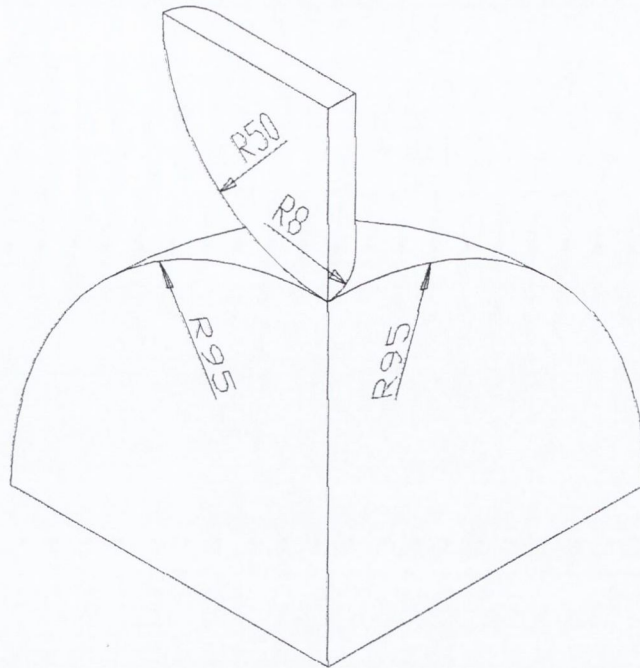


Figure 3.15 An Example of One Quarter Segment of Contacting Solids

In a 2D axisymmetric analysis it is required to represent the two solids as two spheres and so the following formula is used:

$$R_{eq} = \frac{2}{\left\{ \frac{1}{R_1} + \frac{1}{R_2} \right\}} \quad \text{equation 3.2}$$

In this case R_1 and R_2 are the local radii (principal relative radii of curvature) of the contacting surface at the point of contact. Thus an equivalent radius can be calculated for the roller and the former so that they can be modelled using axisymmetric finite element analysis.

To apply actual values to these radii the configuration of the roller and former must be considered. It cannot be assumed that the roller wheel orientation is perpendicular to the surface of the former. Figure 3.15 shows the roller in different positions around the former. The position marked '1' in this figure represents the most inclined position the roller can have to the surface normal at contact. The position marked '2' represents the most direct alignment between the roller and the fillet radius region of the former. This arises from the fact that the planes of the roller and the fillet radius torus are at a fixed angle of 45° to each other. As a result when the roller's point of contact is 22.5° from the crown of the fillet radius or outer diameter of the former the contact condition is the nearest to normal contact.

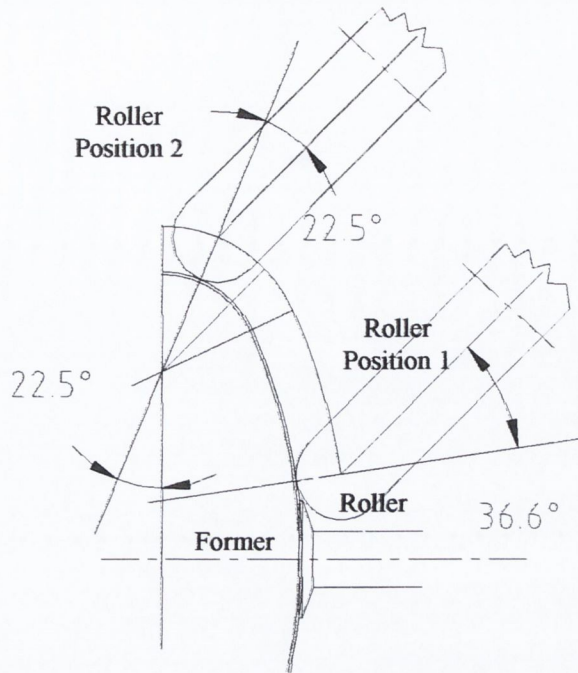


Figure 3.16 Configurations of Roller and Former

The former has two regions; one with a spherical surface of radius 95mm and the second a toroidal region defined by radii of 17 and 33mm. So the contact geometry under consideration is a wheel (a torus) making contact with a sphere or a second torus (the fillet radius region). In position '1' the roller is inclined at 36.6° to the surface normal. In position '2' the roller and the toroidal region of the former are both inclined at 22.5° to the surface normal. These are the two extremes, firstly where the roller is at its greatest inclination to the sphere and secondly where the least angle occurs between the fillet radius torus and the wheel. Equation 3.2 can be applied for these two cases and the equivalent radii calculated. Where the roller is inclined to the common surface normal, the surface experiences the roller as having a larger local radius in the plane perpendicular to the 8mm edge radius. The principal relative radius of curvature must be calculated as the curvature of an ellipse. In particular the ellipse that would be obtained by projecting the roller onto the plane passing through the common surface normal and the perpendicular to the 8mm edge radius.

In position '1'

$$\text{for the roller } R_{eq} = \frac{2}{\left\{ \frac{1}{8} + \frac{1}{\left(\frac{50}{\cos 36.6} \right)} \right\}} = 14.18 \text{ mm}$$

$$\text{for the former } R_{eq} = \frac{2}{\left(\frac{1}{95} + \frac{1}{95} \right)} = 95 \text{ mm}$$

In position '2'

$$\text{for the roller } R_{eq} = \frac{2}{\left\{ \frac{1}{8} + \frac{1}{\left(\frac{50}{\cos 22.5} \right)} \right\}} = 13.94 \text{ mm}$$

$$\text{for the former } R_{eq} = \frac{2}{\left\{ \frac{1}{17} + \frac{1}{\left(\frac{50}{\cos 22.5} \right)} \right\}} = 25.87 \text{ mm}$$

On this basis the following axisymmetric finite element analysis was conducted, in the first case using a radius of 14.18mm and 95mm for the roller and former respectively and 13.94mm and 25.87mm in the second case.

Table 3.3 Table Principal Radii (-all dimension in mm.)

Configuration /Position	1	2
Roller Geometry (mm)	50, 8	50, 8
Orientation to common surface normal	inclined at 36.6°	inclined at 22.5°
Local Principal Radii, and R_{eq} (mm)	8, 50/Cos36.6° 14.18	8, 50/Cos22.5° 13.94
Former Geometry (mm)	95, 95	torus defined by R33 & r17
Orientation to common surface normal	in line	inclined at 22.5°
Local Principal Radii, and R_{eq} (mm)	95, 95 95	17, 50/Cos22.5° 25.87

In the finite element model the values of R_{eq} given in table 3.2 are used to define the radius curves used to represent the roller and former. The workpiece is supported by its contact with the roller and the former. As the problem is axisymmetric the mesh is subject to a boundary condition that ties the edge of the mesh to the axis of symmetry. The design of this mesh is quite different from that used in the previous models which were simply a set of square elements of size 0.0625 mm. The mesh is refined i.e. uses smaller elements, in the area of contact.

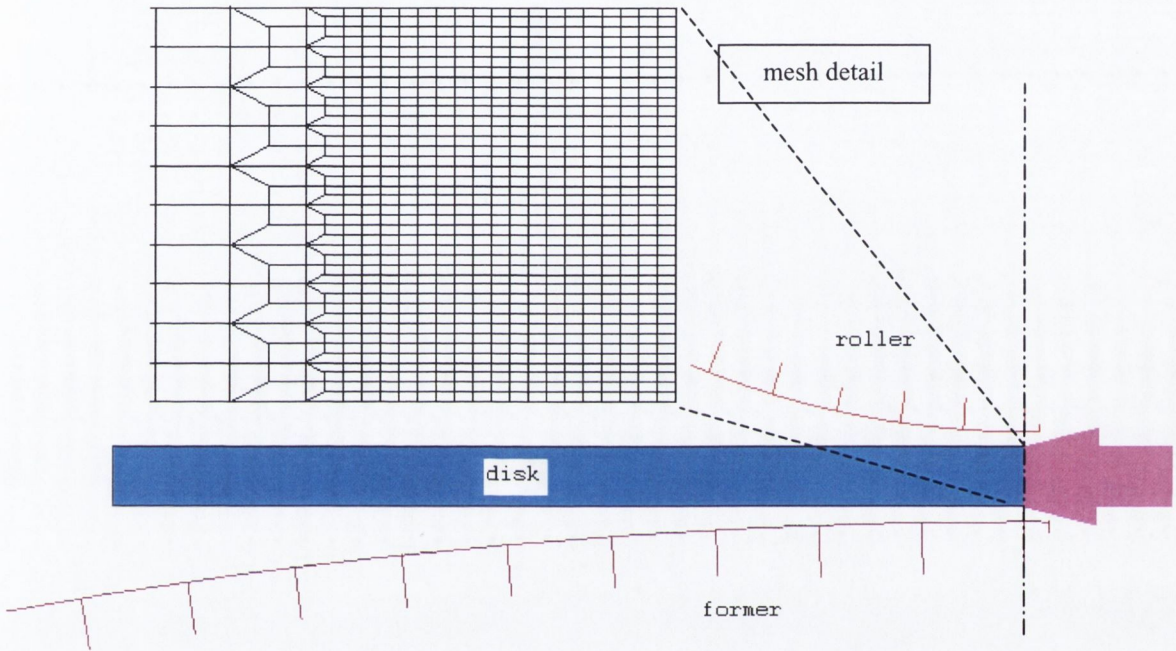


Figure 3.17 Axisymmetric FE model, mesh between rigid body tools

The results of these models are presented in chapter 4 and make interesting comparison with the results of the models in the following section.

3.3.4. Simulating Workpiece Contact Load as Direct Compression by Elastic Tools

These models are designed to show the contact stiffness that would arise when the roller, workpiece and former are brought into static contact, i.e. without the sideways motion that occurs in a spinning process. These models can also predict the strains that a given force can cause by direct compression. Later the results from these simulations will be compared to the strain required in the spinning process itself.

These finite element models, unlike those described in 3.3.1 and 3.3.2, require the finite element code to detect contact. The contact stress is no longer a simple uniform pressure distribution, but it is influenced by the deflection of the contacting surfaces. This requires the setting of various parameters in Marc and the first of which is the definition of the contact bodies. Figure 3.18 shows the contact bodies involved

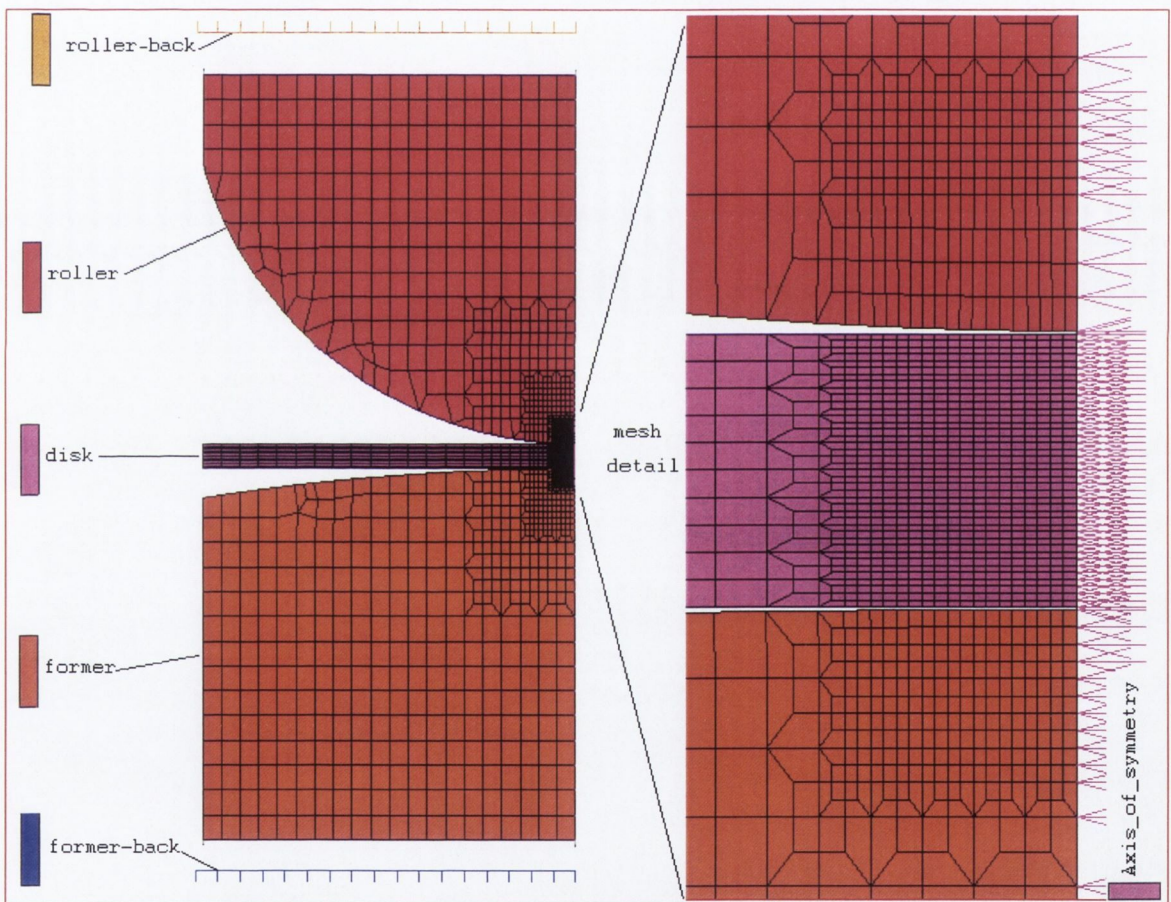


Figure 3.18 Axi-symmetric finite element model –contact bodies

The three principal contact bodies are straightforward. Two additional contact bodies can also be identified these, are the rigid bodies labeled roller-back and former-back. These latter bodies move to make contact with the roller and former at the start of the solution process. Thereafter these two rigid surfaces are used to provide the motion or prescribed displacement to the roller and former in order to compress the workpiece or disk. As the

problem is axisymmetric all three deformable bodies (roller, disk and former) are subject to a boundary condition that ties the edge of the mesh to the axis of symmetry.

The elastic properties of the tools were set to represent Nylon and steel. A modulus of elasticity of 210 000 N/mm² for steel and 2 800 N/mm² Nylon and a Poisson's ratio of 0.3 and 0.33 respectively. Four different simulations were run with various tool material combinations. Both roller and former were modelled as steel and nylon as indicated in Table 3.4 below.

Table 3.4 Variations in materials used

simulation	1	2	3	4
Roller	Steel	Nylon	Steel	Nylon
Former	Steel	Steel	Nylon	Nylon

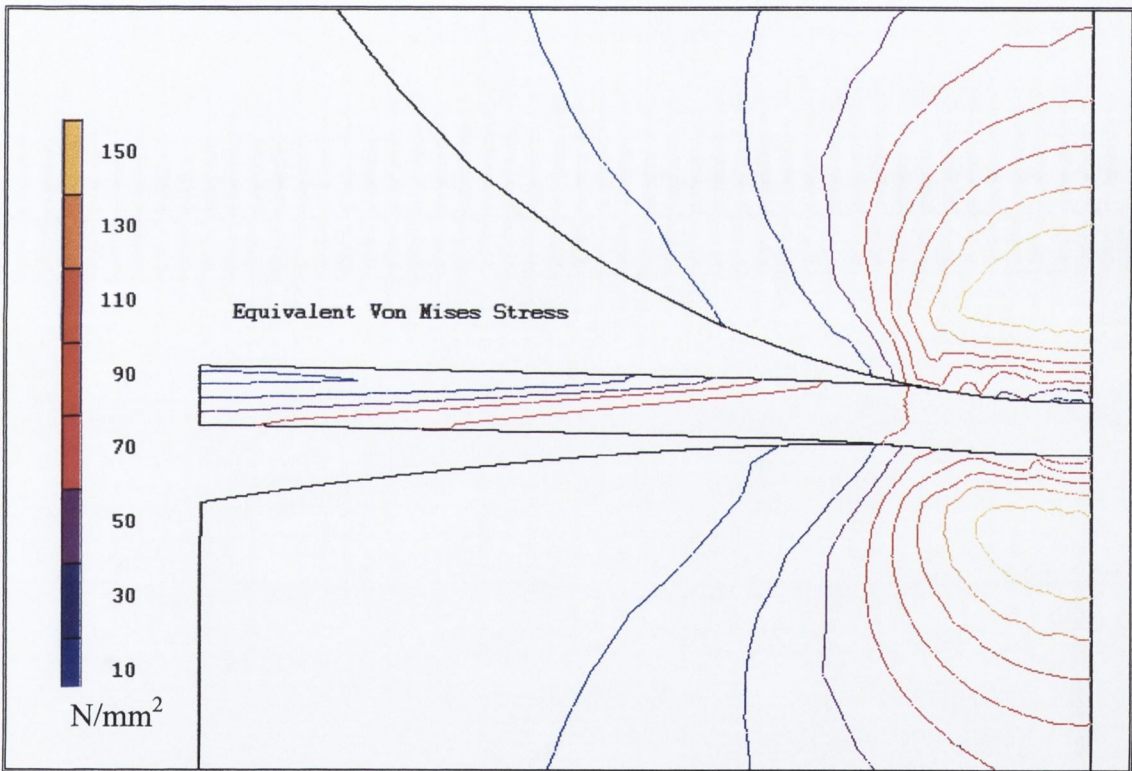


Figure 3.19 Axisymmetric FE model –Elastic Tools Typical Stress Result

3.4. The Experimental Spinning Process

3.4.1. Overview of Spinning Experiments

This section describes the spinning experiments performed on the Hitachi Seiki CNC lathe. The various process parameters, feed per revolution, spindle speed, definition of roller path etc. are described. Force and strain measurement methods are outlined. The workpiece strains enable an investigation of the nature of the deformation that has occurred. The chosen experimental shape was taken from the literature and the toolpath was developed through the use of experimental hand spinning. The shape itself is typical of a lot of parts produced by conventional spinning and involves a considerable variation in the forming process from the center to the outer edge of the workpiece. The process of producing good quality, wrinkle free parts using a conventional NC lathe is described. A spindle speed of 480 rpm was used throughout so that the centrifugal loading is small in these experiments but would require to be reconsidered if higher speeds or softer material were used. Consequently the finite element simulations were entirely quasi-static. The same workpiece material was used as for the experiments described in section 3.1 i.e. light gauge sheet Aluminium (Al 99.0-Werkstoff 30205, Material condition HH, 0.2% yield 110MPa). One of the experimental objectives was to demonstrate that the deformation required to achieve this shape, varies from bending near the tailstock through stretch forming or 'shear forming' to flanging at the outer edge. While direct measurement of the principal strains is not possible the various measurements help to build an understanding of the deformation involved and ultimately determine the nature of deformation in conventional spinning.

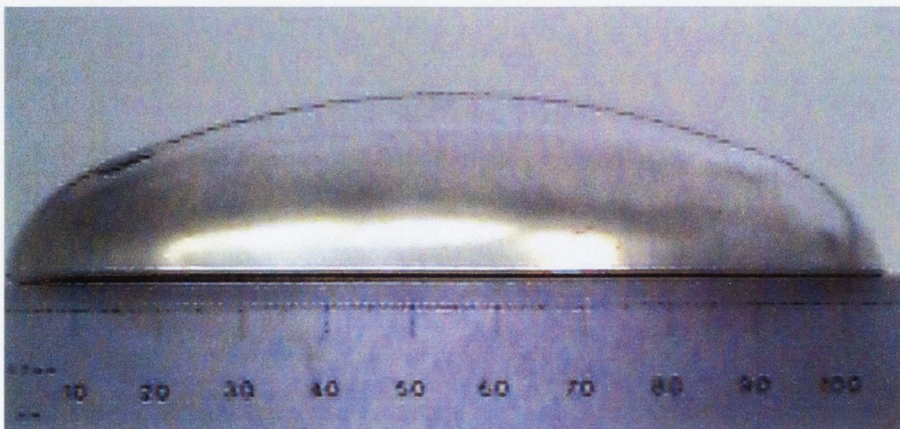


Figure 3.20 An example of a spun part (with steel rule).

Dimensions of required part.

As already described in section 2.1.9 page19, in the context of analysing strains for an ideal deformation a simple shape was chosen which provided a variety of forming conditions i.e. the doubly curved shape should not allow the process to become quasi-steady state as would be the case if a straight cone were used. The shape consisted of outside diameter of 100mm with a central section consisting of a spherical surface of radius 95mm having a blend radius of 17mm between the cylindrical and the spherical sections as shown previously in Figure 3.20. This is same shape as that used in an investigation of working forces in conventional spinning by Qiang et al. [27].

3.4.2. Measurement of Part Shape

The resultant shape following spinning was measured using a TESA Brown and Sharp coordinate measuring machine. Parts were held by means of a vacuum fixture, which consisted of a tailstock held vertically in a vice. The tailstock was drilled so that a central hole could be connected to a vacuum pump. This located the parts at the same position where they were held by the tailstock on the lathe. This means of holding the parts makes use of the one position on the part that was clamped during the forming process and so was subject to the least variation as the process parameters are changed.

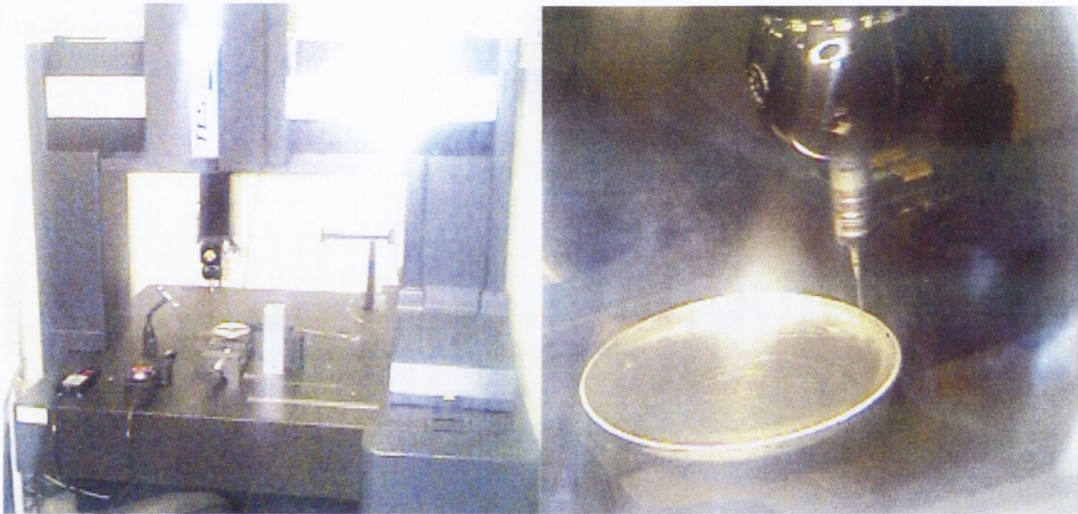


Figure 3.21 Measurement of Parts on TESA CMM

These measurements are critical to gaining an understanding of the effects of varying the process parameters on the geometry of the parts produced. Measurement of the intermediate shapes also enables an assessment of the ability of the finite element simulation to predict these shapes.

3.4.3. Measurement of Strains

The strains were obtained directly from thickness measurements using a sheet metal micrometer. This was done with the aid of a Mitutoyo 0-25mm, 0.01mm micrometer with a 155mm reach and fitted with a 5mm precision ball on the moving anvil. Strains were also measured with the aid of a circle grid etched on the workpiece where this was possible. Unfortunately the use of a steel roller generally obliterated the grid marks during spinning. A grid was applied to the workpiece by an electrochemical etching process using a low voltage, 30Amp, alternating current power supply and a Nylon stencil as shown in Figure 3.22.

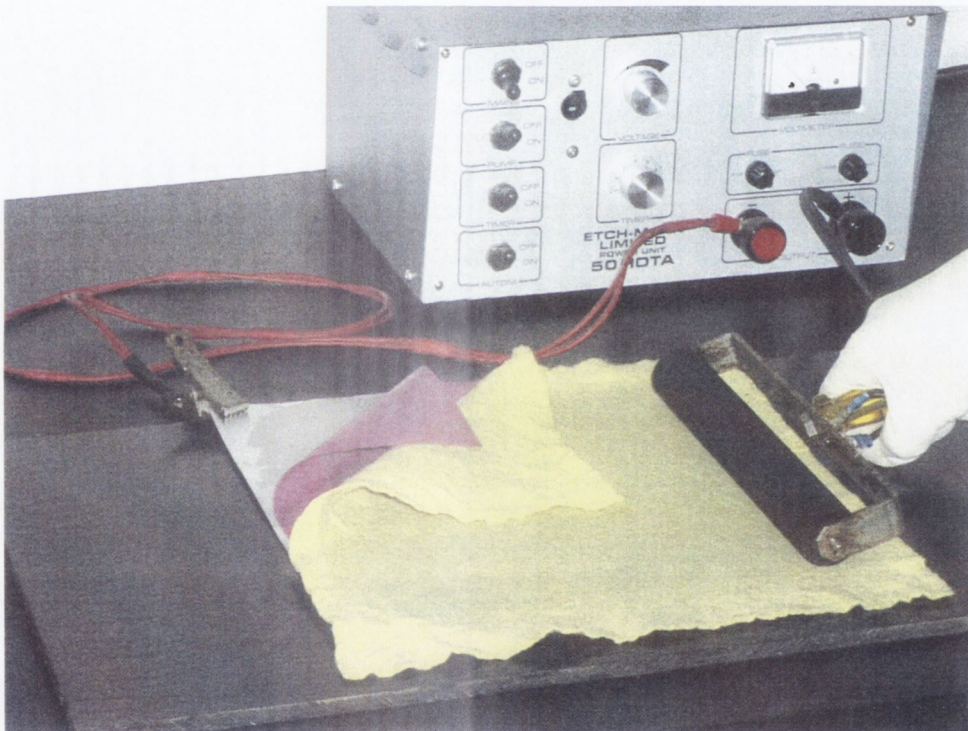


Figure 3.22 The Etching Process

The aluminium sheet was connected to one terminal of the power supply via a crocodile clip attached to some part that was not actually being etched. A stencil was placed on the sheet to be etched and then a felt soaked in electrolyte was placed on top. A ferrite roller electrode was then applied by hand to the felt and current flowed from the roller through the felt and stencil. The stencil pattern determines the areas of the sheet metal to be marked by the electrolyte, thus the stencil pattern is replicated on the sheet metal as shown in Figure 3.23.

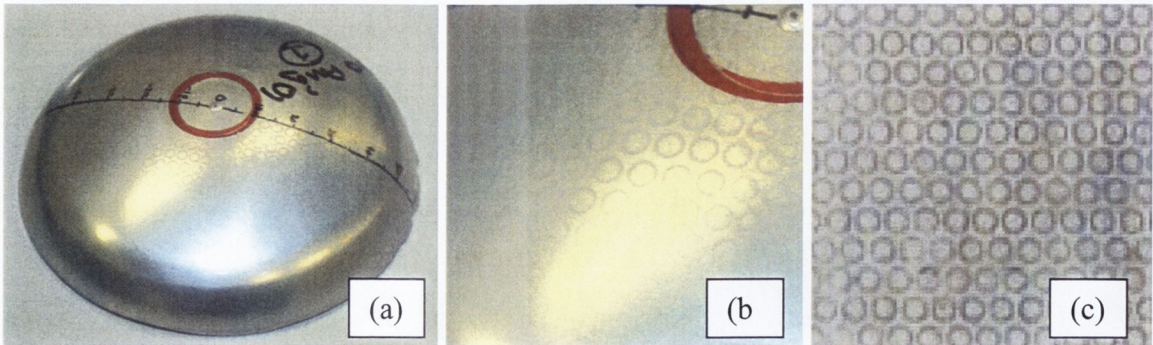
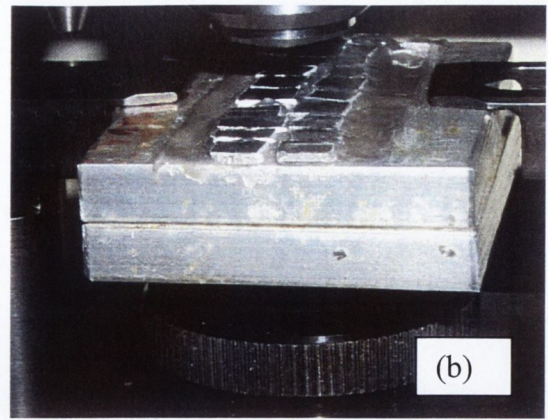
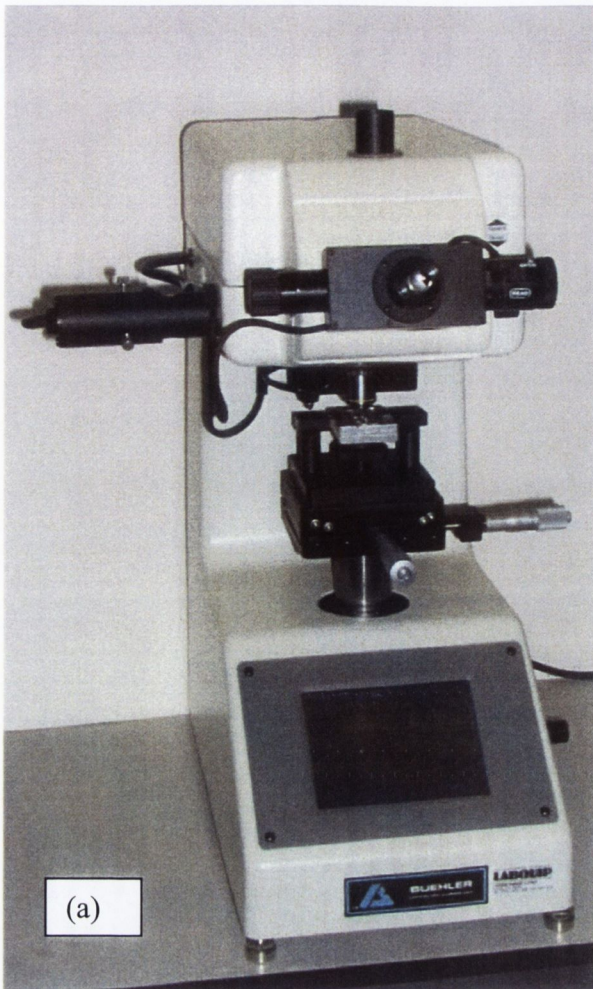


Figure 3.23 Etched Circle Grid (a) on part, (b) detail, (c) on flat workpiece.

A Baty Profile projector was used to measure the size of these grid circles and hence the strains were determined.

3.4.4. Measurement of Work-hardening

The hardness condition of the material after spinning was measured using a Beuhler (Model no. 1600-6300) micro hardness test system. A segment of the disk was cut using a jig saw and then diced into specimens less than 5mm square. These were mounted in an epoxy resin on an aluminium block as illustrated in Figure 3.24. The measurements were made according to BS EN ISO 6507-1. The resulting measurements gave an indication of work hardening for comparison with that predicted by the finite element simulation as well as allowing comparison of results between different spinning process parameters.



P2240090.bmp

Figure 3.24 Beuhler Microhardness Tester (a), Part mounted for test (b) and (c).

The BS EN6507 standard specifies a minimum thickness for the micro hardness test that is satisfied by a mean diagonal measurement of less than $250\ \mu\text{m}$ for a test piece thickness of 1.0mm (nominal).

Annex B (pages 7-9) of this standard specifies a correction factor for indentations made on curved testpieces which allows the appropriate correction to the measurements made depending on the curvature of the surface being measured. On a concave surface the hardness is otherwise slightly under-estimated and on a convex surface the hardness is otherwise slightly over-estimated.

3.4.5. Measurement of Forces

A three-component dynamometer, charge amplifier and recording software were used to measure the forces involved during metal spinning. The dynamometer used was a Kistler 9121 as shown in Figure 3.25.

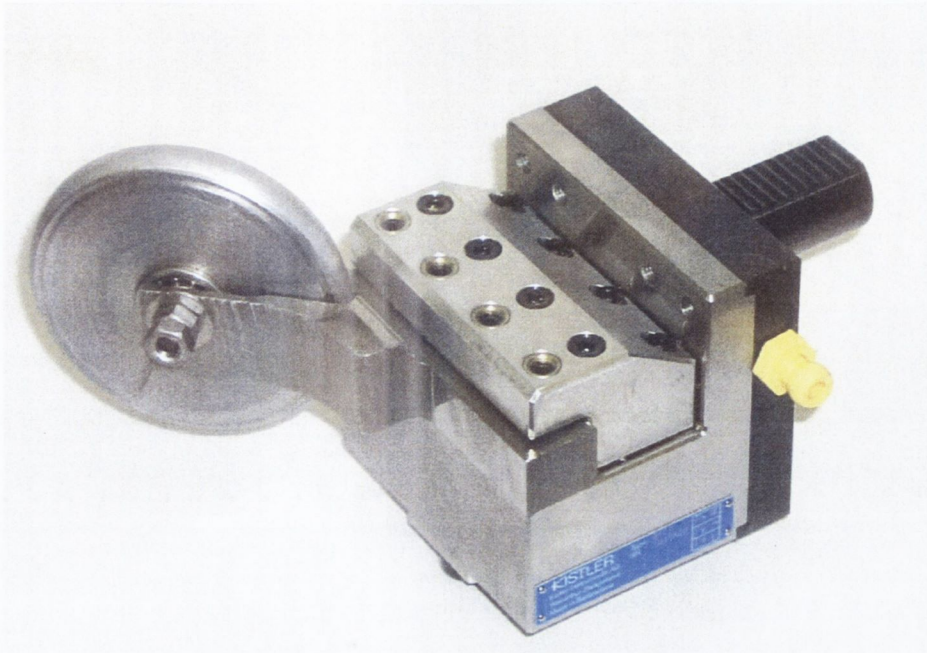


Figure 3.25 Roller Tool Mounted in the Kistler 9121 Dynamometer

A Kistler 5019 adapter, or charge amplifier, was used to convert the analogue electric signal from the dynamometer itself to a signal from -10 to $+10$ volts which was fed to an analogue to digital (A/D) board in a PC. A program (Dynoware version 2.31 © 2002 Kistler Instrumente AG) then converted this signal to usable data that can be stored and accessed on the PC. Typically a recording frequency of 400Hz was used and this gave a results file of about 0.25MByte when recording the three force components over a cycle time of say 16 seconds. The force measurement range was set at $\pm 2000\text{N}$ for each force channel.

3.4.6. The Spinning Equipment

The Former

The greater part of this surface is spherical with a radius of 95mm. The outer diameter of the former is 100mm and a blend radius of 17mm joins this outer cylindrical surface to the spherical surface. These match the inside of the nominal size of the part to be produced.

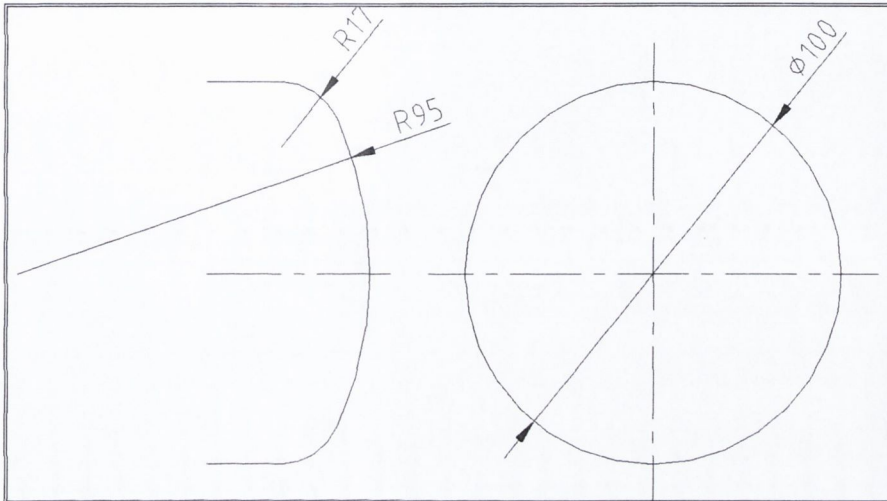


Figure 3.26 Basic dimensions of former

Two formers, constructed to the internal dimensions of the required part, were used one made of steel and the other of nylon.

The Roller

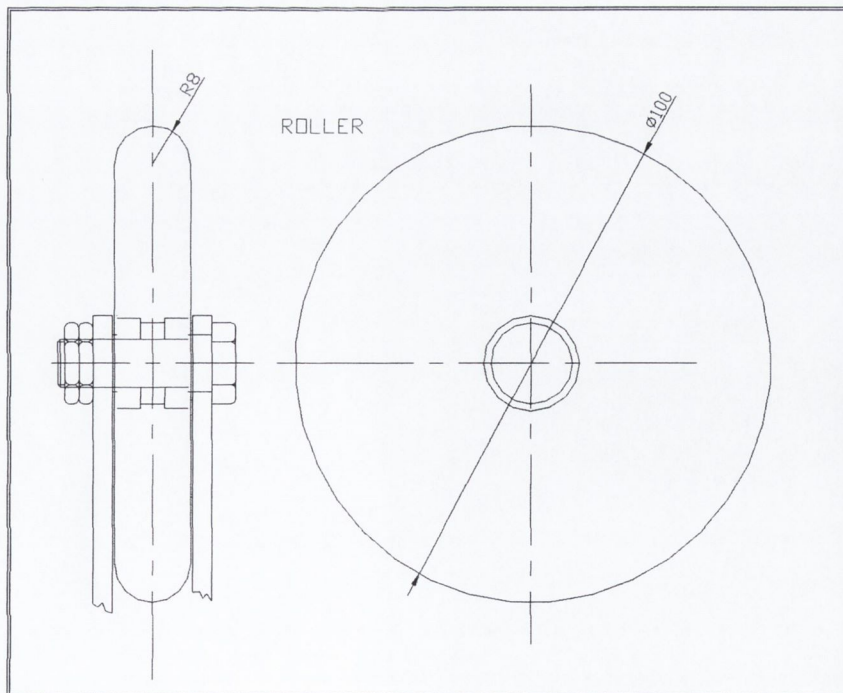


Figure 3.27 Roller

As shown in Figure 3.27 the roller used was 100 mm outside diameter with an edge radius of 8mm.

The Roller Holder

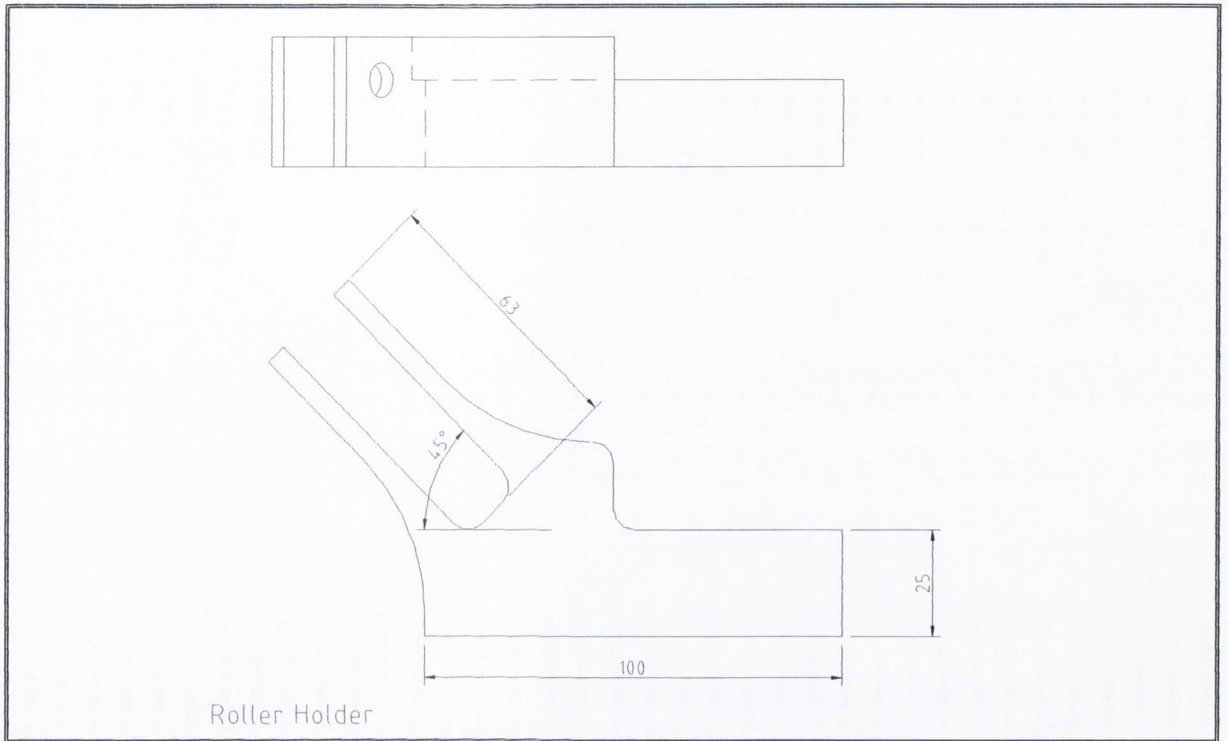


Figure 3.28 Roller holder

The important feature to note about the roller holder is that the angle between the lathe axis of rotation and the roller is fixed at 45 degrees. This is unlike the actual situation in hand spinning where this angle varies continuously as the tool pivots on a fixed tool post, as was shown in Figure 2.3, rather than travels on a slide. The lathe axis of rotation and the roller axis of rotation were coplanar i.e. they both lay in the same plane (a plane parallel to the bed of the lathe).

The Tailstock

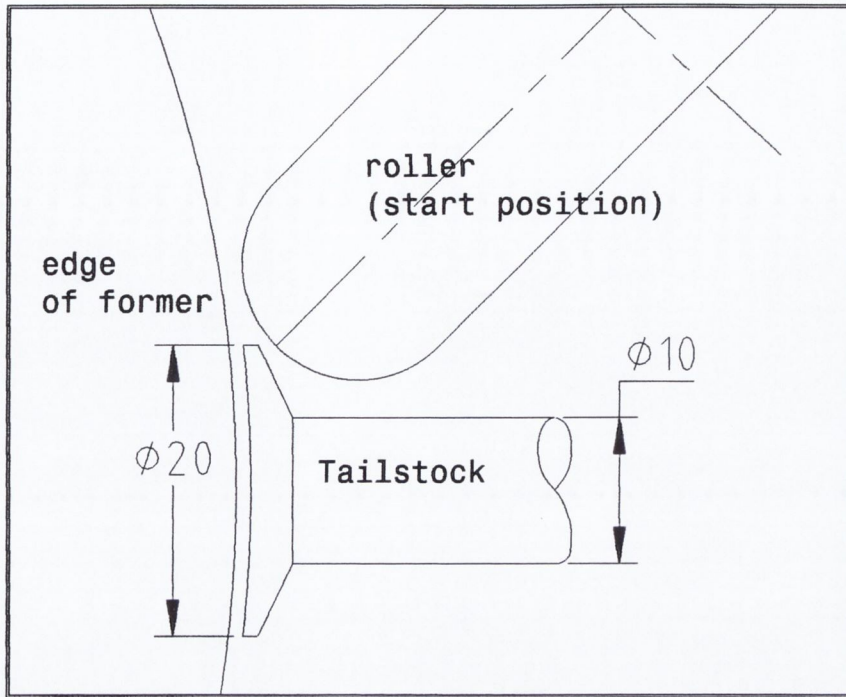


Figure 3.29 Tailstock

The tailstock provided a clamped area of 20mm diameter and was reduced in diameter to allow the roller to contact the workpiece as close to the centre as possible. This is illustrated in Figure 3.29. The remainder of the tailstock was machined to a taper for mounting in the lathe standard live centre holder. All of the main parts are illustrated in figure Figure 3.30 below.

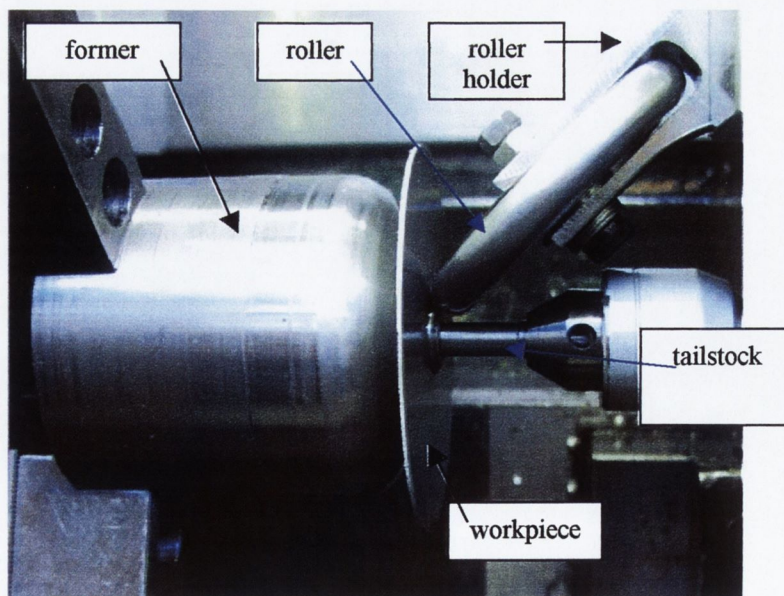


Figure 3.30 Experimental spinning process

3.4.7. The tool path including NC code

The principal for determining the tool path is that the roller brings the workpiece into contact with the former and is then advanced towards the former by a small 'prescribed displacement'. The tool is then moved at a constant distance from the surface of the former, as shown in Figure 3.31, at a defined feed rate, while the workpiece is continuously rotating.

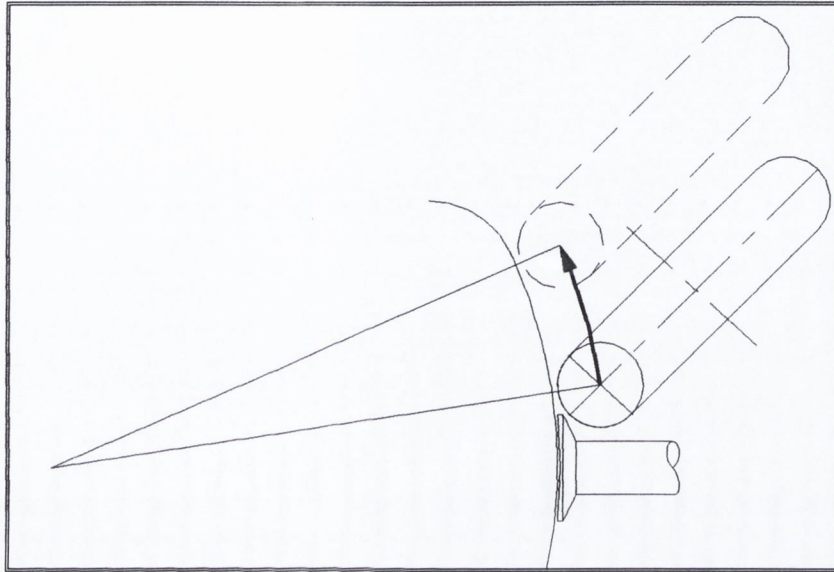


Figure 3.31 Basic Tool Motion Equidistant from the Surface of Former

The selected part was produced with three roller passes. As this worked well in hand spinning experiments the same approach (with three passes) was used when designing a tool path for producing the experimental part using the NC lathe.

Each roller pass then requires three pieces of information; (1) where to make the approach i.e. the radial position where the roller plunges to make contact (2) where to lift off from the constant distance motion i.e. the radial position where the roller lifts off and (3) a curve or line along which the roller moves after lift-off i.e. the direction to move to lift off. These are illustrated in Figure 3.32.

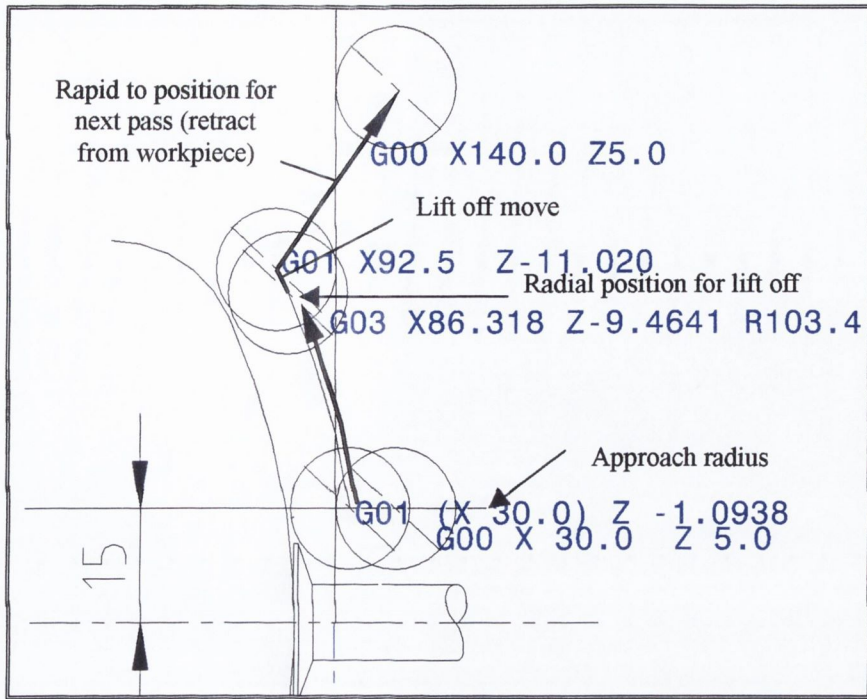


Figure 3.32 First roller pass showing the position of the roller edge radius

For the first pass as shown in Figure 3.32 the centre of the roller edge radius is positioned 15mm (X30.000 in NC code) from the axis of the lathe before moving into contact. It then follows a circular arc until a radial position of 43.159 (X86.318 in NC code). Next it moves off tangentially reaching a radial position of 46.25 (X92.5 in NC code) and finally it retracts from the workpiece entirely. The experimental toolpath moves the roller clear of the workpiece to allow inspection between passes if required. This is unlikely to be a requirement during an actual production operation consequently the toolpath and the cycle time would be shortened.

Figure 3.33 shows the second and third roller pass, each of which moves the flange gradually to the final part shape. Note that during the lift-off stage of the second pass the roller moves tangentially to form the flange. The roller motion along the lift off curve or line can contribute significantly to the working of the blank and help reduce problems such as the flange becoming inverted.

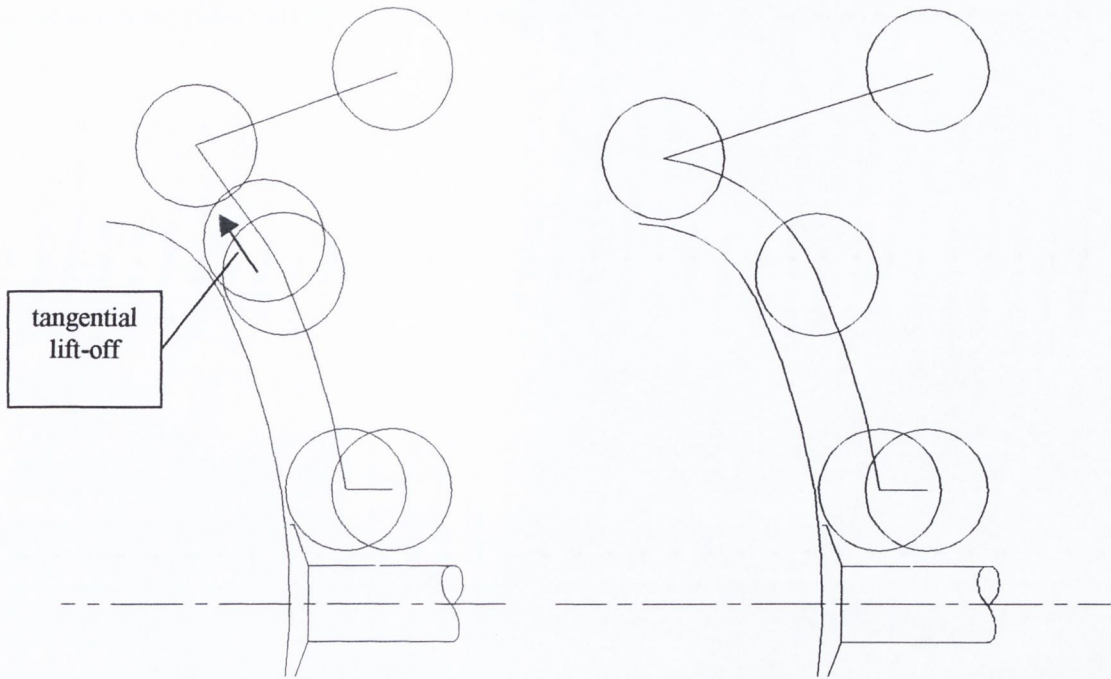


Figure 3.33 Second and Third Roller Pass

Care was necessary to ensure that the roller did not run over the edge of the blank because this frequently lead to the edge of the blank catching and being buckled by the side of the roller. The NC code used for these tool motions is given in Appendix 2 NC code.

Checking the tool path

Great care was taken to ensure that the distance between the roller and former was constant at all points by checking with a feeler gauge during a dry run. Adjustments to tool offsets and path geometry were made as necessary.

Range of experiments

The prescribed displacement or programmed interference between roller and workpiece was varied between 0.1 and 0.3 in the case of the nylon former. Lower values were used in the case of the steel former. Roller Feed was varied from 0.1mm to 2.5 mm per revolution. Mandrel speed was maintained at 450 rpm throughout the experiments. A blank diameter of 115mm was used for all tests.

3.5. The Spinning Process: FE Simulations

3.5.1. An Approach to Simulation of Spinning using 2D-Axisymmetric FEA

The finite element models described below were designed to predict the final shape of the part and the condition of the material in the finished part. They are also capable of providing some detail of contact with both the roller and the former in planes lying on the spinning axis. The models begin with a flat workpiece represented by a mesh of four-node axisymmetric elements as shown in Figure 3.34 and as the simulation proceeds the mesh is deformed around the former by the roller as shown in Figure 3.35

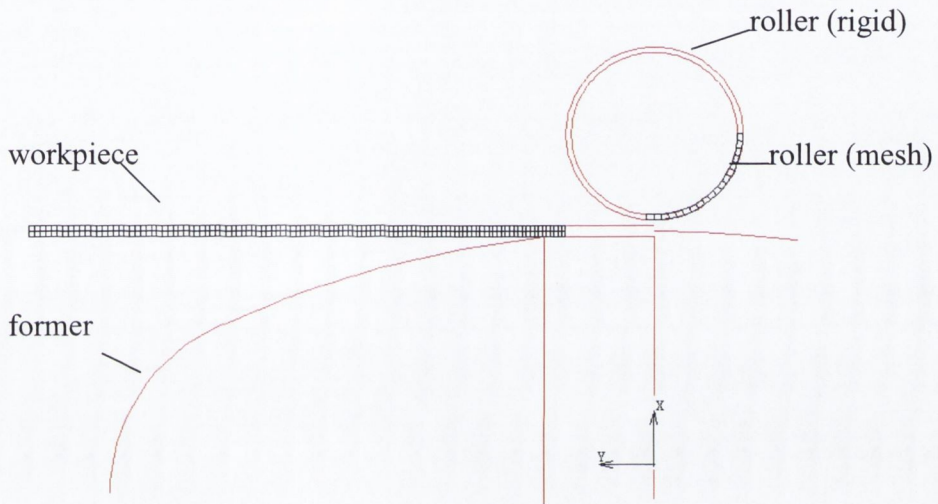


Figure 3.34 2D-Axisymmetric Model of Spinning

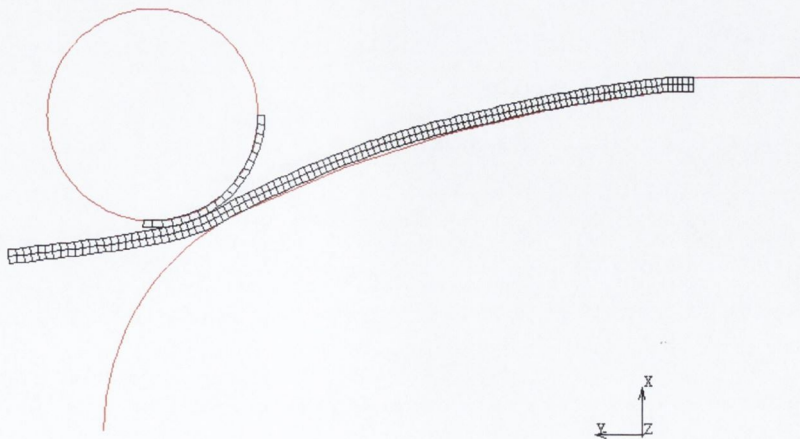


Figure 3.35 2D-Axisymmetric Model of Spinning Typical Deformed Shape

The roller is also represented by four-node elements that are ‘glued’ or constrained into contact with a rigid body which has a programmed motion. The former is represented as a rigid body which remains stationary. These rigid body curves are shown in red in Figure 3.34 and Figure 3.35. These axisymmetric models are only used to simulate the deformation that takes place in an axial plane and so cannot predict any shearing or bending that may occur in the real process in other planes.

Roller motion

The roller movement is in the form of a stepping rather than continuous motion. This approach is different to that of earlier work reported by Alberti [166] on a simulation of cone spinning using the Adina finite element code. This earlier work simply moved the roller along the workpiece while maintaining continuous contact. In these simulations the roller makes a series of moves into and out of contact with the workpiece in order to simulate each revolution of the workpiece. This is illustrated in Figure 3.36 and Figure 3.37.

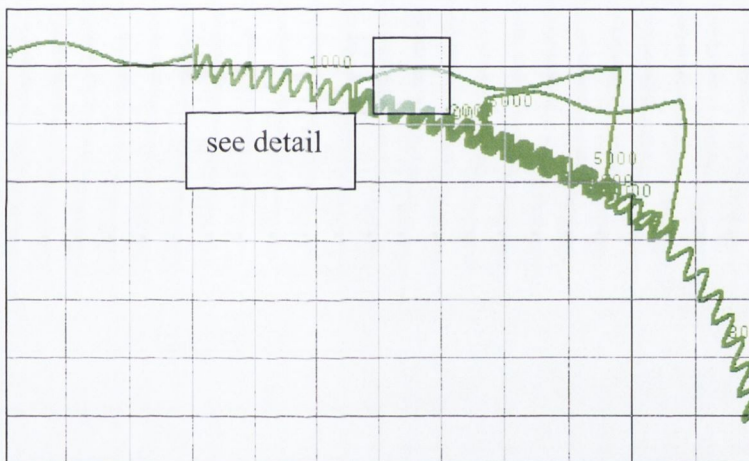


Figure 3.36 Roller Path in Axisymmetric Simulation of Spinning Process

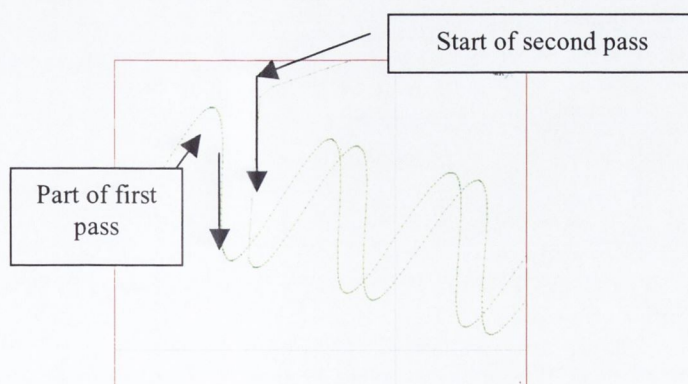


Figure 3.37 Detail of Roller Path in Axisymmetric Simulation

This tool motion is controlled by a Fortran subroutine written by the author, the code of which is presented in Appendix 3 Fortran 6.6 code. The code is very similar to that used to control the tool motion in the full three-dimensional simulations described later in section 3.5.2.

One of the advantages of having deformable elements attached to the rigid roller body is that it is possible to detect contact when the nodes of the roller touch the elements of the disk. This enables a more continuous and effective simulation of the real contact situation because the roller nodes can move continuously along the edge of the workpiece elements. This is unlike the situation with the workpiece nodes touching the roller where each workpiece node would either be in contact or not and so the transfer of working force from one element to the next would not be as smooth. Of course deformable elements on the roller can model elastic deformation which is also of interest.

Outputs from axisymmetric models

These axisymmetric models can be used to predict final shape of the workpiece after a multi-pass spinning operation and the strains imposed in an axial plane. A particularly useful output from these models is the predicted thickness and the strains throughout the part. Some prediction of material condition following forming is available through the output parameter 'total equivalent plastic strain'. This parameter is obtained by an integration of all the incremental equivalent strains as they occur, although some strains are reversed during the spinning process. Evidence that strain reversals occur can be seen to be the case from Figure 3.35. It is seen from this figure that the material is first bent around the roller radius and then leaves the roller to take up a reversed curvature around the former.

The predicted work hardening can be compared to the experimentally measured increase in hardness. The FEA results may underestimate the actual work hardening that occurs because the model does not simulate the full three-dimensional process.

These models do allow the possibility of investigating the width of contact of the workpiece with the roller and the former. Knowledge of roller contact width can be used in determining the appropriate feed per revolution for the spinning process. Prediction of contact with the roller is interesting in terms of understanding the bending and stretching nature of the spinning process.

3.5.2. Simulating the Spinning Process with 3D FEA

Introduction

In this section the term overall process simulation refers to the simulation of the spinning process from flat disk to finished part. The objectives for simulation of the spinning process using 3D finite element analysis included a prediction the final shape of the part including part thickness, a prediction of the condition of the material in the finished part and the forces required for the process.

The 3D simulation allowed a study of the intermediate workpiece shapes generated during the spinning process. It was also used to investigate different tool paths, thus avoiding problems that can arise with poor tool path design such as; excessive working of the material, buckling of the flange or backward folding of the flange.

If these predictions can be made with reasonable accuracy then the 3D simulation could enable an analysis of contact of the workpiece with both the roller and former. More accurate mid-process snapshots of the contact patterns between the roller, workpiece and former could then be achieved by locally refining the mesh during an overall process simulation.

In the development of the overall process model considerable useful results were achieved with a reduced diameter disk. Although such a model could not simulate the overall process the smaller workpiece substantially reduced the solution times and thus allowed various parameters such as contact tolerance and nodal contact release force to be optimised.

Mesh definition; choice of elements

The spinning process under investigation involves the deformation of thin sheet material and this might lead to the conclusion the best type of element to model the process should be a shell element. As mentioned previously there are however certain limitations with the use of the shell elements available in the MSC Marc2001 finite element code. An individual node cannot make contact with two other contact bodies at the same time i.e. it cannot be squeezed against the former by the roller. In effect a node can only be constrained to be in contact with one rigid body at any given time. The process of spinning at least partly involves squeezing the sheet metal between the roller and the former therefore it is critical that the finite element mesh can handle contact with both sides of the sheet simultaneously. For this reason the three-dimensional models in this project used eight-node hexahedral brick full-integration elements.

Although the Marc code does offer reduced integration elements i.e. elements with fewer integration points these were not considered because of their poor capability to simulate bending stress which is clearly one of the major modes of deformation in any spinning process. Higher order elements with mid-side nodes were discounted because the additional or mid-side nodes are not capable of detecting contact. Furthermore in a contact situation it is vital that the element with the contacting node offers the best possible prediction of the shear stresses tending to distort the element, and this is offered by an eight-node hexahedral brick element.

Optimising Mesh Definition

The ability of the mesh to model bending accurately depends on having the maximum possible number of elements along the deformed curve. Figure 3.38 illustrates this issue, the 'improved' mesh not only provides better geometrical definition of the deformed shape but also provides better prediction of the forces involved in creating the deformation.

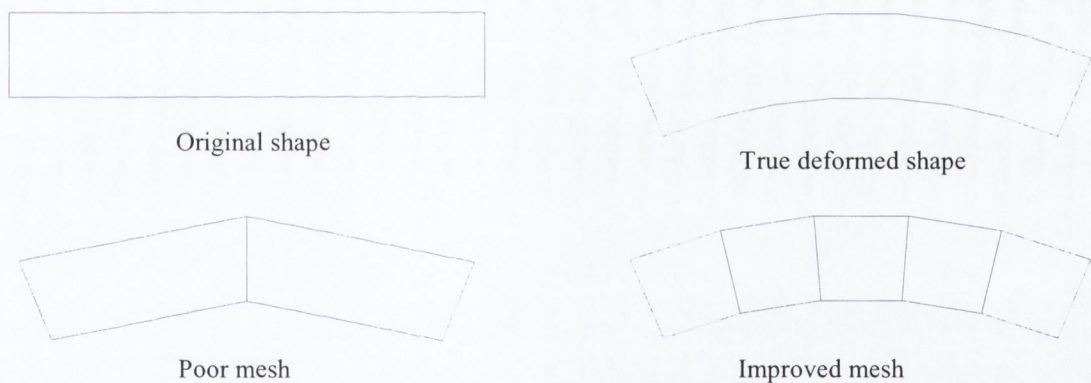


Figure 3.38 Optimum mesh definition

The illustration in Figure 3.38 is of two dimensional bending. When the deformed shape is three dimensional and is also doubly curved with equal curvature in both directions a square element is most appropriate i.e. elements with equal length in radial and tangential direction are desirable in this situation. Figure 3.39 illustrates the three dimensional equivalent of the previous diagram. Of course meshing a circular part with a square or brick shaped element is not straightforward.

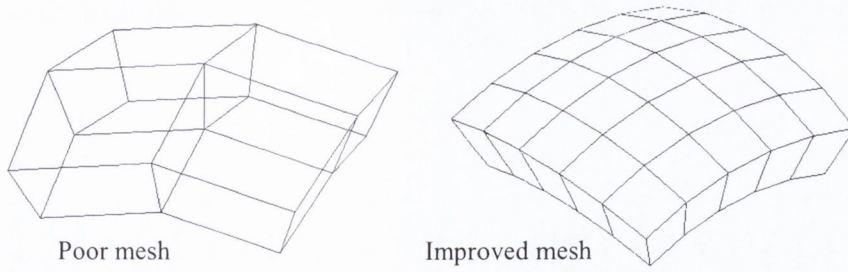


Figure 3.39 Three Dimensional Mesh

The simplest compromise is to divide a radial line into a number of elements and then to convert these into a circular mesh by rotating them in a series of steps around a central axis. This approach has the advantage of being simple but does produce a larger element size at the periphery of the disk. The mesh illustrated in Figure 3.40 was generated by this method. In this mesh the area of elements varies from 1.7mm^2 at the centre to 14.6mm^2 at the outside.

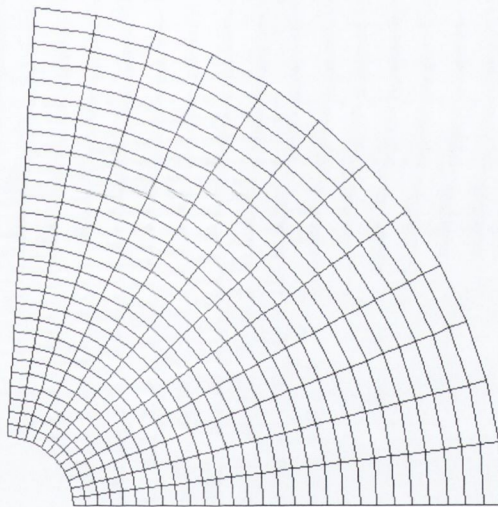


Figure 3.40 A Section of Mesh Generated by Rotation

An Ideal Mesh Based on Curvature.

Simple geometric considerations dictate that the ideal mesh would keep errors associated with representing a curved part shape by straight edged elements to a minimum throughout the mesh. In terms of the mesh describing the final part geometry it follows that the smaller the local radius of curvature the shorter the element edge length required. Where the deformed shape has a small radius, such as at the fillet radius of the experimental part, then the element edge length would ideally be smaller to achieve the same accuracy. A simple way of defining such a mesh would be to allow the same number of degrees of arc for each element along each different radius of curvature. If this same incremental angle,

measured in radians, is multiplied by the radius then we have the appropriate element edge length. In order to determine this element edge length the area of the former part can be divided into two areas in terms of curvature. The central area which is spherical with a radius of 95mm and the fillet area with a curvature of 17mm in one direction and 50mm in the orthogonal direction at the periphery.

Although various models used in this project ran for periods of weeks the practical requirement to have a solution in days rather than weeks dictates that the number of elements in the disk mesh should be kept to less than 1500. With this limit of 1500 elements the resultant mesh would then have elements of 6.47 mm square for that part of the disk that forms the spherical region and elements of 3.4 mm by 1.16 mm in the outer region on fillet radius. This is arrived at through the following calculation;

where x is the element edge length in the spherical region

A_{R95} is the area of the spherical region

A_{R17} is the area of the fillet region at the edge of the part

N is the total number of elements in the disk mesh

$$N = \frac{A_{R95}}{x^2} + \frac{A_{R17}}{\left(\frac{17x}{95}\right)\left(\frac{50x}{95}\right)} \quad \text{equation 3.3}$$

simplifying

$$N = (A_{R95} + 10.62A_{R17})\left(\frac{1}{x^2}\right)$$

solving for x

$$x = \sqrt{\left(\frac{1}{N}\right)(A_{R95} + 10.62A_{R17})} \quad \text{equation 3.4}$$

Given that the areas A_{R95} and A_{R17} are 5381 mm² and 5006 mm² respectively this would give a value of 6.47mm for x . In other words the element size for the spherical region would be 6.47mm by 6.47mm. By a similar calculation the fillet region element size would be 1.16mm by 3.4mm and a mesh similar to Figure 3.41 would be the result.

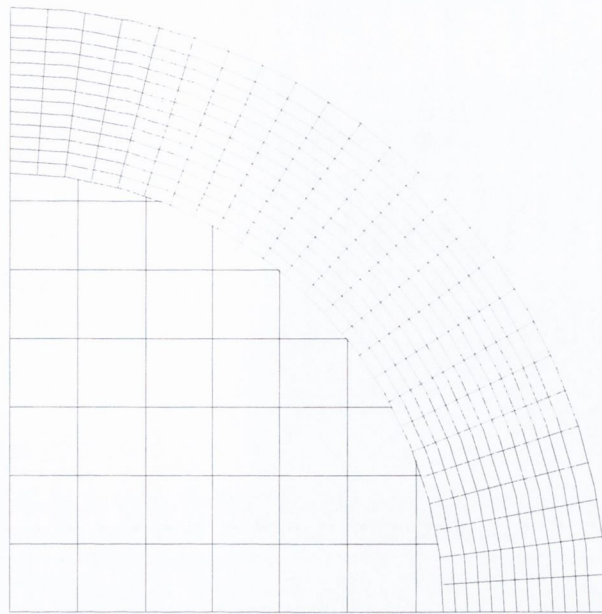


Figure 3.41 Mesh Based on Curvature of Formed Part

A practical difficulty in defining the mesh in the transition between the two regions makes this approach somewhat awkward to implement. In reality the local principal radius of curvature does not suddenly change from 95mm to 50mm at the inner edge of the fillet area but makes a gradual transition from 95 to 50 at the extremity of the disk.

An Ideal Mesh Based on Uniform Element Size.

Another meshing possibility is to use a uniform square mesh with some wedge shaped elements to enable the mesh to match the outside diameter of the disk. On this basis the total of 1400 elements would allow each element to have a surface area on the disk of 7.5mm^2 and an edge length of 2.74mm. This approach offers the advantage that the element size is uniform, consequently each node that experiences contact forces represents the same area and would present the same reaction or deflection stiffness to the roller. Obviously a 2.74mm element edge length can better approximate the 95mm radius of the central area than the 17mm radius of the fillet region. The result of this uniform element size approach is shown in Figure 3.42.

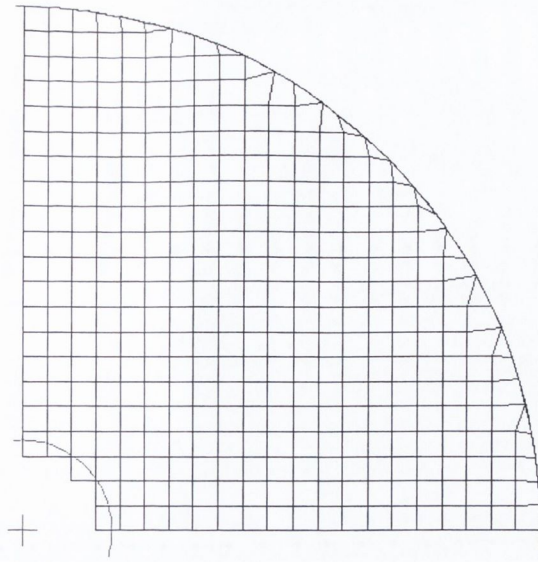


Figure 3.42 Mesh Based on Uniform Element Area

Furthermore a square element mesh will involve many more element edge crossings by the contacting body i.e. the roller than would occur with a circular pattern mesh. As a result longer solution times dictate against this approach.

A Compromise Mesh Definition

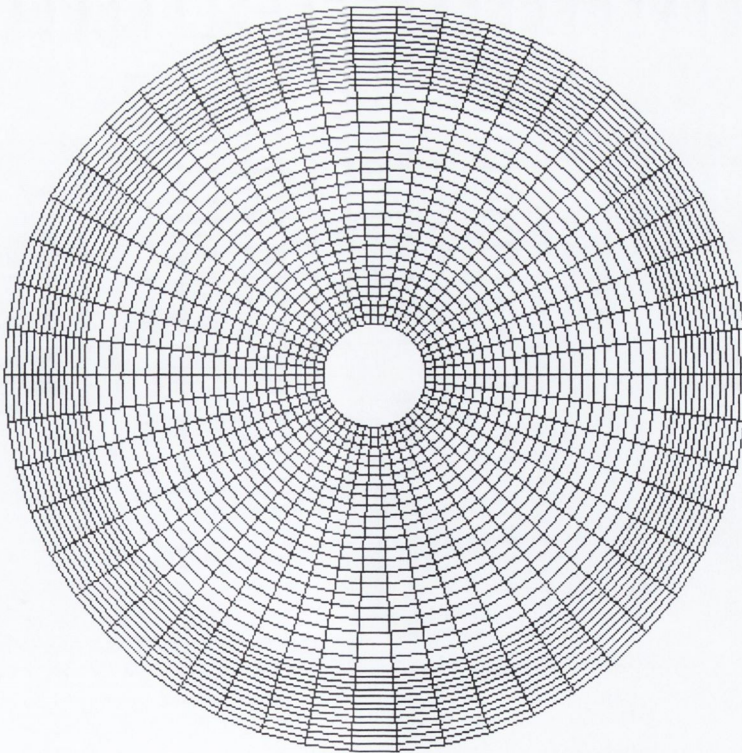


Figure 3.43 A Practical Compromise in Mesh Definition

The disk in Figure 3.43 has in fact 1700 elements. In the mesh there is just a single element through the thickness. This helps keep the number of element down but limits the information available about the stress variation through thickness. Earlier models which had three elements through thickness showed that the variation in strain was reasonably linear so little accuracy should be lost with only one element through the thickness of the disk.

The Material

Because of the repeated loading and reversal of loads it was decided to use the kinematic work hardening model as described in the Marc software documentation [47]. The material properties used are described in Appendix 1 Flow Curves from Plane Strain Compression.

Contact Definition

The MARC software uses a direct constraint contact algorithm. In this procedure the motion of the bodies is tracked and when contact occurs direct constraints (both kinematic and nodal force) are placed on this motion as boundary conditions. A contact tolerance is used to define a zone on either side of the contact surface. If a node is detected within this zone it is moved to the surface. This zone can be biased so that it is unevenly distributed on either side of the contact surface. This is useful in that the contact zone does not have to be very narrow to avoid dragging non-contacting elements onto the surface. It enables a reasonable tolerance to be used and avoids nodes passing through the surface. Typical tolerance values used were in the region 0.0125 to 0.016 mm. with a bias of 0.99, so that the contact zone was twice the tolerance wide and 0.01 times the tolerance above the surface.

If the reaction forces applied by the former to the workpiece are considered, it should only be capable of applying a pressure to the underside of the disk. In fact the contact occasionally fails to release the node in contact and this results in a completely anomalous adhesion force. However this must be viewed in the context of the number of nodes making contact, and whether the occurrence of occasional nodal adhesion forces represent as good a simulation as can be achieved with available computing resources. Generally changes to contact parameters that improve the contact simulation unfortunately also increase the time that it takes to run the simulation.

Further Requirements for an overall process model

The overall process simulation requires more than just an appropriate mesh for the disk. The roller and former and possibly the tailstock also have to be modelled. The model shown in Figure 3.44 represents these as rigid surfaces.

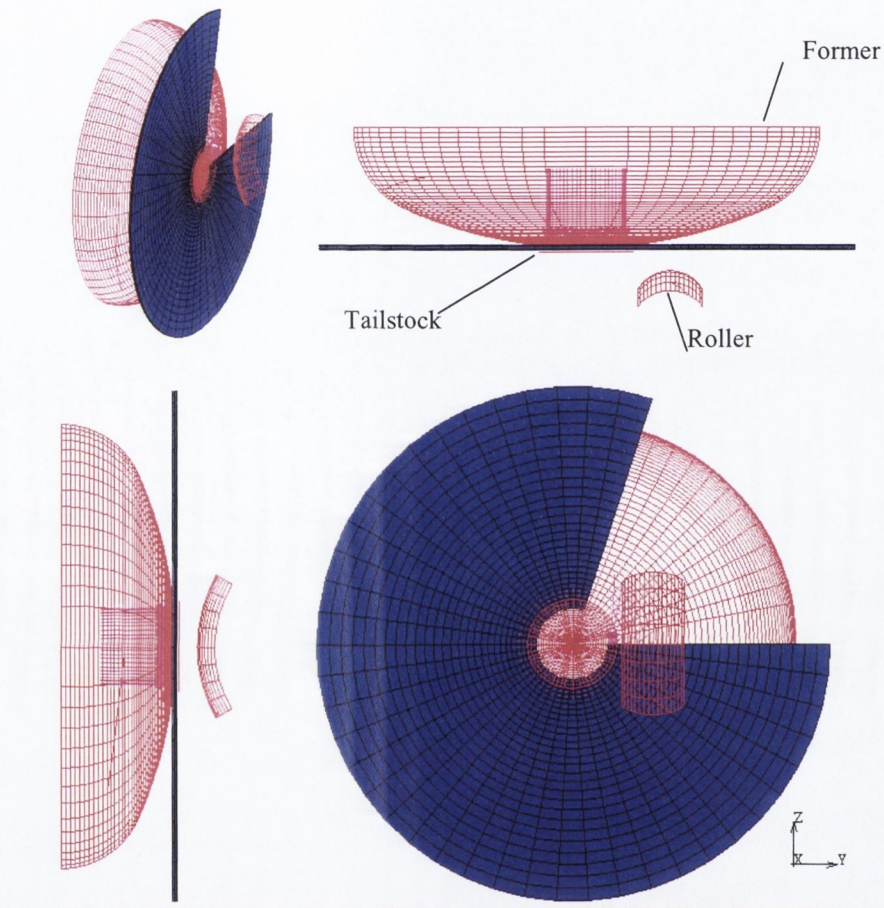


Figure 3.44 Spinning model with rigid roller and rigid former

The roller was simply defined as a segment of the surface of the roller wheel which made contact with the nodes of the meshed disk. The roller provides sliding contact with the disk.

An improved version of the roller which allowed for some elastic contact (surface deflection) with the roller was implemented by attaching a patch of mesh to the roller. This is illustrated in Figure 3.44. This was the type of roller model that was used for the full process simulations. As with the rigid roller, it provides sliding contact rather than true rolling contact. However at the level of detail that is provided by the disk mesh it provides

a reasonable model of the contact situation. Friction in the real rolling contact is small and setting the coefficient of friction to a low value provides a reasonable model. As can be seen in Figure 3.44 the area of roller covered by the mesh has been kept to a minimum and this specific mesh was designed by experimenting with different mesh positions and making adjustments to minimise contact on the edge of the mesh.

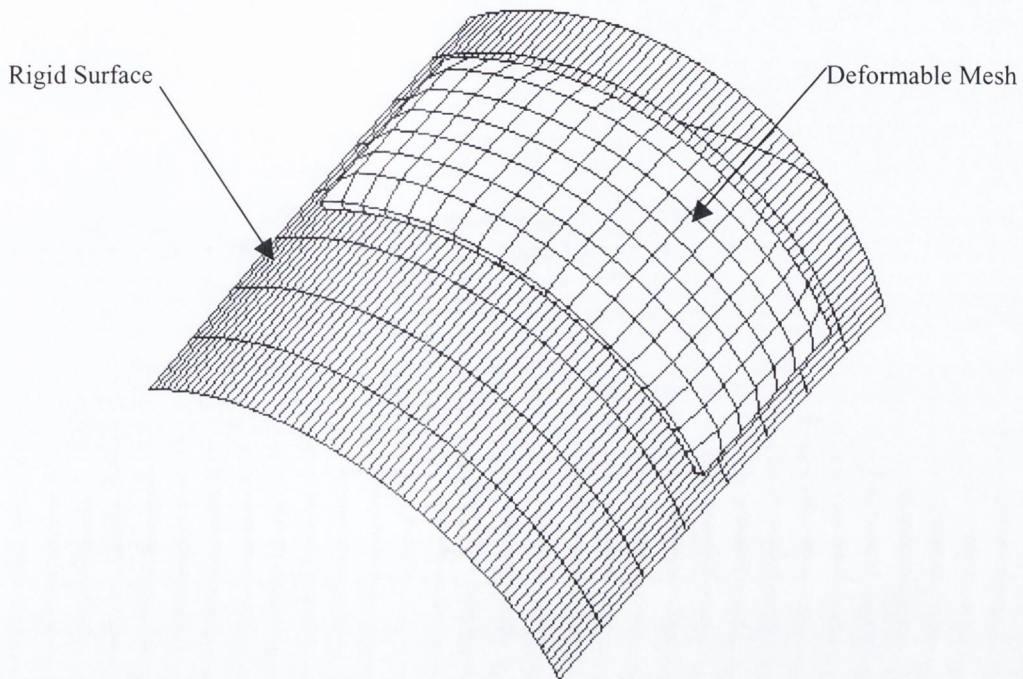


Figure 3.45 Roller model-rigid surface with attached mesh

While it was possible to add some elements to the roller at a strategic location where contact with the workpiece was found to occur there was no possibility of adding a mesh to the former as the entire area of the former would need to be covered. Such an addition of elements would make solution times completely impractical.

Implementing the roller motion

A major choice was required between rotation of the disk (mesh) as in the real spinning operation or the definition of the roller motion in a spiral path along the workpiece. This later option was finally selected, although many simulations were conducted with the entire mesh rotating. The rotation of the mesh disk was accomplished through the use of a flat disk rigid body representing the tailstock. This disk was glued to the mesh and given a fixed rotational velocity. However in order to use the multiprocessor facility in the Marc finite element code the motion of the roller was simply changed from a series of movements in a single plane to these same movements implemented while the roller orbits the stationary disk.

The Fortran code to implement this motion is almost identical to the code used for the two-dimensional axisymmetric models described earlier in section 3.5.1. The application of the rotation to the calculated position is different and this changed part of the code is presented in Appendix 4 Fortran 6.6 code for rotating full three dimensional simulation. This code was used with models such as that shown in Figure 3.46 to provide an overall process simulation.

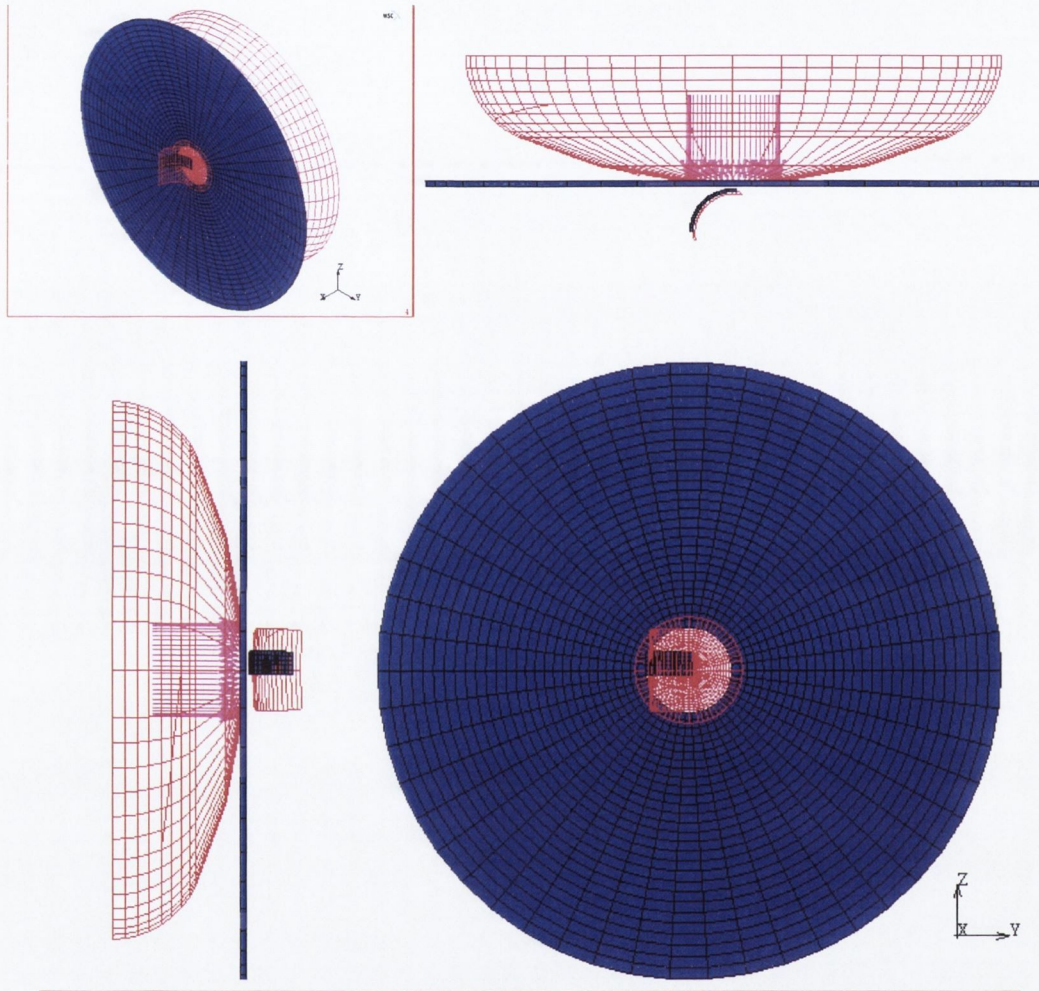


Figure 3.46 Spinning model with deformable elements on roller and rigid former

The main components of this model shown in Figure 3.46 are (1) the disk a 1700 element mesh with an internal diameter of 16mm and an outside diameter of 115mm. (2) the roller consisting of a rigid surface with a deformable 95 element mesh attached (3) the former which consists of a rigid surface and (4) the boundary conditions. The other major items involved in the model are the tool path and the material model as described in the appendices (Appendix 1 Flow Curves from Plane Strain Compression and

Appendix 4 Fortran 6.6 code for rotating full three dimensional simulation). For a full process simulation typical solution times with this model were 60 to 70 hours on a single 1.8GHz personal computer. This was achieved using a feed per revolution of 2.5mm. Reducing the feed directly increases the solution time.

3.6. Summary of Experimental Work

This chapter has outlined the four major types of experiments conducted. Static contact physical and FEA experiments and spinning process physical and FEA experiments. The details of the equipment used and FE models have been outlined. The next chapter presents and compares the outcomes of these experiments and interprets the results to provide insights that can contribute to the design of new incremental forming processes.

CHAPTER 4. RESULTS AND ANALYSIS

4.1. Introduction to Results and Analysis

This chapter begins with the results of the direct contact experiments and simulations. They provide significant insight into what is presented in the subsequent section dealing with the results of the spinning experiments and the finite element simulations. The direct contact experiments provide an understanding of the tool force line stiffness and the variations in this stiffness that occur during the spinning process. Although the same roller and former are used throughout any given experimental spinning process there are changes in tool force line stiffness because of configuration or orientation changes during the process. These direct contact experiments also show where the maximum stress occurs due to simple direct loading and these give some insight into the magnitude of the forces that might be required to achieve the workpiece deformation during a spinning process.

In the spinning process experiments it is shown that a reasonable prediction of the process is achieved with finite element simulation. Finite element prediction of the components of the roller force during the process compare well with the roller force components that were measured experimentally. Deformed shapes of the workpiece from the finite element models are compared to the experimental deformed shapes. Predicted and measured workpiece shapes both during and after the spinning process are compared. Experimental and predicted part thickness and therefore thickness strain also compare favorably. Having assessed the validity of the finite element process model it is shown that the variation in roller force during the spinning process can be attributed to the shape or configuration of the workpiece during the spinning process.

The mesh of the finite element model was locally refined which allowed further analysis to provide new insight into the deformation mechanism occurring as the workpiece contacts the roller during the spinning process. It is possible to determine what strains have been produced and how this is accomplished in the roller contact region. The strains from the finite element model are compared to the experimental and idealised process strains leading towards a conclusion that conventional spinning can be best described as an incremental stretch forming process.

4.2. Results of Static Contact Analysis

Static Analysis of Tool Force Line Stiffness.

The following two subsections present analytical information on the tool force line stiffness. These are firstly classical contact mechanics and secondly static contact simulations using finite element analysis. These analyses provide information on contact conditions arising from the use of different materials in the roller and the former. In particular the stiffness of the contact and the area of contact are evaluated. Establishing the likely area of contact is very relevant to the study of the spinning process and a knowledge of the stiffness gives some basis for predicting forces from programmed displacement particularly as the machine tool to be used in the spinning experiments has no force limiting or control system.

4.2.1. Hertzian Analysis Applied to the Roller and Former in Static Contact.

The basic Hertzian solution to elastic contact between two solids can be applied to the situation where the spinning tools, i.e. the roller and former, are brought into contact with each other with no workpiece present.

Obviously this Hertzian analysis does not directly yield any information about the stress in the workpiece but it does set some boundaries for the size of the elastic contact area between roller and former and for stiffness of the elastic contact i.e. tool force line or load line stiffness.

If the working force generates a certain contact area when it pushes the roller and former together with no workpiece present, it is to be expected that the same working force will generate a larger area with a compliant workpiece in place. Thus the Hertzian elastic contact analysis can provide a lower bound estimate of the size of the contact area.

If however the workpiece thickness is small in comparison with the dimensions of contact between the roller and former, and is therefore reasonably stiff, then it should not greatly change the contact area. Otherwise the workpiece will behave like a thick gasket, and conform to the roller and former shapes, spreading the load over a much larger area than would be the case in the Hertzian analysis.

This Hertzian analysis gives some insight into the effect of changing the elastic modulus of the roller and the former i.e. using say nylon rather than steel as the material for the roller or mandrel.

When two elastic solids are brought into contact with a given force the displacement that occurs after initial contact as the force is applied can be measured as the reduction in

distance between points in each solid that are remote from the area of contact. This change in position of the tools will be termed a 'prescribed displacement'.

In Hertzian analysis the contact between two bodies is approximated by the contact of a sphere and a plate. The exact analytical form of the analysis for Hertzian contact has been expressed in a readily usable form by Slocum [145]. These are given in equations 4.1 through 4.6 below.

$$E_e = \frac{1}{\frac{1-\nu_1^2}{E_1} + \frac{1-\nu_2^2}{E_2}} \quad \text{Equation 4.1}$$

where ν_1 and ν_2 represent Poisson's ratio for the two materials

where E_e is the equivalent modulus of elasticity for the contact, and E_1 and E_2 are the modulus of elasticity for the material of the two bodies and R_{eq} is the radius of the equivalent sphere and R_1 R_2 are the major and minor radii of curvature of one body and R_3 R_4 are the major and minor radii of curvature of the other body.

$$R_{eq} = \frac{1}{\left\{ \frac{1}{R_1} + \frac{1}{R_2} + \frac{1}{R_3} + \frac{1}{R_4} \right\}} \quad \text{Equation 4.2}$$

A function $\text{Cos}\theta$ is defined as

$$\text{Cos}\theta = R_e \left[\left(\frac{1}{R_1} - \frac{1}{R_2} \right)^2 + \left(\frac{1}{R_3} - \frac{1}{R_4} \right)^2 + 2 \left(\frac{1}{R_1} - \frac{1}{R_2} \right) \left(\frac{1}{R_3} - \frac{1}{R_4} \right) \text{Cos}2\phi \right]^{\frac{1}{2}} \quad \text{Equation 4.3}$$

where ϕ is the angle between the planes defined by the local principal radii of curvature and common the surface normal. This angle is zero in the case of the spinning setup described previously.

Factors α, β, γ are defined as

$$\begin{aligned} \alpha &= 1.939e^{-5.26\theta} + 1.78e^{-1.09\theta} + 0.732/\theta + 0.221 \\ \beta &= 35.228e^{-0.98\theta} - 32.424e^{-1.0475\theta} + 1.486\theta - 2.634 \\ \gamma &= -0.214e^{-4.95\theta} - 0.179\theta^2 + 0.555\theta + 0.319 \end{aligned} \quad \text{Equation 4.4}$$

where e is the base for natural logarithms and where θ is defined by Equation 4.3 above

Major and minor semiaxis dimensions of the contact area are given by

$$c = \alpha \left(\frac{3FR_e}{2E_e} \right)^{\frac{1}{3}} \quad \text{and} \quad d = \beta \left(\frac{3FR_e}{2E_e} \right)^{\frac{1}{3}} \quad \text{Equation 4.5}$$

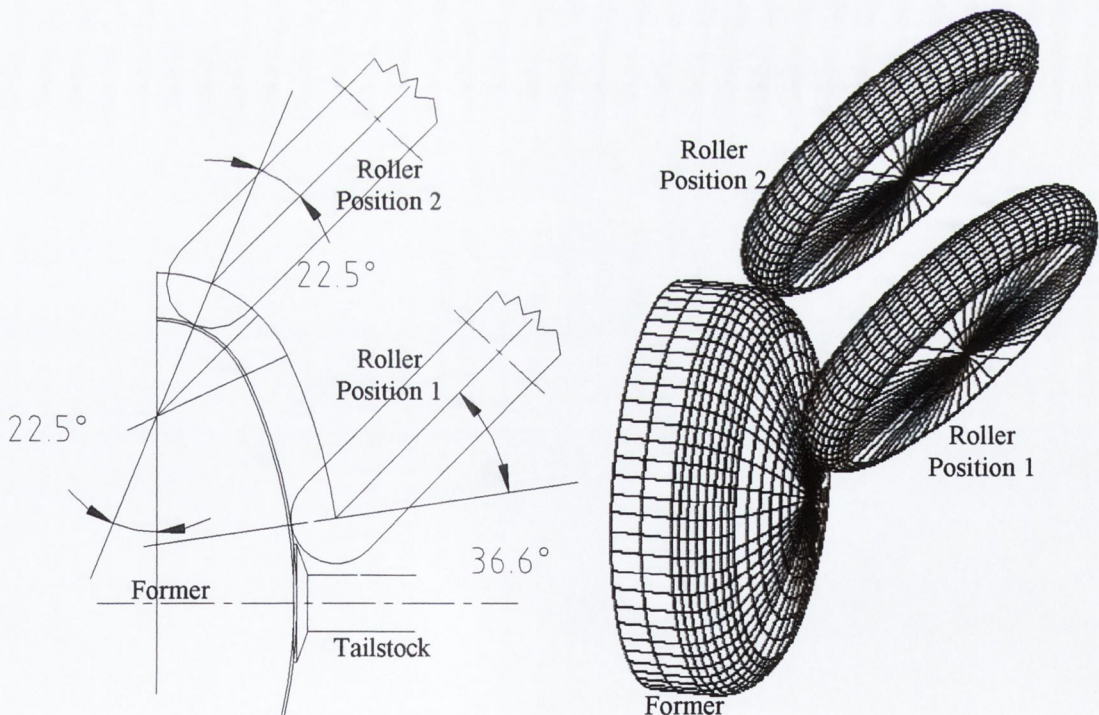
The deflection of the system due to elastic deformation of the bodies

$$\delta = \lambda \left(\frac{2F^2}{3R_e E_c^2} \right)^{1/3}$$

Equation 4.6

Applying these equations the results shown in Table 4.1 were produced. In this case the contact between two solids is assumed, and so it considers only the roller and former and ignores the existence of the workpiece.

The production of Table 4.1 is based on consideration of a roller with a diameter of 100mm and a wheel edge radius of 8mm coming into contact with the former described previously in section 3.4.6. As stated earlier the former has two regions; one with a spherical surface of radius 95mm and the second a toroidal region defined by radii of 17mm and 33mm. So the contact geometry under consideration is a wheel making contact with a sphere and secondly a torus. Local principal radii used in the Hertzian analysis are those of the generating geometry, but modified to allow for inclination of the roller to the former as shown in Figure 4.1. So these principal radii have the following dimensions in position 1: former 95mm, 95mm, roller 8mm, $50/\cos 36.6^\circ$ (=62.28mm) and in position 2: former 17mm, $50/\cos 22.5^\circ$ (=54.12mm) and roller 8mm, $50/\cos 22.5^\circ$ (=54.12mm).



Drawingspin010303-geom-check030118-4.wmf

Figure 4.1 Configurations of Roller and Former

The calculations for Hertzian contact were based on the use of three different material combinations for the roller and former; firstly both steel, secondly nylon and steel, and thirdly both nylon. The Hertz calculation makes no distinction about which body has the lower modulus of elasticity because an equivalent modulus of elasticity is calculated. The values listed in Table 4.1 are as follows; (1) the dimensions of the contact area given as the lengths of the contact ellipse semi axes and the radius of a circle having the same area, (2) the contact stress or pressure, (3) the deflection or distance traveled towards each other by points in each of the contact bodies that are remote from the contact region and (4) the stiffness of the contact between roller and former. The contact stress calculated is the maximum contact pressure which is 1.5 times the average contact pressure and this factor is characteristic of Hertzian pressure distributions as described earlier in section 2.3.1, Figure 2.29.

Size of Contact Area

The ellipse dimensions given in Table 4.1 are the major and minor semi-axis dimensions for the elliptical contact area. The size of the contact area is significant when modeling the process using finite element models. From the point of view of designing an effective finite element simulation it helps to establish the density of nodes that would be required to model the contact area in detail. When it is required to simulate a steel roller it would be desirable to have a finer mesh to simulate the contact because of the smaller area involved. These contact area results in Table 4.1 are a first indication of the size of the deformation zone. It is also of great significance when deciding on the required feed per revolution of the roller on the former.

Comparison of Stresses

It can be seen from Table 4.1 that as would be expected the calculated values of contact normal stresses are large when both the roller and former are made of steel. When Nylon is the material for either the roller or former, the contact normal stress is greatly reduced, and coincidentally the contact pressure approaches a value similar to the flow stress for the workpiece i.e. for commercially pure aluminium.

Table 4.1 Hertzian elastic contact predictions (roller touching former with no workpiece)

Force (N)	100	200	300
Nylon-nylon position 1			
Contact ellipse (mm)	1.54	1.95	2.23
Contact ellipse (mm)	0.53	0.67	0.76
Radius same area circle (mm)	0.90	1.14	1.30
Contact Stress (N/mm ²)	58	74	84
Deflection (mm)	0.050	0.080	0.105
Stiffness (N/mm)	1986	2502	2864
Nylon-nylon position 2			
Contact ellipse (mm)	1.38	1.74	1.99
Contact ellipse (mm)	0.48	0.61	0.69
Radius same area circle (mm)	0.81	1.03	1.17
Contact Stress (N/mm ²)	72	91	104
Deflection (mm)	0.056	0.089	0.117
Stiffness (N/mm)	1785	2249	2574
Nylon-steel position 1			
Contact ellipse (mm)	1.23	1.55	1.78
Contact ellipse (mm)	0.42	0.53	0.61
Radius same area circle (mm)	0.72	0.91	1.04
Contact Stress (N/mm ²)	92	116	132
Deflection (mm)	0.032	0.051	0.067
Stiffness (N/mm)	3123	3935	4505
Nylon-steel position 2			
Contact ellipse (mm)	1.10	1.39	1.59
Contact ellipse (mm)	0.38	0.48	0.55
Radius same area circle (mm)	0.65	0.82	0.94
Contact Stress (N/mm ²)	113	143	163
Deflection (mm)	0.036	0.057	0.074
Stiffness (N/mm)	2807	3537	4049
Steel-steel position 1			
Contact ellipse (mm)	0.37	0.47	0.54
Contact ellipse (mm)	0.13	0.16	0.18
Radius same area circle (mm)	0.22	0.27	0.31
Contact Stress (N/mm ²)	1005	1266	1450
Deflection (mm)	0.003	0.005	0.006
Stiffness (N/mm)	34187	43074	49307
Steel-steel position 2			
Contact ellipse (mm)	0.33	0.42	0.48
Contact ellipse (mm)	0.12	0.15	0.17
Radius same area circle (mm)	0.20	0.25	0.28
Contact Stress (N/mm ²)	1239	1562	1788
Deflection (mm)	0.003	0.005	0.007
Stiffness (N/mm)	30727	38714	44316

Contact Stiffness

Contact stiffness is the force generated by a given prescribed displacement divided by the prescribed displacement. The values of contact stiffness range from 2kN/mm to near 50kN/mm these can be compared to the stiffness of the machine tool or that of the dynamometer 600N/ μ m (600kN/mm) [52]. So the contact system represents a relatively soft spring element in the tool force line. The steel former to steel roller contact stiffness

ranges to nearly 50kN/mm but it is apparent that these tools would need to be made of the hardest of tool steel if the contact stress is to be sustained without the steel components yielding.

It can be seen that by using nylon as the material for the tool or former, the stiffness of the contact system is greatly reduced. The maximum steel-nylon contact stiffness in Table 4.1 is less than 5kN/mm. The use of a softer tool or former reduces the sensitivity to variations from the ideal gap between the roller and the former e.g. due to run-out or geometrical inaccuracies in the shape of the former.

Deflection

The deflection gives useful information to aid programming tool movement and modelling the theoretical gap between the roller and the former. Spinning often requires the gap to be set to a value less than the original thickness of the workpiece. Tool movement was described as 'at a constant distant from the surface' in section 3.4.7, and illustrated in Figure 3.31, so this gap or distance can be more easily set if the deflection of the tool surfaces is known.

It is also useful to consider the results of these calculations in graphical form. Figure 4.2 presents the relationship between force and prescribed displacement i.e. the displacement that occurs after initial contact as the force is increased. This prescribed displacement of the roller and former is measured as the reduction in distance between points in each solid that are remote from the area of contact. (When two elastic solids are brought into contact with a given force the displacement, that occurs after initial point contact as the force is applied, can be measured as the reduction in distance between points in each solid that are remote from the area of contact. This change in position of the tools is termed a 'prescribed displacement'.)

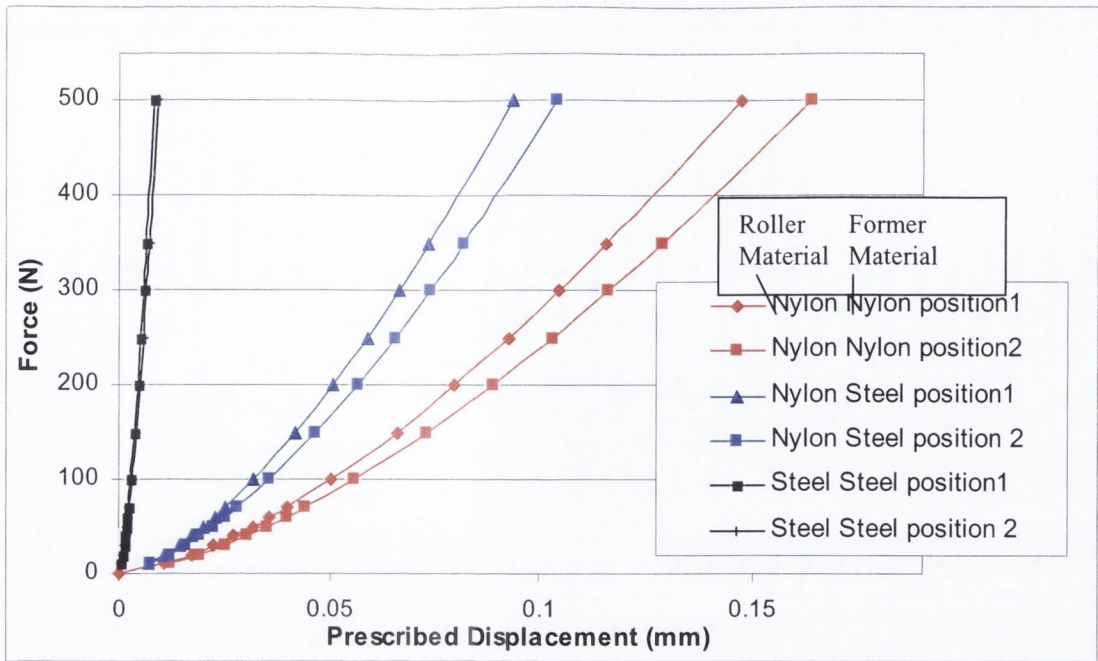


Figure 4.2 Force variation with Prescribed Displacement (Hertz theory)

Note that the labels 'position 1' and 'position 2' in the legend of Figure 4.2 through Figure 4.6 and subsequent diagrams refer to the roller position on the former as depicted in Figure 4.1 page 103. The distinction between the contact characteristics of these two positions show that significant variation occurs during the spinning process without any tool change. Figure 4.3 shows the relationship between force and contact area. It can be seen that in all cases the contact area is larger in position 1 than in position 2

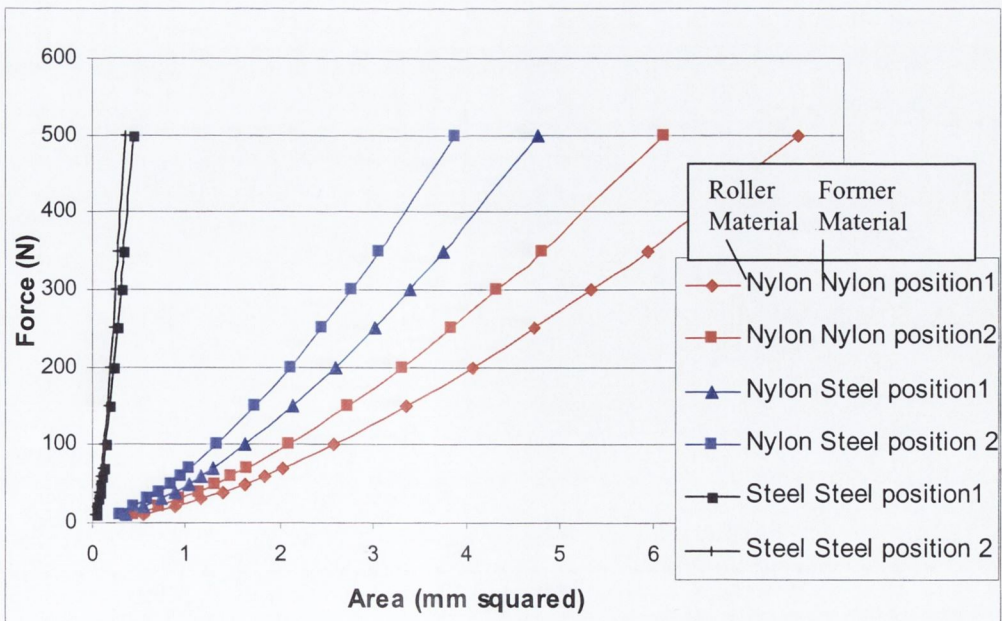


Figure 4.3 Contact area against Force from Hertz Theory

From these figures it can be seen that as would be expected the use of nylon for the former and roller results in a much larger contact area. Also if nylon is used for either of these components there is a major reduction in contact stiffness and a corresponding increase in contact area compared to the steel roller and steel former combination.

4.2.2. Finite Element Predictions of Static Contact

Because these models include a mesh to represent the workpiece they are more likely to give a better prediction of the contact stiffness and the resulting contact area when the roller is pushed towards the former. It is to be expected that the contact area produced when a steel roller and former are pushing on opposite sides of a workpiece will be larger than that predicted by classical contact analysis for direct steel to steel contact. Similarly contact stiffness will be lower. With a nylon roller and former the contact area will also change when the workpiece is introduced.

It is of course possible to run the finite element simulation for elastic tools touching without any workpiece present. This simulation is simply a reduced version of the model described earlier in section 3.3.4. As would be expected the results are in general agreement with the Hertzian predictions. The force displacement curves for this condition are plotted in Figure 4.4 and compared with the corresponding predictions by the Hertzian analysis from Figure 4.2, which are plotted in grey.

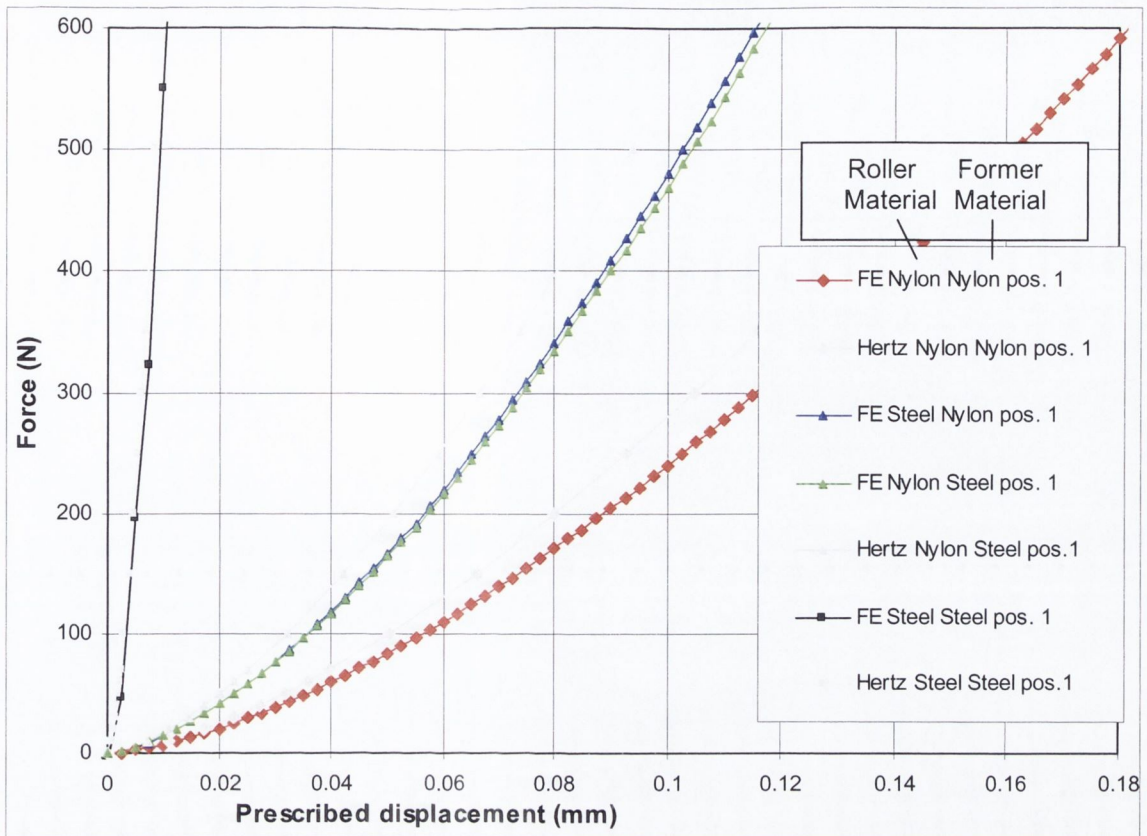


Figure 4.4 Comparison of Hertz and FE Predictions of Contact Force (No Workpiece)

It can be seen from Figure 4.4 that in general there is reasonable agreement about the shapes of the force displacement curves. The finite element predictions are lower than the Hertz theory predictions. This is particularly noticeable where nylon is used, and for which the finite element predictions are about 20% lower than the Hertz theory, while the differences for steel to steel contact in the Figure 4.4 are less than 10%. The smaller deflections involved in this case imply that the calculations were applied to a situation that is nearer to the ideal for which Hertz theory was derived i.e. for small deflections.

There are two curves from the finite element results for the combination of nylon and steel (roller and former). Unlike the Hertz analysis which makes no distinction between which body has the lower modulus of elasticity with the finite element model there is one curve for nylon roller and steel former and the second curve for steel roller and nylon former. The results in Figure 4.4 are for position 1 as illustrated in Figure 4.1. The results for position 2 were entirely comparable. The FE results were somewhat lower than the Hertzian predictions but are omitted from Figure 4.4 for clarity. Figure 4.5 shows the finite element predictions of forces for positions one and two as illustrated in Figure 4.1 page 103. It can be seen that the results are broadly similar for these two positions although

there is a clear distinction. Contact characteristics can vary significantly during a spinning operation even with perfectly accurate roller and former shape and roller positioning.

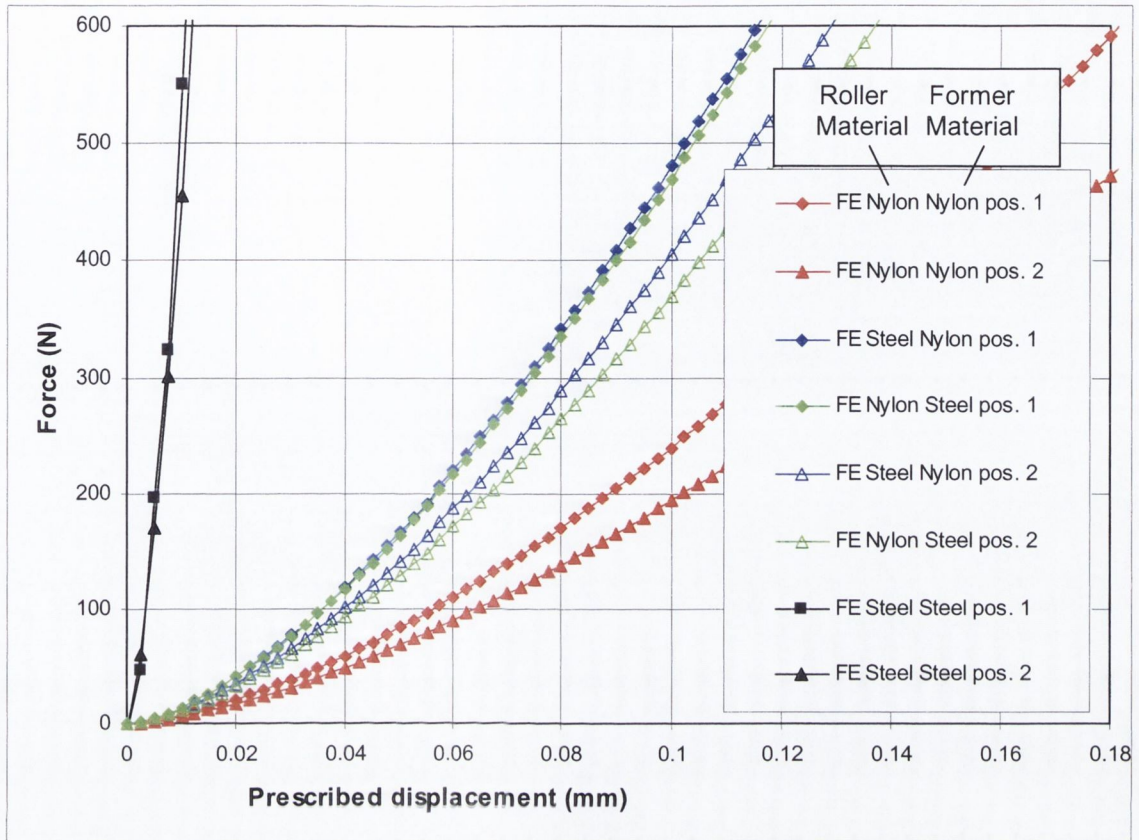


Figure 4.5 Comparison of FE predictions of force for positions 1 and 2 (no workpiece)

4.2.3. FE predictions of Static Contact with the Workpiece in place:-

For the case with the workpiece in place the models described earlier in sections 3.3.3 (page 66) and 3.3.4 (page 71) gave the following results.

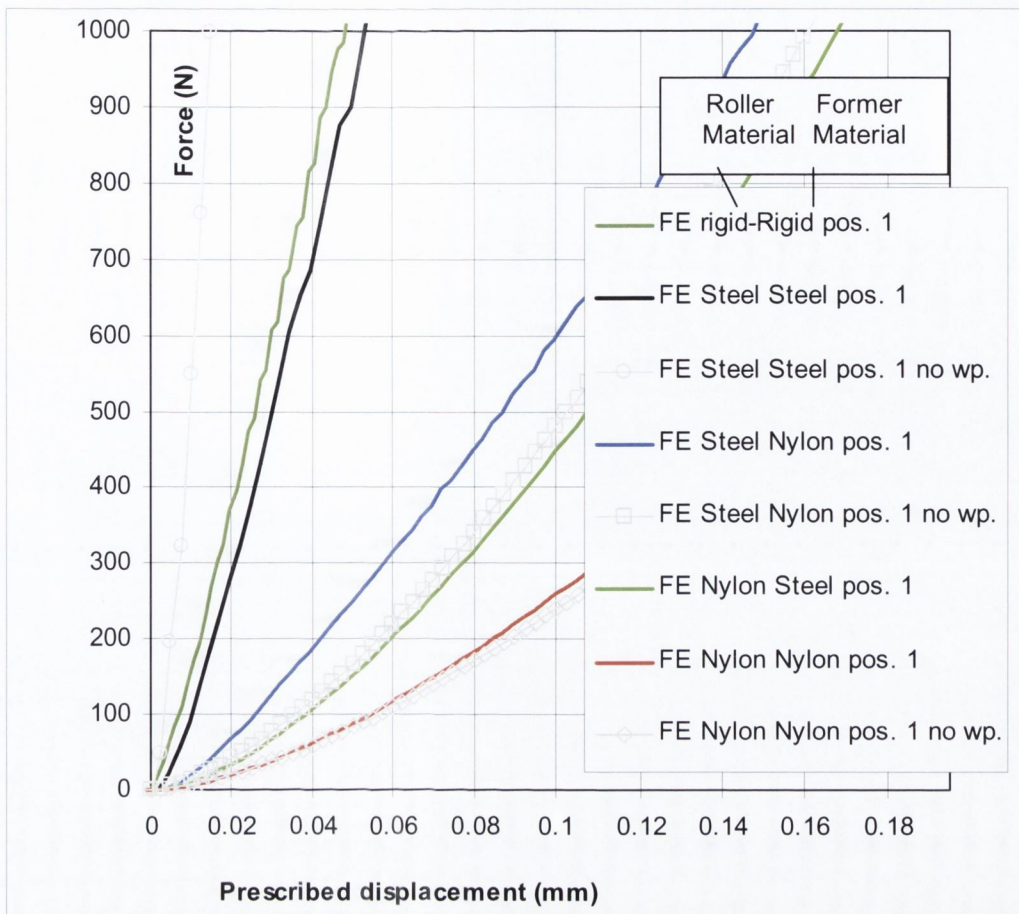


Figure 4.6 FE Predictions of contact force for position 1 (workpiece and no workpiece compared).

The results of this simulation are similar to those from the Hertzian analysis and also to those finite element results with no workpiece present. For comparison the results of FE simulations with no workpiece present are shown in grey in Figure 4.6 (these have already been presented in Figure 4.4 and Figure 4.5). It is worth noting that the introduction of the workpiece has significantly changed the stiffness of the steel roller and steel former combination, it has become much less stiff than the Hertzian predictions for direct contact between the roller and the former. In fact the force displacement curve with steel roller and former with the workpiece in place, is very close to that for rigid roller and rigid former as described in section 3.3.3 page 66. In other words it is the compliance of the workpiece rather than the roller and the former that is the determining factor.

The slight ripple, noticeable in some curves, is due to the fact that the contact is discrete. Each time a new node comes into contact it brings with it an area of contact represented by the element edge length.

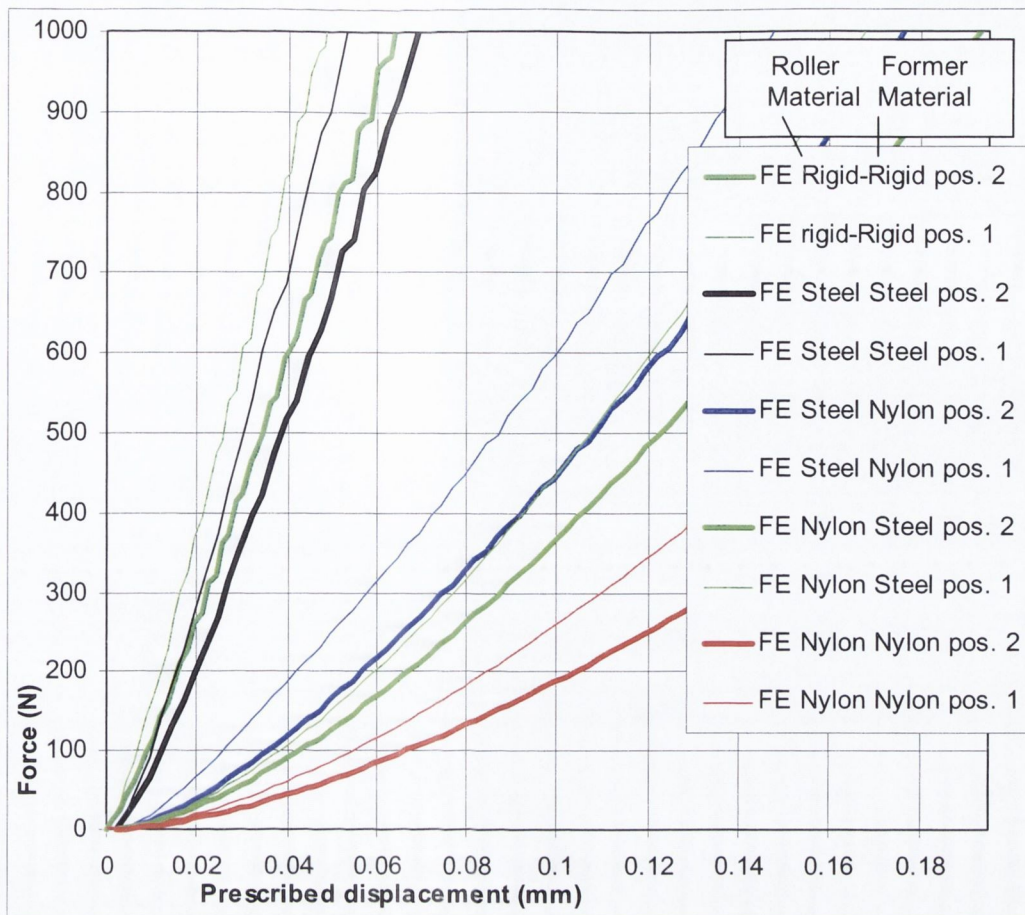


Figure 4.7 Stiffness predictions from finite element models (with workpiece).

Figure 4.7 shows the finite element predictions of forces for positions one and two as illustrated in Figure 4.1. It can be seen from Figure 4.7 that the force for a given displacement is lower for position 2 (shown as thick lines) than for position 1 (shown as thin lines) but results are broadly similar for these two positions. Position 2 has smaller contact radii on both the roller and former and so position 2 will bring a smaller area of the workpiece into contact and so maybe expected to produce a lower force for a given prescribed displacement.

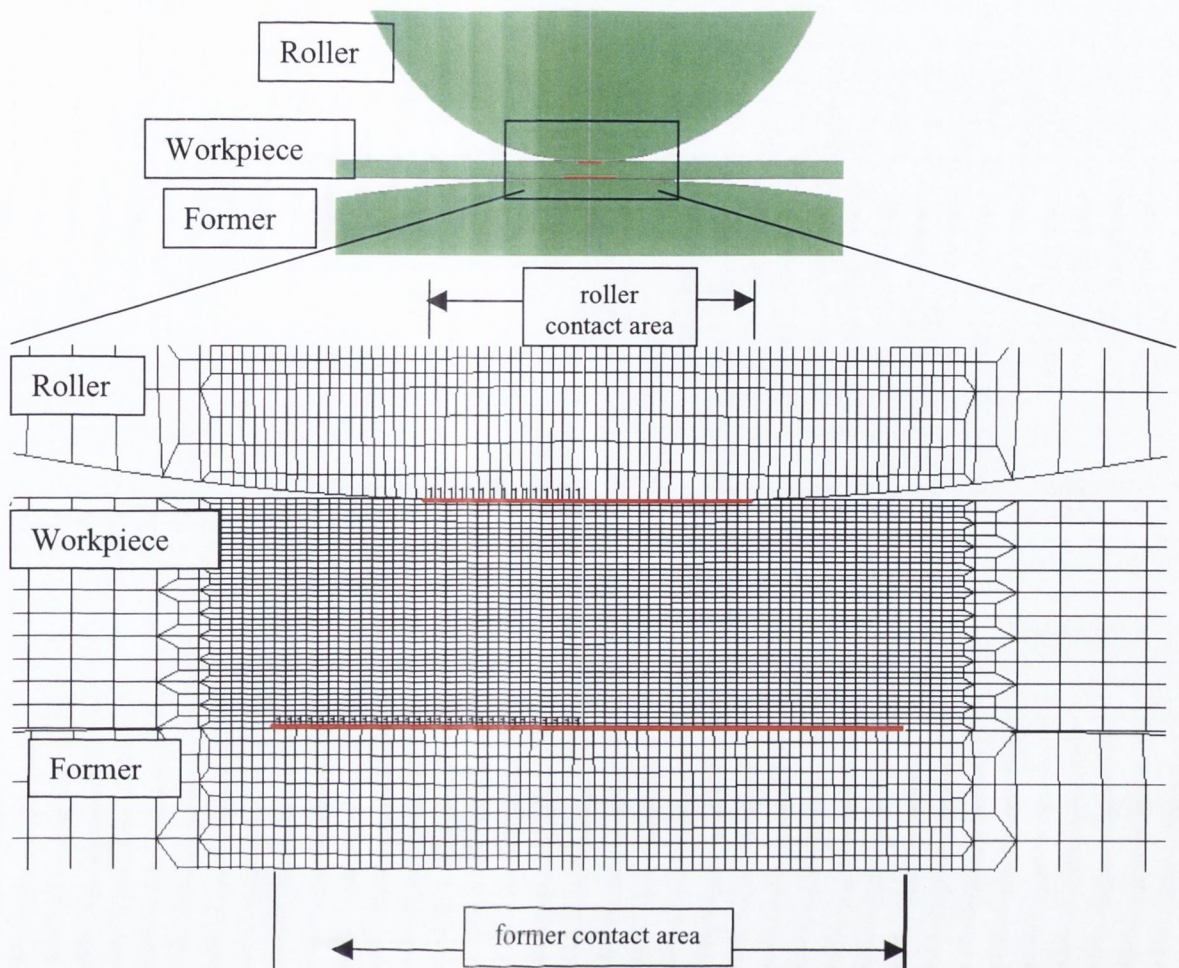


Figure 4.8 Axisymmetric Model –different sizes of contact areas (red on detail))

Area of contact

The predicted contact area can be plotted as a function of applied force. The results will of course have two contact area results i.e. one area for the workpiece in contact with the roller and probably a larger area for contact between the workpiece and the former as shown in Figure 4.8. The geometry of the surface and the elasticity of the materials will determine the actual areas of contact. The flatter surface would in general be expected to have the larger contact area.

Plotting the variation of contact area and force as predicted by the FE simulations gives the curves shown in Figure 4.9. The relationship between force and contact area predicted by Hertz theory is also plotted in green for comparison.

In general this reflects what was already said in connection with Figure 4.4 above i.e. that the Hertz prediction of contact is stiffer than the contact that occurs when the workpiece is in place. In particular comparing the area predicted by Hertzian theory for the nylon roller and nylon former combination it can be seen that the area predicted lies half way between the roller and the former area curves. In this case the area is largely determined by the nylon as it has the lowest modulus of elasticity. In the case of the steel roller and steel former the contact areas are much larger than Hertzian theory predicts for contact between steel tools. This is because the workpiece is more compliant than the steel of the tools so the FE model predicts an increased contact area.

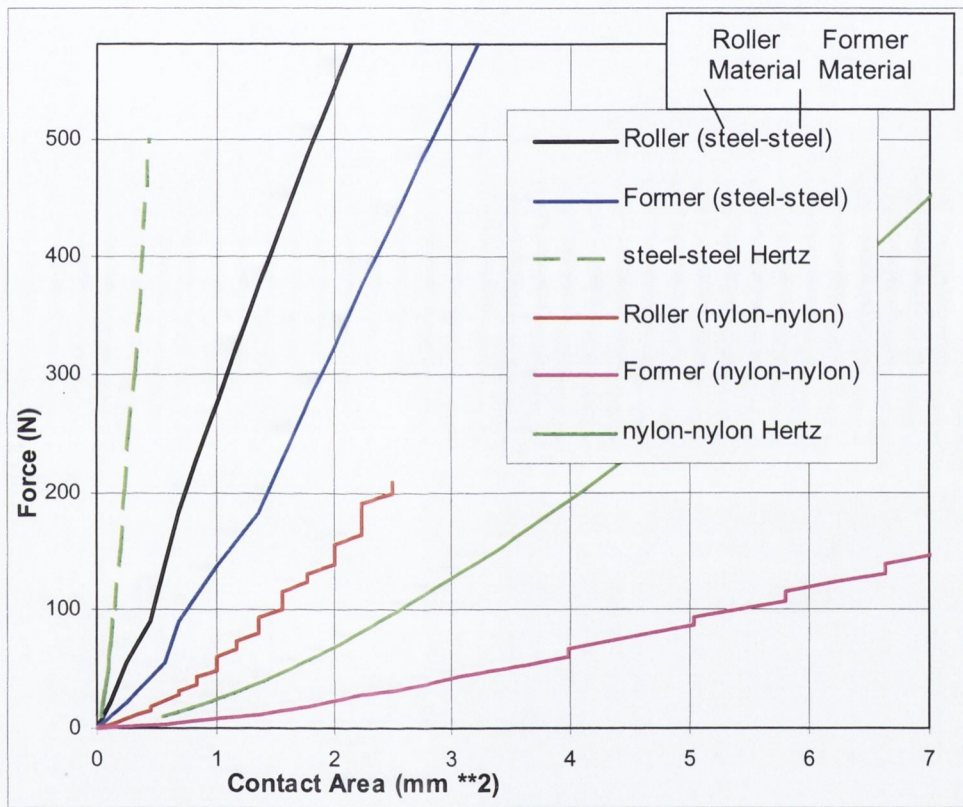


Figure 4.9 Contact Area Relationship with Force: Finite Element Prediction Vs Hertz.

The results for combinations of steel and nylon in roller and former material are plotted in Figure 4.10

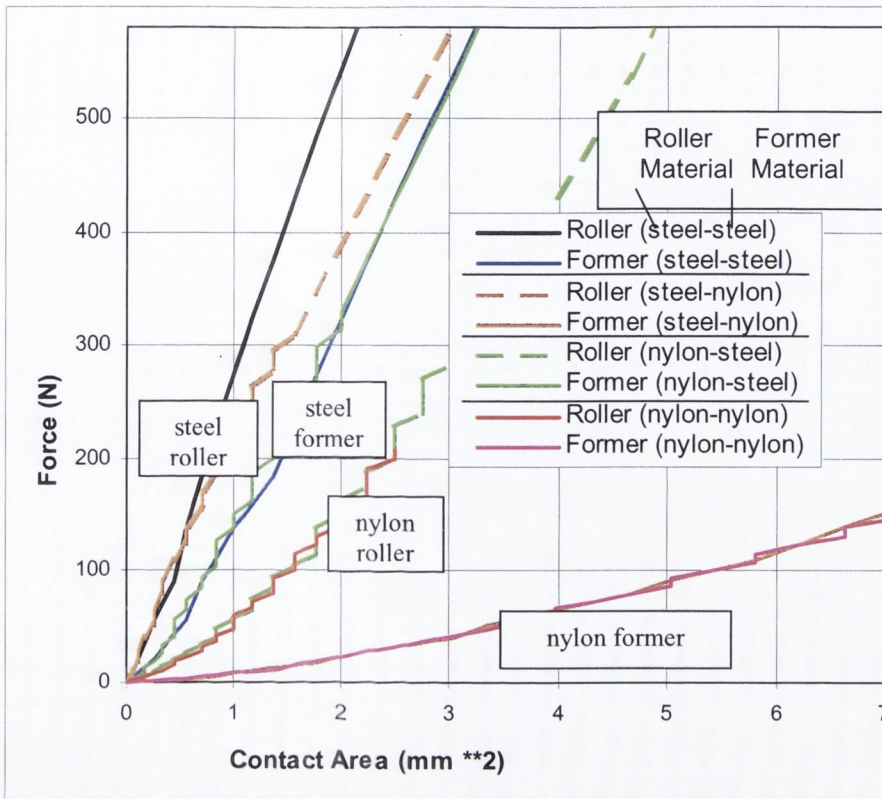


Figure 4.10 Contact Area Relationship with Force: Finite Element Prediction.

As expected the contact area with the roller is in most cases smaller for a given force than the contact area with the former. The combination of a nylon roller and steel former is an exception to this. In general the contact area developed by any individual tool is initially unchanged by the material of the opposing tool. Thus the labels on the curves in Figure 4.10 can be applied. The contact area with the steel roller does diverge for different former materials for loads over 250 Newton.

While it is interesting to see the variation of force and contact area the force is not directly controlled in programming a CNC machine tool rather it is prescribed displacement or tool position that is controlled so the following figures analyse the variation of contact area with prescribed displacement. Where it is required to achieve a certain feed per revolution in a spinning operation a knowledge of the dependence of the width of contact on the prescribed displacement enables the feed per revolution to be chosen with some confidence provided that corresponding force from Figure 4.5 and Figure 4.6 are within the capacity of the spinning equipment.

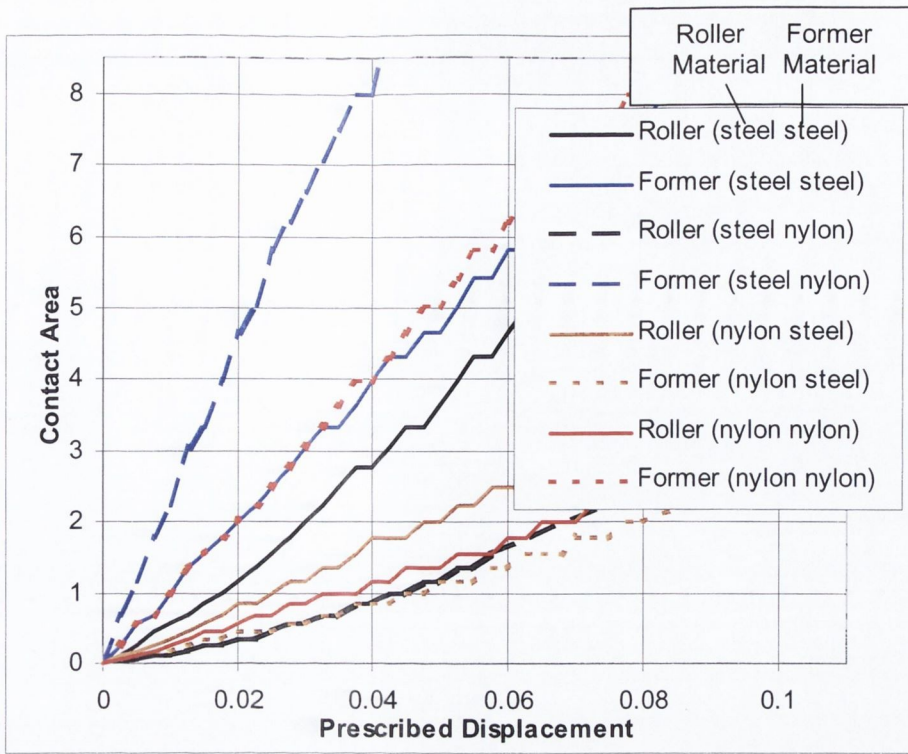
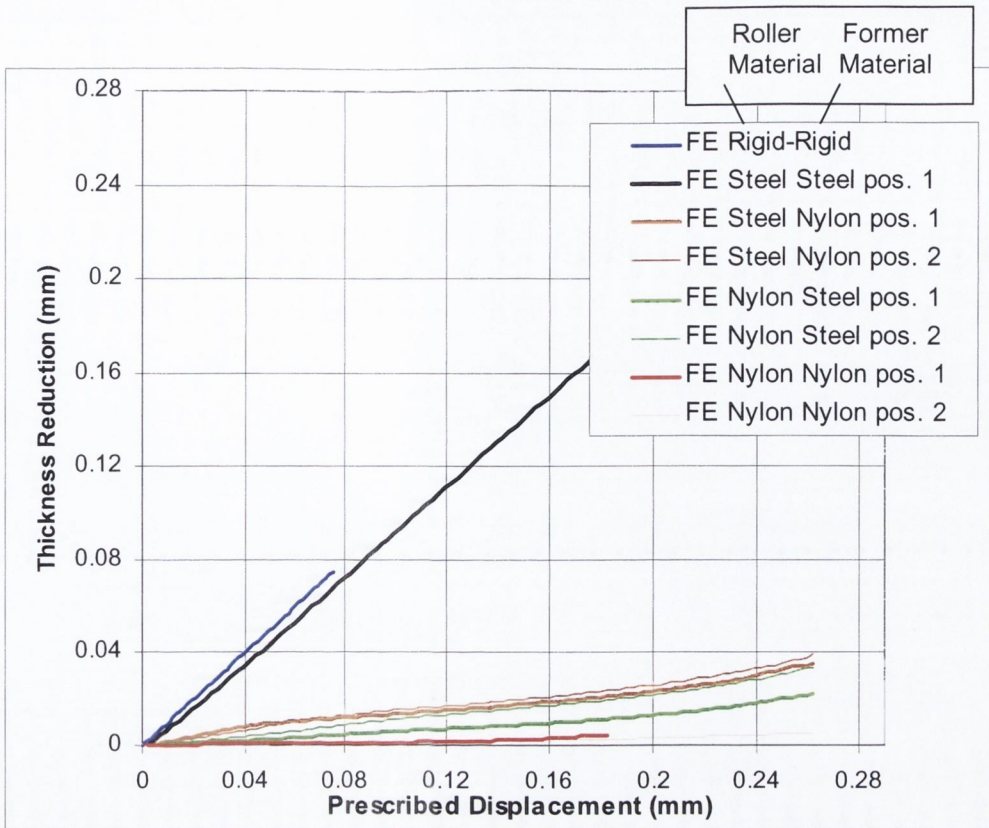


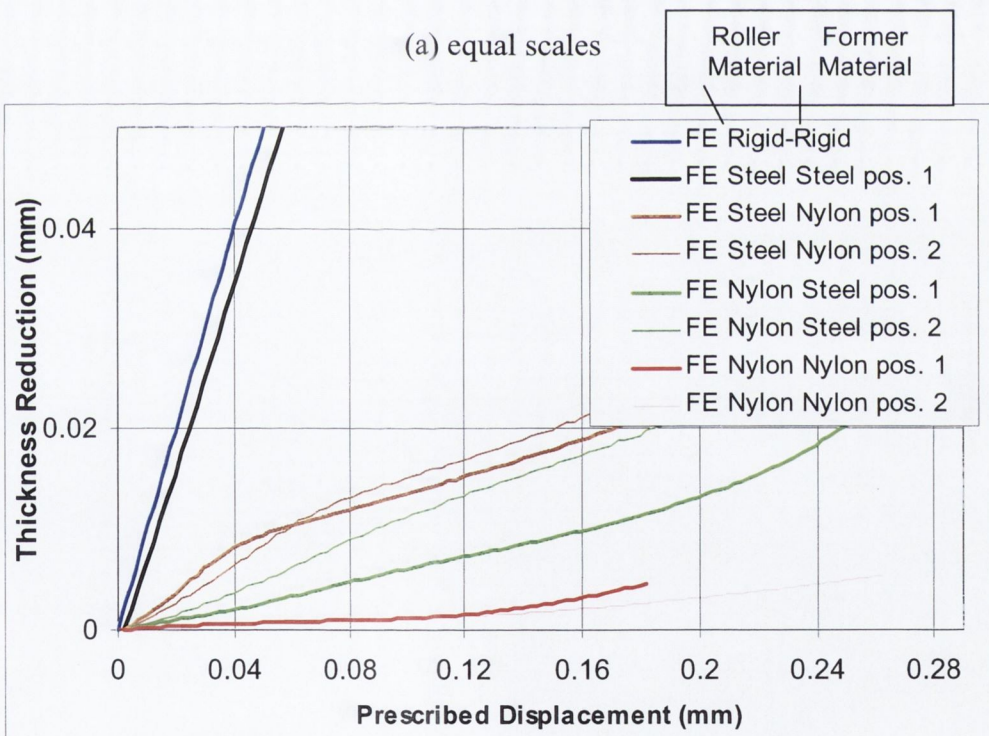
Figure 4.11 Workpiece contact area Vs Prescribed displacement from FE (roller position1).

Thickness Reduction at center of contact

Once deformable tools (roller and former) are introduced into the finite element analysis then the prescribed displacement applied to these tools is not the same as the change in thickness produced in the workpiece. Local flattening, of the roller and former surfaces, accounts for part of the imposed displacement, with the remainder being accounted for by the reduction in thickness of the workpiece itself. This is shown in Figure 4.12 which plots the variation in thickness reduction with prescribed displacement. The greatest reduction in workpiece thickness for a given tool material is achieved with the steel roller and steel former. It is closest to the rigid tool situation, which is simply a line with a 45degree slope.



(a) equal scales



(b) enlarged vertical thickness scale

Figure 4.12 Thickness reduction variation with prescribed displacement.

It is interesting to see how thickness reduction varies with applied force. Figure 4.13 presents thickness reduction against force for the case of rigid tools, steel tools,

nylon tools and combinations of nylon and steel tools. These curves are designated pos.1 and pos.2 in the legends on the graphs referring to the position 1 and position 2 of the roller on the former that is illustrated in Figure 4.1 page 103.

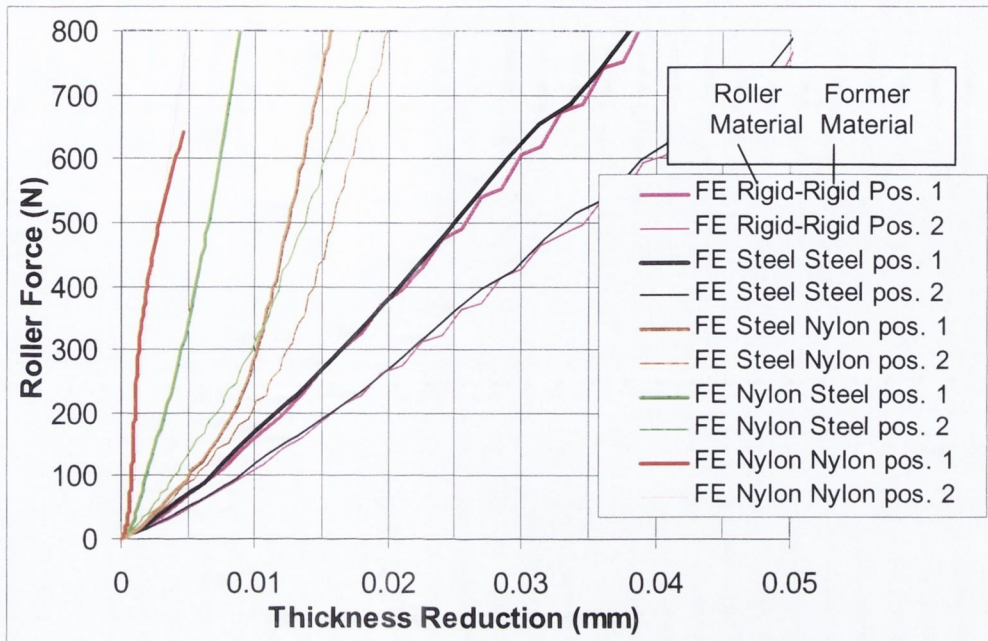


Figure 4.13 Thickness reduction variation with applied force.

It is known from the literature [27] that typical spinning forces for the manufacture in commercially pure aluminium of the experimental shape investigated here, are in the region of 500 Newton. This is also confirmed later in this report where satisfactory manufacture of the experimental part is achieved with similar forces using nylon tools. This force coupled with the hardest tools (the steel roller and former) produces a reduction of less than 0.03 mm (3% on a thickness of 1mm) and less than this again when nylon tools are used.

These small thickness changes can be compared with thickness reduction in a practical spinning operation which are typically of up to 10% [28]. Also if this direct compression was the only mechanism of thickness change every point on the workpiece would have to pass within a very small area of the center of contact to achieve the required reduction. This would imply that a very small feed should be used but feed per revolution of 2.5mm can produce satisfactory parts. A substantial proportion of the deformation must be stretch forming rather than compression.

So some further understanding of the deformation process is required to deal with this apparent discrepancy.

A loading system that does not directly change the material thickness is perhaps ideal for constant thickness spinning or a constant thickness incremental forming process.

A further interesting fact that can be obtained from Figure 4.13 is that if nylon is the material for either the roller or the former the process is reasonably insensitive to force variation in the region 300 to 500 N.

This is very useful characteristic for a practical spinning or forming process: in a real spinning process there will be geometric inaccuracies in the former shape, the roller shape and in the tool path definition but some deviation can be tolerated with little effect on the product.

4.2.4. The Results of Static Contact Physical Experiments

Results of the direct contact physical experiments described in section 3.2.2 are presented in the table below.

Table 4.2 Experimental Measurements of contact area

Roller material	Former Material	Workpiece material	Load (N)	Roller Contact				Former Contact			
				Contact area major axis (mm)	Contact area minor axis (mm)	AREA (mm ²)	Average Contact Pressure MPa	Contact area major axis (mm)	Contact area minor axis (mm)	AREA (mm ²)	Average Contact Pressure MPa
Nylon	Steel	None	350	4.2	1.7	5.6	62.9				
		None	500	4.7	2.0	7.2	69.5				
		1mm Al	500	5.3	1.9	7.8	63.9	3.5	3.2	8.8	56.8
		1mm Al	350	5.0	1.7	6.8	51.8	3.3	3.0	7.5	46.5
Nylon	Nylon	None	500	5.5	2.3	9.9	50.3				
		None	350	5.1	2.0	8.0	43.7				
		1mm Al	500	5.4	1.9	8.2	61.0	5.0	4.3	16.8	29.8
		1mm Al	350	5.1	1.7	6.7	51.9	4.5	3.8	13.4	26.1
Steel	Nylon	None	500	5.2	2.2	8.7	57.5				
		none	200	3.9	1.6	4.7	42.1				
		1mm Al	500	4.0	1.4	4.2	117.9	4.7	4.5	16.4	30.4
		1mm Al	200	3.3	1.2	3.1	64.3	4.4	4.0	13.8	14.5
Steel	Steel	None	200	2.6	1.2	2.5	81.6				
		1mm Al	500	3.8	1.4	4.0	123.7	3.6	3.3	9.2	54.1
		1mm Al	300	3.3	1.3	3.3	90.4	3.2	3.1	7.7	39.1

In the entries where there is no workpiece the roller contacts the former directly and so there is only one area of contact to be measured. The results show larger contact areas than predicted by the finite element simulations. These results can be compared to the predictions graphed in Figure 4.10. It must be remembered that while it is possible to use a contact tolerance of 0.0001mm in a finite element model in this physical test the Fuji Prescale contact detection film itself is itself 0.2mm thick. In general the contact areas detected by the Fuji Prescale film reflect the areas predicted for contact with nylon roller and former more closely than for steel roller or former. It is apparent that the film itself influenced the measurements considerably in the tests with steel tools. Also at lower forces the pattern detected by the film becomes difficult to read. Nonetheless these results provide some evidence that the analytical and finite element results have given results that are the right order of magnitude and set an upper bound on what values for contact areas might be expected to be predicted the finite element analysis.

4.2.5. Linking the study of contact areas involved in direct contact to spinning

In the direct static contact results outlined above, the strains produced are generally quite low. It can be seen from Figure 4.12 and Figure 4.13 that thickness reductions and hence strains caused by static loading are quite small when a nylon roller and former is used. These strains are small compared to those described earlier in section 2.1.9 and illustrated in Figure 2.19, page 26.

It can be clearly seen from the contact pressures presented in Table 4.2, page 120, that the stresses arising in the sheet metal as a result of such pressures are unlikely to cause significant plastic deformation. In general the typical pressure values are well below the yield strength of the aluminum workpiece material (approx. 97MPa). In spite of this it will be shown later in this chapter that a spinning operation can work well with nylon tools.

In order to obtain a better understanding of the spinning process it is useful to examine the deformation zone in some detail. The following section explores the effect of various contact pressures, when applied on a range of different areas, in generating a state of high equivalent stress through the thickness of the sheet metal. These finite element models were described in section 3.3.1, page 60 and section 3.3.2, page 63.

When a sheet is loaded by a uniform pressure applied to a small area, the stress can be raised to the yield point of the aluminium workpiece through most of its thickness i.e. on either side of a neutral surface within the thickness of the sheet. The stress is very much bending in nature where the stress is tensile on one side of the neutral surface and compressive on the other. While the entire thickness is not stressed to yield point the sheet as a whole is in a state of incipient yielding. Static loading by a uniform pressure applied to a small area does not in itself produce significant plastic deformation, in fact the strains are similar to those that were predicted in the direct contact simulations. However in this condition other loads easily deform the sheet material. These loads arise from a combination of the surrounding material and from the contact with roller and / or former.

4.2.6. The Results from Uniform Pressure FE Model

In this section it will be shown that a uniform pressure, of magnitude less than the material yield strength and applied to a small area, can produce a stress state that is close to yielding through more than 90 % of the workpiece thickness. This relates directly to spinning because as described earlier in section 3.3 page 56 the workpiece is not always directly supported.

This section describes the results from FE simulations using the models described earlier in section 3.3.1, page 60. It is of interest to study the effect on the workpiece of applying a load over similar contact areas to those generated in the static contact FE simulations. The application of the load as a uniform pressure over a small area enables this analysis to be carried out without consideration of the particular tools and tool materials and tool displacements required to create the load.

The dimensions and material constants used in the model are those associated with the experimental spinning process using the aluminium workpiece. The results are presented as dimensionless where possible e.g. stress can be plotted as stress divided by pressure.

Figure 4.14 shows typical stress contours obtained from these models. In this particular example the workpiece thickness was 2.5mm. In order to make a comparison between different sets of stress contours obtained with different workpiece thickness, the equivalent stress occurring directly below the center of the applied pressure is plotted against distance below surface.

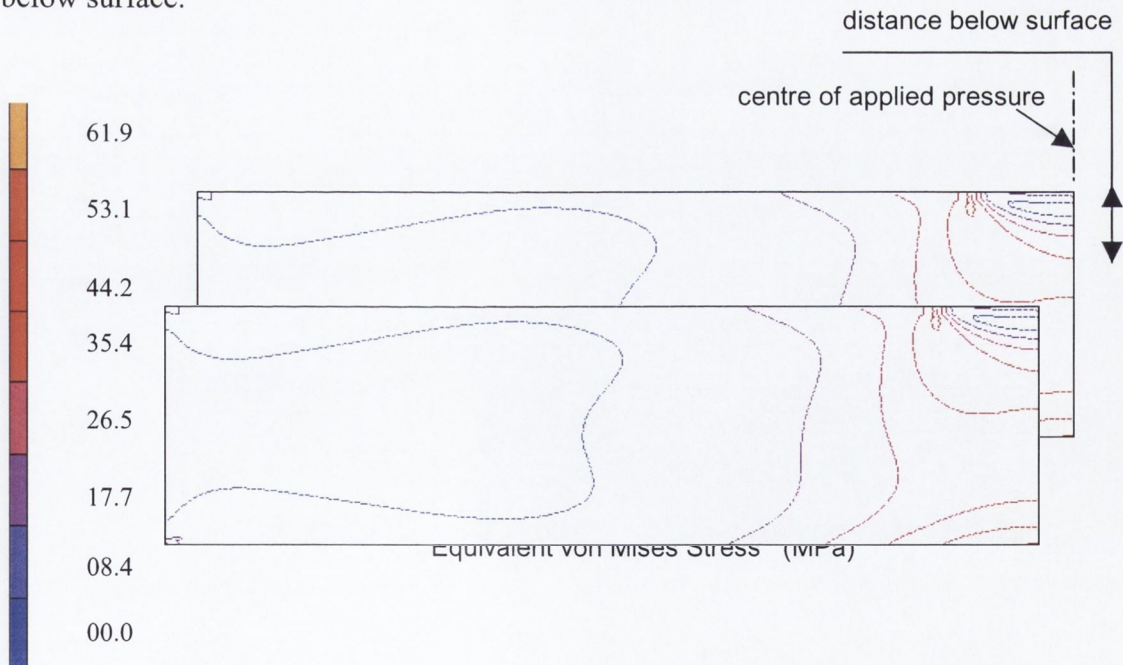


Figure 4.14 Axisymmetric Finite Element Model Constant pressure typical results

Stress variation with Depth below Workpiece Surface

With a workpiece depth of 16mm the stress contours are very similar to those predicted by the closed form analytical solution given by Johnson [41], Figure 4.15. The singularity that occurs at the edge of the loaded area in the analytical model is not reproduced exactly in the finite element simulation. The contours plotted in Figure 4.15 for the finite element simulation are for plane strain to enable comparison with the textbook [41] analytical solution. The maximum stress occurs at a depth equal to half the width of the area to which the pressure is applied in both cases. This agreement on depth to maximum shear stress demonstrates the FE simulation is in good agreement with and the closed form analytical solution.

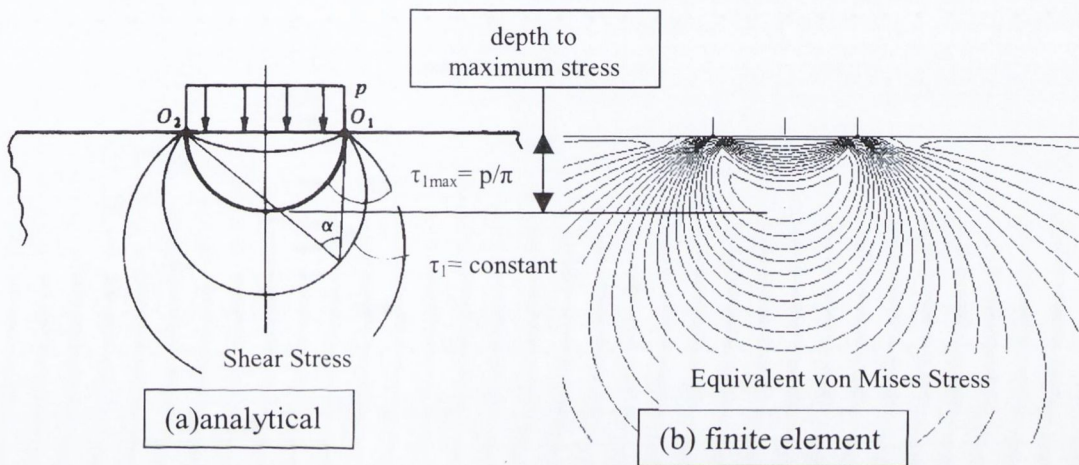


Figure 4.15 Stress contours for a pressure load (a) analytical [41] Vs (b) FE solution

The scale on the vertical axis is the actual distance divided by the radius of the area to which the pressure is applied and so is dimensionless

While the comparison above is for plane strain an axisymmetric analysis will better reflect roller contact in metal spinning. Also to further demonstrate the similarity between the finite element and the analytical solution the variation in principal stress along the line directly below the center of contact is plotted in Figure 4.16. This shows how these stresses vary inside the material with increasing distance from the surface where the load is applied. The stresses presented in Figure 4.16 are σ_z the stress in the direction of the applied pressure, σ_r the stress perpendicular to this direction and $\tau = (\sigma_z - \sigma_r)/2$ the shear stress. These stresses are plotted against the distance below the surface on the vertical axis. Part (a) of Figure 4.16 is from an analytical solution presented by Johnson [41] for axisymmetric loading with constant pressure. Figure 4.16 (b) is the same principal stresses predicted by the finite element simulation. Also added in part (b) of this figure is the von Mises equivalent stress. The von Mises

equivalent stress contour is a convenient form of output from the finite element model rather than plotting two direct stresses and a shear stress.

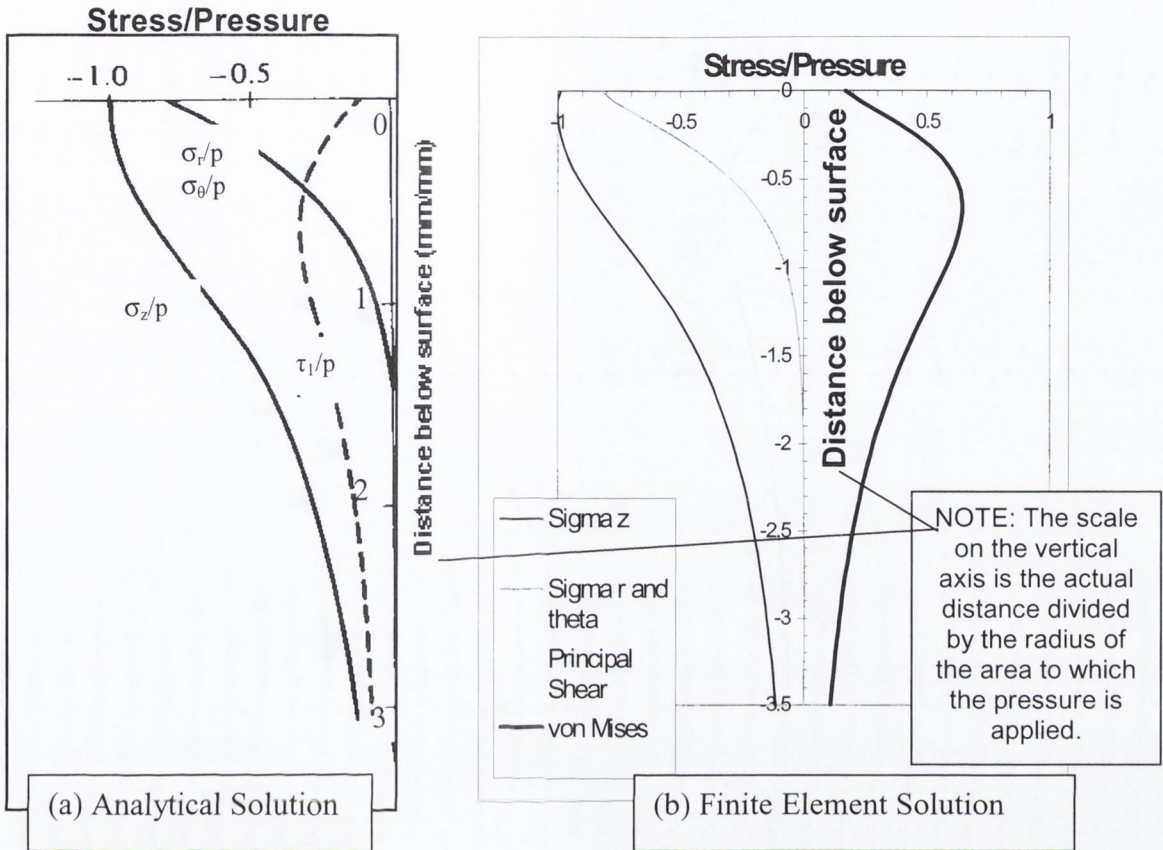


Figure 4.16 Analytical and FE prediction of Stress Vs dimensionless distance below the surface generated by a uniform pressure.

The finite element prediction of variation in the magnitude of the von Mises equivalent stress with increasing distance from the surface where the load is applied is given in Figure 4.17. The figure shows how the distribution of equivalent stress below the contact surface changes with the changing thickness of the workpiece or solid supporting the pressure. As the thickness of the part is reduced the stress distribution changes. The maximum equivalent stress occurs below the surface in the case of a semi-infinite solid but for a thin plate or sheet the maximum equivalent stress occurs at the surface. In fact it occurs on the surface away from the surface where the load is applied and not on the surface where the pressure is applied. The loading becomes largely bending in nature as the thickness of the plate or sheet is reduced.

Stress Variation with Sheet Thickness

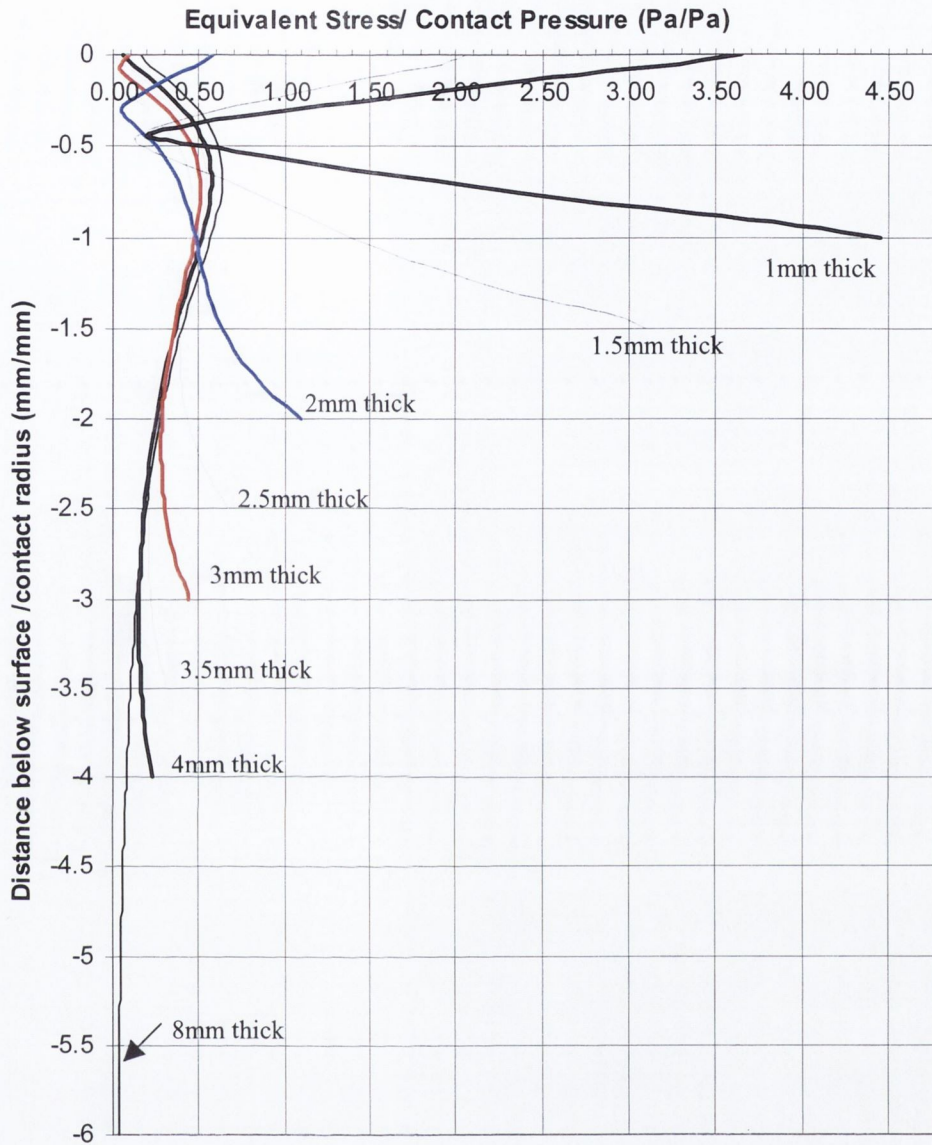


Figure 4.17 Equivalent Stress variation with distance below the surface in Different Thickness plates (uniform pressure load, “no support”).

If the situation represented by the curve labeled “1mm thick” is studied it can be seen that the stress is largely bending in nature. In other words there is a neutral surface where there is relatively little stress with linearly increasing stress in compression and tension on either side of this surface. This is illustrated in Figure 4.18 and can be seen to be a very different stress pattern to that illustrated in Figure 4.16. The maximum stress intensity of 4.45 times

the applied pressure as shown in Figure 4.18 could be calculated from a standard elastic stress formula [50] but the finite element simulation will allow more complex support arrangements and plastic yielding to be considered.

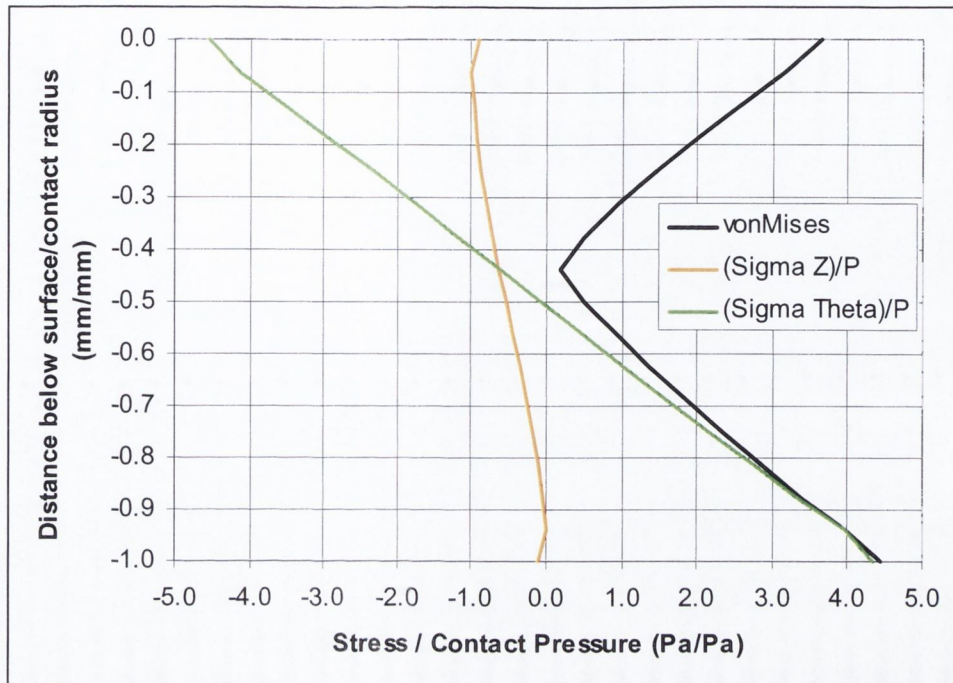


Figure 4.18 Stress Variation with distance below the surface in 1mm thick plate

It can be readily seen that a relatively small local pressure load on a thin plate can produce stress intensities much greater than the magnitude of the applied pressure. Thus it is possible to envisage that a more compliant material such as nylon can create the forming forces involved in spinning. The plastic deformation is initiated as bending and develops into a combined bending and stretching operation. In this context understanding how local stresses are created by the tools is central to spinning and other incremental metal forming processes. It can be seen that the loading of the workpiece is initially by bending, with greater stress being caused on the surface away from the applied load.

The results of the model described in section 3.3.2 offer a further understanding of the stresses arising when the workpiece is loaded by a uniform pressure. These models simulate the loading of the workpiece by opposing pressures. Here the roller load is simulated as being applied on an area of radius 1mm on a workpiece of thickness 1mm. The area where the supporting pressure is applied is then varied while adjusting the pressure to provide force balance. When the opposing or supporting pressure is very low,

so that the load is supported through stress transmitted from a remote region of the workpiece, the situation is exactly as that shown in Figure 4.17. Thus the heavy dashed curve labeled 'No support' in the legend of Figure 4.19 is the same as the curve labeled '1mm thick' in the legend of Figure 4.17.

The continuous curve labeled '1.000' in Figure 4.19 represents the situation where equal forces are applied top and bottom of the workpiece and unsurprisingly the equivalent stress is about equal to the applied pressure through the thickness of the workpiece.

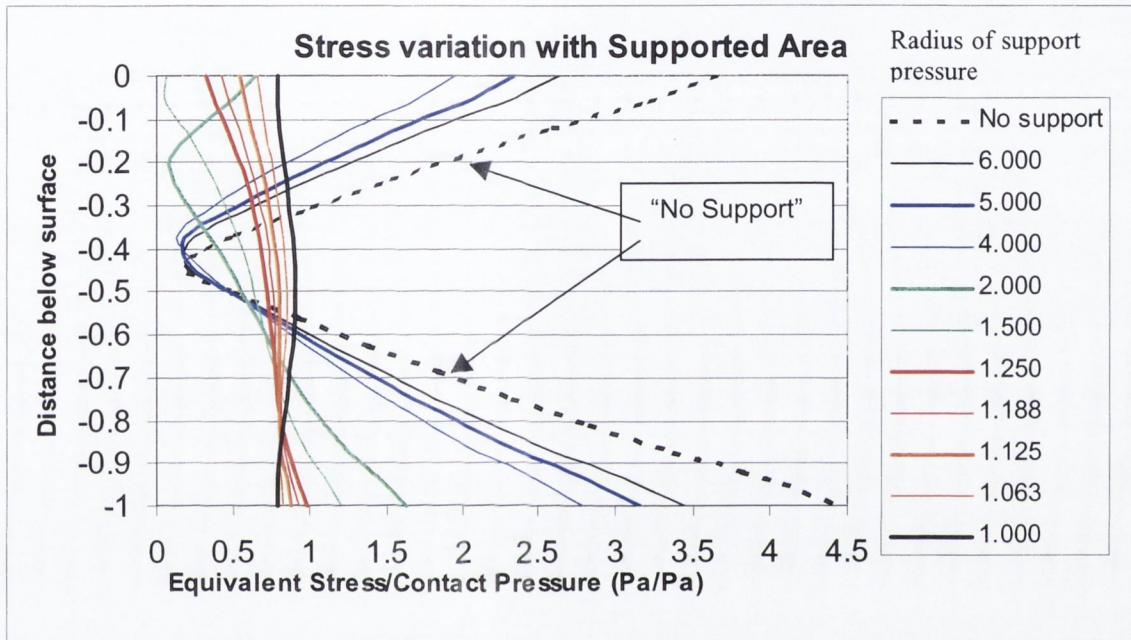


Figure 4.19 Stress variation with supported area

Perhaps the most interesting of the results presented in Figure 4.19 is the curve for a support area of 5mm radius which is shown with a thick blue line. For this curve the area of contact is not very large and so could realistically occur in a spinning process. It is about the size of contact area with a nylon roller detected using Fuji Prescale film as reported in Table 4.2 page 120.

Plastic Deformation

So far the discussion on the creation of equivalent stress intensity greater than the magnitude of the applied pressure has not considered the situation where the elastic limit is reached through all or part of the workpiece thickness. Accordingly the next situation to consider is one in which the metal can deform plastically. The question to be answered is “what proportion of the workpiece thickness will reach the yield point under a given magnitude of pressure.?” Pressure cannot be increased until the entire thickness reaches

yield point in a FE model because in that situation large, almost arbitrary, deformations result that add little to understanding and are difficult to relate to spinning.

The region of material that remains elastic can become quite a small proportion of the overall material thickness. So the material should be very susceptible to deformation by other loads imposed by the surrounding material.

Considering the situation where the workpiece is subject to two pressures as before with pressure on the top surface applied to an area of radius 1mm and the pressure on the bottom surface applied to an area of radius 5mm. This situation generated the '5.000' curve in Figure 4.19. Taking this situation and instead of limiting the simulation to elastic loads but rather increasing the pressure to some fraction of the plastic yield stress for the material the finite element simulation then generated the curves in Figure 4.20.

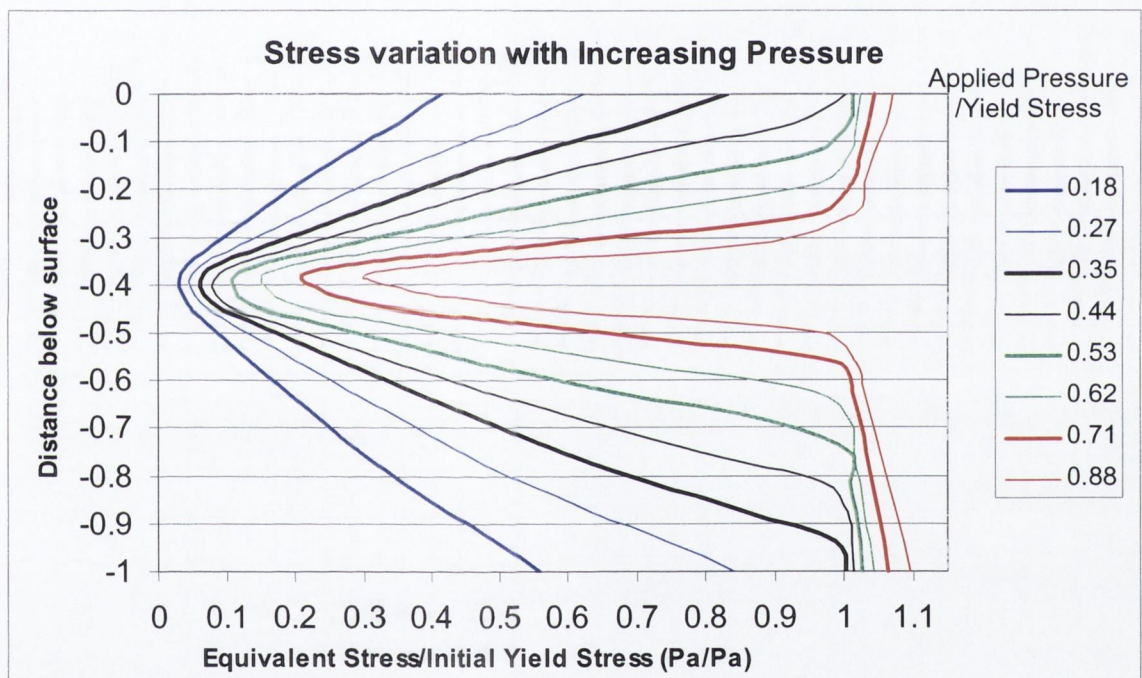


Figure 4.20 Plastic strain occurring under uniform pressure

It can be seen that the curves due to the lower pressure loads are similar to the '5.000' curve in Figure 4.19 because the material behaviour is elastic. They differ only because they are scaled by the material yield stress rather than the applied pressure. However it can be seen that the equivalent stress is greater than the initial yield stress when the magnitude of the applied pressure exceeds one quarter the value of the initial yield stress. The '0.27' curve in Figure 4.20 shows the stress less than yield through the entire thickness while the '0.35' has clearly reached yield on the lower surface. The curve labeled '0.88' shows the

stress exceeding the yield stress throughout over 70% of the workpiece thickness. It will be shown later that this type of loading occurs in a spinning process. Though it is to be expected that there will be regions where there is no neutral layer through the workpiece thickness i.e. regions where the deformation is one of bi-directional stretching at all levels through the workpiece thickness.

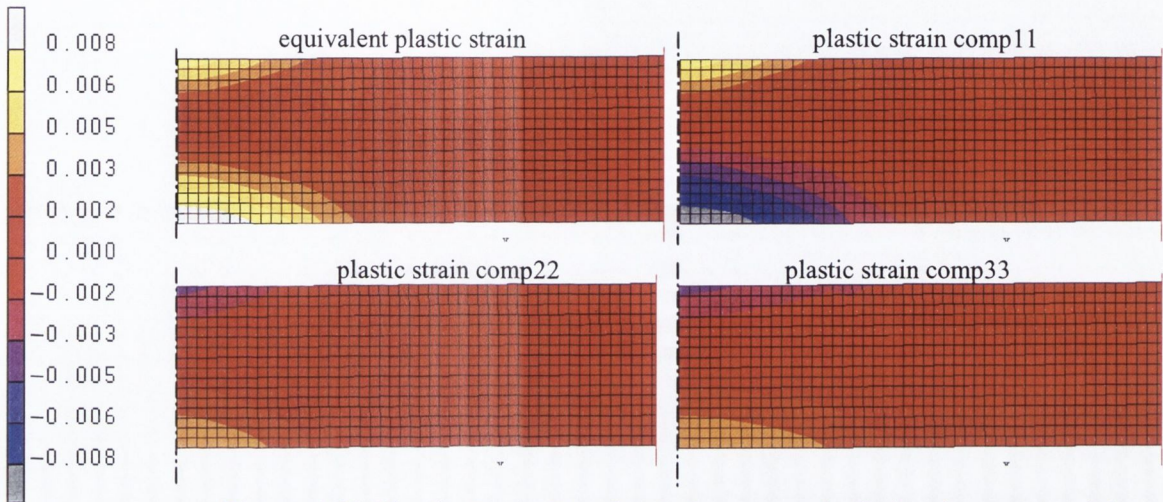


Figure 4.21 Plastic Strain Results Axi-symmetric finite element model

Figure 4.21 illustrates the strain patterns involved, which were obtained using the models described in Figure 3.10, page 60. The equivalent plastic strain and the components of strain in the direction of the applied pressure and in the directions perpendicular to this are presented. Strain in the direction of the applied pressure is labeled 'Comp11' and is in the vertical direction in the diagram and in the perpendicular directions 'Comp22' is horizontal in the diagram and 'Comp33' is the hoop strain and its direction is normal to the plane of the diagram. As in the previous section the strains are quite small. These results for the investigation of contact stress and strains are not going to predict large deformations such as occur in the spinning process. Yet the nature of the stresses generated by contact pressure has been explored.

4.3. Spinning Process Experiments

The first concern is that the experimental spinning process is a 'reasonable' representation of an actual spinning process. Although it is implemented on a CNC (computer numerical control) lathe it is nonetheless representative of a spinning process that might be more typically implemented on a dedicated spinning lathe with playback numerical control. Obviously the first requirement is that spun parts are produced, but further confidence can be gained by comparing the forces involved with published values from an independent source.

4.3.1. Experimental shape: spun part geometry as measured by CMM

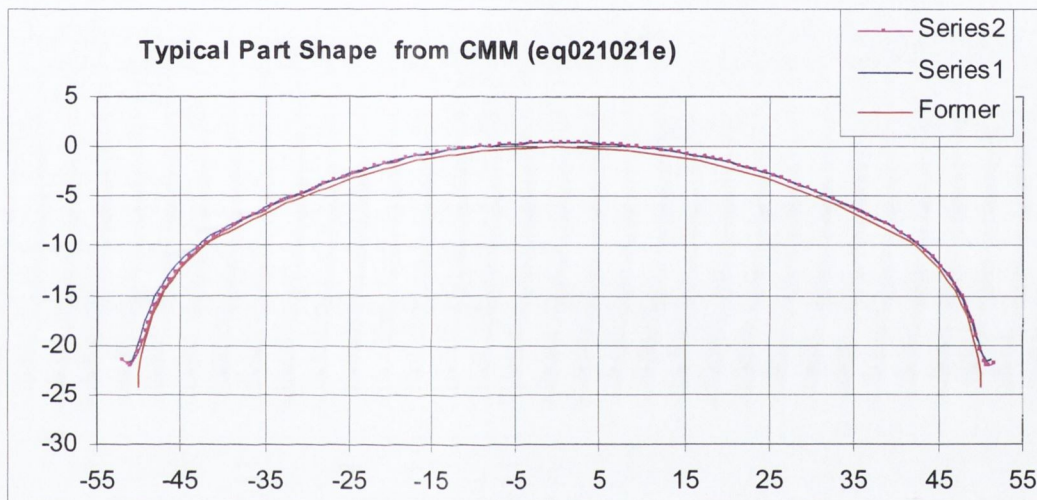
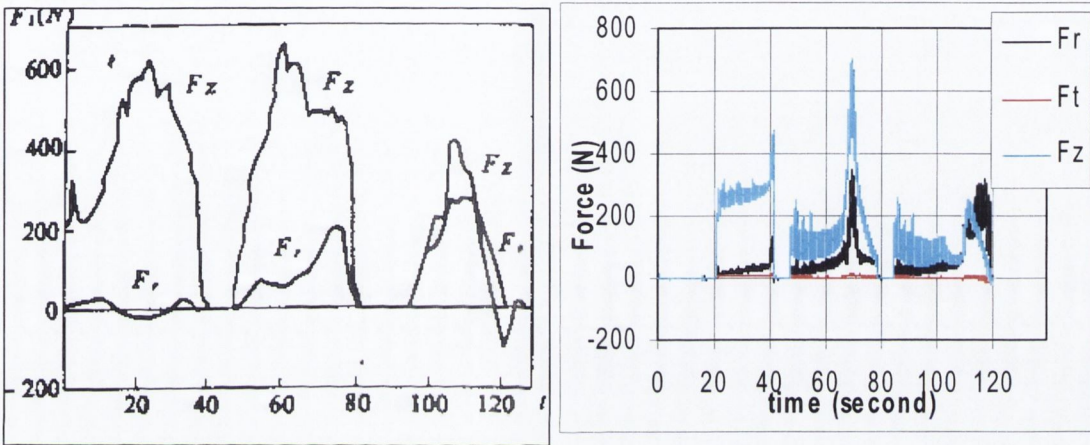


Figure 4.22 A typical profile of a spun part as measured on the CMM (in mm)

In Figure 4.22 the mandrel or former shape is plotted along with two sets of profile measurements that were taken as scans of the inside of the workpiece. It can be seen that there is good agreement between the part shape and the required shape as dictated by the mandrel. The scans were taken in perpendicular directions but match well and so indicate that the part is reasonably circular. The part shape does deviate from the mandrel at the periphery because it was essential to avoid instability that would occur if the roller ran off the edge of the workpiece. (Practical spinning operations often use a trimming or beading tool, which removes or forms the edge of the workpiece and so avoids any requirement to achieve a completely finished edge produced by the roller).

4.3.2. Comparison of Experimental Forces with Published Results

The forces involved in this spinning process were measured using the equipment described earlier in section 3.4.5 and they compare well with forces reported by Qiang [27] for a similar process. This shows that the experimental spinning process is broadly working within normal parameters for a spinning process and so enables the roller force measured in the spinning process to be analysed in the context of the deforming shape of the workpiece. The roller force gives a history of the deformation process. In turn this enables an understanding of the process to be developed. Figure 4.23 below shows typical results from both analyses and in each case the values of the force components are plotted against time.



(a) Typical forces Qiang [27]

(b) from experiment (EQ10831B-.xls)

Figure 4.23 Typical forces in a spinning operation.

Figure 2.24 below shows the directions of the force components F_r , F_t and F_z being measured.

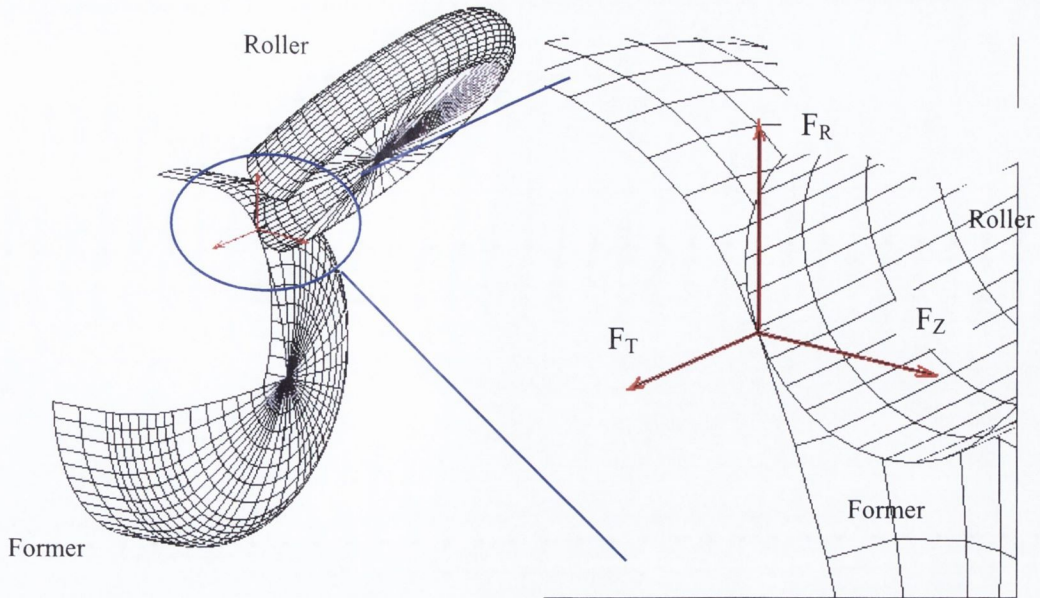


Figure 4.24 Force Measurement Coordinate System

It can be seen that while these two sets of results in Figure 4.23 are not identical they are broadly similar. They reflect a three pass tool path in both cases i.e. the value of the force components drops to zero when the roller lifts off the workpiece between each pass. They show the roller force components as follows. The axial component labelled F_Z is the largest force component. It can be seen to diminish from the first pass to the third pass in both cases. The radial component labelled F_r is increasing with each pass. The third force component the tangential component is only plotted in Figure 4.23(b) and can be seen to be very small in comparison to the other components.

The fact that a playback numerical control machine was used for the tests described by Qiang [27] and the fact that the exact details of the tool path used were not available to this author is clearly a source for some of the differences in the two sets of results. In the Figure 4.23(b) there is a period at the beginning of the second and third passes where the roller is doing relatively little forming and so the forces are substantially lower than those reported by Qiang and shown in Figure 4.23(a).

4.3.3. Thickness strain measurements

Using a sheet metal micrometer the following results were obtained for workpiece thickness at various positions.

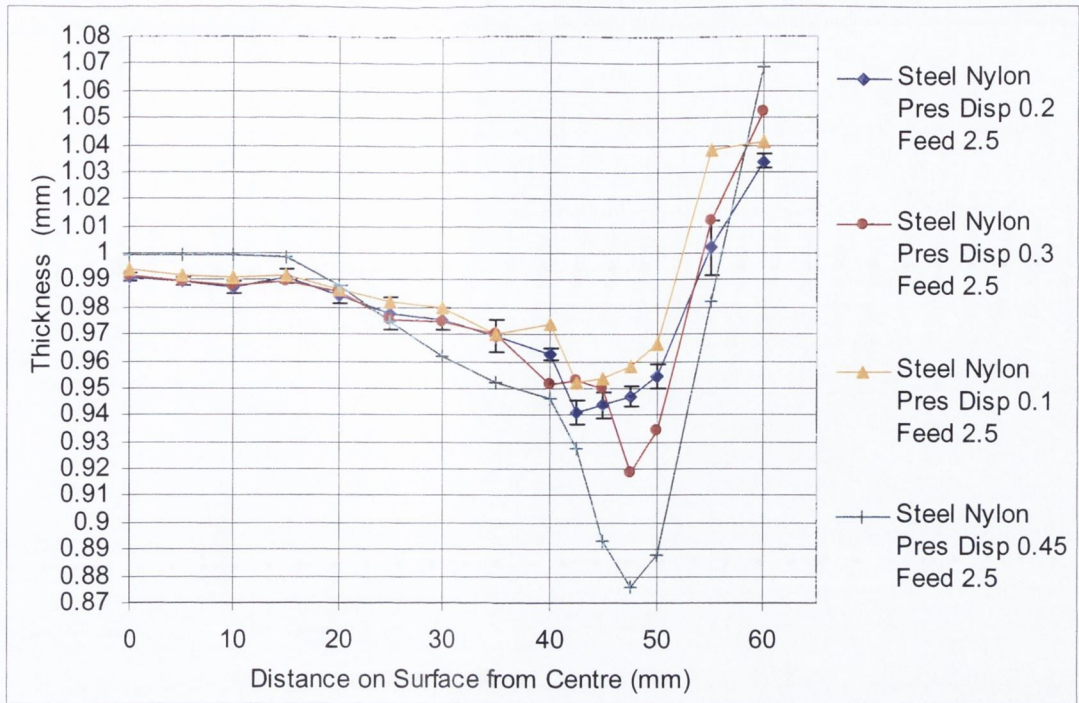


Figure 4.25 Experimental Thickness Variation

It can be seen that the thickness reduction varies by less than 0.03 in the inner region of the workpiece over a wide range of prescribed displacements. As the prescribed displacement is increased from 0.1 to 0.45mm i.e. a change of 0.35mm and it can be seen that the resulting thickness change is less than 10% of this. This stability of the process over a variety of prescribed displacements is foreseeable from the results for static contact in Figure 4.12 which illustrated how thickness reduction varies with prescribed displacement for static contact. In the case of static contact a prescribed displacement of 0.24mm produces a change in thickness of the workpiece is of less than 0.035mm i.e. less than 15% of the prescribed displacement.

The force time history curves presented in Figure 4.23 present three different components of the roller force however if it is required to make comparisons between different spinning process parameters it is simpler to plot the total roller force which is the vector addition of the three individual force components.

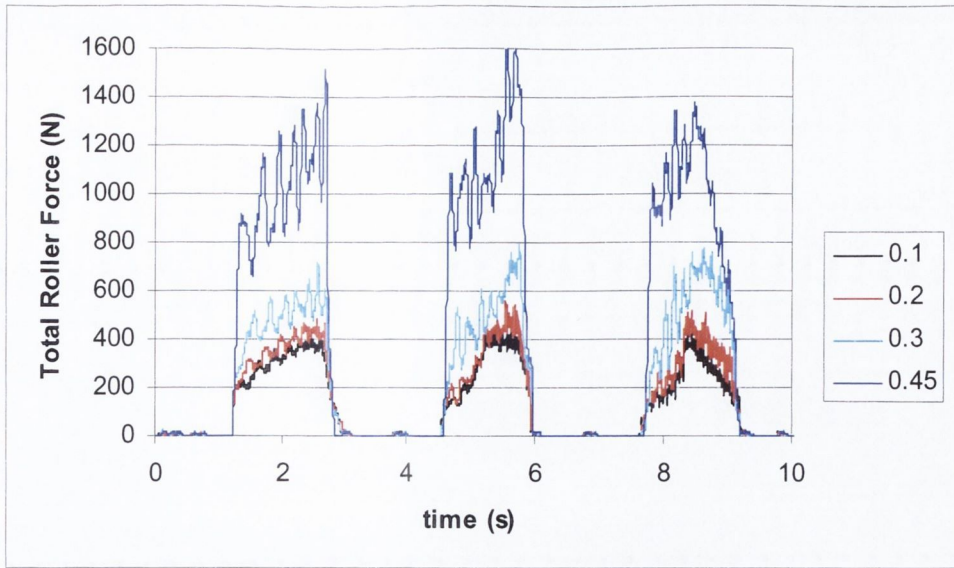


Figure 4.26 Experimental Force History Curves for different Prescribed Displacements

This analysis gives some indication of the stiffness of the system, or how the roller force increases with prescribed displacement.

4.3.4. Tool Force Line Stiffness in Spinning

Using a number of different spinning experiments, with different prescribed displacements, it is possible to calculate a spinning stiffness that can then be compared to direct contact tool force line stiffness. This stiffness can be used to ‘calibrate’ the spinning process simulations.

In order to make a comparison with the static simulations an average force was calculated for each history curve. The times between each pass were excluded when calculating this average value. These time-averaged values for roller force are plotted against prescribed displacement in Figure 4.27 and the results are compared with predictions from the analysis of the static contact simulations presented earlier in Figure 4.4 and subsequent figures.

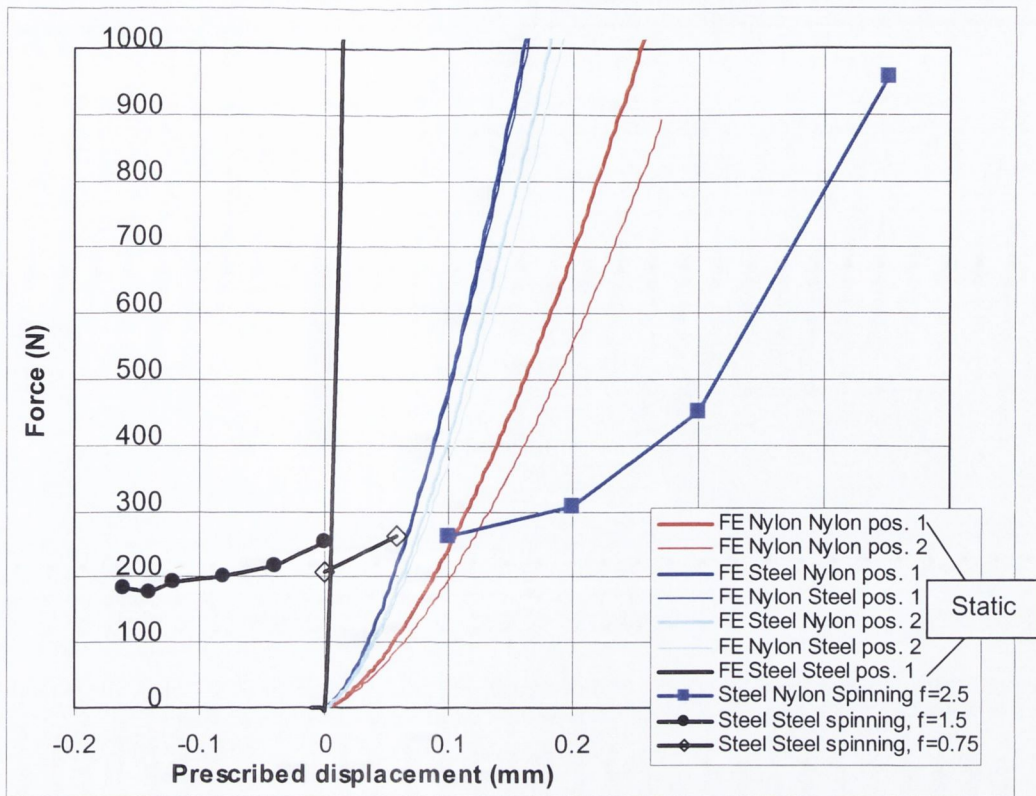


Figure 4.27 Force Variation with Prescribed displacement of Roller

It can be clearly seen that the contact stiffness is substantially lower for the actual spinning operation compared to the static contact situation. The question might be asked as to whether this lower stiffness is due to other components in the tool force line rather than the contact between the roller workpiece and former. The Kistler dynamometer is rated at $600\text{N}/\mu\text{m}$ and the NC lathe machine frame can be expected to be the same order of magnitude. Clearly these do not compromise the tool force line stiffness. The stiffness of the roller holder as illustrated in Figure 3.28 (page81) could be the subject a major design investigation and it is clearly stiffer if loaded directly rather than from the side of the forks. A simple beam calculation for the lateral deflection of the roller holder forks indicates a relatively low stiffness of $1\text{kN}/\text{mm}$ for the independent deflection of each fork. It can be assumed that the coupling of the forks through the roller axle will increase the combined stiffness from a simple addition, giving $2\text{kN}/\text{mm}$, to a substantially higher value. Furthermore the spinning force is never simply a lateral load.

It is noteworthy that the force displacement curve has a non zero intercept on the vertical axis. This is to be expected because when the roller is programmed to move at a distance greater than the workpiece thickness from the former it will still make contact with the (initially flat) workpiece and carry out some metal forming.

4.3.5. Comparison of Experimental Strains with Strains for Landmark Processes

The plastic deformations of spinning must respect volume constancy, just as with all metal forming processes, and so there must be reciprocal contractions in directions perpendicular to each tensile strain and vice versa. This fact is apparent from the results obtained for predicted deformation at various locations in the workpiece.

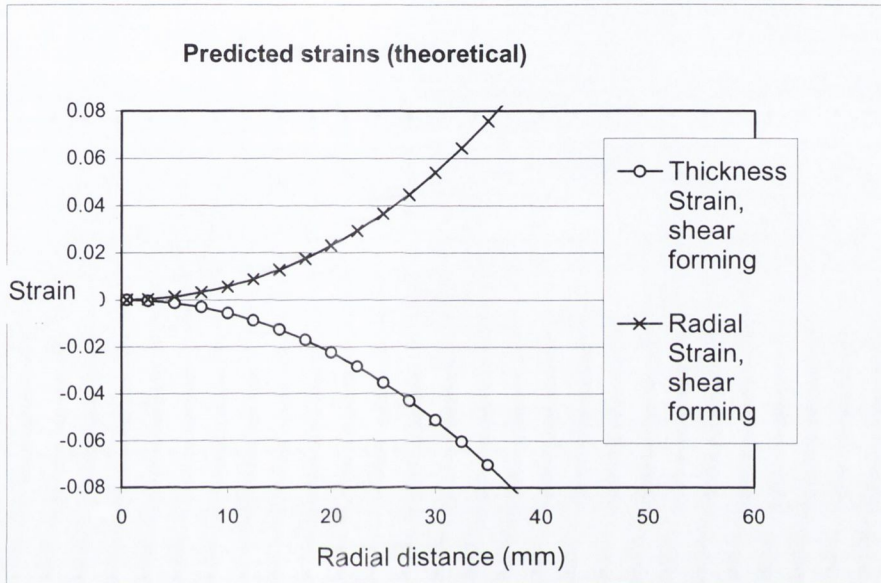


Figure 4.28 Theoretical strains for shear forming a spherical part of radius 95mm

It was shown earlier in section 2.2 that theoretical strain fields can be calculated by considering part geometry. These results shown in Figure 4.28 were obtained by analysing the spherical region of the workpiece (radius 95mm) and assuming a shear-forming process. This gives radial strain and thickness strain, and recall that the hoop strain is zero for a shear forming process. When these radial and thickness strains are expressed as natural strains they are equal in magnitude and opposite in sign and this pattern of strain is independent of sheet thickness.

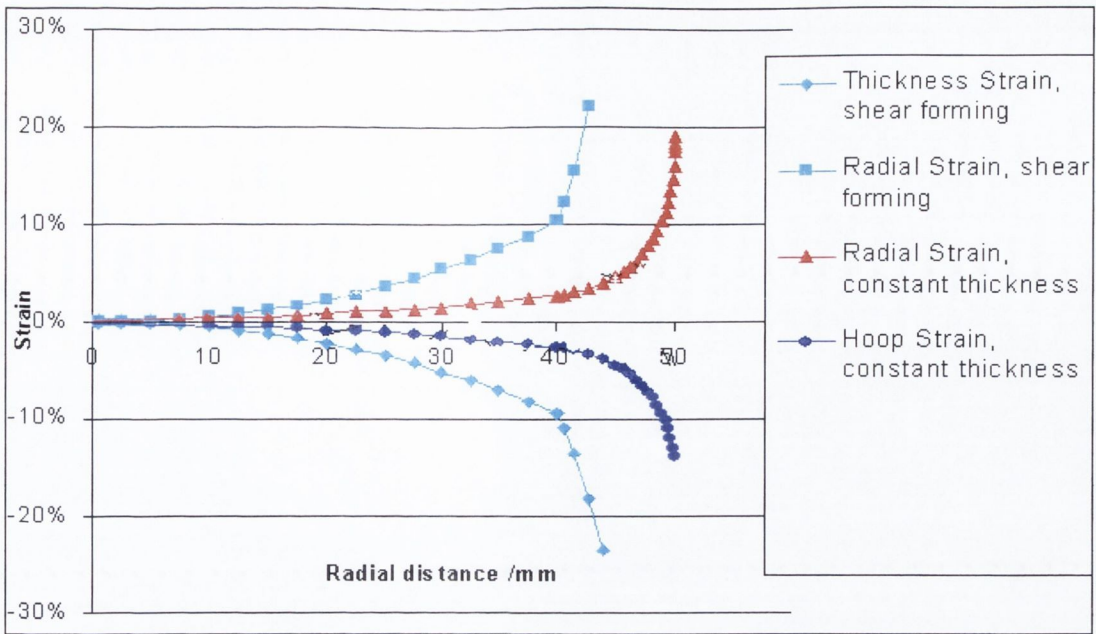


Figure 4.29 Ideal constant thickness and shear forming strains for the experimental shape.

Figure 4.29 presents the results of an analysis performed by this author [28] for a constant thickness process applied to the experimental shape. The radial and hoop strains represented by the red and blue curves respectively and their magnitudes are equal and opposite. Of course the thickness strain is zero as the name of the process implies. The theoretical calculation of these strain curves does not consider the sheet thickness, consequently in the case of a sheet of finite thickness these graphs would represent the strains at a neutral layer. The characteristic strain curves for the shear forming of the experimental shape are also presented for completeness (the light blue curves). A significant change in the slope of these curves occurs at a radial distance of approximately 40mm from the workpiece center where the shape changes from a spherical radius of 95mm to a blend radius of 17mm.

In the case of the constant thickness process allowance must also be made for the sheet thickness when considering the curvature of the part. If the problem of bending a straight strip of material to a spherical radius is considered then classical simple bending theory would be expected to give positive or tensile strains on the outer fibres of the bend and negative or compressive strains on the inside of the bend. The inner surface will be compressed and the outer surface stretched by an amount related to the thickness. Specifically additional strains of

$$\epsilon = (r \pm t/2)/r$$

Equation 4.7

can be evaluated as natural strains of ± 0.0052 for a sheet of thickness, t of 1mm forming a part of the spherical radius, r of 95mm. So the given curves could be shifted by this amount to calculate theoretical strains for the inner and outer surface.

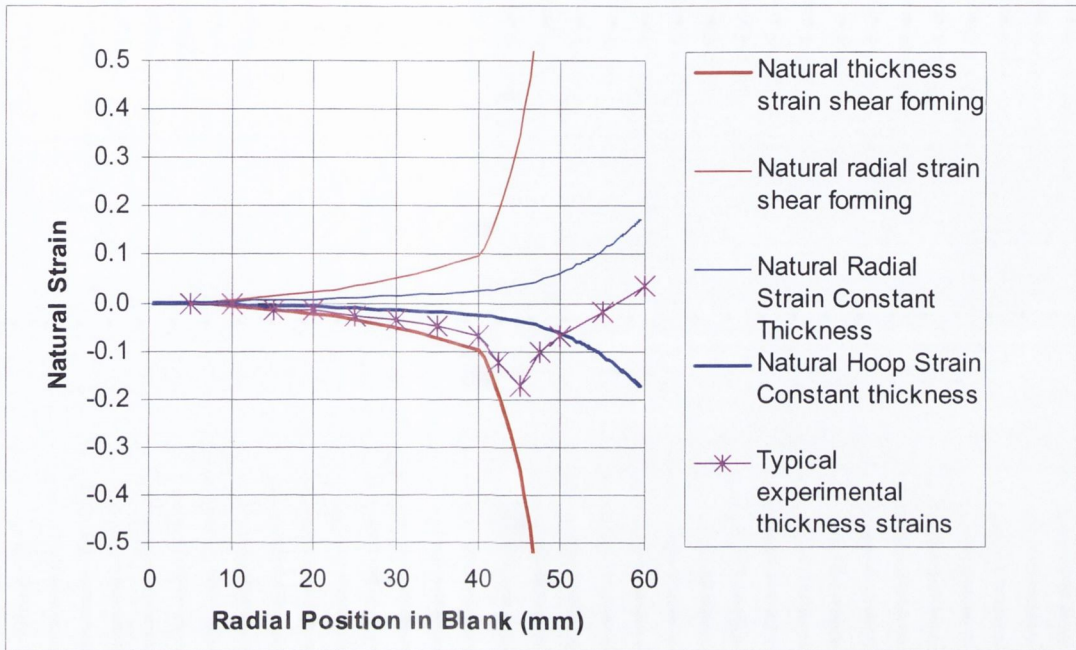


Figure 4.30 Experimental thickness strain compared with theoretical process strains

Figure 4.30 shows the measured thickness strains overlaid on the theoretical strains. It can be seen that the thickness reduction is similar to but somewhat less than the reduction predicted for a theoretical shear forming process as was presented from constant volume calculations in Figure 2.19 on page 26. This similarity ends abruptly near the edge of the workpiece when the flange is no longer large enough to constrain the deformation zone.

4.4. Finite Element Simulation of the Spinning Process

4.4.1. Comparison of experimental strains with FE predictions

Once it has been established that the finite element simulation can provide a reasonable prediction of the strains in the spinning process, the results of the finite element model can therefore be analysed or post processed to provide information on the nature of the spinning deformation process. In addition the FEA results provide detailed information on the stress tensor and the plastic strain tensor throughout the process. It is not possible to present and all this data, but by comparing the output strains with the idealised models of

shear forming and constant thickness spinning a more detailed understanding of the process can be achieved.

By looking at the predicted finite element results of the process it can be seen that the experimental results and FEA predictions are in good agreement, and that the additional results provided by FEA enables the spinning process to be better understood. The results presented here are for the chosen experimental shape as described previously.

4.4.2. FE predictions of spinning forces using full 3D process simulation

Finite element models were described previously in section 3.5.2. The credibility of the finite element simulations can be assessed by comparing the predicted force output with the experimentally measured force output.

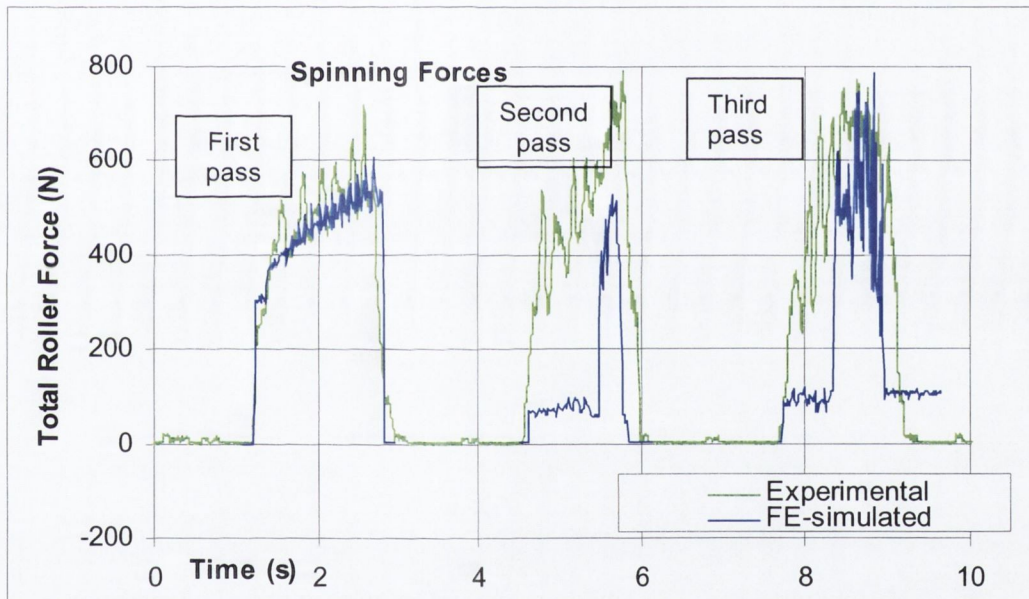


Figure 4.31 Predicted forces from FEA compared with experimental forces.

Figure 4.31 shows an experimentally measured roller force and the FEA predicted roller force for a three roller pass spinning operation with a 1mm thick workpiece. Both force curves carry a considerable amount of noise. The cause of the noise is somewhat different in each case. In the case of the simulation noise arises because the coarseness of the mesh combined with the nature of the contact model. The contact algorithm in the Marc2001 finite element code was described previously in section 2.4.3. At any point in the simulation contact is simulated by a relatively small number of nodes if a node separates or a new node makes contact the result will appear as noise on the predicted force output

from the simulation. In the case of the experimentally measured force it is primarily due to geometrical inaccuracies or eccentricity in the roller and former.

The FE simulations as described previously in section 3.5.2 use a rigid former and a deformable roller (Figure 3.45, page97). The experimental spinning operation was carried out using a steel roller and a nylon former.

These force curves match well particularly for the first roller pass.

The experimental prescribed displacement was 0.3mm

The finite element prescribed displacement was 0.1mm

In this way the comparative rigidity of the model requires a calibration of the models.

Thus if it is desired to simulate a prescribed displacement of 0.3mm a displacement of 0.1 may be used in the finite element simulation. This calibration can be best achieved by matching the average force curves on the basis that it is the force that is causing the deformation of the workpiece.

Clearly the ability of the finite element model to simulate a deformable former is missing and so the finite element simulation will tend to be too rigid. Thus justifying the use of a smaller prescribed displacement.

The second and third passes provide a reasonable prediction of the spinning force but do not match the experimental force curve as well as the first pass. The fact that the finite element model is over rigid can account for some of the discrepancy. Also the relative simplicity of the flow curve for the material probably also contributes. It can be seen that at the beginning of the second pass the simulation predicts a substantially lower force than occurs in the experimental spinning process. Indicating that the first pass has produced the formed that part of the product and passing the roller over that part a second time maybe unnecessary although the experimental force is not as low the FE predicted value.

4.4.3. Presentation /Analysis of force in surface normal coordinate system

Figure 4.32 shows the spinning force analysed in terms of component normal to the surface of the former, tangential to the surface of the former, and thirdly in the feed direction.

It can be seen that the component in the feed direction increases steadily during the first pass. This can be associated to the deforming shape that is being acquired by the

workpiece. The flange becomes slightly upturned like a hat rim and as the first pass proceeds is at an increasing angle from the surface of the former as can be seen in the Figure 4.33.

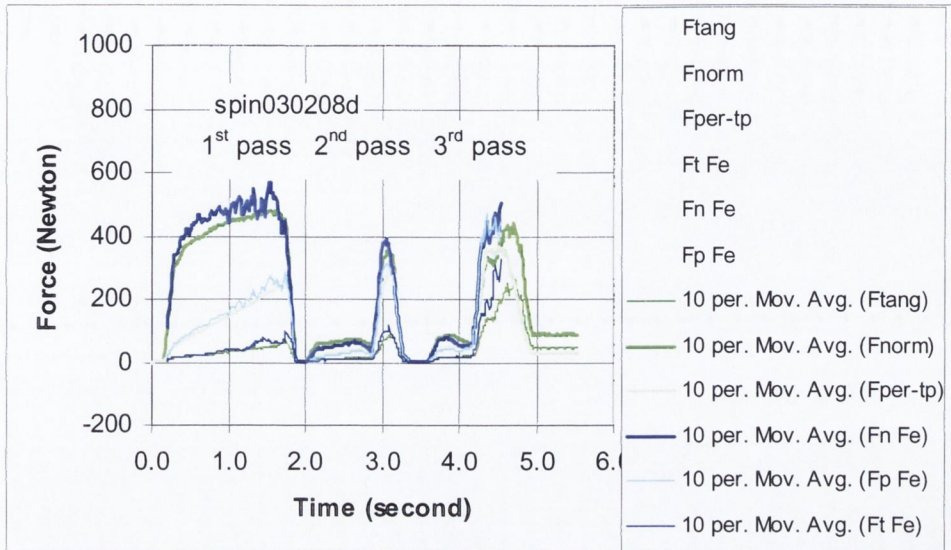


Figure 4.32 Force Components in Surface Normal Coordinate System

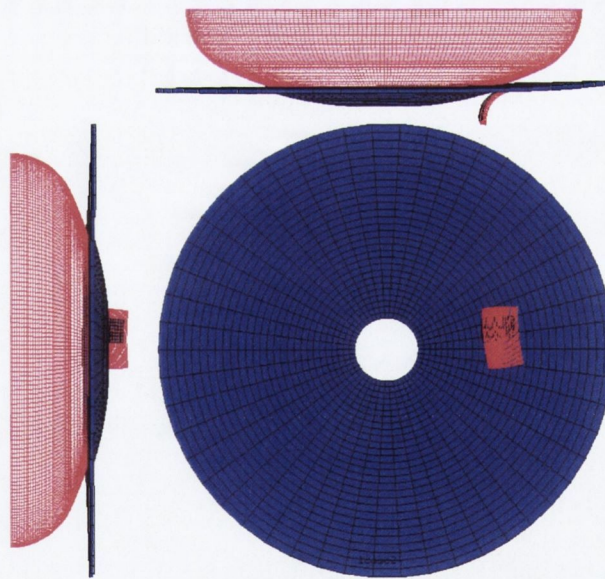


Figure 4.33 Prediction of deformed shape during first pass (t=1.0s)

The deformed shape during the second pass is illustrated in the following

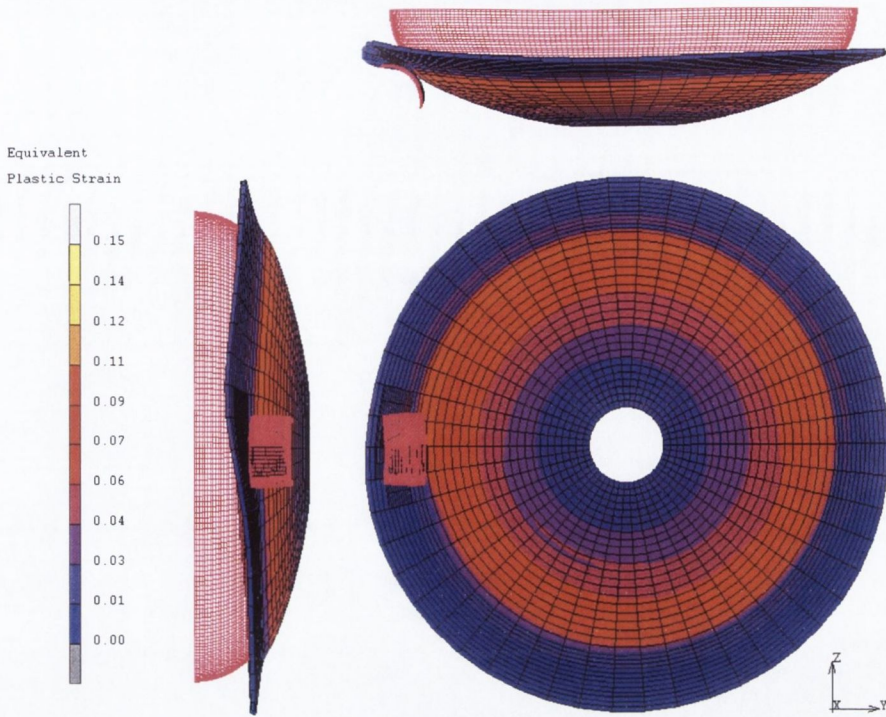


Figure 4.34. It can be seen that the flange is no longer large enough to maintain an almost flat shape as was apparent in the previous figure.

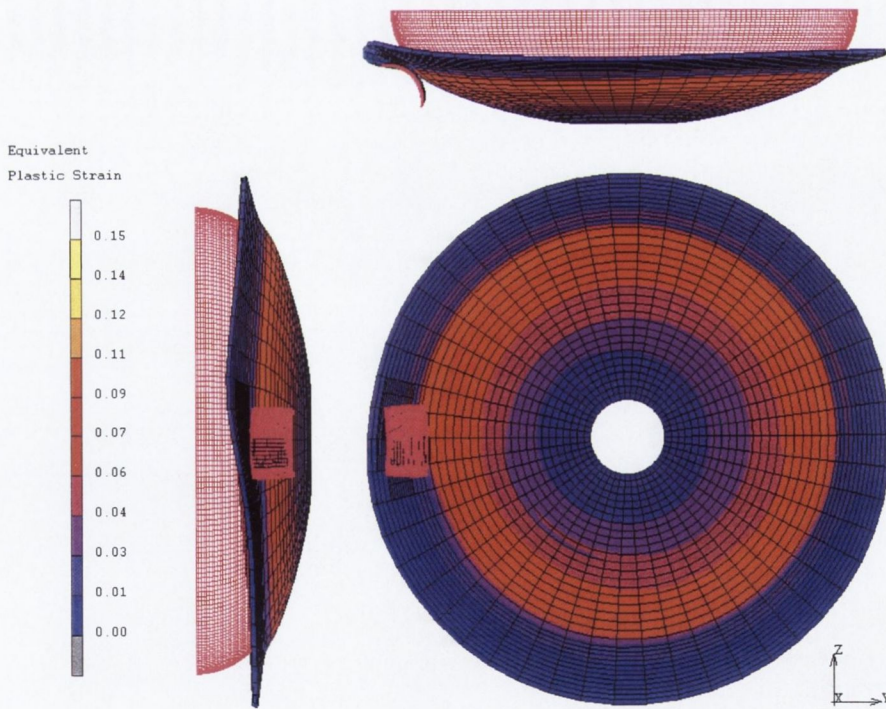


Figure 4.34 Prediction of deformed shape during second pass ($t=3.1s$)

4.4.4. Tool Force Line Stiffness in Spinning from FEA

Previously in section 4.3.4 the spinning stiffness was compared to the static contact stiffness. The corresponding characteristic of the full process simulations shows how the full process simulation is significantly more stiff due to limitations of the finite element model. Because of being restricted to the use of rigid surfaces to represent the former and also because of the relative coarseness of the mesh representing the workpiece the predicted forces are higher for a given prescribed displacement. Nonetheless the comparison the average force predicted by the finite element simulation with experimental results enables a calibration or cross-reference between the predicted and the experimental. The finite element model uses a mesh attached to a rigid surface as a model of the roller. There are two different materials applied to this mesh; one nylon and the other steel. The results of using both of these are given in the Figure 4.35 below, Where the pink curve represents the prediction for steel roller and the green curve represents the prediction for the nylon roller.

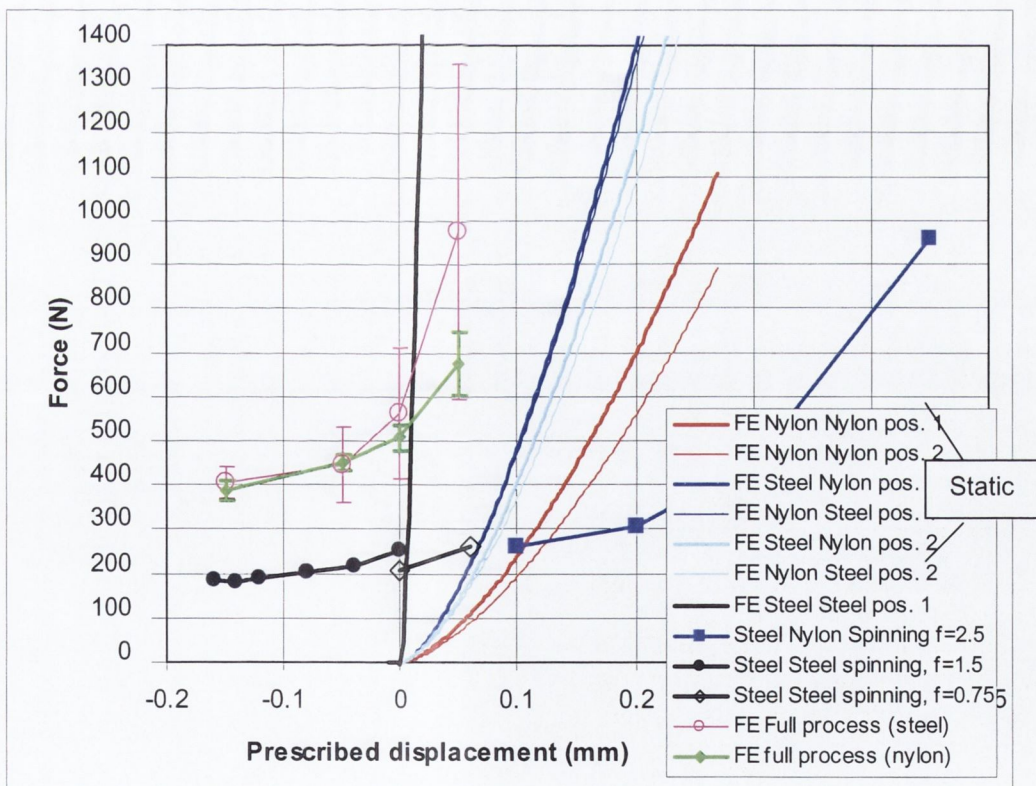


Figure 4.35 Force Vs Prescribed displacement (experimental and FE full process)

The error bars on both of these curves are indicative of the difficulty that Marc finite element code has in simulating the contact particularly in the case of the steel roller. It is very evident that a finer mesh would be desirable to simulate contact with steel tools than

with nylon. This was anticipated from the static results presented earlier in Table 4.1 and Figure 4.11, which showed a smaller contact area with the steel roller.

It can be seen that rate at which the contact force increases is similar to the stiffness of the steel nylon static simulation (blue curve no markers) but that the force never becomes as low as experimental. This would be expected from the over prediction of stiffness associated with the simulation of bending with a very limited number of elements [49].

4.4.5. Comparison of experimental strains with FE predictions

Finite element modelling of the spinning process also allows for a detailed examination of the process and for a prediction of the final condition of the finished product or workpiece. The strains imposed on the workpiece blank to provide the finished part are readily extracted from the FE output or results file. It is of course possible to physically measure the strains on an actual deformed workpiece and in the course of this project the circle grid technique was used, from which to strain measurements could be obtained on the top surface of the spun part. These experimentally measured strains provided additional data for comparison with, and validation of, finite element models.

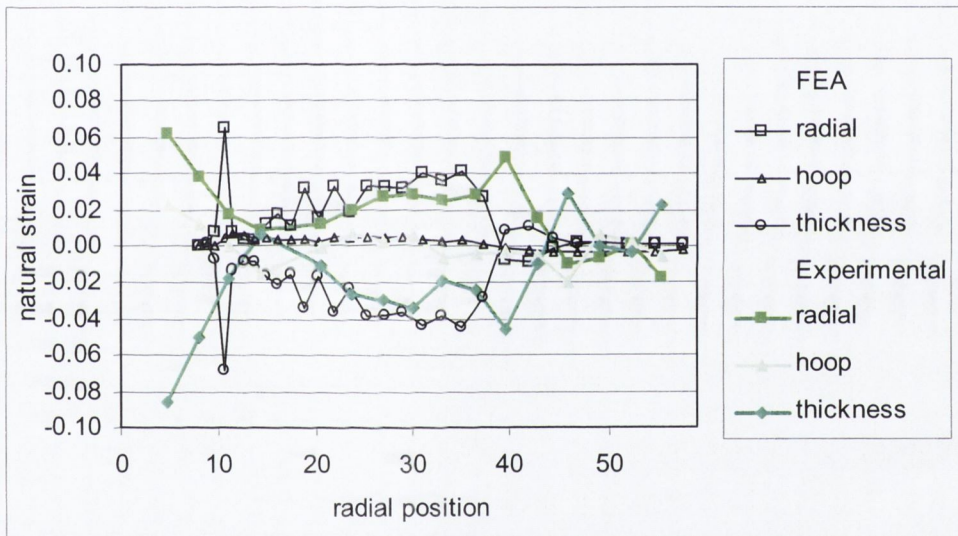


Figure 4.36 Predicted top surface strains from FEA compared with experimental grid circle strains.

In Figure 4.36 the three strain components ϵ_r and ϵ_h and ϵ_t , the radial, hoop and thickness strains respectively are plotted from a finite element model while in Figure 4.36 the radial and hoop strains determined experimentally are shown for comparison. As described by the author in [53] these experimental strains were obtained from an analysis of an etched circular grid. In both cases it can be seen that the hoop strain is relatively small compared to the radial strain. However in a region close to the tailstock there is a high level of radial strain. This is accentuated in the FE results because a single element at the edge of the mesh accounts for most of the deformation in this region. (The mesh does not extend under the tailstock). Both the circle grid analysis and the finite element model show that the main

region of deformation occurred from a radial position of 15mm and up to a radial position of 30mm. The radial strains increase from 0.01 to 0.04 natural strain, while the hoop strains in the same region are less than 0.005. It should be noted that both the circle grid analysis and the finite element model can only provide strain values at discrete positions. Notwithstanding this there is reasonable agreement between the experimental results and the FE predictions. This again gives confidence in the use of finite element method to analyse a spinning process.

4.4.6. Contour plots of Strains from FE models

A familiar output from finite element models is a coloured contour plot showing variations in strain throughout the model. Therefore output plots, such as that shown in Figure 4.37 illustrate in some detail how different regions of the deforming part are strained.

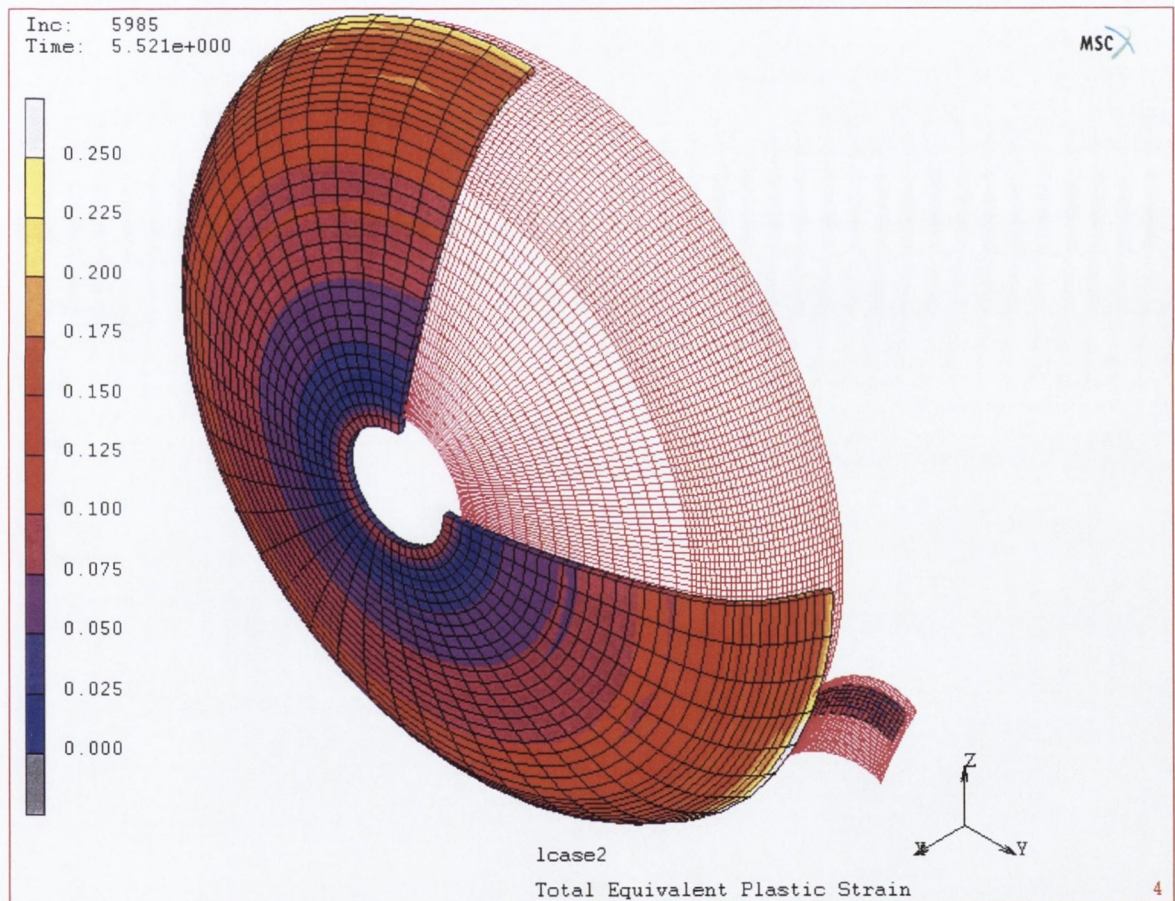


Figure 4.37 Equivalent strains from finite element model.

The element edges for the workpiece are plotted as black lines. The roller and former are also plotted as segmented surfaces indicated by purple-red lines. While this is a reasonable approach, and gives an overall picture of how strain is distributed around the part, it only shows results for one side of the part in any given diagram. To better present the results a

series of close-up plots of strains could be used to provide more detail with the mesh shown cutaway to illustrate the through thickness distribution of stress and strain. Working with a sheet material a frequent approach is to consider the strains in a coordinate system aligned with the surface of the sheet. While this option is readily available with the Marc 2001 code for shell elements the results for a solid hexahedral brick mesh such as has been used in this project can only be plotted in one coordinate system at a time and not in a local element based coordinate systems. It follows that thickness strain etc. has to be studied in a separate plot for each position in the workpiece. As the workpiece reaches a more fully formed shape it is essential to analyse the strains in the correct local co-ordinate system

Alternatively, the strain tensor can be plotted as a three orthogonal vector entity at the center of each element. This will not show variation within any element but will illustrate the nature of the average deformation that each element has undergone in the spinning process. Figure 4.38 shows a segment of workpiece with plastic strain tensors. The arrows that point into the elements represent compressive strain components and the outward pointing elements represent tensile strain components. The length of the vectors plotted in Figure 4.38 is indicative of its magnitude. So it can be seen that the strains increase in magnitude from the center of the part to the outer edge. The vectors are also colour coded according the legend given in the figure.

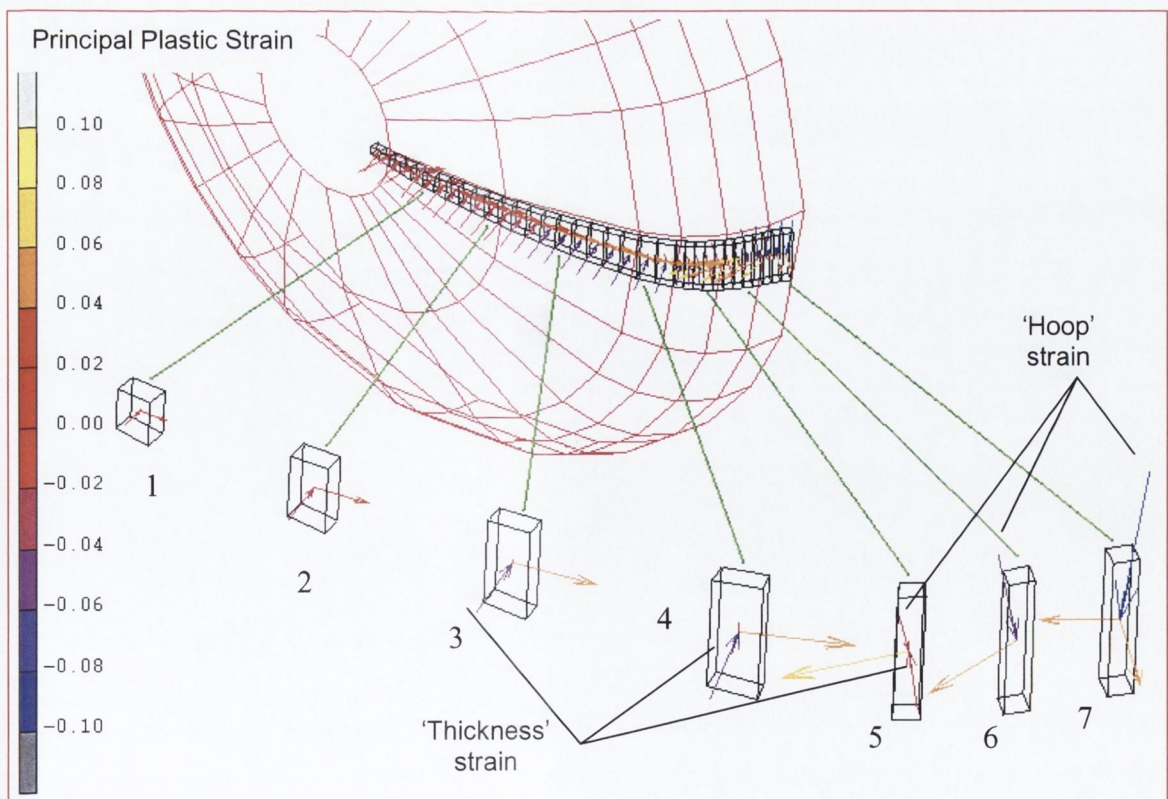


Figure 4.38 Principal plastic strain tensors

The central area (elements 1 through 4) of the part is characterised by a plane strain deformation. The deformation is accounted for by strain in two orthogonal directions there is little strain in the third direction although on the fourth element a small strain component is just visible. Effectively the hoop strain is zero for this region of the part. Elements 5, 6 and 7 as numbered in Figure 4.38 show increasing hoop strain components although these tensor components are not exactly in the hoop direction i.e. not completely vertical in the diagram. Element 5 has undergone some reduction in the thickness direction whereas element 6 shows no thickness strain and element 7 displays some positive strain in the thickness direction.

The tensor plot in Figure 4.38 presents the average strain for a particular element for this reasons a different approach has been adopted to plotting the FE results for further analysis. Specific positions in the part are selected and the results co-ordinate system is aligned with appropriate directions to given the plots of strain variation through thickness presented in the following section.

4.4.7. Strain variation through thickness from FE analysis

In Figure 4.38 the average strains predicted by finite element analysis were presented as principal strain tensors. This did not show what is happening in terms of strain variations through the thickness of the sheet. So the following figures, Figure 4.40 through Figure 4.42, provide this information and allow the output of the FE simulation to be better presented. As the variation of strains through the sheet thickness is of interest a series of distinct locations were analysed.

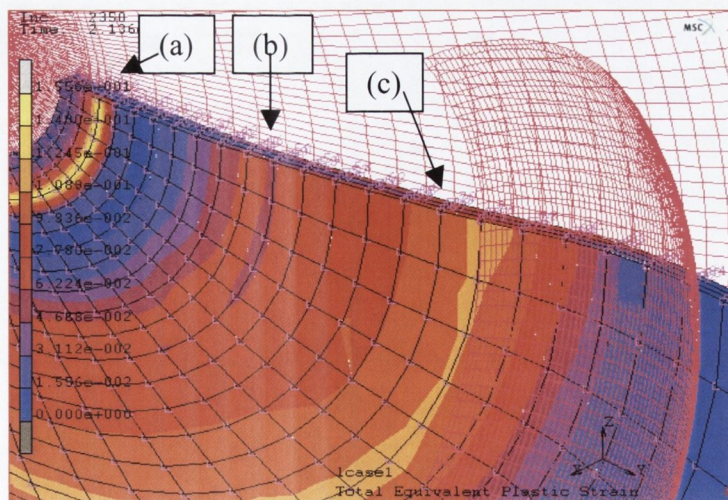


Figure 4.39 A section of the finite element model during spinning

A partial section of the finite element model is shown in Figure 4.39 and these locations are labelled (a) through (c). Location (a) is nearest the tailstock and location (c) is near the deforming region. The following figures illustrate the strain variation through the part thickness.

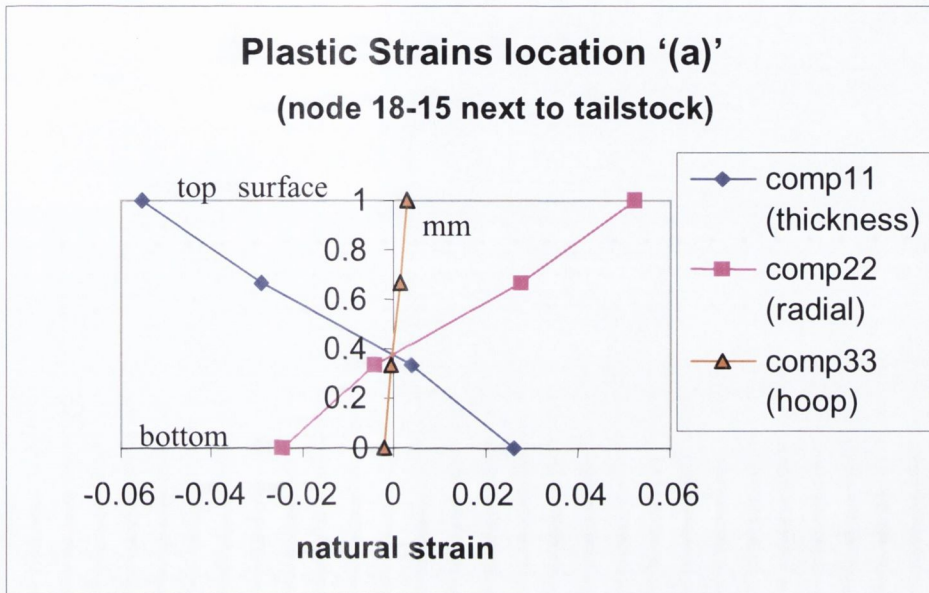


Figure 4.40 Strain Variation through Sheet Thickness at 'a' near tailstock

The workpiece is 1mm thick and the position within the sheet is measured in mm from zero at the inner surface to 1.0 at the outer surface. For the purpose of Figure 4.40 through Figure 4.42 any actual thickness change is not measured on the vertical axis, rather the strains are plotted against the undeformed positions of the nodes within the sheet.

The first, Figure 4.40 for location 'a' of Figure 4.39 shows a deformation that can be characterised as almost pure bending. All three strains are zero at about 0.4mm from the inner surface. So there is neutral layer at this level. So although the process might be expected to have the characteristics of shear forming further from the tailstock, however at location (a) it is largely plane strain bending which would presumably leave the neutral layer located near the middle of the sheet thickness. It can be seen that little or no strain has been imposed in the hoop direction. The small strain in the hoop direction that does occur is less than that to allow for the curvature of the part as discussed above in the context of constant thickness forming on page 137.

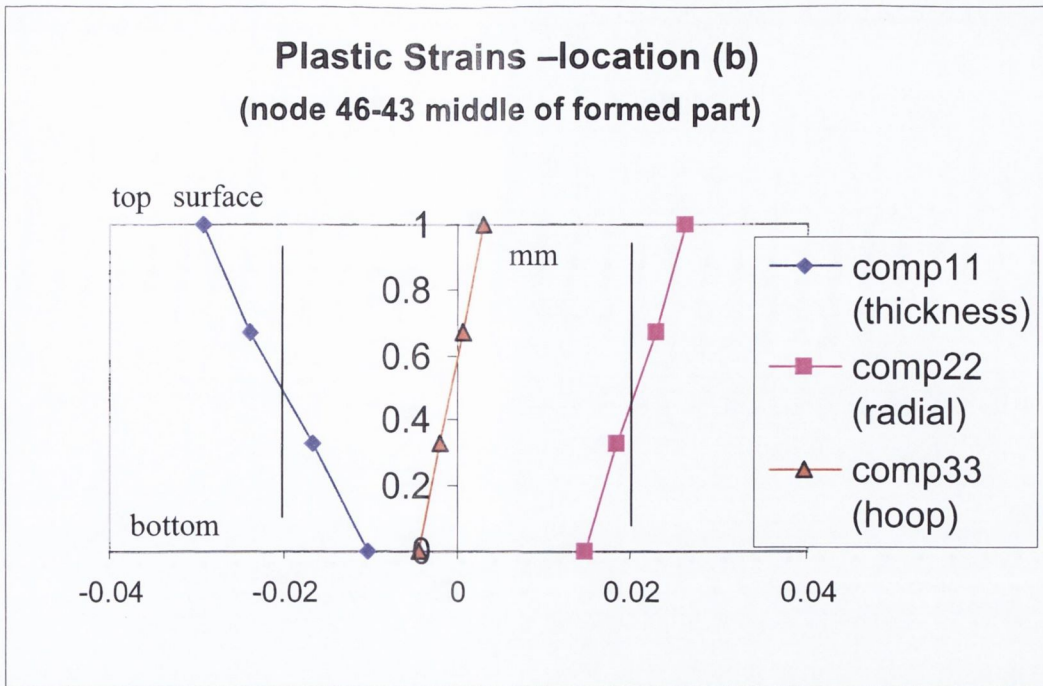


Figure 4.41 Strain Variation through Sheet Thickness at ‘(b)’(of Figure 4.39)

The next plot of strain variation through thickness is Figure 4.41 for location (b) of Figure 4.39, which is at a radius of approximately 19mm from the center of rotation. It has some similarities to that for location (a) but there is no longer a neutral surface or layer within the sheet. Strains in the hoop direction remain small and the radial direction has been stretched. If reference is made to Figure 4.29 for the strains for a theoretical shear forming process it can be seen that the radial strain should be approximately 2% and the thickness strain should indicate a 2% reduction in thickness. This is a reasonable description of the average radial and thickness strains but the actual deformation that has occurred is more complicated. Again the strains in the hoop direction are small. Variation of strains through thickness can be related to the curvature of the part as discussed above in the context of constant thickness forming i.e. +0.5% on the outside and -0.5% on the inside. This is seen to occur in the radial direction and in the hoop direction. It is as if a bending strain were superimposed on the shear forming theoretical strains. The strains in the radial direction seem to reflect the curvature of the part imposed by the 95mm radius of the spherical area of the former i.e. the difference in strain between the two sides of the sheet is, as predicted by Equation 4.7 for simple bending, about 1%.

The strains are much larger than the theoretical constant thickness model, which would require a hoop strain of -0.8% and a radial strain of 0.8% and no thickness strain. So again ‘shear forming’ is a more accurate description of the deformation process of this simple model.

The third through thickness strain plot is for location '(c)' which is approximately 30mm from the center of rotation. The strains are similar but larger than the strains for location '(b)' with the hoop strain still very small. The 'shear forming' analysis predicts a thickness strain of 0.0525 (natural strain) for this location in the workpiece. The magnitudes of the thickness and radial strains in Figure 4.42 are close to but less than this value.

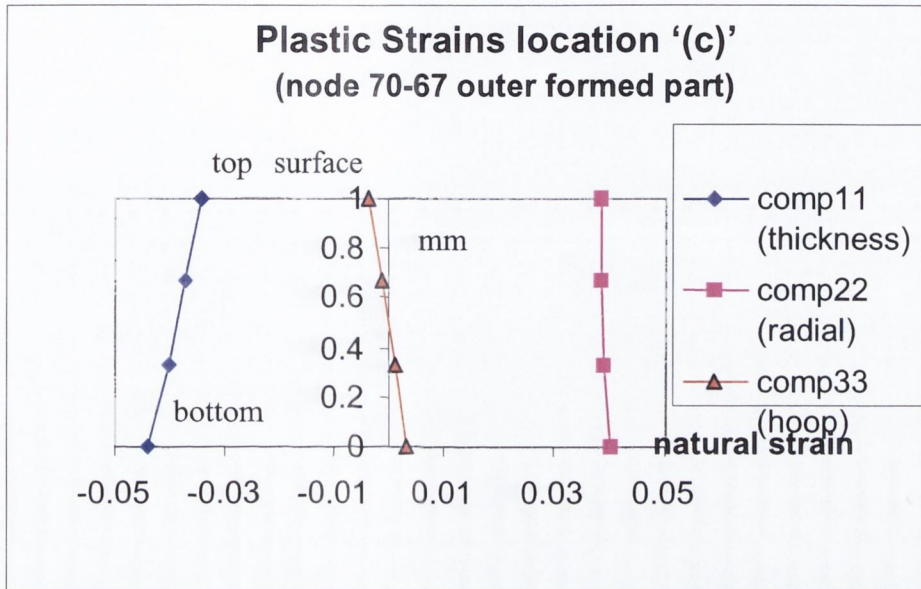


Figure 4.42 Strain Variation through Sheet Thickness at '(c)'

In summary studying the strain variation through the sheet thickness has shown that the nature of the deformation in two of the three locations investigated is close to that predicted by the idealised 'shear forming' process but results from the first location beside the tailstock show strains that can be characterised as pure bending. These results are taken from a finite element simulation near the end of the first roller pass. This model used three elements through the workpiece thickness. The strains resulting vary linearly through workpiece thickness so results taken from a model with only one element through workpiece thickness should still achieve reasonable accuracy. Accordingly the simulation of the entire three pass spinning process was run with only one element through the material or sheet thickness. Further analysis of the variation of strains through thickness was carried out at the locations shown in Figure 4.43

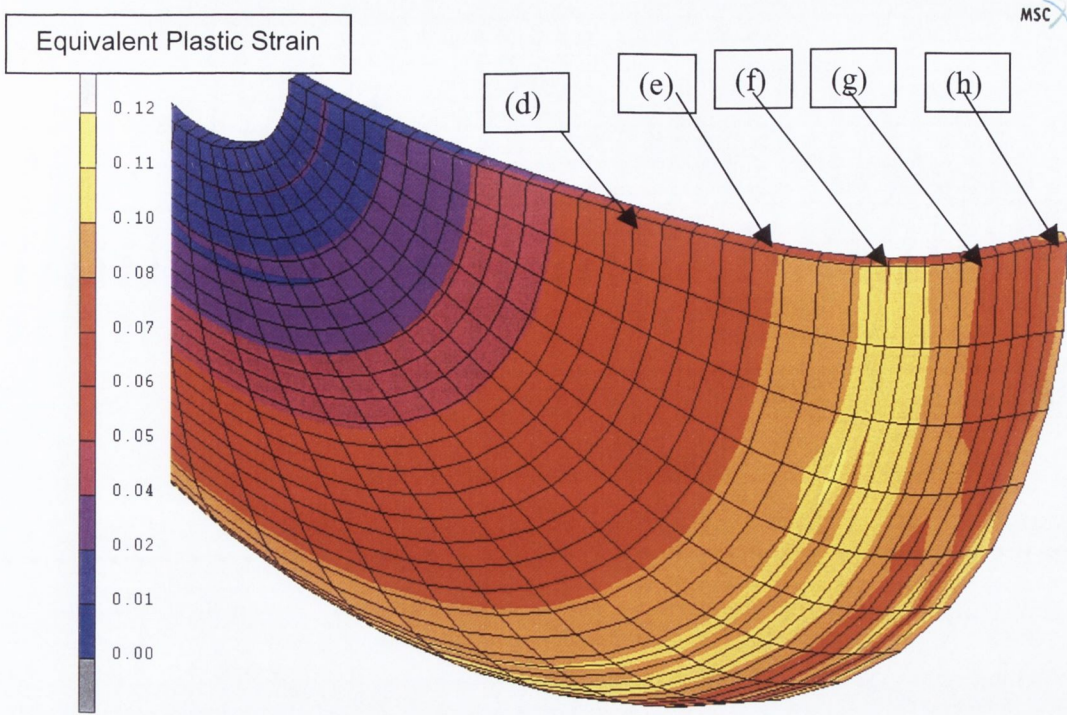


Figure 4.43 A section of the finite element model - spinning completed

In Figure 4.44 the results for the location ‘(d)’ in Figure 4.43 are similar to the results for location ‘(c)’ in the partially formed part Figure 4.42. both are for positions about 30mm from the centre of the workpiece.

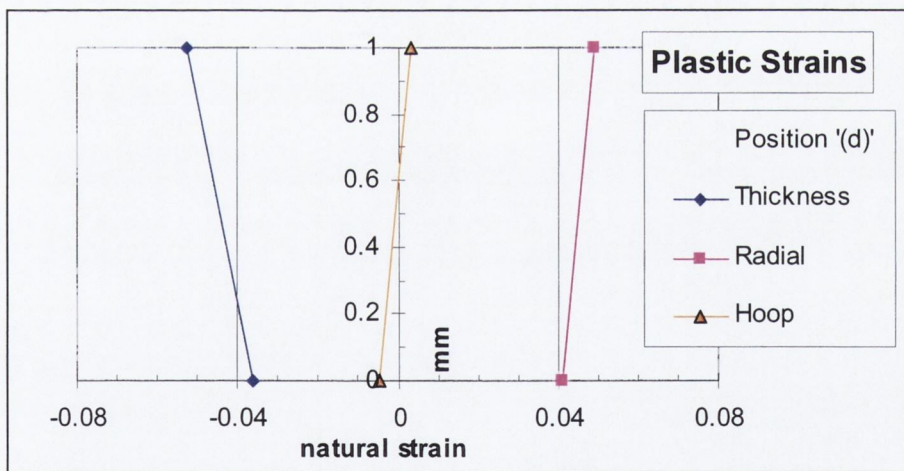


Figure 4.44 Strain Variation through Sheet Thickness at ‘(d)’

In Figure 4.45 the results for the location ‘(e)’ in Figure 4.43 are for a position 43mm from the center of rotation just at the transition between the spherical region of the part to the fillet radius. It can be seen that there is far greater difference between the inner and outer surfaces as a result of the smaller radius.

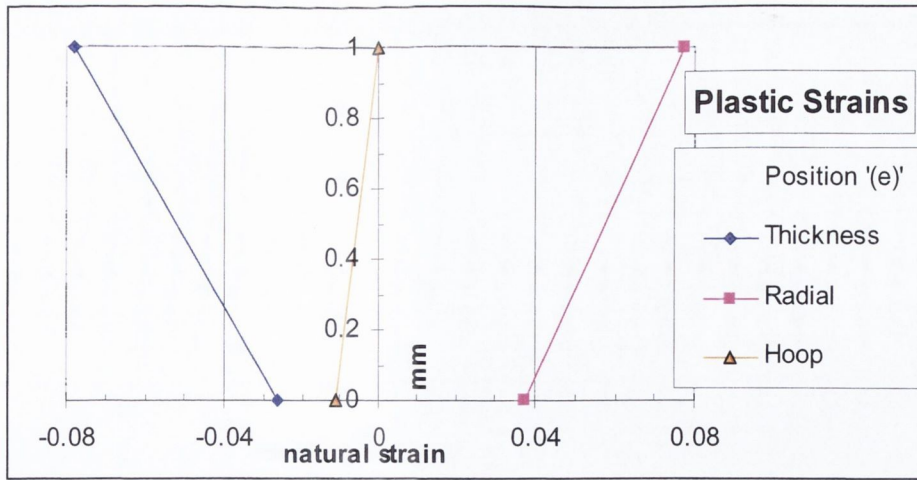


Figure 4.45 Strain Variation through Sheet Thickness at '(e)'

In Figure 4.46 position '(f)' which is at a distance of 48 mm from the center in the original blank it can be seen that significant hoop strain is occurring and in can be seen that the hoop strain increases in the following diagrams for locations '(g)' and '(h)' of Figure 4.43

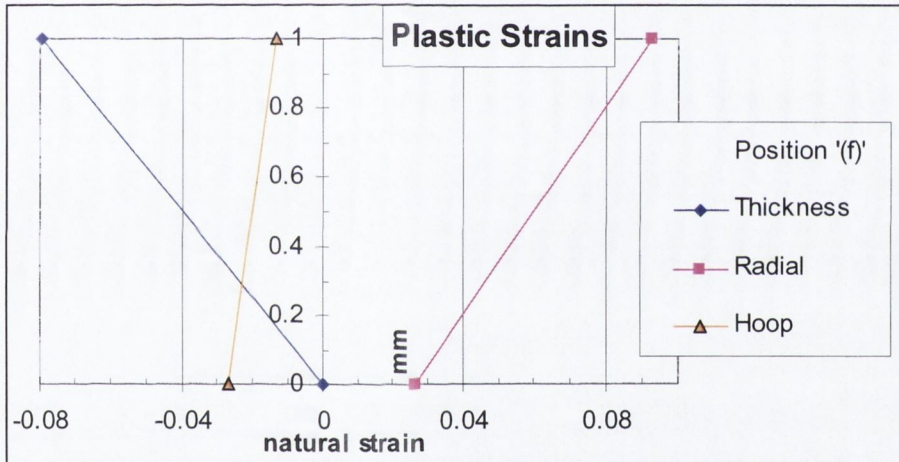


Figure 4.46 Strain Variation through Sheet Thickness at '(f)'

In Figure 4.47 this increasing hoop strain exceeds 0.06 as a negative hoop strain. And the large variation in the other strains between the outer or top surface and the inner or bottom surface reflects the much smaller radius at the edge of the part.

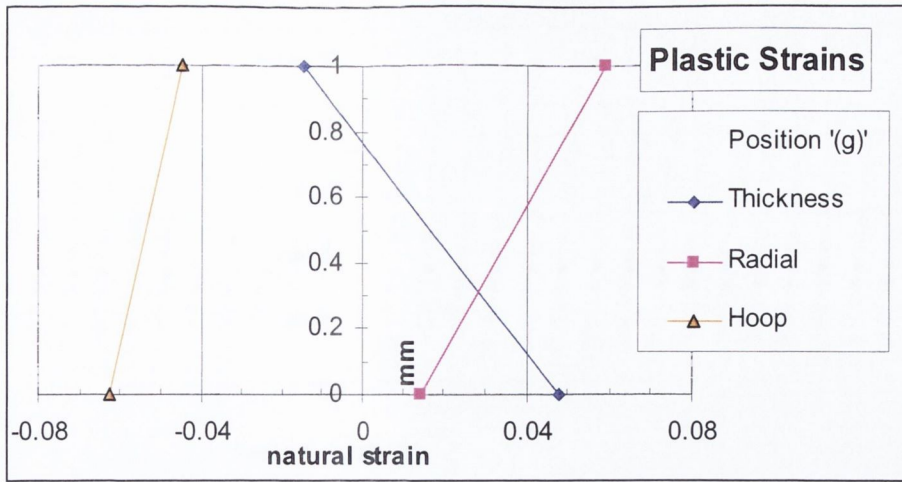


Figure 4.47 Strain Variation through Sheet Thickness at 'g'

In Figure 4.48 which is the result for the very edge of the part we see positive thickness strain and positive radial strain while the hoop strain is reduced. The variation in strains from inner to outer surface is much lower reflecting that this is effectively not part of the edge radius but has remained flat.

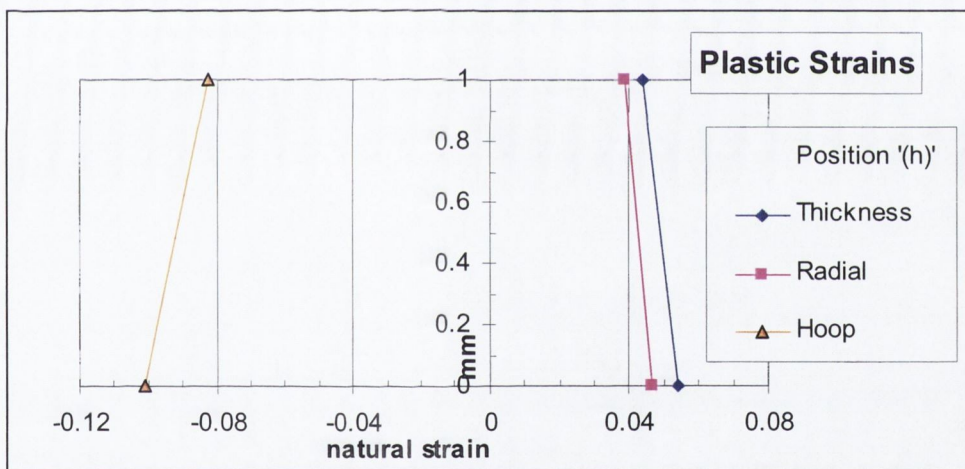


Figure 4.48 Strain Variation through Sheet Thickness at 'h'

The magnitudes of strains imposed by the simulated spinning process were larger in magnitude than the constant thickness ideals in the central region but smaller than the shear forming strains.

The results presented in Figure 4.29 for the strains for a theoretical shear forming and constant thickness spinning are plotted again in Figure 4.49 to make the comparison with the strains predicted by the finite element simulation. The finite element strain results are the average of principal strains at the inner and outer surfaces of the part. As such they do

not reflect the through thickness variation that has been presented in Figure 4.40 through Figure 4.48.

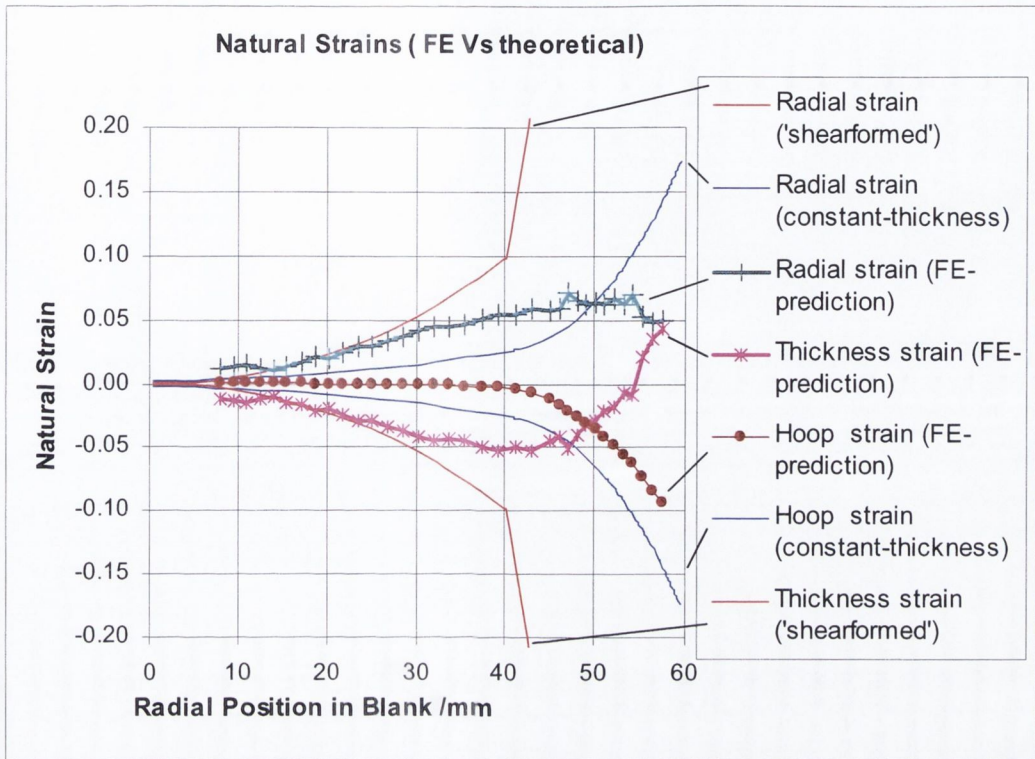


Figure 4.49 Strains from FE simulation compared to theoretical

The fact that the hoop strain is effectively zero in the central region supports the concept of a certain critical flange size allowing 'shear forming' to take place. This concept is key to cone spinning without a mandrel [38] and has implications for designing tool paths for any spinning process.

4.4.8. Strain hardening results

This section gives a brief outline of the results of a series of micro-hardness tests that were made on the experimental parts after spinning as described in chapter 3. The results show that substantial strain hardening is achieved in regions of the spun part that would not be expected from the deformed shape itself i.e. in terms of the idealised constant thickness process. It can be seen in Figure 4.50 that greater hardness has been achieved nearer the center of the part. The results also offer a benchmark to assess the prediction of work hardening by finite element analysis.

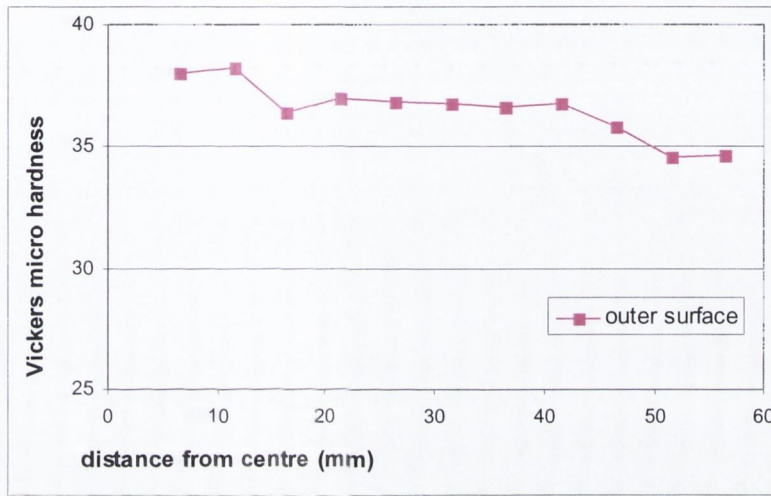


Figure 4.50 Typical hardness profile

In Figure 4.51 the hardness measurements are converted to a tensile yield strength using a factor of 3.235 calculated from data given in [54] using a zero intercept. The predicted yield strength from the finite element simulation is also plotted.

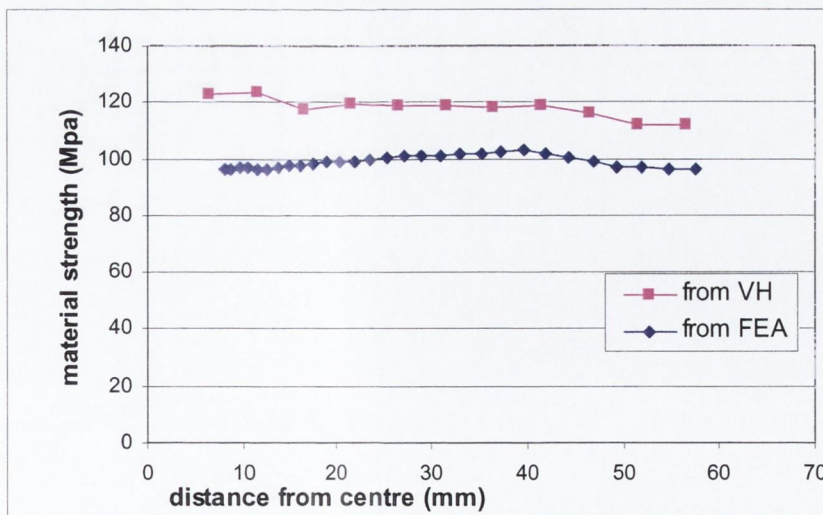


Figure 4.51 Strength from hardness measurements and FE predicted

The total equivalent plastic strain is the parameter that is used in the simulation to look up the material flow curve and so total equivalent plastic strain was converted to yield strength using this flow curve. It can be seen that although there is some scaling difference between these curves, both curves reflect the fact that workhardening reduces at the periphery. Although the imposed strains are larger at the periphery the material there has only been subjected to one roller pass.

4.5. USING MESH REFINEMENT TO STUDY CONTACT.

4.5.1. Results showing size of contact area

The first approach used to assess the size of the contact area was to set up a region of the disk where the mesh was sufficiently fine so that there would be several nodes in contact simultaneously, and not simply one or two reacting most of the contact force

This model was solved using domain decomposition. This technique was used to produce several of the finite element results presented in this work. The author in [55] discusses some aspects of using this technique, which involves parallel processing. The main feature of this technique is that the mesh of elements is divided up into a small number of sets or domains and each domain is then solved on a separate computer. The shared boundary between the domains is then solved as a separate problem on one of the computers which operates as the master computer. In general the solution time for this shared boundary or inter-domain problem is small compared to the size of the domains and so the technique has the benefit of several computers working at close full capacity to substantially reduce the overall solution times.

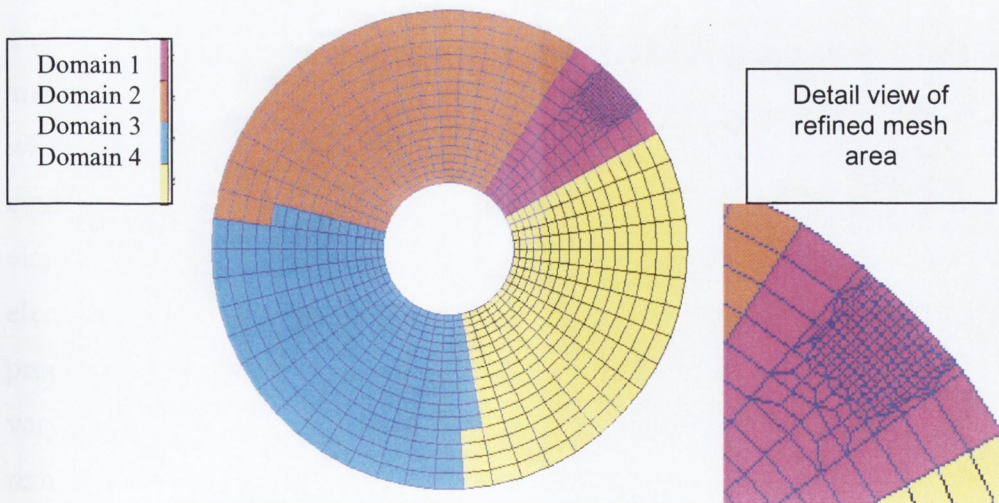


Figure 4.52 Mesh divided into four domains (spin020128)

In this case of the mesh is shown in Figure 4.52 Each domain contains approximately 740 elements, but Domain 1 appears smaller because of the finer mesh. The fine elements

visible at the edge of the disk measure approximately 0.45mm square on the surface of the disk and are 0.33mm deep and so three elements are being used through the workpiece thickness of 1mm.

Looking at the fine mesh region shown in Figure 4.53, as the roller passes over it, it can be seen that contact is made with approximately fourteen nodes, representing an area of just less than 3 mm². Also as would be expected, the contact region is in front of the center line of the roller. It is of interest that the contact region is not particularly circular in shape but extends from the area of highest contact stress and trails both behind and toward the center of the workpiece. This result is with the roller close to the edge of the part.

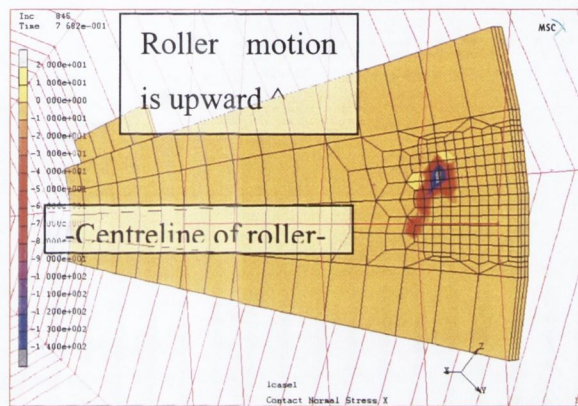


Figure 4.53 Contact area between roller and workpiece

Another approach to studying the contact area is to use mesh adaptivity. In this technique a coarse mesh is initially defined for the entire workpiece and a small number of elements are designated as being in an adaptive set. These elements can be automatically refined when contact occurs. The maximum level of subdivision used was four i.e. each element could be subdivided four times. This allows a single element to generate 8⁴ or 4096 elements i.e. if a brick element is refined in by dividing each edge in half it will become 8 elements and if this refinement process is allowed to proceed four times 4096 element are produced. Clearly the number of elements that can be handled to this level of refinement is very limited, fortunately after each level of subdivision it is only those elements that remain in contact that are subdivided again so this restricts the growth in the number of elements.

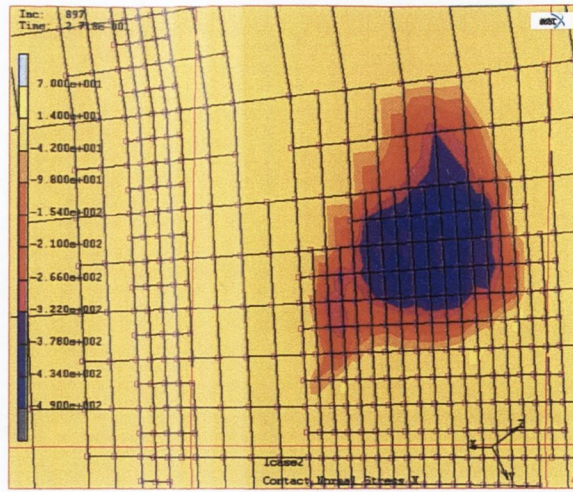
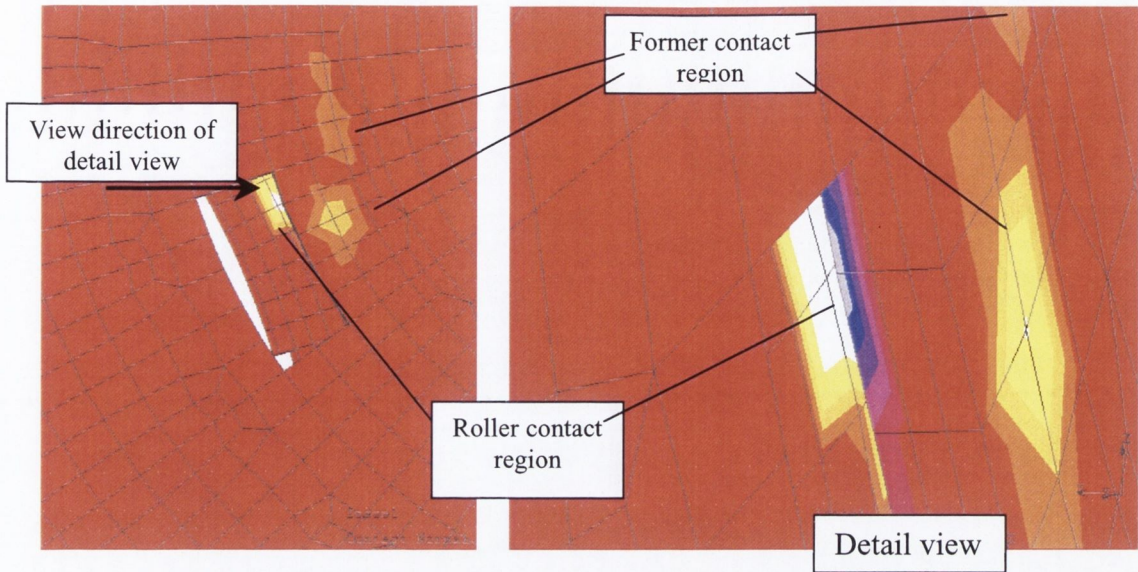


Figure 4.54 Contact area between roller and workpiece using adaptive meshing

The smallest elements measure 0.09 mm by 0.14mm on the surface of the workpiece and there are approximately 100 nodes in contact so a contact area of 1.3mm^2 is predicted. This smaller area is occurring earlier in the spinning process. (The adjacent area of refined mesh shown in Figure 4.54 is the result of a previous roller pass).

Limitations of the capabilities of Marc2001 finite element code prevent the combination of parallel processing and local mesh adaptivity. This may seem an obvious approach to problems such as the simulation of incremental forming or spinning and it is announced that this restriction is partially resolved in the Marc2003 code.

4.5.2. Offset Contact Forces and Areas (insight Deformation Mechanics in spinning)



(view from inside the former with mesh cutaway to show roller contact region)

Figure 4.55 Offset of contact areas on roller and former

It is of interest to explore how the contact area with the roller and former differ during a spinning process. Even using a relatively coarse mesh that has enabled the simulation of the full three pass spinning process as previously described in Section 4.4

Figure 4.55 shows how the contact areas with the roller and former are not directly opposite each other on either side of the workpiece but are in fact offset by a significant distance.

By using local mesh refinement during the first pass greater detail can be seen in terms of the shape and location of contact areas with the roller and former.

Figure 4.56 provides a cutaway view of the model to clarify the position of the tools and contact areas and the motion of the roller.

Contour plots of the contact stress are shown in Figure 4.57. In part (a) of this figure the mesh is viewed from inside the workpiece i.e. through the former. The contact area can be seen to be quite elongated. In part (b) of this figure some of the workpiece mesh is hidden to reveal the contact stress on the roller surface where it is in contact with the workpiece.

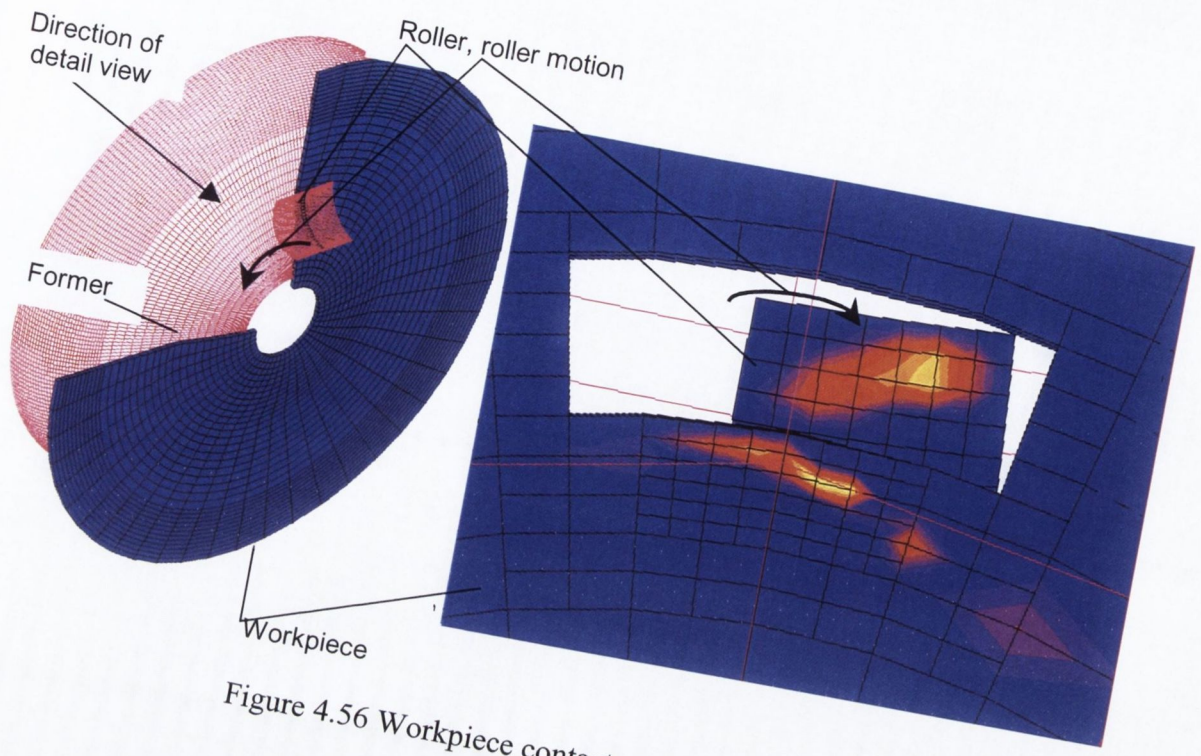
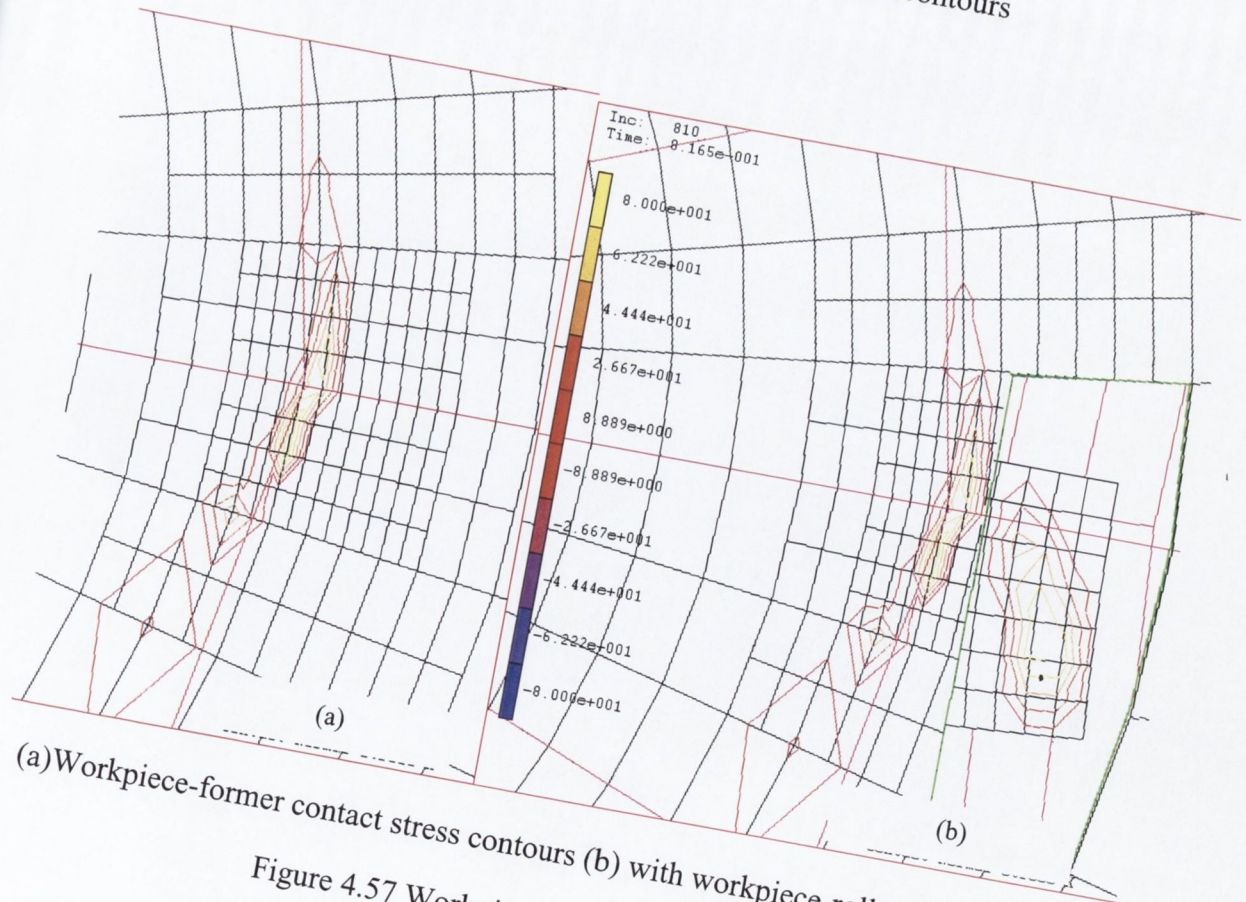


Figure 4.56 Workpiece contact stress contours



(a) Workpiece-former contact stress contours (b) with workpiece-roller stress contours
 Figure 4.57 Workpiece contact stress contours

Studying this small area of workpiece in greater detail it is of interest to look at the plastic strain rate.

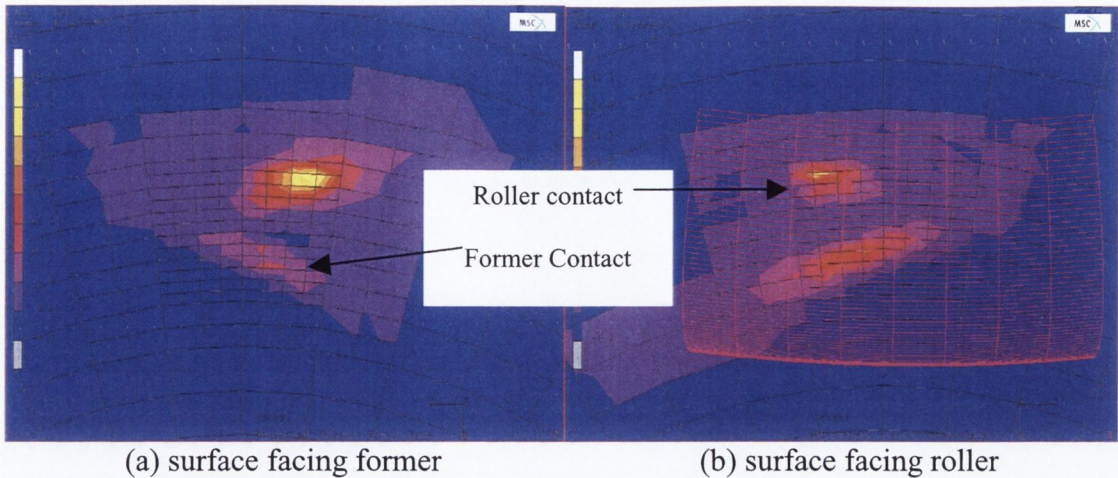


Figure 4.58 Contour plots of Equivalent Plastic Strain Rate

Taking the same area of the workpiece and plotting plastic strain rate it can be seen that the areas of high strain rate are reasonably similar to the areas of highest contact stress. There are in fact two separate zones of high strain rate. The first where the roller makes contact with the workpiece and a second where the former makes contact. These views are taken from opposite sides of the workpiece and so appear somewhat like mirror images of each other.

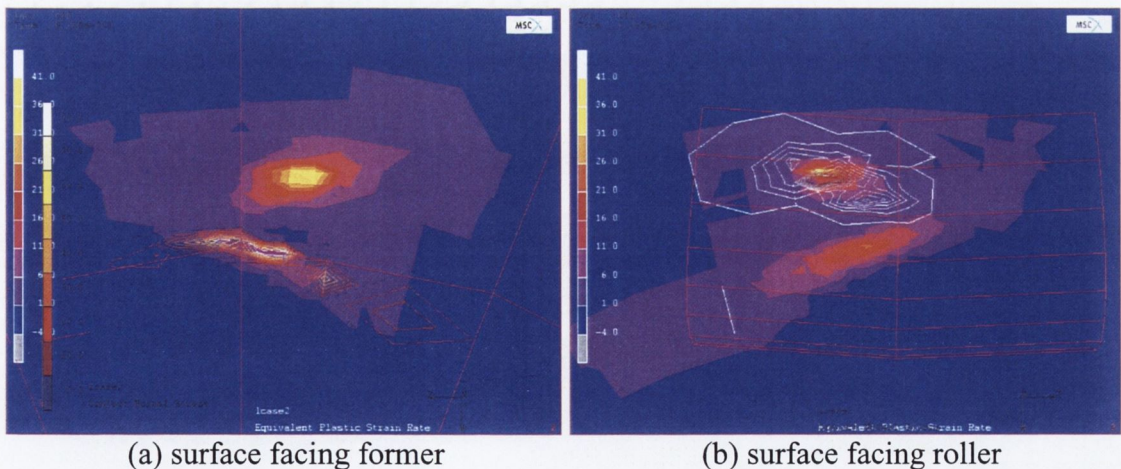


Figure 4.59 Plots of Equivalent Plastic Strain Rate with stress contours superimposed.

These areas are quite distinct. The area around the roller contact region extends some distance in front of the roller while the area around the former contact region ends reasonably abruptly where former contact stress occurs. This is illustrated in Figure 4.59. In this figure the contact stress contours that were presented in Figure 4.56 are superimposed on the plastic strain rate plots of Figure 4.58. The actual levels of strain rate

are significant a strain rate of 60(1/sec) might not be anticipated in a process that has a cycle time of anything from 15 to 150seconds and where the maximum strain created by the process may be no more than 0.3 (natural strain). The value of strain rate could indicate an increase in flow stress of the order of 10-15% [56].

Also of note is the size of the straining area: the areas are larger on the surface away from the tool. Considering the area of high strain directly related to contact with the roller: in Figure 4.58 (a) the area of high strain rate is higher and more intense than in (b) although it is the surface illustrated in (b) that makes contact with the roller. This would be expected with a stretching process being imposed by the roller.

Considering the area related to contact with the former the reverse is the case: the area of high strain directly related to former contact: in Figure 4.58 (b) the area of high strain rate is higher and more intense than in (a)

CHAPTER 5. CONCLUSIONS

5.1. Conclusions

- Comparison of the results for static contact with the results from the experimental spinning process has shown that tool forces in spinning are very much less than the force required to produce the same thickness change by direct compression. This has provided clear evidence of the stretch forming nature of conventional spinning.

Static contact analysis has been used to determine contact stiffness. It predicts a larger tool force line stiffness than was found in the experimental spinning tests. It has been shown that the effective tool force line stiffness is greatly reduced in a spinning process because of the stretch forming nature of the process. A static force of 500N would be far from sufficient to achieve the change in wall thickness involved in manufacture of the experimental part but it has been demonstrated how through local contact loads this magnitude of force can effectively produce the experimental part.

- The spinning process is robust because it is insensitive to normal force changes. The thickness reduction achieved in static contact by a given force does not have a linear relationship with its magnitude and correspondingly the thickness reduction in spinning, achieved by a given roller force, does not have a linear relationship with the magnitude of the roller force.

The robustness of the spinning process is predicted by the results of the static contact analysis using 2D finite element analysis. This robustness or insensitivity to roller force change has been confirmed by experimental spinning tests. The insensitivity to roller force variation is a significant factor in assuring the stability of the spinning operation.

- Static stress analysis has been used to quantify the stress magnification that occurs when a workpiece is loaded with forces applied to unequal areas. This leads to a stress condition that is wholly consistent with a description of spinning as stretch forming. Using a 3D spinning process simulation, it has been shown that this stress condition occurs in the deformation zone.

- The use of a low elastic modulus tool material enhances this robustness and furthermore the use of soft tool material in conjunction with a large feed or stepover is a very effective incremental forming strategy particularly because of the larger tool contact areas achieved with low elastic modulus tools. Correspondingly, dwell during roller motion and small feed or stepover combined with hard tools provide a less stable forming strategy that can lead to backward bulging or in the worst case trepanning.

- It has been demonstrated how thickness strain in ‘shear forming’ can be assumed to be a principal strain thereby reflecting the stretch forming nature of spinning processes. Comparison of the results of a full process finite element simulation and the principal strains for a shear formed element as obtained from classical continuum mechanics confirm this.

It has been shown that the distinction between shear forming and conventional spinning is quite blurred. The final stages of a conventional spinning process demands the most in terms of machine tool rigidity in order to achieve the required thickness reduction. This is apparent in the general rise in roller force in the experimental process just as predicted by the finite element simulation.

The start of the conventional spinning process which has been described in the literature as shear forming is almost entirely stretch forming in nature. The results presented here show conclusively that while ‘shear forming’ provides a useful model for volume calculations it does not give a true description of the deformation and underestimates the complexity of the process. The various graphs for stress and strain paths and histories from FE simulations have illustrated this very clearly.

- Full process finite element simulation has been demonstrated using a single solid element through the workpiece thickness. The validity of this approach has been confirmed by the linear variation in strains found using several elements through the workpiece thickness and also supported by static stress and contact analysis. This is consistent with the bending and stretching nature of conventional spinning. The finite element simulations and the experimental results show very good agreement in terms of the characteristics of the forces, the shape of the workpiece during the forming process and the final shape of the product. The agreement on the shape of the force histories is best for the first pass.

- Spinning serves as a useful archetype for investigation of contact and forces in incremental forming. The understanding that has been developed can be applied to a variety of incremental forming processes.

It is foreseen that as incremental stretch forming processes become more widely used, they could be applied to direct manufacture and not simply to prototype production which is largely the case at present.

- An understanding of the system stiffness, or process stiffness is key to the design of any incremental forming process i.e. toolpath and the forming tools and the machine tool. It has been demonstrated that this is the case for conventional spinning.

5.2. Recommendations for future work.

The investigation of incremental sheet forming using FE models will help the development of this technology just as it has done for process and tooling design in the sheet metal stamping industry. The knowledge that has been gained on the size of the deformation zone can be applied to incremental forming in order to better mimic deep drawing or stamping.

The results of this work present implications for the design of incremental forming processes for parts that are not rotationally symmetric. For example if it is sought to develop a process that mimics the material flow in deep drawing the roller must work the material close to the edge of the blank first to avoid a simple stretch forming operation

The possibilities of applying incremental forming to sheet like products e.g. half round sections or tubes remains largely unexplored. It is envisaged that forming a sheet into a singly curved shape prior to incremental stretch forming could provide advantages where the required part shape has a certain predominant curvature, i.e. it should be possible to prototype more efficiently by starting an incremental forming process after an initial rolling operation.

The use of materials that have different values of elastic modulus for incremental forming tooling begs exploration for materials with values in the range above 2.8Gpa. The experimental work in this project was confined to aluminium but to achieve similar advantages with steel it may require a proportionally stiffer tool materials.

As considerable investigations are reported in the use of dieless incremental forming techniques it appears to the author that there is scope for an investigation that would parameterise incremental forming in terms of tool radius, workpiece thickness and plunge depth. An effective plunge depth would need to be calculated to account for the fact that one side of the tool has preformed material and the other side is largely unstrained sheet. Such an investigation would of course also require consideration of flow stress and elastic modulus.

Finite element simulation has formed the basis of a large part of this investigation and can contribute increasingly powerful analysis to all the above problems as computation costs decline.

References

- 1 Matsubara, M., Tanaka, S., Nakamura, T., *Development of Incremental Sheet-Metal-Forming System Using Elastic Tools (1st report principle of forming process and formation of some fundamental curved shapes)* Transactions of the Japanese Soc. Mech. Eng. 1994 Vol.60c pages349-356.
- 2 Jeswiet, J., Hagan, E. and Szekeres, A., *Forming Parameters for Incremental Forming of Aluminum Sheet Metal*, Proc. Inst. Mech Engrs, Vol216 Part B J Engineering Manufacture. IMechE 2002. Page1367-1371.
- 3 Leach, D., Green, A.J., Bramley, A.N., *A New Incremental Sheet Forming Process for Small Batch and Prototype Parts*, 'Shemet2001' proceedings of the 9th International Conference on Sheet Metal, K.U.Leuven, Belgium 2001 page 211-218.
- 4 Strano, M., *Current and Potential Applications of Incremental Processes in Sheet Forming*, (conference on) Recent developments on Metal Forming Technology, ERC/NSM The Ohio State University, October 2002.
- 5 Fax Dated 23Mar'98 from MASATO IMAMURA . 14th RP Symposium Amino Corp to present machine products, , Matsubara, M., (in Japanese) description of incremental sheet metal forming system part translated by A.Miller/EQ .
- 6 Iseki, H., *An approximate deformation analysis and FEM analysis for the incremental bulging of sheet metal using a spherical roller*, Journal of Material Processing Technology, 111 (2001) 150-154
- 7 Finckenstein, E.v., *Handbuch der Fertigungstechnik*, editors Gunter Spur and Dieter Schmoeckel, Band2/3 *Umformen und Zerteilen*, Carl Hanser Verlag Munchen Wien 1985 (in german) pages 1250 –1263
- 8 Jeswiet, J., *Incremental Point forming with a Tool Post*, 'Shemet2001' proceedings of the 9th International Conference on Sheet Metal, K. U. Leuven, Belgium 2001 page 37-42
- 9 Fries-Knoblach, J., *Sheet Metal Working in the Bronze and Iron Age in Southern Central Europe*, Shemet99, The 7th International Conference on Sheet Metal, Friedrich-Alexander-University, Nuremberg-Erlangen Germany, 1999 page23-34
- 10 Raftery, B., *A catalogue of Irish Iron Age Antiquities*, Marburg 1983 page 213-214
- 11 Jope, E.M., *The Keshcarrigan Bowl and a Bronze Mirror-Handle from Ballymoney*, Ulster Journal of Archaeology 1954. page92-96.
- 12 Packham, C.L., *Shear and Flow Forming of austenitic chrome-nickle steel* Sheet Metal Industries, Jan 1978. page 12-14,22
- 13 Fletter, P.R., *Metal Spinning Tutorial 1995*, <http://prl.stanford.edu/Documents/spinning.html> 13th Oct 2001
- 14 Kleiner, M., Heller, B., Göbel, R., Klimmek, Ch., Kantz, H., *Investigation of Dynamic Instabilities in Sheet Metal Spinning*, 3rd Int. Symposium Investigation of Nonlinear Dynamic Effects in Production Systems 26-27 Sept. 2000 Cottbus Germany
- 15 Reid, W., *Metal Spinning and Anodising*, Oliver and Boyd Edinburgh and London 1968
- 16 Merkblatt stahl 351 *Drücken von Stahlblech*, Beratungsstelle für Stahlverwendung Düsseldorf1 1969 (in german)
- 17 Lange, K. *Handbook of Metal Forming*, Society of Manufacturing Engineers, Dearborn, Mich. 1995
- 18 Lange, K., ed., *Umformtechnik, Handbuch für Industrie und Wissenschaft, Band 3 Blecharbeitung*, Springer-Verlag Berlin Heidelberg New York London Paris 1990 page 500-521 (in german)

-
- 19 Brown,C.C., *A Microprocessor Based Learning System for Hydraulic Metal Spinning*, Proceedings of the Second International Conference on Rotary Metal-Working Processes, October 6th-8th,1982.
- 20 Runge,M., (translated by D.H.Pollitt) *Spinning and flow forming*, Leifield GmbH &Co. Werkzeugmaschinenbau / verlag moderne industrie AG, D-86895 Landsberg/Lech 1994
- 21 Agarwala,B.K., *The shear spinning of tubes with high dimensional precision*, Proc. of Advanced technology of plasticity 1st ICTP 1984 vol 1 pp401-409
- 22 Sortais,H.C., Kobayashi,S., Thomsen,E.G., *Mechanics of Conventional Spinning*, Transactions of ASME, Journal of Engineering for Industry Nov. 1963.
- 23 El-Sheikh,M.N., *Production of Aluminium Bowls through a Process Combination of Spinning and Deep Drawing*, pages 189-203, (conference proceedings), Neuere Entwicklungen in der Blechumformung, IFU-Universität-Stuttgart /Werkstoffinformationsgesellschaft, May 1998
- 24 Hosford,W.F. and Caddell,R.M. *Metal forming Mechanics and Metallurgy* New Jersey PTR Prentice Hall 1993 ISBN 0135885264 p290, p14
- 25 Dierig,H., *Verbesserung der Form- und Massgenauigkeit beim NC- und CNC-Drücken* (survey of parameters governing spinning), Industrie-Anzeiger 109(1987)77.p.92-93
- 26 www.leifield.com Leifield GmbH &Co 2003
- 27 Qiang, W., Tao, T., Wang, Z.R., *A study of the working force in conventional spinning*, Proceedings of the Second International Conference on Technology of Plasticity Stuttgart, August 24-28, 1987 Ed. by K. Lange for Arbeitsgemeinschaft Umformtechnik, Springer-Verlag, Berlin Heidelberg. 1987 ISBN 3-540-17915-1 page103-108
- 28 Quigley,E., Monaghan,J., *Metal forming, an Analysis of Spinning Processes*, Journal of Materials Processing Technology 103 (2000) page 114-119.
- 29 Packham,C.L., *Metal spinning and shear and flow forming*, Sheet Metal Industries, Apr., May and June 1977.
- 30 Kobayashi,S., *Instability in Conventional Spinning of Cones*, Transactions of ASME, Journal of Engineering for Industry, Feb. 1963. page 44-48
- 31 Nagarajan,H.N., Kotrappa,H., Mallanna,C., Venkatesh,V.C., *Mechanics of Flow Forming*, Central Machine Tool Institute, India. 1979
- 32 Spencer A.J.M., *Continuum mechanics*, Longman London, 1980. Page 74-75
- 33 Wada,T., Nanba,T., *Spin-forging deformation mechanism of Sheet Metal Cone*, Proceedings of the Twenty Sixth International Machine Tool Design and Research Conference Sept. 1986 UMIST/Macmillan page 483-488
- 34 Sortais,H.C., Kobayashi,S., Thomsen,E.G., *Mechanics of Conventional Spinning*, Transactions of ASME, Journal of Engineering for Industry Nov. 1963. page 346-350
- 35 Köhne,R., *NC-Drücken unter Verwendung eines Programmier- und Erfassungssystems* (in german~ NC spinning /roller path programming systems), Industrie Anzeiger Nr.15 v.20.2 1981 /103.Jg. page 14-16
- 36 Kawai,K., and Hayama,M., *Roller Pass Programming in Conventional Spinning*, Proceedings of the second international conference on Advanced Technology of Plasticity vol. II. Stuttgart,August24-28,1987, Springer Verlag, page 711-718
- 37 Winkelmann,H., Brüntrup,O.,Hauk,H., *Multifunktionale rotationsymmetrische Formteile aus Blech* , Umformtechnisches Kolloquium Darmstadt, PtU Darmstadt, March 1997 (in German)page 97-102

-
- 38 Kawai, K., Yang, L.-N., Kudo, H., *A flexible shear spinning of truncated conical shells with a general-purpose mandrel*. Journal of Material Processing Technology, 113 (2001) 28-33
- 39 Slater, R.A.C., *A review of Analytical and Experimental Investigations of the Spin-Forging of Sheet Metal Cones*, pages33-60, Proceeding of the first International Conference on Rotary Metal-Working Processes, November20-22, 1979.
- 40 Wada,T., Nanba,T., *Spin-forging deformation mechanism of Sheet Metal Cone*, Proceedings of the Twenty Sixth International Machine Tool Design and Research Conference Sept. 1986 UMIST/Macmillan page 483-488
- 41 Johnson,K.L., *Contact Mechanics*, Cambridge University Press, 1985
- 42 Essenburg,F., *On surface constraints in plate problems*, Trans. ASME, series E, Journal of applied mechanics vol. 29, 1962, page340-344
- 43 Updike,D.P., Kalnins, A., *Contact pressure between elastic spherical shells compressed between rigid plates*, Trans ASME, Series E, Journal of Applied Mechanics, vol. 39, 1972 , page 1110-1114
- 44 Gladwell,G.M.L., England,A.H., *Contact problems for the spherical shell*, Proceedings 12th Annual Meeting of Society of Engineering Sciences, Austin, University of Texas, 1975 page 869-875
- 45 Powell,N.N., *Incremental Forming of Flanged Sheet Metal Components*, PhD thesis, Cambridge University, England 1991.
- 46 MSC.Marc *Theory and User Information, Vol. A*, MSC Software Corporation, Santa Ana, California, U.S.A., 2001. page 8-12 to 8-19 and page 10-33
- 47 MSC.MARC *Training Course Documentation MAR101* Marc Analysis and Research Corp. Palo Alto USA.
- 48 Quigley, E., Monaghan, J., *Limitations of finite element models of spinning and incremental forming processes*, IMC19 19th International Manufacturing Conference, Queens University Belfast, August 2002
- 49 <http://web.mit.edu/2.31/www/fall01/ps5sol.pdf> *Finite element analysis in computer-aided mechanical design*, Massachusetts Institute of Technology, June 2002
- 50 Warren C. Young, *Roark's formulas for Stress and Strain* 6th Ed. McGraw-Hill 1989 ISBN 0-07-100373-8 page 440
- 51 Fuji Prescale films, *technical information on pressure sensing films*, April 2001 (c167)
- 52 www.kistler.com Kistler Instrumente AG, 2002
- 53 Quigley,E., Monaghan,J., *Using a finite element model to study plastic strains in Metal Spinning*, 'Shemet2001' proceedings of the 9th International Conference on Sheet Metal, K.U.Leuven, Belgium 2001 pp 255-262.
- 54 Brooks Hardness Conversion Chart, Brooks Inspection Equipment, Colchester, England, ~1995.
- 55 Quigley,E., Monaghan,J., *The Finite Element modelling of Conventional Spinning using Multi-domain Models*, IMC18 Conference of Irish Manufacturing Committee, 2001
- 56 Byrer,T.G., Semiatin,S.L.,and Vollmer D.C., (editors) *Forging Handbook*, Forging Industry Association, American Society for Metals, 1985 Ohio ISBN 0-87170-194-4 page 90.

Appendix 1 Flow Curves from Plane Strain Compression

Plane Strain Compression Test

In order to determine the material behaviour under large plastic deformation, measurements are made of force and position as specimens are compressed in the test apparatus shown in fig. 1 below. The test rig is shown mounted in the Instron Universal test machine Type (100kN).

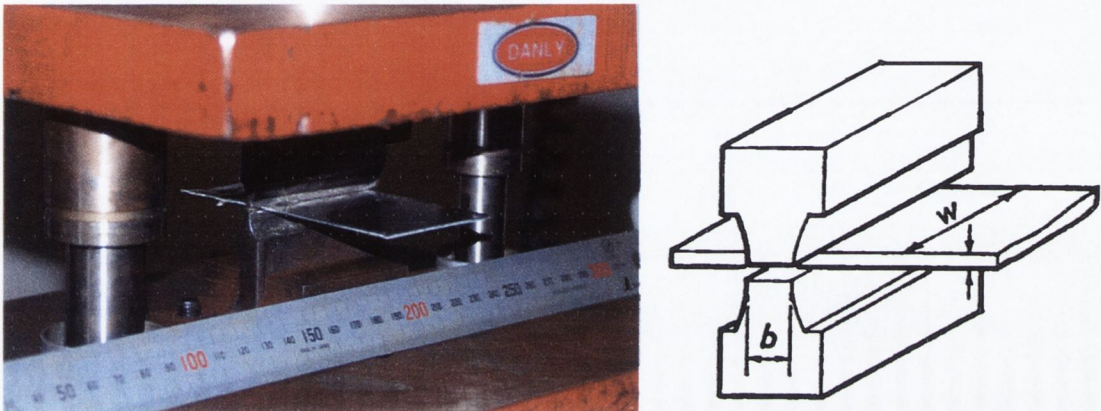


Figure 1 Plane strain compression test apparatus

Determining a maximum strain point on the flow curve

What is required is a mapping of flow stress against natural strain. The final thickness of the part is produced by the highest load (see figure 2). This gives a definite point on the flow curve that is easily calculated. The final thickness (l_{final}) of the specimen can be measured after it is removed from the test apparatus. The original thickness (l_o) is also easily measured. The natural strain is then calculated as

$$\varepsilon = \ln\left(\frac{l_{final}}{l_o}\right)$$

The stress required to produce this strain can be calculated from the measured load. The stress is calculated by dividing the measured load by the area of the specimen that has been compressed.

$$\text{Area} = (\text{width of blade}) \times (\text{width of specimen})$$

$$\sigma_{flow} = \left(\frac{\text{load}}{\text{area}}\right) = \left(\frac{\text{load}}{b \times w}\right)$$

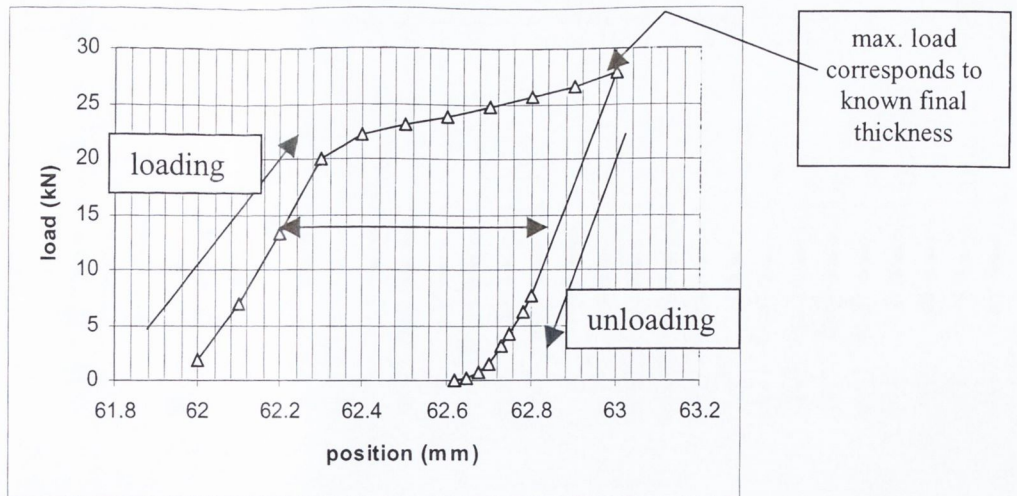


Figure 2 Raw test data; load displacement results

Conversion from plane strain to uniaxial.

The test being conducted is a plane strain test and not a uniaxial test. Because it is desired to have the flow stress information that can be related to uniaxial stress conditions it is required to reduce the stress data by a certain factor ^[1]. This reduction is required because under plane strain conditions material flow is more constrained than in a uniaxial test. The

conversion factor used is $\frac{\sqrt{3}}{2} = 0.866$

Thus the flow stress equivalent to a tensile test can be written

$$\sigma_{flow} = 0.866 \left(\frac{Load}{Area} \right)$$

[1] Rowe, G.W., Elements of Metal Working Theory, Edward Arnold Ltd, London 1979

Other points on the flow curve

The above calculations give the maximum load point on the flow curve. For other points on the flow curve the thickness can be calculated from the displacement. To calculate the thickness it is necessary to subtract the measured displacement from the final displacement and to add this difference to the final thickness. The result is shown in fig3

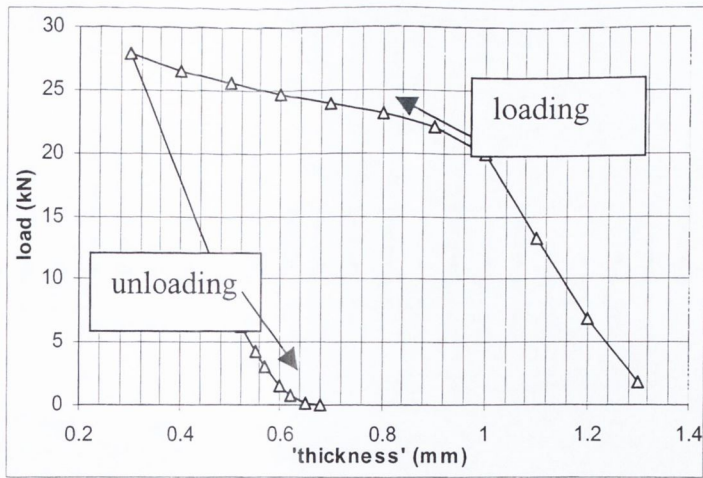


Figure 3 Load Vs. Uncorrected thickness

From figure 3 it is evident that there is considerable elastic windup occurring as the load is applied. Without correction for elastic windup there will appear to be load measurements where the test specimen is thicker than it was before the test (1.0mm) which is clearly impossible. To get an accurate result it is vital to know the elastic characteristic of the apparatus. This can be determined by measuring the force displacement output of the system, as it is unloaded.

Therefore instead of taking the difference between the final displacement and the displacement at a given load, the difference should be taken between the displacement corresponding to the same load on the unloading curve and the displacement at a given load. This is effectively the horizontal distance between the curves in figure 2. (This may be done graphically)

The flow curve in figure 4 is then obtained by plotting the stress, calculated from the load measurements and the strain, i.e. calculated by taking the log of the thickness corrected for elastic windup.

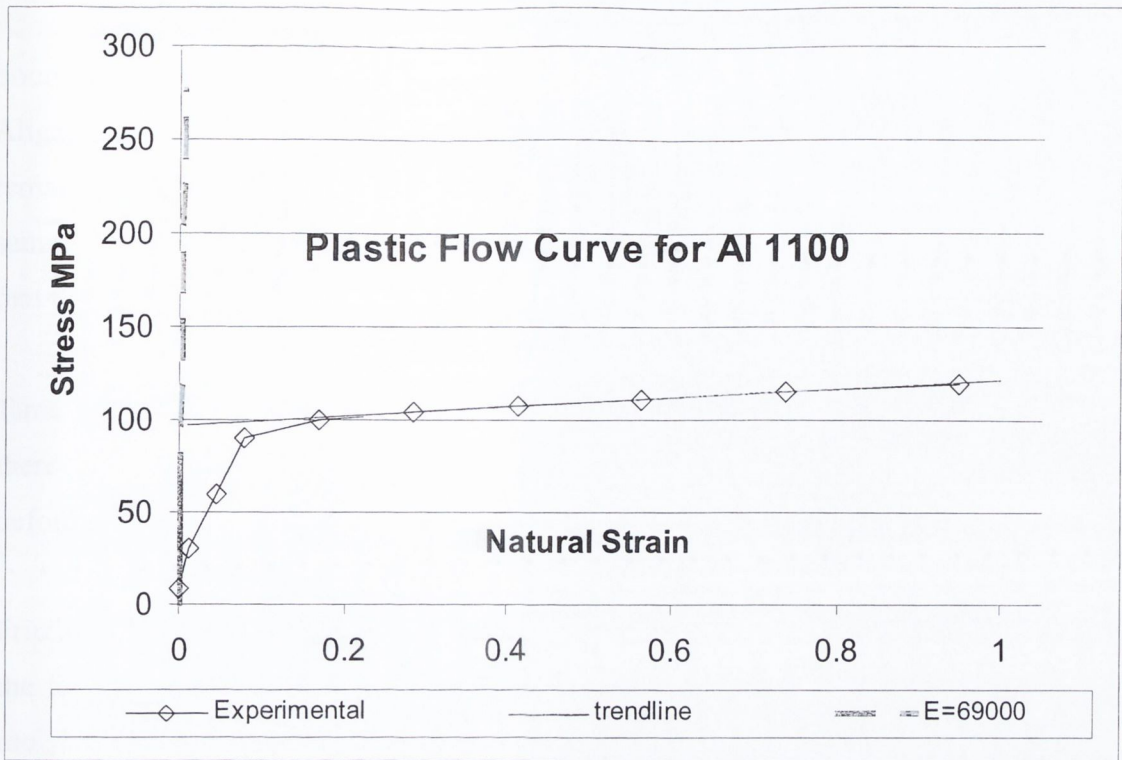


Figure 4 Experimental Flow Curve

This data now must be made available in a meaningful form to the finite element code. This can be done as a series of data points or as a characteristic equation for the line. There is of course some serious doubt about the accuracy of the early part of the curve. The slope of this region of the curve might be expected to be equal to the Elastic modulus for aluminium which is plotted for reference on the graph in figure 4. It can be seen that it is an almost vertical line. What is required is a reasonable extrapolation of the large strain plastic flow curve back towards the vertical axis. This can be done by adding a trend line to the large strain measurements. The intercept of this line and the Elastic modulus line is clearly the yield stress that will be used to determine initial plastic deformation in the simulations.

$$\sigma_{flow} = 96.7 + 24.95\varepsilon$$

It is also noteworthy that this intercept value is in good agreement with a published [229] figure for the yield strength of Al 1100 H12 of 105MPa given that the material was sourced as an 'equivalent' to this grade of pure aluminium.

[229] Baucchio, Michael(Ed.), ASM Metals Reference Book, Third Edition, ASM International, 1993, pp414-415 tensile / yield strength for various Aluminium alloys.

Sources of error

Alignment. It is obviously critical that the blades of the test apparatus are parallel and remain well aligned during the test. It can be checked that the width of the specimen is the same across the full width of the indentation after the test in order to confirm this. Also that there is no misalignment between the upper and lower indentations on the test piece.

Time dependency. It is also important that the readings be taken without undue delay as there is a tendency for material that is plastically deforming to continue plastically deforming without any additional load being applied.

Friction. As is known from any analysis of forging the higher the friction on the surface of the forging tool the greater the forging pressure or force required. To minimise friction a molybdenum grease was used. In order to relieve any friction that does occur the test load should be reduced to zero after each measurement point.

Appendix 2 NC code

N01G50S1500

N02G28U0

N03G28W0

N04G00Z100.0

N05M01

N500T1200M41

G99G97S478M03

G00X120.0Z5.0

X30.0

G01Z-0.3906F1.5

G03X86.280Z-8.8971R103.7

G01X96.0000Z-7.2430

G00X140.0Z5.0M01

G99G97S478M03

G00X56.0000

G01Z-3.1517F1.5

G03X87.5942Z-9.2011R103.7000

G03X100.8474Z-13.4328R25.7000

G01X106.0000Z-15.5109

G00X140.0Z5.0 M01

G99G97S478M03

G00X76.00

G01Z-6.5133F1.5

G03X87.5942Z-9.2011R103.7000

G03X116.0662Z-26.5079R25.7000

G01X120.0000

G00X140.0Z5.0

M01

G97G00X160.0Z210.0

G28U0.0

G28W0.0

M30

Appendix 3 Fortran 6.6 code for Axisymmetric Spinning Process Simulation

```
0001 subroutine motion(x,f,v,time,dtime,nsurf,inc)
C
0002 implicit real*8 (a-h,o-z)                                dp
0003 dimension x(6),v(4),f(6)
c if it's not the roller it ain't movin
0005 if(nsurf.ne.4) then
    v(1)=0.0
    v(2)=0.0
    v(3)=0.0
    v(4)=0.0
0006 return
0007 elseif(nsurf.eq.4) then
c    do the sums

c SPINNING GEOMETRY *****

c Former Geometry
c Former spherical Radius
0011 RSPHER=95.0
c Former fillet Radius
0012 RFILLT=17.0
c Former Outside Diameter
0013 OUTDIA=100.0
c Tailstock Geometry Tailstock Diameter
0014 TSTKDIA=20.0
c Roller Geometry Roller Edge Radius(roller wheel diameter does not affect the
toolmotion)
0015 RREDGE=8.0
C Workpiece thickness (sheet thickness)
0016 WPTHICK=1.0
c spindle speed in radians per sec
0017 OMEGA= 5.00
c Declare the starting position of the roller.
```

```

C ..DISTANCE OF ROLLER ABOVE DISK..FROM CENTRE OF RREDGE TO
TOPFACE OF DISK
0018  ZSTART=8.5
c Set clearance(negative for Interfernce)=surface deflection for real process
0019  CLEAR=-0.1
c calculate the angle to the change in radius from rspher to rfillt
0020  THETABRK=ASIN(((OUTDIA/2.0)-RFILLT)/(RSPHER-RFILLT))
c calculate the radius to the shange in radius from rspher to rfillt
0021  RBRK=(RSPHER+WPTHICK+CLEAR)*(((OUTDIA/2.0)-RFILLT)/(RSPHER-
RFILLT))
c calculate height lost from spherical surface because of flat under tailstock
0022  FLATHT=(RSPHER-SQRT((RSPHER**2)-((TSTKDIA/2)**2)))
C WRITE  ----- W R I T E  -----
2001  format('2001Inc:',i5,'Time:',g12.5,'rbrk',g12.5,'thetabr',g12.5,
      '*FLATHT',g12.5)
c      if (inc.EQ.0) then
0023  IF(INC.eq.1)open (unit=60,file='subroutine.out',status='unknown')
0024  IF(INC.eq.1)write (60,2001)Inc,time,rbrk,thetabr,FLATHT
C      else

c TOOL MOTION GEOMETRY *****
c FIRST PASS
c Radius for starting the first plunge
0101  RPLUNGE1=15.0
c Radius where first pass along surface of former ends
0102  RSTLN1=43.216
c Angle/direction of feeds off surface 0=TANGENTIAL 90DEGREES=NORMAL
0103  ANGSTL1=3.14159/6.0
c Radius where roller starts rapid (contact release loadcaseef)
0104  RLIFT1=48.0
c Lift Z position to move to from end of str line (as ZSTART=DIST FROM TOPFACE
TO CENTRE RREDGE
0105  ZLIFT1=-2.0

c SECOND PASS

```

c Radius for starting the second plunge

0106 RPLUNGE2=28.0

c Radius where second pass along surface of former ends

0107 RSTLN2=45.0

c Angle/direction of feed off surface on second pass

0108 ANGSTL2=3.14159/12.0

c Radius where roller starts rapid (contact release loadcase?)

0109 RLIFT2=53.0

c Lift Z position to move to from end of straight line

0111 ZLIFT2=-4.0

c THIRD PASS

c Radius for starting the third plunge

0112 RPLUNGE3=38.0

c Radius where third pass along surface of former+w'piece ends

c must not be greater than $OUTDIA/2+WPTHICK+CLEAR$!!!!!

0113 RSTLN3=50.80

c Angle/direction of feed off surface

0114 ANGSTL3=3.14159/2.0

c Radius where roller starts rapid (contact release loadcase?)

0115 RLIFT3=58.9

c Lift Z position to move to from end of straight line

0116 ZLIFT3=9.0

c SPEED FOR FEED and RAPID

c calculate feed rate in mm /sec (from NC feed per rev

0117 FEED=1.5*(OMEGA/(2.0*3.1415926))

c calculate rapid speed in mm /sec (from NC feed per rev

0118 RAPID=15.0*(OMEGA/(2.0*3.1415926))

c CALCULATE LENGTH OF EACH MOTION

c

c---rapid go to start radius NC X30

0200 RAPIDDIST01=RPLUNGE1

```

c---feed (plunge) to one thickness + clearance from former NC Z-1.0938
0202 THETA1=ASIN(RPLUNGE1/(RSPHER+WPTHICK+CLEAR+RREDGE))
0204 FLATHT=(RSPHER-SQRT((RSPHER**2)-((TSTKDIA/2)**2)))
C
0206 PLUNGEDIST02=ZSTART-RREDGE-FLATHT
    *(1-COS(THETA1))*((RSPHER+WPTHICK+CLEAR+RREDGE))
C
c---feed to given radius RSTLN1 along RSPHER and RFILLT
c  check that theta2 is less than theta break
0208 TESTTHETA2=ASIN(RSTLN1/(RSPHER+WPTHICK+CLEAR))
0210 IF (TESTTHETA2.LT.THETABRK) THEN
0212 THETA2=ASIN(RSTLN1/(RSPHER+WPTHICK+CLEAR))
0214 FEEDDIST03=(RSPHER+WPTHICK+CLEAR)*(THETA2-THETA1)
C  else RECALCULATE THETA2
0216 ELSE IF (TESTTHETA2.GE.THETABRK) THEN
0218 THETA2=ASIN((RSTLN1-((OUTDIA/2)-
RFILLT))/(RFILLT+WPTHICK+CLEAR))
0220 FEEDDIST03=(RSPHER+WPTHICK+CLEAR)*(THETABRK-
THETA1)+(RFILLT+
    *WPTHICK+CLEAR)*(THETA2-THETABRK)
0222 ENDIF
0223 RSTLN1C=RSTLN1+RREDGE*(SIN(THETA2))
c RSTLN1C Calculates the position of the Centre of the roller edge radius
C WRITE - - - - - W R I T E - - - - -
2002 format('/2002Inc:',i5,'Time:',g12.5,'PLUNGEDIST02',g12.5,'THETA1',
    *g12.5,'THETABRK',g12.5,'THETA2',g12.5,'FEED',g12.5,'RAPID',g12.5)
    IF(INC.eq.1) open (unit=60,file='subroutine.out',status='unknown')
    IF(INC.EQ.1) WRITE (60,2002)Inc,time,PLUNGEDIST02,THETA1,
    *THETABRK,THETA2,FEED,RAPID
0224
c---feed off
0224 STL_DIST04=(RLIFT1-RSTLN1C)/COS(ANGSTL1-THETA2)
C
C---rapid up in Z

```

0226 IF (THETA2.LT.THETABRK) THEN

0228 RAPIDDIST05=((-RSPHER-WPTHICK-CLEAR+FLATHT-ZSTART
C24/09/02

C above is the z position of the centre of rspher

$$*+(RSPHER+WPTHICK+CLEAR+RREDGE)*\text{COS}(THETA2)$$

C centre of roller before straightline move adds above

$$*+(RLIFT1-RSTLN1C)*\text{TAN}(ANGSTL1-THETA2)$$

C straightline move adds above

$$*-ZLIFT1)**2)**0.5$$

C NOW SUBTRACT 'ZLIFT' TO GET RAPID DISTANCE REQUIRED

0230 ELSEIF (THETA2.GE.THETABRK) THEN

0232 RAPIDDIST05=((-RSPHER-WPTHICK-CLEAR+FLATHT-ZSTART

C above is the z position of the centre of rspher

$$*+(RSPHER-RFILLT)*\text{COS}(THETABRK)$$

C above:centre of rfillt adds this

$$*+(RFILLT+WPTHICK+CLEAR+RREDGE)*\text{COS}(THETA2)$$

C centre of roller before straightline move adds above

$$*+(RLIFT1-RSTLN1C)*\text{TAN}(ANGSTL1-THETA2)$$

C straightline move adds above

$$*-ZLIFT1)**2)**0.5$$

C NOW SUBTRACT 'ZLIFT' TO GET RAPID DISTANCE REQUIRED

0238 ENDIF

c---rapid in toward centre (from RSTLN1 to RPLUNGE2)

0240 RAPIDDIST06=RLIFT1 - RPLUNGE2

C=====SECOND PASS

DISTANCES+++++

c---plunge to make contact

C feed (plunge) to one thickness + clearance from former NC Z-1.0938

0242 THETA07=ASIN(RPLUNGE2/(RSPHER+WPTHICK+CLEAR+RREDGE))

C-----

0244 PLUNGEDIST07=((-RSPHER-WPTHICK-CLEAR+FLATHT-ZSTART

c 24/9/02 added 'clear' in line 0244 above

C above is the z position of the centre of rspher

*+(RSPHER+WPTHICK+CLEAR+RREDGE)*COS(THETA07)

C above dist to centre of roller AFTERPLUNGE

*-ZLIFT1)**2)**0.5

C0244 PLUNGEDIST07=ZLIFT1-RREDGE-FLATHHT

c * +(1-COS(THETA07))*((RSPHER+WPTHICK+CLEAR+RREDGE))

C

c---feed along former to given radius RSTLN2 along RSPHER and RFILLT

0246 TESTTHETA08=ASIN(RSTLN2/(RSPHER+WPTHICK+CLEAR))

c check that theta8 is less than theta break

0248 IF (TESTTHETA08.LT.THETABRK) THEN

THETA08=ASIN(RSTLN2/(RSPHER+WPTHICK+CLEAR))

FEEDDIST08=(RSPHER+WPTHICK+CLEAR)*(THETA08-THETA07)

C else RECALCULATE THETA08

0250 ELSE IF (TESTTHETA08.GE.THETABRK) THEN

0252 THETA08=ASIN((RSTLN2-((OUTDIA/2)-

RFILLT))/(RFILLT+WPTHICK+CLEAR))

0254 FEEDDIST08=(RSPHER+WPTHICK+CLEAR)*(THETABRK-

THETA07)+(RFILLT+

WPTHICK+CLEAR)(THETA08-THETABRK)

0256 ENDIF

0257 RSTLN2C=RSTLN2+RREDGE*(SIN(THETA08))

c RSTLN2C Calculates the position of the Centre of the roller edge radius

C

c---straight line feed off former

0258 STL_DIST09=(RLIFT2-RSTLN2C)/COS(ANGSTL2-THETA08)

C

c---rapid up in Z

0260 IF (THETA08.LT.THETABRK) THEN

0262 RAPIDDIST10=(-RSPHER-WPTHICK-CLEAR+FLATHT-ZSTART

c 24/9/02 added 'clear' in line 0244 above

C above is the z position of the centre of rspher

*+(RSPHER+WPTHICK+CLEAR+RREDGE)*COS(THETA08)

C centre of roller before straightline move adds above

*+(RLIFT2-RSTLN2C)*TAN(ANGSTL2-THETA08)

C straightline move adds above

*-ZLIFT2)**2)**0.5

C NOW SUBTRACT 'ZLIFT' TO GET RAPID DISTANCE REQUIRED

0264 ELSEIF (THETA08.GE.THETABRK) THEN

0266 RAPIDDIST10=(-RSPHER-WPTHICK-CLEAR+FLATHT-ZSTART

C above is the z position of the centre of rspher

*+(RSPHER-RFILLT)*COS(THETABRK)

C above:centre of rfillt adds this

*+(RFILLT+WPTHICK+CLEAR+RREDGE)*COS(THETA08)

C centre of roller before straightline move adds above

*+(RLIFT2-RSTLN2C)*TAN(ANGSTL2-THETA08)

C straightline move adds above

*-ZLIFT2)**2)**0.5

C NOW SUBTRACT 'ZLIFT' TO GET RAPID DISTANCE REQUIRED

0268 ENDIF

c---rapid in toward centre

0272 RAPIDDIST11=RLIFT2 - RPLUNGE3

c

c---plunge to make contact

C feed (plunge) to one thickness + clearance from former NC Z-1.0~9~3~8

0273 THETA12=ASIN(RPLUNGE3/(RSPHER+WPTHICK+CLEAR+RREDGE))

C-----

c0274 PLUNGEDIST12=ZLIFT2-RREDGE-FLATHT

c * +(1-COS(THETA12))*((RSPHER+WPTHICK+CLEAR+RREDGE))

C

PLUNGEDIST12=((-RSPHER-WPTHICK-CLEAR+FLATHT-ZSTART

c 24/9/02 added 'clear' in line 0244 above

C above is the z position of the centre of rspher

*+(RSPHER+WPTHICK+CLEAR+RREDGE)*COS(THETA12)

C above dist to centre of roller AFTERPLUNGE

*-ZLIFT2)**2)**0.5

c---feed along former

c check that theta12 is less than theta break

0277 TESTTHETA13=ASIN(RSTLN3/(RSPHER+WPTHICK+CLEAR))

0278 IF (TESTTHETA13.LT.THETABRK) THEN

0279 THETA13=ASIN(RSTLN3/(RSPHER+WPTHICK+CLEAR))

0280 FEEDDIST13=(RSPHER+WPTHICK+CLEAR)*(THETA13-THETA12)

C else RECALCULATE THETA2

0282 ELSE IF (TESTTHETA13.GE.THETABRK) THEN

0283 THETA13=ASIN((RSTLN3-((OUTDIA/2)-
RFILLT))/(RFILLT+WPTHICK+CLEAR))

0284 FEEDDIST13=(RSPHER+WPTHICK+CLEAR)*(THETABRK-
THETA12)+(RFILLT+

WPTHICK+CLEAR)(THETA13-THETABRK)

0285 ENDIF

0286 RSTLN3C=RSTLN3+RREDGE*(SIN(THETA13))

c RSTLN1C Calculates the position of the Centre of the roller edge radius

c---Straight line feed off former

0287 STL_DIST14=(RLIFT3-RSTLN3C)/COS(ANGSTL3-THETA13)

Cc

c

c

c

2008 format('/2008_Inc',i5,'Time:',g12.5,'THETA12_',g12.5,'STL_DIST14_',
*g12.5,'ANGSTL3',g12.5,


```
*'THETA13_',g12.5,'TESTTHETA13_',g12.5,'FEED',g12.5,'RAPID',g12.5)
  IF(INC.eq.1) open (unit=60,file='subroutine.out',status='unknown')
  IF(INC.EQ.1) WRITE (60,2009)Inc,time,THETA12,STL_DIST14,
*ANGSTL3,THETA13,TESTTHETA13,FEED,RAPID
```

c

c

c

```
c      *****CALCULATE      TIMES      FOR      EACH      TOOLMOTION
*****
```

c go to start radius NC X30

0310 RAPIDTIME01=RAPIDDIST01/rapid

C plunge to one thickness from former

0315 PLUNGETIME02=PLUNGEDIST02/feed

c circ move

0320 R95TIME03=FEEDDIST03/feed

c feed off

0325 STL_TIME04=STL_DIST04/feed

c rapid up in Z

0330 RAPIDTIME05=RAPIDDIST05/rapid

c rapid in toward centre

0335 RAPIDTIME06=RAPIDDIST06/rapid

c plunge to make contact

0340 PLUNGETIME07=PLUNGEDIST07/rapid

c feed along former

0345 R95_R17TIME08=FEEDDIST08/feed

c straight line feed off former

0350 STL_TIME09=STL_DIST09/feed

c rapid up in Z

0355 RAPIDTIME10=RAPIDDIST10/rapid

c rapid in toward centre

0360 RAPIDTIME11=RAPIDDIST11/rapid

c plunge to make contact

0365 PLUNGETIME12=PLUNGEDIST12/feed

c feed along former

0370 R95_R17TIME13=FEEDDIST13/feed

c straight line feed off former

0375 STL_TIME14=STL_DIST14/feed

0378 format('/0378Inc:',i5,'Time:',g12.7,'RAPIDTIME01',g12.7,'PLNGTM02'
*,g12.7,'R95TIME03',g12.7,'STL_TIME04',g12.7,'RAPIDTIME05',g12.7,
*'RAPIDTIME06',g12.7,'PLUNGETIME07',g12.7,'R95_R17TIME08',g12.7,
*'STL_TIME09',g12.7,'RAPIDTIME10',g12.7,'RAPIDTIME11',g12.7,
*'PLUNGETIME12',g12.7,'R95_R17TIME13',g12.7,'STL_TIME14',g12.7)

0379 IF(INC.EQ.1) open (unit=60,file='subroutine.out',status='unknown')

0380 IF(INC.EQ.1) write (60,0378)Inc,time,RAPIDTIME01,PLUNGETIME02,
* R95TIME03,STL_TIME04,RAPIDTIME05,RAPIDTIME06,PLUNGETIME07,
*
R95_R17TIME08,STL_TIME09,RAPIDTIME10,RAPIDTIME11,PLUNGETIME12,
* R95_R17TIME13,STL_TIME14

c2000 format('/Inc:',i5,'Time:',g12.5,'Theta:',g12.5)

C

c*****TEST TIME AND CALCULATE TOOL
MOTION*****

c**DEFINITION OF ROLLER TOOL POSITIONS and CALCULATION OF TOOL
VELOCITY*****

0400 if(((TIME+DTIME).GT.0.0).AND.

*((TIME+DTIME).LE.RAPIDTIME01))then

0402 R=RAPID*(TIME+DTIME)

0404 Z=0

c roller stays at ZSTART

c RPLUNGE1

0406 else if((TIME+DTIME).GT.RAPIDTIME01.AND.

*(TIME+DTIME).le.RAPIDTIME01+PLUNGETIME02)

*then

0408 R=RPLUNGE1

0410 Z=-FEED*(TIME+DTIME-RAPIDTIME01)

C

```

0412 ELSEIF (((TIME+DTIME).GT.
      *RAPIDTIME01+PLUNGETIME02).AND.
      *((TIME+DTIME).LE.RAPIDTIME01+PLUNGETIME02+R95TIME03)) THEN
C THIS MOVE STARTS AT THETA1 AND ENDS AT THETA2
0414 THETADOT_1=FEED/(RSPHER+WPTHICK+CLEAR)
c      calculate theta as if on r95 setion of former
0416 THETA=THETA1+THETADOT_1*(TIME-(RAPIDTIME01+PLUNGETIME02))

0418 IF (THETA.LT.THETABRK) THEN
0420 CR=0
C      CZ=-ZSTART+FLATHT-(RSPHER+WPTHICK+CLEAR+RREDGE)
0422 R=CR+(RSPHER+WPTHICK+CLEAR+RREDGE)*SIN(THETA)
0424 Z=-ZSTART+FLATHT+RREDGE-
      *(RSPHER+WPTHICK+CLEAR+RREDGE)*(1-COS(THETA))

0426 ELSE IF (THETA.GE.THETABRK) THEN
C      change calculation for theta and thetadot if past r95 section of former
0428 THETADOT_2=FEED/(RFILLT+WPTHICK+CLEAR)
0430 THETA=THETABRK+THETADOT_2*(TIME-
(RAPIDTIME01+PLUNGETIME02+
      *(THETABRK-THETA1)/THETADOT_1))
0432 CR=(OUTDIA/2)-RFILLT
0434 CZ=-ZSTART+FLATHT+RREDGE-(RSPHER+WPTHICK+CLEAR+RREDGE)
      **(1-COS(THETABRK))-
(RFILLT+WPTHICK+CLEAR+RREDGE)*COS(THETABRK)
C
0436 R=CR+(RFILLT+WPTHICK+CLEAR+RREDGE)*SIN(THETA)
0438 Z=(CZ+(RFILLT+WPTHICK+CLEAR+RREDGE)*COS(THETA))
0440 endif

C0441 format('/0441Inc:',i5,'Time:',g12.5,'PLUNGEDIST02',g12.5,'THETA1',
c      *g12.5,'THETABRK',g12.5,'THETA2',g12.5,
c      *'THETA2',g12.5, 'THETADOT_1',g12.5 'THETADOT_2',g12.5)
c      open (unit=60,file='subroutine.out',status='unknown')

```

```

c WRITE (60,0441)Inc,time,PLUNGEDIST02,THETA1,
c *THETABRK,THETA2,THETA,THETADOT_1,THETADOT_2

0444 ELSEIF (((TIME+DTIME).GT.
    *RAPIDTIME01+PLUNGETIME02+R95TIME03).AND.
    *((TIME+DTIME).LE.
    *RAPIDTIME01+PLUNGETIME02+R95TIME03+STL_TIME04)) THEN
0446 R=RSTLN1+RREDGE*SIN(THETA2)+
    *(TIME-(RAPIDTIME01+PLUNGETIME02+R95TIME03))*
    *FEED*COS(ANGSTL1-THETA2)
0448 CZ=-ZSTART+FLATHT+RREDGE-(RSPHER+WPTHICK+CLEAR+RREDGE)
    *(1-COS(THETABRK))-
(RFILLT+WPTHICK+CLEAR+RREDGE)*COS(THETABRK)
0450 Z=CZ+(RFILLT+WPTHICK+CLEAR+RREDGE)*COS(THETA2)
    *(TIME-(RAPIDTIME01+PLUNGETIME02+R95TIME03))*
    *FEED*SIN(ANGSTL1-THETA2)

0452 ELSEIF (((TIME+DTIME).GT.
    *RAPIDTIME01+PLUNGETIME02+R95TIME03+STL_TIME04).AND.
    *((TIME+DTIME).LE.
    *RAPIDTIME01+PLUNGETIME02+R95TIME03+STL_TIME04+RAPIDTIME05))
THEN

0454 Z=-RSPHER-WPTHICK-CLEAR+FLATHT-ZSTART
c 24/09/02 added 'CLEAR'
C above is the z position of the centre of rspher
    *(RSPHER-RFILLT)*COS(THETABRK)
C above:centre of rfillt adds this
    *(RFILLT+WPTHICK+CLEAR+RREDGE)*COS(THETA2)
C centre of roller before straightline move adds above
    *(RLIFT1-RSTLN1C)*TAN(ANGSTL1-THETA2)
C straightline move adds above
    *RAPID*(TIME-(RAPIDTIME01+PLUNGETIME02+R95TIME03+STL_TIME04))
C RAPID MOTION ADDS ABOVE
0458 R=RLIFT1

```

C=RSTLN1+RREDGE*SIN(THETA2)+

C *(STL_TIME04)*FEED*COS(ANGSTL1-THETA2)

0460 ELSEIF (((TIME+DTIME).GT.

*RAPIDTIME01+PLUNGETIME02+R95TIME03+STL_TIME04+RAPIDTIME05).AN

D.

*((TIME+DTIME).LE.

*RAPIDTIME01+PLUNGETIME02+R95TIME03+STL_TIME04+RAPIDTIME05+

*RAPIDTIME06)) THEN

c moves roller in towards centre

0462 Z=ZLIFT1

0464 R=RLIFT1-RAPID*(TIME

*-(RAPIDTIME01+PLUNGETIME02+R95TIME03+STL_TIME04+RAPIDTIME05))

0466 ELSEIF (((TIME+DTIME).GT.

*RAPIDTIME01+PLUNGETIME02+R95TIME03+STL_TIME04+RAPIDTIME05+

*RAPIDTIME06).AND.

*((TIME+DTIME).LE.

*RAPIDTIME01+PLUNGETIME02+R95TIME03+STL_TIME04+RAPIDTIME05+

*RAPIDTIME06+PLUNGETIME07)) THEN

0468 Z=ZLIFT1-RAPID*(TIME-(RAPIDTIME01+PLUNGETIME02+R95TIME03

*+STL_TIME04+RAPIDTIME05+RAPIDTIME06))

0470 R=RPLUNGE2

0472 ELSEIF (((TIME+DTIME).GT.

*RAPIDTIME01+PLUNGETIME02+R95TIME03+STL_TIME04+RAPIDTIME05+

*RAPIDTIME06+PLUNGETIME07).AND.

*((TIME+DTIME).LE.

*RAPIDTIME01+PLUNGETIME02+R95TIME03+STL_TIME04+RAPIDTIME05+

*RAPIDTIME06+PLUNGETIME07+R95_R17TIME08)) THEN

C-----

```

C THIS MOVE STARTS AT THETA07 AND ENDS AT THETA08
0474 THETADOT_1=FEED/(RSPHER+WPTHICK+CLEAR)
c    calculate theta as if on r95 setion of former
0476 THETA=THETA07+THETADOT_1*(TIME-(
    *RAPIDTIME01+PLUNGETIME02+R95TIME03+STL_TIME04+RAPIDTIME05+
    *RAPIDTIME06+PLUNGETIME07))

0478 IF (THETA.LT.THETABRK) THEN
0480 CR=0

0482 R=CR+(RSPHER+WPTHICK+CLEAR+RREDGE)*SIN(THETA)
0484 Z=-ZSTART+FLATHT+RREDGE-
    *(RSPHER+WPTHICK+CLEAR+RREDGE)*(1-COS(THETA))

0486 ELSE IF (THETA.GE.THETABRK) THEN
C    change calculation for theta and thetadot if past r95 section of former
0488 THETADOT_2=FEED/(RFILLT+WPTHICK+CLEAR)
0490 THETA=THETABRK+THETADOT_2*(TIME-(
    *RAPIDTIME01+PLUNGETIME02+R95TIME03+STL_TIME04+RAPIDTIME05+
    *RAPIDTIME06+PLUNGETIME07+
    *(THETABRK-THETA07)/THETADOT_1))
0491 CR=(OUTDIA/2)-RFILLT
0492 CZ=-ZSTART+FLATHT+RREDGE-(RSPHER+WPTHICK+CLEAR+RREDGE)
    *(1-COS(THETABRK))-
(RFILLT+WPTHICK+CLEAR+RREDGE)*COS(THETABRK)
C
0493 R=CR+(RFILLT+WPTHICK+CLEAR+RREDGE)*SIN(THETA)
0494 Z=(CZ+(RFILLT+WPTHICK+CLEAR+RREDGE)*COS(THETA))
0495 endif

c 2003 format('/2003Inc',i5,'Time:',g12.5,'PLUNGEDIST07',g12.5,'THETA07',
c    *g12.5,'THETABRK',g12.5,'THETA08',g12.5,
c    *'THETA',g12.5, 'THETADOT_1',g12.5 'THETADOT_2',g12.5)

```

```

c      open (unit=60,file='subroutine.out',status='unknown')
c
c      WRITE (60,2003)Inc,time,PLUNGETIME07,THETA07,
c      *THETABRK,THETA08,THETA,THETADOT_1,THETADOT_2

```

```

C-----

```

```

0496  ELSEIF (((TIME+DTIME).GT.
      *RAPIDTIME01+PLUNGETIME02+R95TIME03+STL_TIME04+RAPIDTIME05+
      *RAPIDTIME06+PLUNGETIME07+R95_R17TIME08).AND.
      *((TIME+DTIME).LE.
      *RAPIDTIME01+PLUNGETIME02+R95TIME03+STL_TIME04+RAPIDTIME05+
      *RAPIDTIME06+PLUNGETIME07+R95_R17TIME08+STL_TIME09)) THEN
C MOVE OFF WORKPIECE ALONG STL2
      R=RSTLN2+RREDGE*SIN(THETA08)+
      *(TIME-
(RAPIDTIME01+PLUNGETIME02+R95TIME03+STL_TIME04+RAPIDTIME05+
      *RAPIDTIME06+PLUNGETIME07+R95_R17TIME08))*
      *FEED*COS(ANGSTL2-THETA08)
      CZ=-ZSTART+FLATHT+RREDGE-(RSPHER+WPTHICK+CLEAR+RREDGE)
      *(1-COS(THETABRK))-
(RFILLT+WPTHICK+CLEAR+RREDGE)*COS(THETABRK)
      Z=CZ+(RFILLT+WPTHICK+CLEAR+RREDGE)*COS(THETA08)
      *(TIME-
(RAPIDTIME01+PLUNGETIME02+R95TIME03+STL_TIME04+RAPIDTIME05+
      *RAPIDTIME06+PLUNGETIME07+R95_R17TIME08))*
      *FEED*SIN(ANGSTL2-THETA08)

0497  ELSEIF (((TIME+DTIME).GT.
      *RAPIDTIME01+PLUNGETIME02+R95TIME03+STL_TIME04+RAPIDTIME05+
      *RAPIDTIME06+PLUNGETIME07+R95_R17TIME08+STL_TIME09).AND.
      *((TIME+DTIME).LE.
      *RAPIDTIME01+PLUNGETIME02+R95TIME03+STL_TIME04+RAPIDTIME05+

```

*RAPIDTIME06+PLUNGETIME07+R95_R17TIME08+STL_TIME09+RAPIDTIME10)
)

* THEN

c RAPID UP TO ZLIFT2

Z=-RSPHER-WPTHICK-CLEAR+FLATHT-ZSTART

C 24/09/02

C above is the z position of the centre of rspher

*+(RSPHER-RFILLT)*COS(THETABRK)

C above:centre of rfillt adds this

*+(RFILLT+WPTHICK+CLEAR+RREDGE)*COS(THETA08)

C centre of roller before straightline move adds above

*+(RLIFT2-RSTLN2C)*TAN(ANGSTL2-THETA08)

C straightline move adds above

+RAPID(TIME-(RAPIDTIME01+PLUNGETIME02+R95TIME03+STL_TIME04

*+RAPIDTIME05+RAPIDTIME06+PLUNGETIME07+R95_R17TIME08+STL_TIME09))

C RAPID MOTION ADDS ABOVE

R=RLIFT2

0498 ELSEIF (((TIME+DTIME).GT.

*RAPIDTIME01+PLUNGETIME02+R95TIME03+STL_TIME04+RAPIDTIME05+

*RAPIDTIME06+PLUNGETIME07+R95_R17TIME08+STL_TIME09+RAPIDTIME10)

.AND

*.((TIME+DTIME).LE.

*RAPIDTIME01+PLUNGETIME02+R95TIME03+STL_TIME04+RAPIDTIME05+

*RAPIDTIME06+PLUNGETIME07+R95_R17TIME08+STL_TIME09+RAPIDTIME10

+

*RAPIDTIME11)) THEN

c moves roller in towards centre

Z=ZLIFT2

R=RLIFT2-RAPID*(TIME

*(RAPIDTIME01+PLUNGETIME02+R95TIME03+STL_TIME04+RAPIDTIME05

+RAPIDTIME06+PLUNGETIME07+R95_R17TIME08+STL_TIME09+RAPIDTIME10))

0499 ELSEIF (((TIME+DTIME).GT.

*RAPIDTIME01+PLUNGETIME02+R95TIME03+STL_TIME04+RAPIDTIME05+

*RAPIDTIME06+PLUNGETIME07+R95_R17TIME08+STL_TIME09+RAPIDTIME10

+

*RAPIDTIME11).AND.

*((TIME+DTIME).LE.

*RAPIDTIME01+PLUNGETIME02+R95TIME03+STL_TIME04+RAPIDTIME05+

*RAPIDTIME06+PLUNGETIME07+R95_R17TIME08+STL_TIME09+RAPIDTIME10

+

*RAPIDTIME11+PLUNGETIME12)) THEN

C PLUNGE TO MAKE CONTACT

R=RPLUNGE3

Z=ZLIFT2-FEED*(TIME-(RAPIDTIME01+PLUNGETIME02+R95TIME03+

*STL_TIME04+RAPIDTIME05+RAPIDTIME06+PLUNGETIME07+R95_R17TIME08

+

*STL_TIME09+RAPIDTIME10+RAPIDTIME11))

0500 ELSEIF (((TIME+DTIME).GT.

*RAPIDTIME01+PLUNGETIME02+R95TIME03+STL_TIME04+RAPIDTIME05+

*RAPIDTIME06+PLUNGETIME07+R95_R17TIME08+STL_TIME09+RAPIDTIME10

+

*RAPIDTIME11+PLUNGETIME12).AND.

```

*((TIME+DTIME).LE.
*RAPIDTIME01+PLUNGETIME02+R95TIME03+STL_TIME04+RAPIDTIME05+

*RAPIDTIME06+PLUNGETIME07+R95_R17TIME08+STL_TIME09+RAPIDTIME10
+
*RAPIDTIME11+PLUNGETIME12+R95_R17TIME13)) THEN
C FEED ALONG FORMER

C THIS MOVE STARTS AT THETA13 AND ENDS AT THETA14
0514 THETADOT_1=FEED/(RSPHER+WPTHICK+CLEAR)
c calculate theta as if on r95 setion of former
0516 THETA=THETA12+THETADOT_1*(TIME-(RAPIDTIME01+PLUNGETIME02
*+R95TIME03+STL_TIME04+RAPIDTIME05+

*RAPIDTIME06+PLUNGETIME07+R95_R17TIME08+STL_TIME09+RAPIDTIME10
+
*RAPIDTIME11+PLUNGETIME12))

0518 IF (THETA.LT.THETABRK) THEN
0520 CR=0
C CZ=-ZSTART+FLATHT-(RSPHER+WPTHICK+CLEAR+RREDGE)
0522 R=CR+(RSPHER+WPTHICK+CLEAR+RREDGE)*SIN(THETA)
0524 Z=-ZSTART+FLATHT+RREDGE-
*(RSPHER+WPTHICK+CLEAR+RREDGE)*(1-COS(THETA))

0526 ELSE IF (THETA.GE.THETABRK) THEN
C change calulation for theta and thetadot if past r95 section of former
0528 THETADOT_2=FEED/(RFILLT+WPTHICK+CLEAR)
0530 THETA=THETABRK+THETADOT_2*(TIME-
(RAPIDTIME01+PLUNGETIME02+
*+R95TIME03+STL_TIME04+RAPIDTIME05+

*RAPIDTIME06+PLUNGETIME07+R95_R17TIME08+STL_TIME09+RAPIDTIME10
+
*RAPIDTIME11+PLUNGETIME12+

```

```

*(THETABRK-THETA12)/THETADOT_1))
0532 CR=(OUTDIA/2)-RFILLT
0534 CZ=-ZSTART+FLATHT+RREDGE-(RSPHER+WPTHICK+CLEAR+RREDGE)
** (1-COS(THETABRK))-
(RFILLT+WPTHICK+CLEAR+RREDGE)*COS(THETABRK)
C
0536 R=CR+(RFILLT+WPTHICK+CLEAR+RREDGE)*SIN(THETA)
0538 Z=(CZ+(RFILLT+WPTHICK+CLEAR+RREDGE)*COS(THETA))
0539 endif

0550 ELSEIF (((TIME+DTIME).GT.
*RAPIDTIME01+PLUNGETIME02+R95TIME03+STL_TIME04+RAPIDTIME05+
*RAPIDTIME06+PLUNGETIME07+R95_R17TIME08+STL_TIME09+RAPIDTIME10
+
*RAPIDTIME11+PLUNGETIME12+R95_R17TIME13).AND.
*((TIME+DTIME).LE.
*RAPIDTIME01+PLUNGETIME02+R95TIME03+STL_TIME04+RAPIDTIME05+
*RAPIDTIME06+PLUNGETIME07+R95_R17TIME08+STL_TIME09+RAPIDTIME10
+
*RAPIDTIME11+PLUNGETIME12+R95_R17TIME13+STL_TIME14)) THEN

C MOVE OFF WORKPIECE ALONG STL3
R=RSTLN3+RREDGE*SIN(THETA13)+
*(TIME-
(RAPIDTIME01+PLUNGETIME02+R95TIME03+STL_TIME04+RAPIDTIME05+
*RAPIDTIME06+PLUNGETIME07+R95_R17TIME08+STL_TIME09+RAPIDTIME10
+
*RAPIDTIME11+PLUNGETIME12+R95_R17TIME13))*
*FEED*COS(ANGSTL3-THETA13)
CZ=-ZSTART+FLATHT+RREDGE-(RSPHER+WPTHICK+CLEAR+RREDGE)
** (1-COS(THETABRK))-
(RFILLT+WPTHICK+CLEAR+RREDGE)*COS(THETABRK)

```

```

Z=CZ+(RFILLT+WPTHICK+CLEAR+RREDGE)*COS(THETA13)
*+(TIME-
(RAPIDTIME01+PLUNGETIME02+R95TIME03+STL_TIME04+RAPIDTIME05+
*RAPIDTIME06+PLUNGETIME07+R95_R17TIME08+STL_TIME09+RAPIDTIME10
+
*RAPIDTIME11+PLUNGETIME12+R95_R17TIME13))*
*FEED*SIN(ANGSTL3-THETA13)

```

```

2010 format('/2010Inc',i5,'Time:',g12.5,'THETA12_',g12.5,'STL_DIST14_',
*g12.5,'ANGSTL3',g12.5,
*'THETA13_',g12.5,'TESTTHETA13_',g12.5,'FEED',g12.5,'RAPID',g12.5)
open (unit=60,file='subroutine.out',status='unknown')
WRITE (60,2010)Inc,time,THETA12,STL_DIST14,
*ANGSTL3,THETA13,TESTTHETA13,FEED,RAPID

```

```

2009 format('/2009Inc',i5,'Time:',g12.5,'THETA12_',g12.5,'STL_DIST14_',
*g12.5,'ANGSTL3',g12.5,
*'THETA13_',g12.5,'TESTTHETA13_',g12.5,'FEED',g12.5,'RAPID',g12.5)
c IF(INC.eq.1)
open (unit=60,file='subroutine.out',status='unknown')
c IF(INC.EQ.1)
WRITE (60,2009)Inc,time,THETA12,STL_DIST14,
*ANGSTL3,THETA13,TESTTHETA13,FEED,RAPID

```

```

c 0552 endif
C C
0554 endif

```

C *****

c allocation of XYZ directions to motions calculated as R and Z

c STEPOFF allows tool to move off workpiece periodically for axisymmetric

STEPOFF=1.0

0600 X3=0.0

C R*SIN(OMEGA*(TIME+DTIME))

0605 X2=R+STEPOFF*(1+SIN(OMEGA*(TIME+DTIME)))*(R/95.0)

C *COS(OMEGA*(TIME+DTIME))

0610 X1=Z+STEPOFF*(1+SIN(OMEGA*(TIME+DTIME)))*(SQRT(1-((R/95)**2)))

0615 V(1)=(X1-X(1))/DTIME

0620 V(2)=(X2-X(2))/DTIME

0625 V(3)=(X3-X(3))/DTIME

0630 V(4)=0.0

C OMEGA

c

0635 if(inc.eq.0)v(1)=0.0

0640 if(inc.eq.0)v(2)=0.0

0645 if(inc.eq.0)v(3)=0.0

0650 if(inc.eq.0)v(4)=0.0

C *****

c it was the roller, sums done

0655 endif

0660 write(6,*)v(1),v(2),v(3),v(4)

c

0665 return

0670 end

Appendix 4 Fortran 6.6 code for rotating full three dimensional simulation

Note the code is identical to that in appendix 3 up line 0554 (and so is omitted) then the output for the three dimensional motion differs from the stepping motion in appendix 3

```
0552 endif
C C
0554 endif
C *****
c allocation of XYZ directions to motions calculated as R and Z
0600 X3= R*SIN(OMEGA*(TIME+DTIME))
0605 X2= R*COS(OMEGA*(TIME+DTIME))
0610 X1=Z
0615 V(1)=(X1-X(1))/DTIME
0620 V(2)=(X2-X(2))/DTIME
0625 V(3)=(X3-X(3))/DTIME
0630 V(4)=OMEGA
c
0635 if(inc.eq.0)v(1)=0.0
0640 if(inc.eq.0)v(2)=0.0
0645 if(inc.eq.0)v(3)=0.0
0650 if(inc.eq.0)v(4)=0.0

C *****

c it was the roller, sums done
0655 endif

0660 write(6,*)v(1),v(2),v(3),v(4)
c
0665 return
0670 end
```